Origin and paragenetic relations of chert nodules in the Florence Limestone, Flint Hills, Kansas

by

Minindu Mallawa Nanayakkaralage Gedara

B.Sc.(Hons), University of Peradeniya, 2021

A THESIS

submitted in partial fulfillment of the requirements for the degree

MASTER OF SCIENCE

Department of Geology
College of Arts and Sciences

KANSAS STATE UNIVERSITY
Manhattan, Kansas

2024

Approved by:

Major Professor
Dr. Karin Goldberg

Copyright

Abstract

The presence of chert nodules within Florence Limestones in the Flint Hills, Kansas, is partially responsible for its "rolling hills" landscape, as chert is resistant to weathering, holding the topography in this limestone-dominated terrain. It is also an important archeological material, since prehistoric communities used it for tools and trade due to its inherent strength. Despite its ubiquitous presence in the area, the source of silica and paragenetic relations of the minerals in these nodular cherts have not been investigated. This research used a variety of approaches to unravel the source of silica and understand the timing of the formation of the chert nodules. Fieldwork, petrographic analysis, X-Ray Diffraction, and Raman spectroscopy indicated that the Florence Limestone underwent multiphase silicification, starting with the precipitation of opaline silica along burrow pathways during eodiagenesis, followed by other silica polymorphs (microcrystalline quartz and chalcedony) precipitated at later stages. The identification of moganite, along with the presence of halite molds and gypsum nodules in the succession, indicates that evaporite conditions contributed to silica supersaturation. Oxygen isotopes reveal that samples underwent paleotemperatures around 35° C – 40° C minimum, corroborating the interpretation of burial under eodiagenetic conditions. The silica-germanium ratios of 0.4×10^6 - 1.25×10^6, obtained for the different silica phases (opaline, chert, chalcedony, and megaquartz), are compatible with a biogenic origin for the silicifying solutions, which is in agreement with the presence of siliceous organisms (sponge spicules and radiolarians) in the limestones. Therefore, the silica nodules were formed shortly after deposition by the percolation of silica-rich solutions along burrow networks, resulting in the precipitation of opaline silica, followed by chert, chalcedony and finally megaquartz. Silicifying solutions were derived from the dissolution of siliceous organisms, augmented by highly evaporite conditions.

Table of Contents

List of Figures v
List of Tables xi
Acknowledgments xii
Dedication xiii
Chapter 1 - Introduction 1
Chapter 2 - Methodology 15
Chapter 3 - Results 27
Chapter 4 - Discussion 56
Chapter 5 - Conclusions 70
Bibliography 72
Appendix A - Petrographic Descriptions 85
Appendix B - Thin Section Quantification 145
Appendix C - Raman Spectroscopy Data 157
Appendix D - ICP-MS Analysis Data 161

List of Figures

Figure 1.1- Outcrops around Manhattan, Kansas, selected for this study. Site 01- Near Milford Lake, Site 02- Near Tuttle Creek dam, Site 03- Along I-70 highway, exit 307. 2
Figure 1.2- Stratigraphic position of the Barneston Limestone (which includes the Florence Limestone) in the Wolfcampian Chase Group (Miller & Twiss, 1994). Both Council Grove and Chase Group are characterized by alternating shales (Sh) and limestones (Ls). 5
Figure 1.3- Exposed "burrow network" formed by coalescing chert nodules near Milfod Reservoir (Miller, 2010). Length of hammer is 28 cm. 6
Figure 1.4- (a and b)-A "wood-grained" chert layer from Portland Limestone (Maliva et al., 1999). (C= Dark grey chert nodule, E= Earlier-generated dark-grey nodular chert, L= Limestone, W= Wood grained chert)..... 7
Figure 1.5- Meteoric water and saline water mixing forming zone of chertification (Knauth, 1979). 11
Figure 1.6- Solubility of quartz and amorphous silica varying with temperature (Rimstidt & Cole, 1983)..... 12
Figure 1.7- Different forms of silica precipitating from solution (Knauth, 1970)..... 13
Figure 1.8- Silica phases stability fields at a given temperature and pressure (Hesse, 1989). 14
Figure 2.1- Nodular chert exposures near Milford Lake. (a) Chert "layers" can be seen in the top and side views. Distribution of chert along horizontal "beds." (b) 8-10 cm thick chert layers exposed on the vertical plane. Yellow stars indicate the sampled chert beds..... 16
Figure 2.2- Outcrop along the I-70 highway, displaying multiple chert intervals on a vertical exposure. Height of outcrop is ~3.5 m and yellow stars indicate sampled chert horizons. .. 17
Figure 2.3- Outcrop near Tuttle Creek Lake. Height of outcrop varied from ~3.5 m to 4.5 m. The yellow stars indicate different chert horizons where samples were collected.. 18
Figure 2.4- Raman shifts vs. intensity for different silica phases in an enstatite chondrite (Kimura et al., 2005)... 22
Figure 2.5- XRD scans for Opal-A, Opal-CT, and Opal-C (Elzea & Rice, 1996)..... 23
Figure 2.6- Chert granules reacting with dilute HCl to remove carbonates and organic matter (samples FL-KS-7-2, FL-KS-6-2, FL-KS-5-2-2, FL-KS-6-3, FL-KS-7-1 from left to right)... 24

Figure 3.1- Horizontal chert layers with diagonal or vertical connections (white arrows), similar to burrow pathways. 27
Figure 3.2- Chert layers in the middle section at Site 03 (Tuttle Creek) exposure, displaying (a) a wood-grained texture and (b) intense vertical fracturing. 28
Figure 3.3- Isolated chert nodules (arrows) appear in the top layers of host limestone at Site 03 (Tuttle Creek). 29
Figure 3.4- Isolated chert nodules with lighter-rimmed boundaries and darker cores. 30
Figure 3.5- Common texture and fabric in studied thin sections:(a) wackestone (micritic calcarenite) and (b) loose grain packing with chaotic orientation of grains. 34
Figure 3.6- Different types of bioclasts in the studied thin sections: (a) a bryozoan with preserved primary porosity (plane polarized light, PP), (b) a silicified brachiopod (on the far right side shown by a black arrow) and sponge spicules (shown by yellow arrows) (PP), (c) an accumulation of sponge spicules (PP), (d) a rarely preserved radiolarian (shown by a white arrow in crossed polarized light, XP). The blue dye mark the pore spaces in the thin section, and pink color in calcite is due to staining with Alizarin Red. 37
Figure 3.7- Four major silica phases: (a) opaline silica replacing micrite (indicated by yellow arrows, crossed polarized light, XP), (b) chert replacing micrite and sponge spicules (indicated by yellow arrows, XP), (c) silica rosettes (indicated by yellow arrows) filling interparticle and vug pores (plane polarized light, PP), and (d) chalcedony replacing bioclast. 39
Figure 3.8- Different optical orientations of chalcedony fibers, indicating the occurrence of (a and b) length-fast chalcedony (f) within a bioclast and (c and d) length-slow (s) chalcedony (moganite) within a bioclast. (a) and (c) is the PP view, and (b) and (d) are the XP view with the addition of a gypsum plate. 40
Figure 3.9- Spherulitic chalcedony (brownish color, abundant on the upper left corner) grading to euhedral quartz (more abundant toward the lower right) in a vug pore under (a) plane-polarized light (PP) and (b) crossed-polarized light (XP)..... 41
Figure 3.10- Paragenetic relations between silica phases. (a) Opaline silica (Opl) replaced by chert (Chrt), (b) chert replaced by chalcedony (Chl) along the margin of a bioclast, (c) opaline silica replaced by chalcedony, (d) silica rosettes (Ro) lining and filling dissolution pores. 42

Figure 3.11- Calcite replacing (a) a carbonate bioclast, (b) a sponge spicule (shown in yellow arrow), (c) opaline silica, (d) chalcedony. 43
Figure 3.12- Other diagenetic minerals include (a) coarse barites replaced by chalcedony, precipitated within partially dissolved anhydrite nodules (b and c). The nodules are partially silicified by chalcedony, which contains anhydrite inclusions in the center (d)..... 44
Figure 3.13- Porosity included (a) intraparticle pores within a bryozoan, (b) vug pores due to dissolution of micrite and chert, (c) moldic pores due to dissolution of bioclasts, (d) fracture pores. 46
Figure 3.14- Stylolites are commonly accompanied by (a) interparticle and moldic pores, (b-c) silica rosettes, and (d) opaline silica precipitation. The preferential location of secondary pores (in blue) along stylolites suggests that the latter provided a pathway for the percolation of dissolving solutions that generated the pores, as well as late-stage solutions for the precipitation of silica rosettes and opaline silica during burial. 47
Figure 3.15- Luminescence observed on bioclasts in thin section FL-KS-7-2. The non-luminescent dark line in the middle is opaline silica in the wood-grained nodule. Dark spots surrounding luminescent carbonate particles are the chert replacements. 48
Figure 3.16- Raman shift corresponding to silica replacing a bioclast in sample FL-KS-3-1..... 50
Figure 3.17- Raman shift signal for FL-KS-6-1, overlayed with the instrument's chalcedony reference signal (below). 51
Figure 3.18- Diffractogram for FL-KS-7-1 showing Moganite-Quartz associations (MQz). 52
Figure 3.19- Diffractogram for FL-KS-7-1 showing Moganite-Quartz associations (MQz). 52
Figure 3.20- $\delta^{18}O$ values for the six samples analyzed, according to the major silica type (Opl- Opaline silica, Chrt- chert, Chl+MQz- Chalcedony with megaquartz). The markers (black circles) in the graph are larger than the analytical error of 0.28‰. 54
Figure 3.21- Ge/Si ($x10^6$) ratios analyzed in six samples with different types of silica (Opl- Opaline silica, Chrt- Chert, Chl+MQz- Chalcedony with megaquartz). 55
Figure 4.1- Measured oxygen isotope values of burial chert from ODP 795 from (Brumsack et al., 1992) vs depth of burial (Yanchilina et al, 2020). (mbsf = meters below the seafloor) 57
Figure 4.2- Diagenetic processes and products observed during the formation of silica nodules in the Florence Limestone. 59

Figure 4.3- Ge/Si ratios from this study (blue circles) compared with Ge/Si ratio from different sources of silica (Tribovillard et al., 2011; Tribovillard, 2013). 61
Figure 4.4- Schematic illustration of an evaporite nodule observed in the studied thin sections. A- Quartzine spherulites of different sizes, B- Megaquartz with undulous extinction, C- Megaquartz with anhydrite inclusions, D- Prismatic barite crystals. 62
Figure 4.5- Paleogeography of North America in the Early Permian. Kansas is marked by solid black margins and paleoequator is marked by a red solid line (Modified after Goldberg & Miller, 2019). 63
Figure 4.6- Paleogeographic reconstruction of North America, with Kansas (red arrow) located close to the paleo equator (yellow line) (Blakey & Ranney, 2018). 65
Figure 4.7- Alternating opaline silica and micrite zones, forming the wood-grained texture. Note the abundant sponge spicules within the micrite matrix (Opl- opaline silica, Cal- micrite matrix). 68
Figure A.1- (a) Opaline silica replaced by chert (b) Silica rosettes filling dissolution pores (c) Abundant moldic pores (d) Brachiopod intraparticle pore filled by chalcedony. 87
Figure A.2- Wood-grained nodule boundary with opaline silica and chert (b) Opaline silica with bioclasts replaced by chalcedony (c) A bryozoan bioclast with abundant intraparticular pores (d) Silica rosettes filling dissolution pores. 90
Figure A.3- (a) Wackestone with abundant bioclasts (including sponge spicules) (b) Chert replacing micrite matrix (c) Silica rosettes lining moldic pores (d) Blocky calcite replacing chalcedony. 93
Figure A.4- (a) Abundant bioclasts with moldic pores within micrite (b) Remains of micritic mud replaced by chert (c) Opaline silica formations adjacent to silica rosettes (d) Titanium oxide rhombs(secondary) in micrite matrix. 96
Figure A.5- (a) Abundant sponge spicules close to wood-grained chert boundary (b) Silica rosettes bordering with wood-grained chert (c) Possible “growth front” looking wood-grained chert boundaries (d) Spherulitic chalcedony replaced by blocky calcite. 99
Figure A.6- Intraparticle pores of corals and bryozoans partially filled by silica rosettes (b) Abundant calcispheres (c) Brachiopod shell replaced by Moganite (M) (d) Undifferentiated carbonate bioclast replaced by chalcedony and chalcedony replaced by diagenetic calcite rhombs. 102

Figure A.7- (a) Calcisphere bioclasts embedded within micritic matrix (b and c) Moldic and dissolution pores within chert (d) Calcite rhombs replacing chert. 105
Figure A.8- (a) Moldic pores within micrite filled by opaline silica (b) Chert replacing micrite (c) Carbonate bioclast replaced by chalcedony and chalcedony later replaced by blocky calcite (d) Well-formed/spherical silica rosettes filling dissolution pores. 108
Figure A.9- (a) Abundant calcisphere bioclasts (b) Diagenetic silica rims replacing carbonate bioclast indicating a replacive reaction (c) Blocky calcite replacing chert (d) Silica rosettes filling dissolution pores. 111
Figure A.10- (a and b) Intraparticular pore of a brachiopod shell filled by length fast chalcedony (a = XPL and b = XPL with gypsum plate). Note the surrounding chert matrix with some parts of bioclast replaced by calcite (c) Chalcedony replacing carbonate bioclast (d) Stylolite formed through a phosphate grain. 115
Figure A.11- (a) Calcispheres silicified with some micrite remnants within the silica-replaced matrix (b) Silicified brachiopod shell replaced by chalcedony with dissolution pores at the boundaries of fossil. 118
Figure A.12- (a) Opaline silica precipitated within a stylolite cutting an undifferentiated carbonate bioclast (b) Blocky calcite replacing a recrystalized sponge spicule (c) Spherulitic chalcedony replacing a brachiopod spine (d) Dolomite rhomb replacing chert. 121
Figure A.13- (a and b) Diagenetic calcite and dolomite rhombs replacing chert. 124
Figure A.14- (a) Abundant anhydrite crystals within megaquartz (b) Varying sizes of spherulitic chalcedony (c) Opaline silica filling pores within baryte grains (d) Subhedral megaquartz filling a vuggy pore. 127
Figure A.15- (a) Aggregate of sponge spicules (b) Chalcedony and megaquartz replacing an undifferentiated carbonate bioclast (c) Dissolution of micrite forming abundant pores (d) A vuggy pore. 130
Figure A.16- (a and b) Prismatic quartz replaced by calcite within the cherty matrix. (c and d) Partially replaced euhedral prismatic quartz (PQ) with granules of anhydrite inside the grains. 133
Figure A.17- (a) Mud micrite replaced by chert (b) A stylolite with opaline silica precipite. Later, opaline silica was replaced by blocky calcite crystals growing inwards. 135

Figure A.18- (a and b) Opaline silica (Opl) replacing micrite and carbonate bioclasts. Opaline silica replaced by chert (Chrt) and blocky calcite. (c and d) Euhedral calcite rhomb replacing siliceous bioclast. 138
Figure A.19- (a) Dissolution pores filled by opaline silica (Opl) (b) A moldic pore partially filled by chalcedony (Chl) (c and d) Opaline silica (Opl) replaced by blocky calcite. 141
Figure A.20- (a and b) A carbonate bioclast replaced by chalcedony, the latter replaced by calcite. (c and d) Intraparticle dissolution of a brachiopod shell, with pore-filling silica rosettes. 144
Figure C.21- FL-KS-1-2 Wood-grained chert full signal. 157
Figure C.22- Complete FL-KS-1-2 chert reference signal (top) overlapped with quartz reference signal (below)..... 157
Figure C.23- Full signal for FL-KS-2-2 with a peak around 464 cm^{-1}. 158
Figure C.24-Full signal for FL-KS-3-1 for wood-grained chert boundary. Peaks around 464 cm^{-1} (quartz) and 1019 cm^{-1} (calcite) were observed. 158
Figure C.25- Full signal observed for FL-KS-3-2 silicified bioclast with peak signal around 464 cm^{-1}. 158
Figure C.26-FL-KS-4 Full signal with 464cm^{-1} peak for chert matrix. 159
Figure C.27- Full signal for FL-KS-5-2-1. 159
Figure C.28- Truncated signal wave with a peak around 464.23 cm^{-1} for micrite-replacing silica. 159
Figure C.29- Full signal for FL-KS-5-3, silicified bioclast boundary with peaks observed around 127.23cm^{-1} (quartz), 206.53 cm^{-1} (quartz), 464.06 cm^{-1}(quartz) and 1086.37 cm^{-1} (calcite). 160
Figure C.30- Full signal for Chalcedony and megaquartz associations in FL-KS-6-1. 160

List of Tables

Table 2.1- Sample locations. 15
Table 2.2- Cathodoluminescence colors observed and interpretations on different silica forming environments and conditions (Füchtbauer et al., 1982; Ramseyer et al., 1988; Ètze et al., 2001). 20
Table 3.1-Detailed chert nodule classification based on the color and shape of the nodule. The parameters are defined in Chapter 2 (Y= rim present, N= rim absent). 31
Table 3.2- A summary of main constituents and their percentages (relative to total sample volume, based on counting of 300 points for each slide). 34
Table 3.3- A summary of major constituents in analyzed thin sections (n=20), showing the average and maximum percent volume (based on counting of 300 points for each slide) for relevant primary, diagenetic constituents and porosity. 36
Table 3.4- Percentage of silica minerals in the different silica nodule types. 45
Table 3.5- Peak and minor signals observed for each thin section analyzed. The uncertainity of the instrument was $2cm^{-1}$. 49
Table 3.6- Oxygen isotopic data of analyzed chert samples (1σ). 53
Table 3.7- Si and Ge concentrations and the calculated Ge/Si ratios. 54
Table B.1- Quantification of thin sections. 145
Table B.2- Summary of the Quantification. 155
Table D.1- ICP-MS Analysis Data. 161

Acknowledgments

Firstly, I would like to express my sincere and heartfelt gratitude to my major supervisor, Dr. Karin Goldberg, for her immense support and guidance throughout my graduate career. This research would have been only a dream without her. I would like to thank my committee members, Dr. Pamela D. Kempton, Dr. Matthew Brueseke, and Dr. C. Marshall, for accepting the invitation to join my research committee and for their invaluable contributions. I would also like to thank Dr. Matthew Kirk, Dr. Claudia Adam, and Dr. Brice Lacroix for supporting the smooth flow of my research in different aspects. I sincerely appreciate Dr. Fred Longstaffe of Western Ontario University, Dr. Scott Boroughs, and Dr. Arron Steiner of Washington State University for supporting my research by performing essential analyses. I dearly remember Sarah Lamm, Rajavel Krishnamoorthi, and Ethan Senne for their valuable time and effort in supporting me during equipment operations.

I would also like to acknowledge Kansas State's Geology Department, the Kansas Geological Foundation, and the Geological Society of America for making my research feasible through funding and providing various facilities during research.

My special thanks to all faculty members in the Department of Geology and all fellow graduate students for their love and support during my time as a master's student. I would like to express my indebtedness to Hunter Rose, who effectively coordinated departmental tasks.

Special thanks to my wife, Asini Konpola, for being my strength. The love and support from my parents, Asoka and Daya, my sister Nipuni, and my uncle and aunt, Sheela and Chandradasa, were crucial. Finally, I would like to thank the Sri Lankan community in Manhattan and the well-wishers and supporters who were always around me.

Dedication

"To my mother, Daya Muhandiram, my father, Ashoka Kumarage, my wife, Asini Konpola and my sister Nipuni Kumarage."

Chapter 1 - Introduction

The state of Kansas is famous for its vast grasslands and flat landscapes. Nevertheless, in the Flint Hills, extending from northeastern Kansas to the southeastern border of Oklahoma, one can observe some uniquely shaped hills whose erosional outlines appear like the steps of a staircase. The "rolling hills" landscape is a consequence of the presence of chert within some limestone layers, which reinforces these rock units against weathering and erosion relative to more easily eroded shales with which they are interbedded, creating the observed 'stairstep' topography.

The alternating layers of shale and limestone in Kansas represent cyclothems formed during the Pennsylvanian to Permian as a result of cyclic sea-level changes (Goldberg & Miller, 2019). Some limestone layers contain chert nodules and lenses that coalesce laterally, forming "layers" clearly visible in outcrops along roadcuts. The Florence Limestone Member is the most prominent limestone in the Manhattan- Fort Riley area, that contains "layered" nodular chert.

The origin of these chert nodules is yet to be unraveled. Three outcrops of the Florence Limestone were selected for this study (Figure 1.1). The Milford Lake spillway (Site 01) offers a top view of the uppermost bedding surface of the Florence Limestone (Miller, 2001) and the outcrop on the road K-24 near Tuttle Creek Reservoir (Site 02; Stop 05 of Goldberg & Miller, 2019) displays a vertical succession of the Florence Limestone. Site 03 was selected along highway I-70 east of exit 307, because it offers a clear view of multiple silicified horizons.

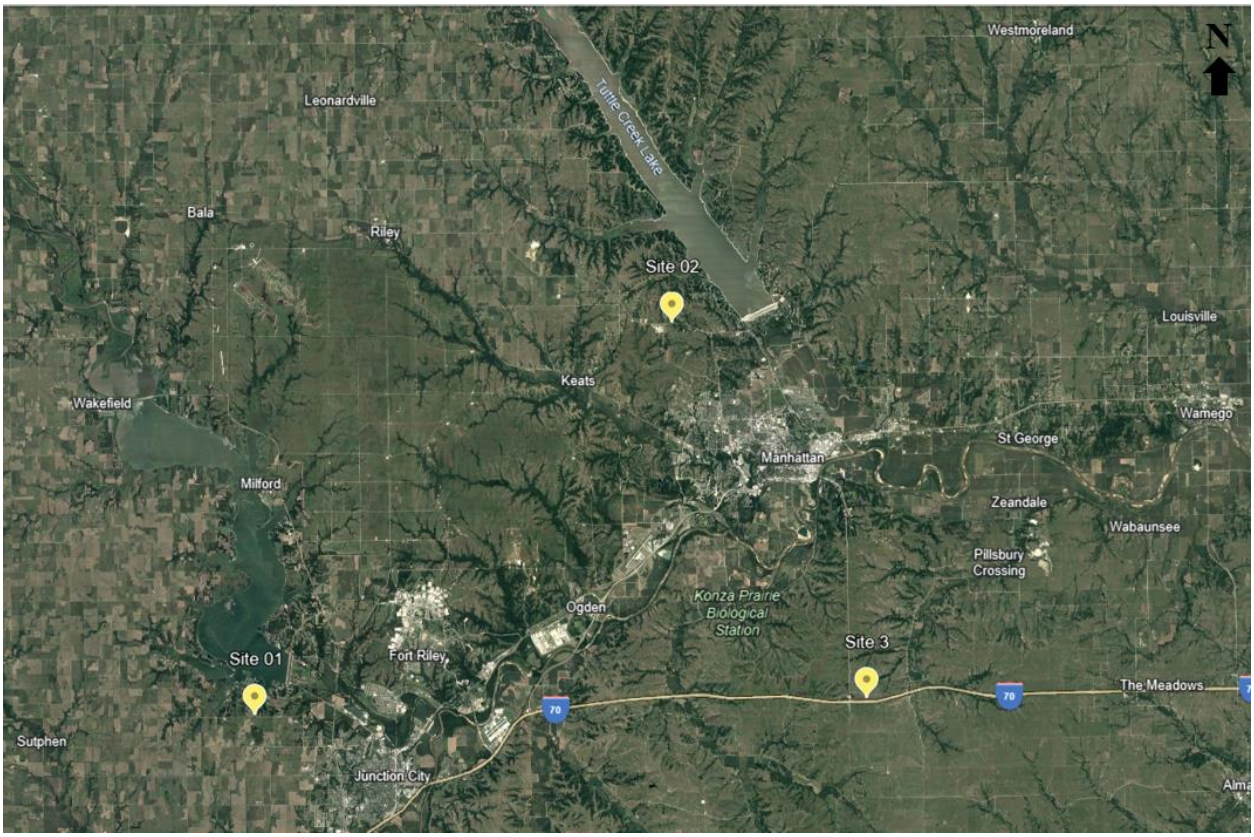

Figure 1.1- Outcrops around Manhattan, Kansas, selected for this study. Site 01- Near Milford Lake, Site 02- Near Tuttle Creek dam, Site 03- Along I-70 highway, exit 307.

1.1 Statement of Research Problem

Nodular chert is found in numerous formations around the world, which are discussed later in this chapter. Many studies provide evidence for the timing of formation and source of silica for these nodules (White et al., 1956; Chanda et al., 1976; Brenna, 2016), which can be a result of palaeogeographic and paleoclimate conditions experienced by different parts of the world. Regardless of the mechanism of formation, chert precipitation has been studied because of its role in more prominent processes in the Earth system. For example, it allowed the preservation of some of the oldest life records on Earth (e.g., the Apex Chert in Australia; Allwood et al., 2006; Marshall et al., 2012), and it has been investigated on Mars as a possible record of planetary life (Frydenvang et al., 2017; Bosak et al., 2021). Chert replacements within

dolomitic terrains can preserve pervasive porosity, allowing for the accumulation of petroleum deposits (Packard et al., 2001; Matysik et al., 2021). This material also has historical and archeological significance, as nodular chert has been used as a primary tool-making material in the past, and chert from Flint Hills was highly prized due to its inherent strength (Johnson, 1973; Hofman, 2020).

The geology of the Flint Hills area has been extensively studied (Miller & Twiss, 1994; Miller, 2001; Goldberg & Miller, 2019), but the source of silica to form chert nodules still needs to be determined (Miller & Twiss, 1994; Miller, 2001), along with the timing of silicification. Some sponge spicules have been found within the Florence Limestone (Miller & Twiss, 1994), but the extent/concentration of spicules has been deemed insufficient to explain the volume of silica observed, which would imply the contribution of other sources of silica (Miller, 2001).

This work aim to define the origin and timing of formation of the silica nodules in the Florence Limestone. Specific objectives are to: 1) create a catalog of the different types of nodules, 2) identify the silica mineralogy, 3) define the paragenetic sequence of the silica phases, 4) estimate the temperature of silica precipitation, and 5) identify the source of silicifying solutions that led to the formation of chert nodules in the Florence Limestone.

1.2 Geological Context

During the Wolfcampian, paleogeographic reconstructions indicate that the North American midcontinent lay within the lower relief of the supercontinent Pangaea (Scotese & Langford, 1995; Blakey, 2003; Scotese & Schettino, 2017; Blakey, 2021). The Permian succession in the Flint Hills area is characterized by an alternating sequence of limestones and shales (Figure 1.2), interpreted as cyclothems formed as a result of sea level fluctuations driven

by Milankovitch orbital modulations (Miller & Twiss, 1994; Mccahon & Miller, 1997; Goldberg & Miller, 2019). The Lower Permian Chase Group, exposed in the Manhattan area, Kansas, is excellent for studying these cyclothems (Miller & Twiss, 1994; Miller, 2001; Goldberg & Miller, 2019).

The carbonate and fine-grained clastic facies of the Council Grove and Chase Groups in northeastern Kansas suggest a shallow marine to marginal marine shelf periodically exposed during relative sea-level low stands (Miller & Twiss, 1994). Through the Permian into the Triassic, the Pangeae landmass slowly drifted towards higher latitudes from equatorial region (Rowley et al., 1985; Witzke, 1990), which prompted long-term climate change from humid to arid conditions in Pangeae (Tabor & Poulsen, 2008).

According to field observations of Goldberg & Miller (2019), chert formations within the Florence Limestone exhibit a box-work structure with a vertical and horizontal polygonal network similar to Thalassinoid burrowing (Figure 1.3), with at least six chert “beds” ranging from 20 cm to 30 cm in thickness (Miller, 2001). Repeated filling of these burrows by skeletal debris indicates relatively rapid sedimentation due to climate fluctuations (Miller, 2001). Although similar chert horizons are visible in Fort Riley Limestone, Florence Limestone chert beds are predominant and well exposed, making them easily to study. Similar burrows-shaped chert nodules have been observed in northern Europe associated with shelf-sea conditions (Ekdale & Bromley, 1984) and in Utah's Permian Trapper Creek Formation (Wistort et al., 2019).

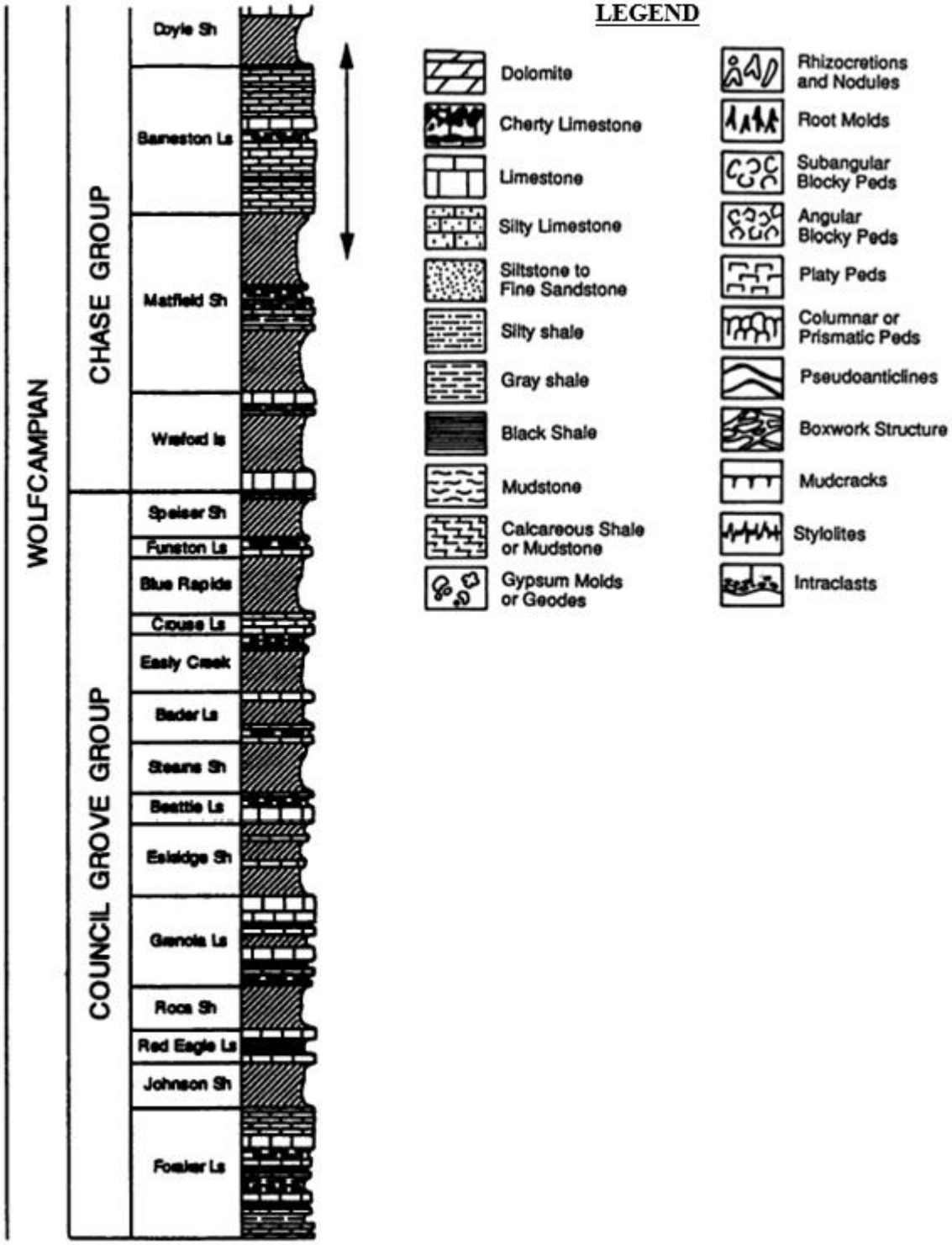

Figure 1.2- Stratigraphic position of the Barneston Limestone (which includes the Florence Limestone) in the Wolfcampian Chase Group (Miller & Twiss, 1994). Both Council Grove and Chase Group are characterized by alternating shales (Sh) and limestones (Ls).

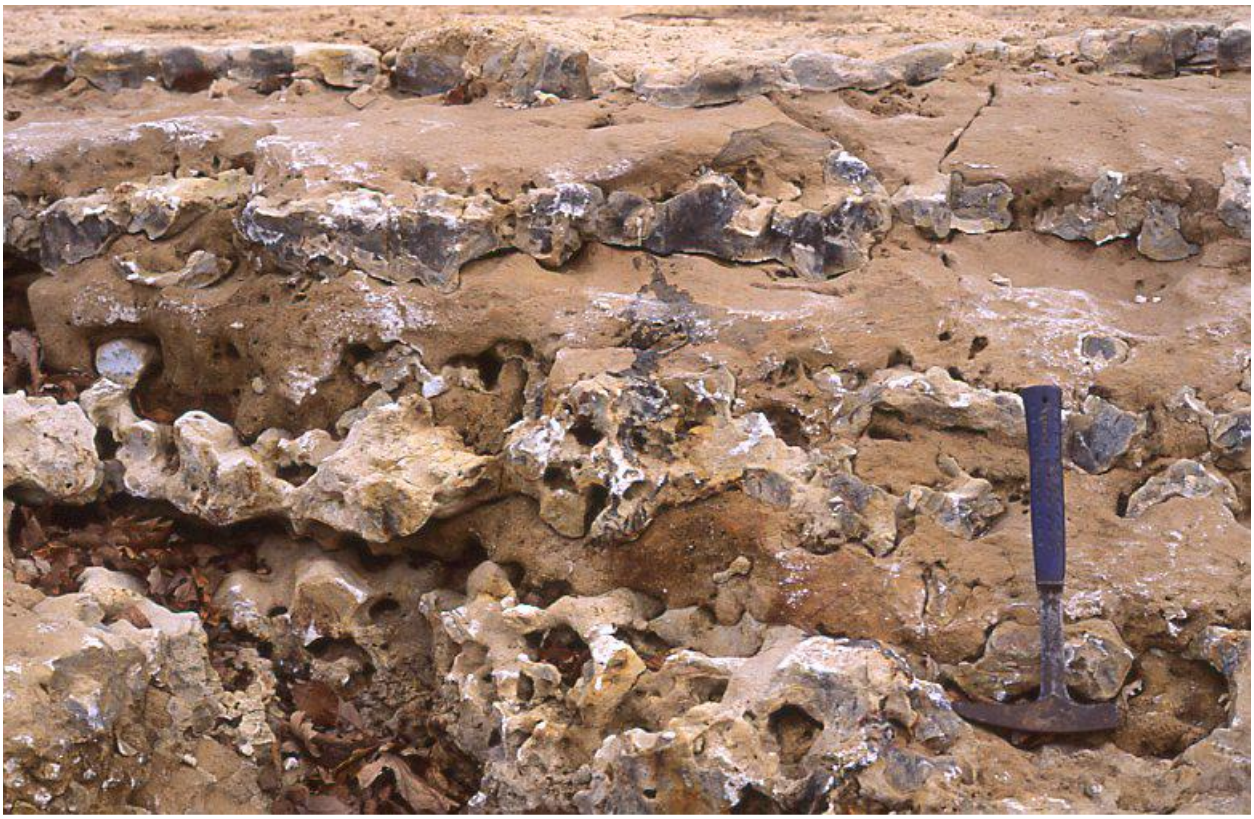

Figure 1.3- Exposed "burrow network" formed by coalescing chert nodules near Milfod Reservoir (Miller, 2010). Length of hammer is 28 cm.

Some nodules in the Florence Limestone contains "wood-grained" texture, with sharp boundaries between chert and limestone in many samples. Similar appearances have been recorded in chert of the Monterey Formation (Maliva & Siever, 1989; Behl, 2011) and Portland limestones (Figure 1.4; Maliva et al., 1999). In both cases, alternate light and dark-colored bands represent variations in opal-CT concentration (Behl, 2011).

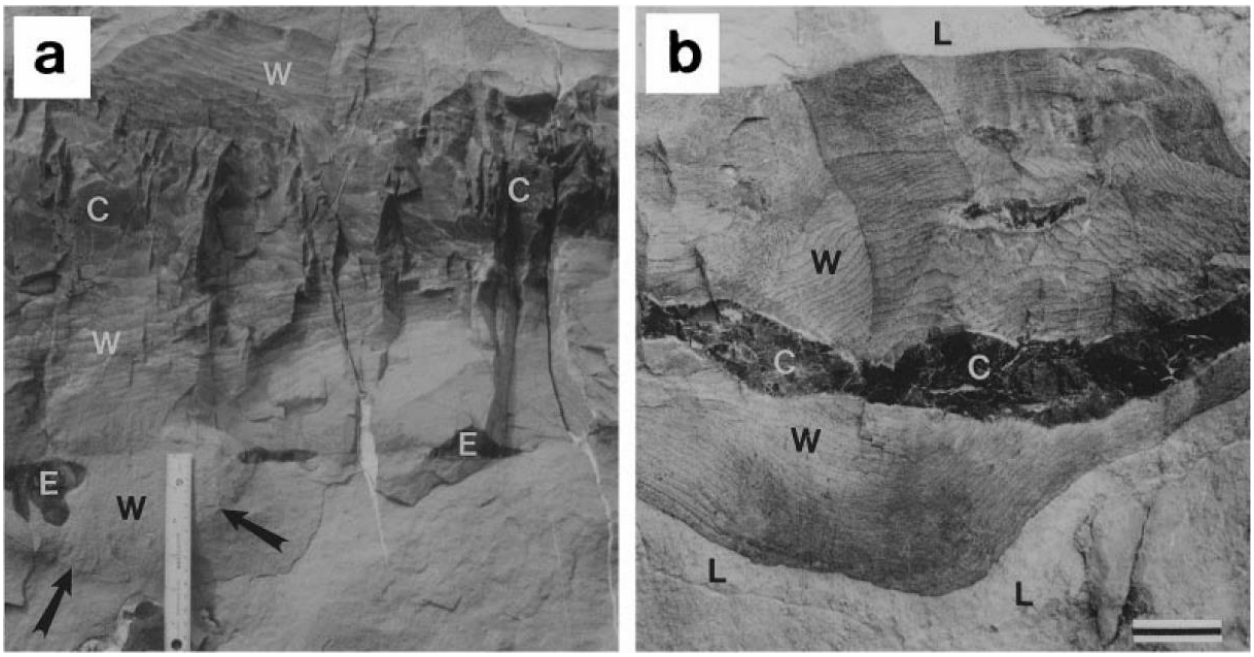

Figure 1.4- (a and b)-A "wood-grained" chert layer from Portland Limestone (Maliva et al., 1999). (C= Dark grey chert nodule, E= Earlier-generated dark-grey nodular chert, L= Limestone, W= Wood grained chert).

In addition, several horizontal silica "layers" occur within the Florence Limestone. The realization that these embody hardgrounds (i.e., a synsedimentary lithified seafloor; Wilson & Palmer, 1992) has a profound stratigraphic meaning since these surfaces represent stratigraphic discontinuities, commonly developed under low sedimentation rates in starved basins, marking the position of flooding surfaces (Pandey et al., 2018; Richiano et al., 2019). As such, the spacing between these hardgrounds (and their frequency) might reflect the tempo of the allogenic control(s) of these flooding surfaces, opening the door to the possibility that these horizons might represent Milankovitch cycles, for instance.

1.3 Sources of Silica in Cherts

Chert formations in different localities derive from various silica sources. Common sources of silica in chemical sedimentary rocks include fluids with a biogenic, hydrothermal, or diagenetic origin or a combination of these sources (Behr, 2002; Trewin & Fallick, 2009; Gao et al., 2020; Yao et al., 2021). A biogenic origin of silica requires the rapid burial of siliceous tests of microorganisms that inhabited oceans in large numbers. Upon death, their shells are deposited on relatively calm, undisturbed ocean bottoms, which, with time, form bedded deposits. During diagenesis, siliceous oozes, composed of opal-A (Williams et al., 1985; Varkouhi & Wells, 2020), are transformed into different silica types including chert. The reactivity of silica is substantially reduced with the burial depth, resulting in silica preservation (Van Cappellen & Qiu, 1997). Precambrian silica cycling was insignificant until the appearance of Neoproterozoic silica-shelled protists and Ediacaran sponges (Perry & Lefticariu, 2007), which peaked in the Phanerozoic (Siever, 1962; Maliva et al., 2005; Tarhan et al., 2016). Permian chert deposits found along the western coast of the United States represent deposits of the above biogenic silica origin (Murray et al., 1992;Wistort et al., 2022).

Hydrothermal activity is a significant silica source for chert formed associated with sedimentary rocks in mid-oceanic ridge hydrothermal systems and seamount-bearing regions in the deep ocean. Submarine hydrothermal processes have played a significant role during the precipitation of chert in the Taiyuan Formation, North China Craton (Yao et al., 2021), bedded chert formation in the northern Pacific, DSDP Leg 32 near Japan (Adachi et al., 1986), and Laiban nodular cherts of Guangxi, China (Qiu & Wang, 2011). Similarly, the Mesoproterozoic Wumishan banded and nodular chert formations in China (Shen et al., 2018) are interpreted as the products of hydrothermal silicification within dolomitic rocks. In continental settings,

hydrothermally derived silica is also observed to be associated with hot springs, and the deposits are often sinter or geyserite (Fournier & Rowe, 1966; Jones & Renautt, 1997; Campbell et al., 2015). These settings need some kind of magmatic heat source to drive the hydrothermal systems and also a source of silica (Chen et al., 2006; Gao et al., 2020) For example, modern Yellowstone Plateau volcanic field geysers have abundant amorphous silica either as geyserite deposited within hydrothermal conduits or along the walls of hydrothermal vents or sinter deposited as the cooling, silica-rich water flows away from the hot springs vent (Walter, 1976; Shanks et al., 2005; Jones, 2021).

Diagenetic processes may also expel silica during burial and compaction, forming silica-rich diagenetic fluids. Grain dissolution in point-to-point contact between quartz grains releases silica into diagenetic fluids during chemical compaction (Trewin & Fallick, 2009). While temperature and pressure are critical in governing liquid saturation with silica, any fluid carrying 6 mg/g or higher of dissolved silica is a potential silicifying fluid (Knauth, 1970). Alteration of volcaniclastic sediments may form silica deposits, such as those in Kitty's Gap, Pilbara Craton in Australia (van den Boorn et al., 2007), or clay minerals in replacement reactions (Aoyagi & Kazama, 1980; Peltonen et al., 2009), as in Coorong Lagoon, Southern Australia (Hart & Steinhart, 1965). Porcellanite chert formations found during deep-sea drilling in the Atlantic sector (Site PS2070-1, Maud Rise and Site PS2089-2, Southwest Indian Ridge) of the Southern Ocean indicate diagenetic silica formed as a result of the transformation of opal-A (biogenically derived) into microcrystalline silica with burial (Bohrmann et al., 1994).

Two or more silica sources can combine to form silicified deposits. Nodular chert in the middle Permian Maokou Formation in southern China precipitated from hydrothermally derived and biogenic silica (Gao et al., 2020). Coupled chert-shale deposits from the Franciscan and

Claremont Formations in California display variable degrees of silicification, resulting from the precipitation of diagenetic silica remobilized from the surrounding host deposits (Wachs & Hein, 1974). An example of chert formation with a mixed origin is the Upper Jurassic Portland nodular chert in Dorset, England, where former siliceous sponge spicules were replaced by calcite, thus releasing silica into diagenetic solutions to be reprecipitated as chert nodules (Hart, 1993).

Magadi chert is a freshwater-derived chert deposit in highly alkaline waters, evaporated at a shallow depth in Magadi Lake, Kenya (Hesse, 1989; Behr, 2002; Brenna, 2016). Sodium silicate precursors like magadiite (Zipser, 1967) and kenyaite are believed to have provided silica for these chert deposits (Schubev & Simonson, 1990).

1.4 Factors Affecting Supersaturation

Silica derived from the above sources forms silicifying solutions. Undissociated silica in most natural waters exists as silicic acid (H_4SiO_4), which is termed "silica" (Dapples, 1967; Hesse, 1988). For the deposition to occur, the dissolved solution should be supersaturated with silica. Discussed below are some critical processes of silica supersaturation.

The pH is crucial for silica mobilization and redistribution within the depositional environment (Banks, 1970; Maliva & Siever, 1989; van den Boorn et al., 2007). Higher, basic pH under hypersaline conditions favors the dissolution of detrital silica, while lower pH (acidification and drying up of lakes) promotes the precipitation of silica (Hart & Steinhart, 1965; Knauth, 1979). Often, these pH changes cause replacement reactions within carbonate environments (Walker, 1962). Oceanic and lake pH changes commonly occur due to photosynthesis by microorganisms like *Ruppia maritima*, seasonal changes that cause water level

fluctuations, and chemical zonation due to sediment/organic matter degradation (Hart & Steinhart, 1965).

Silica-rich fluids derived from hydrothermal or diagenetic processes can directly interact with marine water in mixing zones, making the solutions supersaturated (Adachi et al., 1986; Gao et al., 2020; Yao et al., 2021). Meteoric water percolating within carbonate terrains can form mixing zones supersaturated with silica and undersaturated with calcite and aragonite (Figure 1.5; Knauth, 1979). Porosity and permeability in the carbonates may enhance the mixing (Maliva & Siever, 1989; Banerjee et al., 2021) while allowing space for replacement chert deposits. Many examples above that led to supersaturation are associated with shallow carbonate environments (Banks, 1970; Knauth, 1979; Maliva & Siever, 1989; Banerjee et al., 2021).

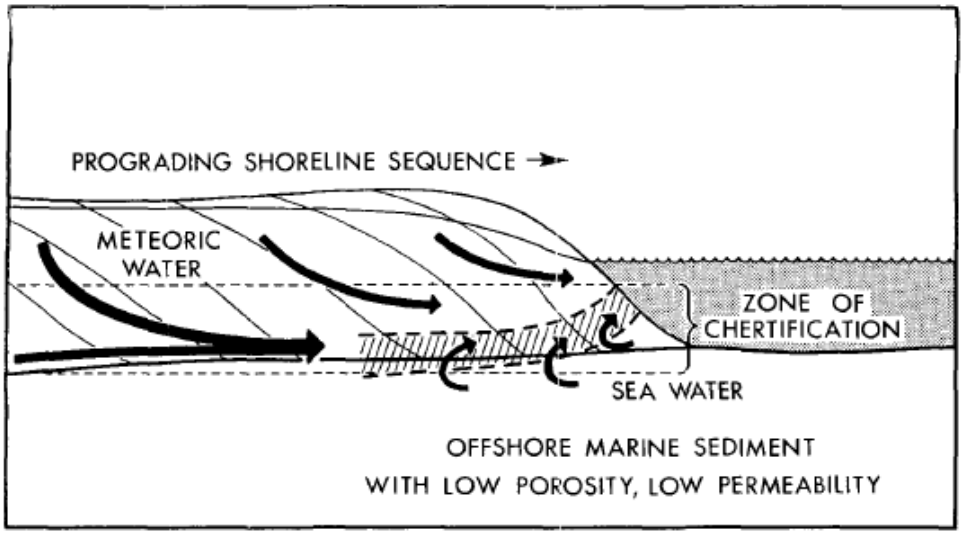

Figure 1.5- Meteoric water and saline water mixing forming zone of chertification (Knauth, 1979).

The activation energy of the silica phase transition (from solid to liquid) lowers with higher temperatures (Williams et al., 1985). The solubility of quartz and amorphous silica increases exponentially with increasing temperature (Figure 1.6; Rimstidt & Cole, 1983). This

has been proven experimentally that the silica concentration of pure water may reach up to ~750 ppm at 350º C exponentially for chemically clean Brazilian quartz sample (Crerar & Anderson, 1971). Thus, increasing temperature increases the degree of supersaturation and silica concentration in a solution (Stein & Kirkpatrick, 1976).

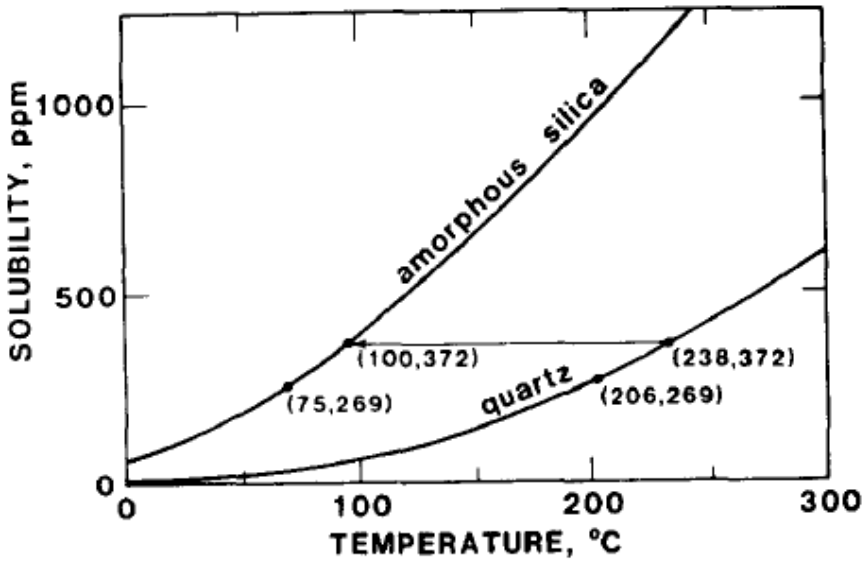

Figure 1.6- Solubility of quartz and amorphous silica varying with temperature (Rimstidt & Cole, 1983).

Pressure is directly proportional to silica solubility (Willey, 1974; Walther & Harold, 1977), but the effect of pressure on solubility is negligible compared to temperature (Crerar et al., 1985).

Hydrothermal hot water springs possess a different type of supersaturation process. When ascending to the surface rapidly, silica-rich water becomes supersaturated due to cooling, and thus, the rapid onset of silica precipitation results in amorphous silica types, like geyserite or sinter (Renaut et al., 1996; Jones & Renautt, 1997).

1.5 Silica in Solution and Transformation to Chert

Silicifying solutions can give rise to both amorphous silica forms (opal-A, opal-C, opal-CT, chalcedony) and crystalline forms such as quartz (and sometimes high temperature forms like cristobalite, and tridymite; Figure 1.7; Knauth, 1970). Opal-A is typically biogenic in origin (Winter & Knauth, 1992).

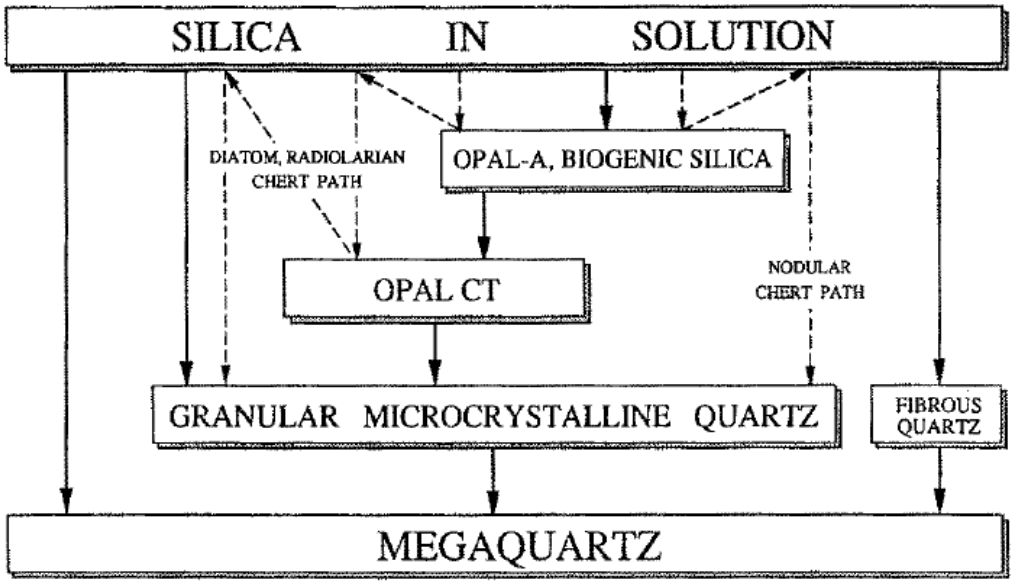

Figure 1.7- Different forms of silica precipitating from solution (Knauth, 1970).

In nature, amorphous silica transforms into stable crystalline polymorphs due to diagenesis(Thiry & Millot, 1987). The opal-A to opal-CT to low quartz transformation is commonly observed in nature (Mizutani, 1970; Calvert, 1974; Aoyagi & Kazama, 1980). These reactions proceed as numerous dissolution-reprecipitation reactions (Williams et al., 1985; Hesse & Schacht, 2011). Temperature (which affects both solubility and pH of the solution), the alkali concentration in the solution, pressure, and reaction time of silica determine the end product of transformation (Aoyagi & Kazama, 1980; Williams et al., 1985; Hesse & Schacht, 2011). The transition from low to high quartz occurs with increasing temperature and pressure (Figure 1.8;

Hesse, 1989). Coesite and stishovite are high-pressure polymorphs of quartz and, therefore, irrelevant to this study. Similarly, since the Florence Limestone (and associated stratigraphic formations) does not bear evidence of coeval volcanism (Miller & Twiss, 1994; Miller, 2001), silica originated from igneous sources is likely not importance for the study.

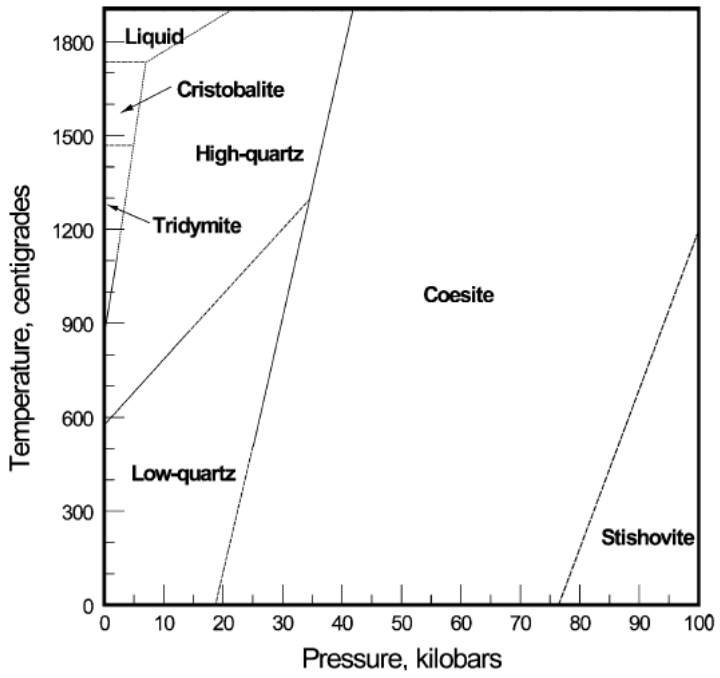

Figure 1.8- Silica phases stability fields at a given temperature and pressure (Hesse, 1989).

Chapter 2 - Methodology

This research included field and laboratory studies. The field studies focused on the detailed description of the distribution of chert nodules and the collection of samples representative of the different types of nodules. The laboratory studies included petrographic and complementary analyses, detailed below.

2.1 Field Analysis

Field analysis was based on three sites around Manhattan, as displayed in Figure 1.1. Site 01 (latitude 39.0660599, longitude -96.8961833), near Milford Lake, was selected because the exposure allowed us to observe the distribution of chert nodules on both horizontal and vertical planes (Figure 2.1). Sites 02 (lat. 39.0660562, long. -96.6765959) and 03 (lat. 39.2515499, long. -96.6464372) exhibited vertical exposures of the Florence Limestone with multiple chert layers (Figures 2.2 and 2.3). The different types of chert nodules were measured, described in detail, and photographed, and their spatial and vertical relations annotated. Eight representative hand samples were collected from the three sites (Table 2.1). Five additional samples from other locations (collected by Dr. K.B. Miller) were included for laboratory analyses.

Table 2.1- Sample locations.

Sample	Sampling Location
FL-KS-1	Collected by Dr. K. B. Miller.
FL-KS-2	
FL-KS-3	

FL-KS-4	
FL-KS-5	Milford Lake State Park, south of Highway 57, off of Highway 244 towards east of creek.
FL-KS-6	Along I-70 east of exit 307, on north side of the road.
FL-KS-7	Along Highway 24, north of junction with K-13, Seth Child road.
FL-KS-8	Hickory Court, Manhattan (collected by Dr. Matthew Kirk).

Figure 2.1- Nodular chert exposures near Milford Lake. (a) Chert "layers" can be seen in the top and side views. Distribution of chert along horizontal "beds." (b) 8-10 cm thick chert layers exposed on the vertical plane. Yellow stars indicate the sampled chert beds.

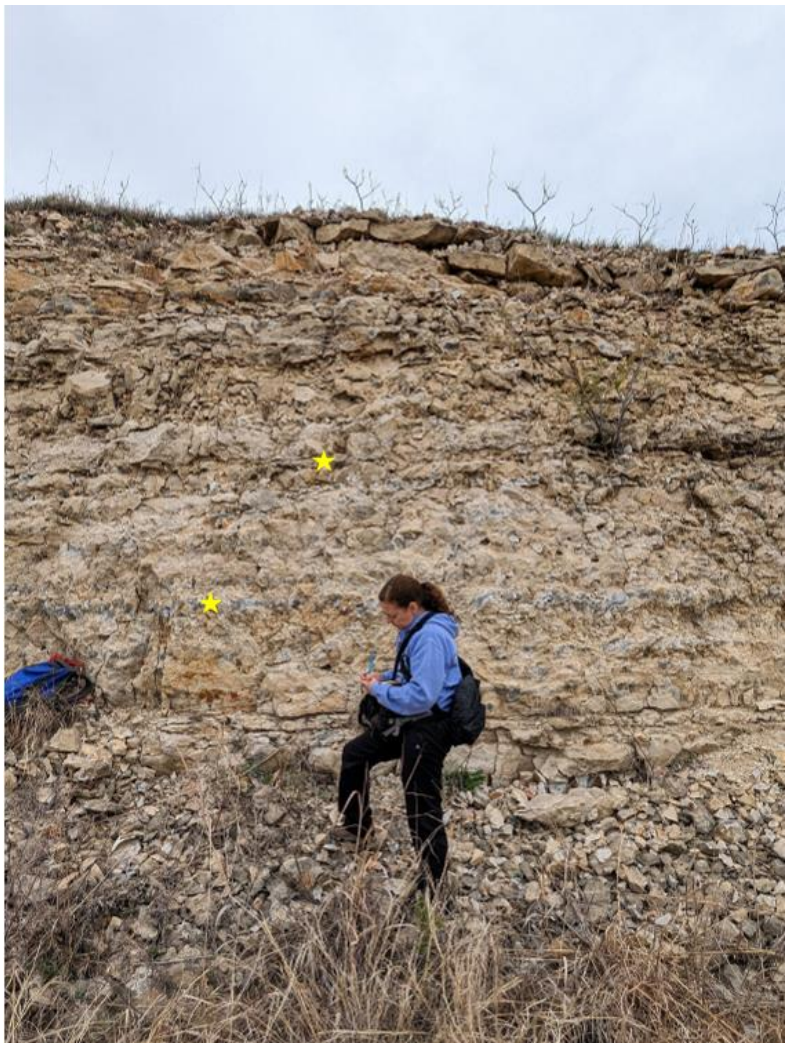

Figure 2.2- Outcrop along the I-70 highway, displaying multiple chert intervals on a vertical exposure. Height of outcrop is ~3.5 m and yellow stars indicate sampled chert horizons.

Figure 2.3- Outcrop near Tuttle Creek Lake. Height of outcrop varied from ~3.5 m to 4.5 m. The yellow stars indicate different chert horizons where samples were collected.

2.2 Macroscopic Sample Analysis

Chert samples were cataloged based on color, texture (internal: wood-grained or homogeneous, external: botryoidal or smooth), boundary type (abrupt or gradual, smooth or jagged), shape (spheroidal or irregular), presence or absence of rims and distribution within the host limestone (isolated or coalescent). This analysis aimed to separate the chert nodules based on macroscopic characters to check whether their external appearance reflected their mineralogy. Hand samples were described, photographed, and organized into a table.

2.3 Petrographic Analysis

Twenty thin sections were prepared out of the samples collected. Their codes indicate the sample number and whether more than one thin section was made for any given sample. For

example, FL-KS-8 indicates the only thin section made for sample 8, whereas FL-KS-1-2 denotes thin section #2 of sample 1. Thin sections were described and quantified under a Leica DM2700 optical microscope with 10x eyepiece power and a combination of 2.5x, 5x, 10x, 20x, and 40x objectives. The petrographic description included textural properties, compositional constituents (primary and diagenetic constituents), pore types, and their paragenetic relations. Compositional quantification was performed through point-counting of three hundred points per thin section. Total points counted were used to calculate model mineralogy, which was assumed to represent the composition of total sample volume. Petrographic data were stored in a database using the software Petroledge®. A Zeiss optical camera attached to the microscope was used to capture photomicrographs of thin sections.

2.4 Cathodoluminescence Analysis

Thin sections representative of different silica phases were analyzed under cathodoluminescence. Cathodoluminescence microscopy involves the study of emitted light or photons (in visible wavelength) when the sample is bombarded with an electron beam generated by a luminoscope. The luminescence depends on the sample's composition, formation history, replacements, and degree of compaction (Mclemore & Barker, 1987; Raviolo et al., 2009). Authigenic quartz, formed in temperatures ranging from near ambient to over 100^{o} C, has weak or no luminescence, so this property can be used to differentiate it from higher-temperature (above 300º C) quartz types (Ruppert, 1986).

Luminescence will depend on the concentration of activators (mostly Ti), quenchers, and sensitizers in the sample, resulting in different image textures (Frelinger et al., 2015). Detrital plutonic quartz shows dark cores with bright rims; Volcanic quartz typically shows well-preserved growth zones with oscillating intensities. Metamorphic quartz tends to be, brown, dull

with homogenous luminescence. Hydrothermal quartz usually displays, blue to violet luminescence in Red-Green-Blue (RGB) filters. A summary of cathodoluminescence color for each quartz formed at different environments along with crystallization temperatures are given below in Table 2.2.

Table 2.2- Cathodoluminescence colors observed and interpretations on different silica forming environments and conditions (Füchtbauer et al., 1982; Ramseyer et al., 1988; Ètze et al., 2001).

Stable Temperature Range for Quartz	Cathodoluminescence Color	Interpretation on Quartz Origin
>573º C	Blue	Phenocryst quartz in rapidly-cooled magmatic rocks or low grade metamorphic quartz
>573º C	Violet	Quartz in plutonic and volcanic rocks
300º – 573º C	Brown-violet	Strongly metamorphosed quartz
<300º C	Green	Hydrothermal quartz
<300º C	Pink/yellow	Agate/quartz replacing sulfate minerals
>300º C	Red	Quartz formed close to volcanic dykes and sills

Cathodoluminescence was used to identify possible compositional variations in chert samples, as well as changes in precipitation conditions since above formation conditions of silica can be used as an indirect evidence to temperature of quartz crystallization.

An optical cathodoluminescence equipment from the Department of Geology at K-State was used in this analysis. For the study, a pressure of 80 millitorr within the vacuum chamber and a beam current of 0.5 milliampheres were maintained. The electron beam was generated using a luminoscope with around 8-9 kilovolts and a current of one milliamphere. Two movable magnets were used to direct the electron beam over the thin section, and luminescence was observed through a Nikon Eclipse petrographic microscope equipped with a camera.

2.5 Raman Spectroscopy Analysis

In Raman spectroscopy, the emitted intensity of scattered light is measured when a sample interacts with a laser beam with a specific wavelength. The intensity bands were plotted against shifted relative wavenumbers, termed Raman shift (cm^{-1}). Since the band changes with the different crystallography of silica (Ilieva et al., 2007), tridymite, cristobalite, and microcrystalline quartz can be differentiated by this light scattering technique (Figure 2.4; Kimura et al., 2005). Moganite, which is hard to detect by XRD (Pop et al., 2004; Ilieva et al., 2007), can be accurately identified. Experiments indicate that the availability of opaline silica like Opal-A, Opal-C and Opal-CT can be determined by Raman spectroscopy, however XRD is primarily used for identification of opaline silica (Curtis et al., 2019).

A Renishaw inVia Raman spectroscopy machine, available in the Department of Geology, Kansas State University, was used for ten thin sections to identify the different silica phases. All samples were analyzed using a green laser beam (532 nm wavelength), under exposure times of 1,2 and 5 seconds, with the intensity of 100% and 50% and the number of accumulations varying from 1 to 10, where necessary.

When the laser emits monochromatic light (in visible or near-infrared range), the sample interacts with the light producing Rayleigh (elastic) scattering and Raman (inelastic) scattering. As a result of Raman scattering, sample's molecules are vibrated in different ways which causes a shift in frequency of scattered light. This energy/frequency shift corresponds to structure and chemical bonding of sample. The peaks collected using the detector is finally analyzed with laser wavelength to detect the sample mineralogy. Shorter bond lengths can provide higher wavenumbers and viceversa.

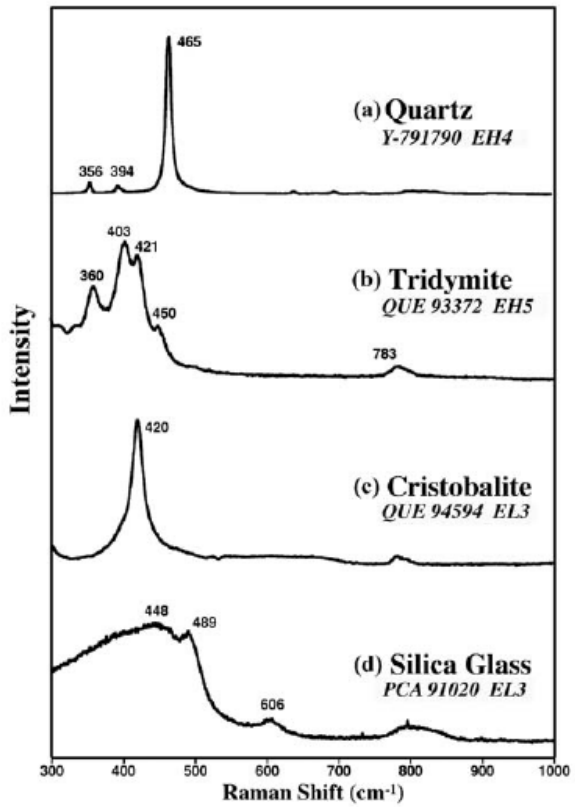

Figure 2.4 - Raman shifts vs. intensity for different silica phases in an enstatite chondrite (Kimura et al., 2005).

2.6 X-Ray Diffraction Analysis

X-ray diffraction (XRD) analysis is a method for determining the composition of solid samples. It is based on the principle of constructive interference of X-ray waves, in which the diffraction angle can be used to calculate d-spacing value(s), which is then used to identify the crystalline solid. Chert samples can be analyzed by XRD to differentiate between opal-CT, opal-A, lutecite (moganite), and microcrystalline quartz (Jones & Segnit, 1971; Curtis et al., 2019) based on output waveform (Figure 2.5; (Elzea & Rice, 1996). This analysis was used as a complementary technique to Raman spectroscopy.

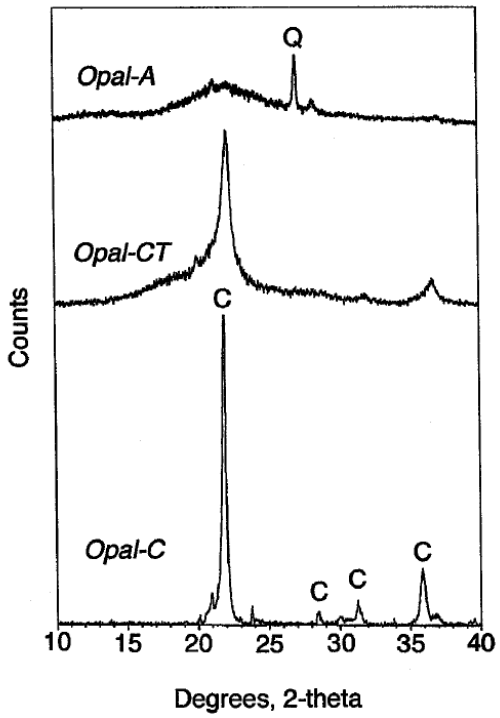

Figure 2.5 - XRD scans for Opal-A, Opal-CT, and Opal-C (Elzea & Rice, 1996).

Chert samples for XRD analysis were selected and prepared based on the abundance of different silica phases (opaline silica, chert, chalcedony, and megaquartz) identified in thin sections. A total of six samples were selected, and the same samples were used to conduct oxygen isotope analysis and LA-ICPMS analysis. Hand samples were crushed into 2 - 8 mm granules using a mortar and a pestle for XRD analysis. Then sample grains were acid-digested using 1:3 diluted HCl acid (400 ml) to remove carbonate and organic matter (Figure 2.6). The granules were air-dried for three days and finally ground into a fine powder using an agate mortar and pestle before being inserted into the XRD.

Figure 2.6 - Chert granules reacting with dilute HCl to remove carbonates and organic matter (samples FL-KS-7-2, FL-KS-6-2, FL-KS-5-2-2, FL-KS-6-3, FL-KS-7-1 from left to right).

Samples were analyzed using the PANalytical Empyrean XRD instrument, and the output signal was interpreted using Profex software with specific CIF files being used for each silica phase identification. Final signals were compared with the International Center for Diffraction Data (ICDD) and RRUFF databases.

2.7 Oxygen Isotope Analysis

Six samples (same silica phases used for XRD) were analyzed at Western Ontario University, Laboratory for Stable Isotope Science, with a classical extraction line CIF_3-253 instrument. 2 ml of each sample was run using the CO_2 equilibration technique with a precision of 0.28‰ (1σ). Quality analysis and control were performed using quartz and kaolinite laboratory in-house standards. Data are reported in the typical delta notation relative to the VSMOW standard.

2.8 LA-ICPMS Analysis

Germanium (Ge) and silicon (Si) have similar properties in the marine environment (Hatem et al., 2017), and for that reason, the substitution of Ge for Si in mineral phases forming

in seawater is common. The two main sources of Ge and Si in the ocean are mineral weathering and hydrothermal fluids (McManus et al., 2003; Wheat & McManus, 2005), whereas the precipitation of biogenic opal removes Si and Ge from the ocean. The Ge/Si ratio can be used to identify the source of silica. Hydrothermally-derived silicifying fluids can have extreme values of Ge/Si around 50-1000 µmol/mol, while lower values of around 0.5 µmol/mol indicate surface water-related silica sources (Evans & Derry, 2002). The significant difference between these ratios for fluids derived from continental weathering (0.54), seawater (0.69), and hydrothermal (11) (McManus et al., 2003) makes Ge/Si a valuable indicator of silica sources. As such, the Ge/Si ratio has been used to identify the biogenic origin of chert in the Cretaceous Chalk Formation in northern France (Tribovillard, 2013).

Thick sections of samples were made by mounting a piece of the sample onto slides with epoxy, trimming to ~1 mm thick and polishing the upper surface for ablation. All samples were analyzed at Washington State University's School of the Environment Lab Facility. A Finnigan Element 2 ICPMS with laser ablation instrument (LA-ICPMS) was used, with a sensitivity of >1.5x10 e^9 counts/ppm at 115Indium. Samples were analyzed at 100-micron spot size, and a minimum average detection limit of 436.5 ppm and 0.02 ppm was maintained for Si and Ge, respectively. Each sample was analyzed five times before averaging the measurements. The measured uncertainty of concentrations for Si and Ge were 0.56% and 4.86%.

An electron microprobe was used to measure several locations on each sample to get SiO_2 values to internally normalize the LA-ICPMS count data for all the trace elements to account for ablation/instrument drift during individual ablation runs, as well as throughout the day. The analyses returned 100% SiO_2 in each run, within the instrument precision. Images of the

sample surfaces were also taken and used to avoid hitting carbonate and other inclusions when picking up spots for LA-ICPMS.

The internal SiO_2 normalization for the LA-ICPMS data is a linear calculation, so the error associated with the SiO_2 concentration will propagate to the same amount for the LA-ICPMS trace element data (i.e., a 1% relative error in assumed SiO_2 concentration equals a 1% relative error in Ge concentration). Since the error in SiO_2 from the microprobe was ~2% relative, the values obtained for SiO_2 ranged from ~98.5% to ~101%, so rather than attempting to use those measured values, we assumed a value of 99.5% SiO_2 for normalization purposes. This procedure not only reduced the analyses time, since analyzing the exact same spot with two different instruments is tedious and time consuming, but it also probably actually reduced the error *versus* using microprobe data (e.g. using a measured value of 101% would obviously be less accurate than an assumed value of 99.5%).

The following equation was used to calculate the concentration of Si from measured SiO_2 in the samples (99.5%).

$$Si\ (ppm) = \frac{Atomic\ weight\ of\ Si}{Atomic\ weight\ of\ SiO2} \times 100{,}000 \times \frac{99.5}{100}$$

Elemental Ge and Si concentrations were then used to calculate the Ge/Si ratios. Finally, the integration of the data obtained in the analyses (described in Chapter 3) allowed the interpretation of the source, timing, and mechanism of the formation of the chert nodules in the Florence Limestone (discussed in Chapter 4).

Chapter 3 - Results

3.1 Field Analysis

All three sampling sites have multiple chert layers within the host limestone. The thickness of individual chert layers varies from 6 to 12 cm, and approximately 4 to 8 horizontally distributed layers occur on a vertical section depending on the height of exposed outcrop. Site 01 (Milford Lake State Park) had branching chert nodules that extend as beds, similar to burrows (Figure 2.1).

Diagonal branching of chert nodules, connecting horizontal horizons are rare at Sites 01 and 2 (Milford Lake and Tuttle Creek) exposures, but abundant at the exposure in Site 03 (along I-70) on the north side of the road. The diagonal chert nodules appear as silicified connections between two chert layers, similar to vertical burrows (Figure 3.1).

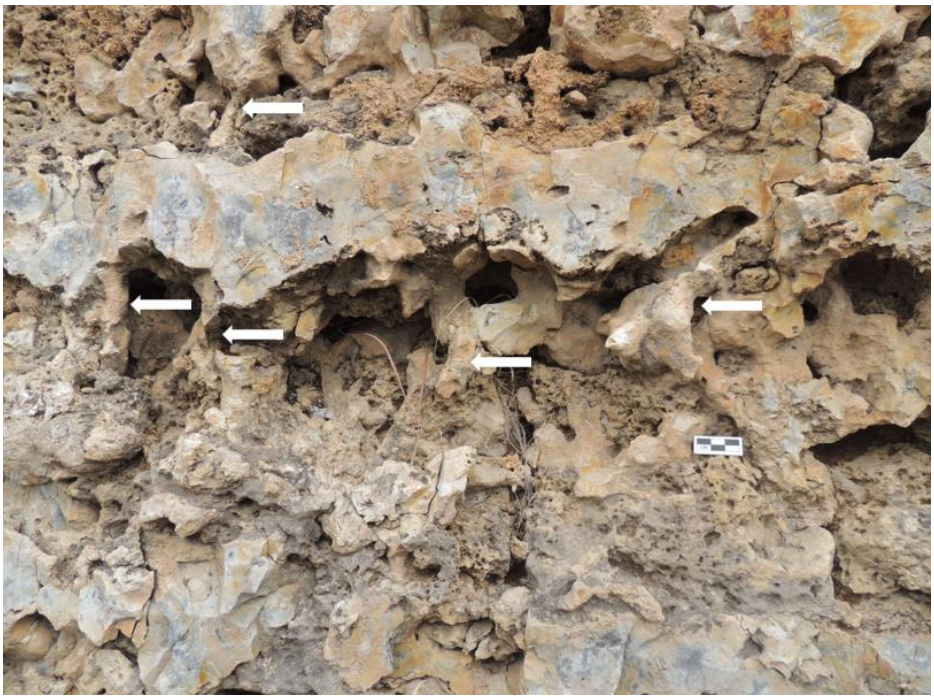

Figure 3.1- Horizontal chert layers with diagonal or vertical connections (white arrows), similar to burrow pathways.

Different chert nodule types occur at Site 03 (Tuttle Creek) in a clear stratigraphic order. The lowermost chert layers display horizontal levels connected by diagonal and vertical nodules, resembling the distribution of burrow networks at Sites 01 and 02 (Fig. 3.1). In the central part of the succession at Site 03, however, wood-grained chert nodules are abundant (Figure 3.2a), often displaying vertical fractures (Figure 3.2b). The wood-grained texture in the nodules always occurs at the top of the chert layers, suggesting that the solution responsible for the wood-grained chert percolated from the top down.

Figure 3.2- Chert layers in the middle section at Site 03 (Tuttle Creek) exposure, displaying (a) a wood-grained texture and (b) intense vertical fracturing.

At the top of the exposure, more isolated, rimmed chert nodules were observed (Figure 3.3). These isolated chert nodules are circular in cross-section and exhibit a lighter ring and a dark core, resembling a reaction or a replacement border (Figure 3.4).

Figure 3.3- Isolated chert nodules (arrows) appear in the top layers of host limestone at Site 03 (Tuttle Creek).

Figure 3.4- Isolated chert nodules with lighter-rimmed boundaries and darker cores.

3.2 Macroscopic Sample Analysis

Upon closer inspection of the samples, the three main chert nodule types identified in the field (homogeneous, wood-grained, and rimmed) were further classified based on features like color, the nature of the boundary, shape, etc. (Table 3.1).

Table 3.1-Detailed chart nodule classification based on the color and shape of the nodule. The parameters are defined in Chapter 2 (Y= rim present, N= rim absent).

Nodule type	Color	Texture	Boundary	Shape	Rim	Distribution	Hand Sample # (FL-KS-)	Defining criteria
Type 1	Gray	Homogeneous	Abrupt, jagged	Irregular	N	Isolated	5-1-1	Homogeneous texture, abrupt and jagged boundaries, irregular shape, isolated distribution
Type 2	Gray	Wood-grained	Abrupt, jagged	Spheroidal	N	Isolated	5-3	Wood-grained texture, abrupt and jagged boundaries, spheroidal shape, isolated distribution
Type 3	Gray	Homogeneous	Abrupt, jagged	Spheroidal	Y	Isolated	5-1-2	Homogeneous texture, abrupt and mostly smooth boundaries, spheroidal shape, rimmed, isolated distribution
	Gray/brown rim 5GY4/1 core 5GY7/4	Homogeneous	Abrupt, smooth	Spheroidal	Y	Isolated	2-2	
	Gray/yellow	Homogeneous	Abrupt, smooth	Spheroidal	Y	Isolated	6-3	
	Gray/yellow	Homogeneous	Abrupt, smooth	Spheroidal	Y	Isolated	7-1	
Type 4	Yellow	Homogeneous	Abrupt, smooth	Irregular	N	Coalescent, branching	8	Homogeneous texture, abrupt and smooth boundaries, irregular shape, coalescent and branching distribution

Type 5	Tannish gray	Wood-grained	Abrupt, smooth	Spheroidal	N	Isolated	1-2	Wood-grained texture, abrupt and smooth boundaries, mostly spheroidal shape, isolated distribution
	Gray	Wood-grained	Abrupt, smooth	Spheroidal	N	Isolated	3-1	
	Gray	Wood-grained	Abrupt, smooth	Spheroidal	N	Isolated	5-2-2	
	Gray	Wood-grained	Abrupt, smooth	Irregular	N	Isolated	5-2-3	
	Gray	Wood-grained	Abrupt, smooth	Spheroidal	N	Isolated	7-2	
Type 6	(N7) Gray	Botryoidal, homogeneous	Gradual, jagged	Irregular	N	Isolated	1-1	Homogeneous texture, gradual and jagged boundaries, irregular shape, coalescent or isolated distribution
	Gray	Homogeneous	Gradual, jagged	Irregular	N	Coalescent	2-1	
	Gray N6	Homogeneous	Gradual, jagged	Irregular	N	Coalescent	4	
	Gray	Homogeneous	Gradual, jagged	Irregular	N	Isolated	5-2-1	
	Gray	Homogeneous	Gradual, jagged	Irregular	N	Isolated	6-1	
	Gray	Homogeneous	Gradual, jagged	Irregular	N	Coalescent, branching	6-2	
	Gray	Homogeneous	Gradual, jagged	Irregular	N	Coalescent	7-3	

This analysis allowed the identification of six types of chert nodules (Table 3.1). Type 1 is characterized by homogeneous texture, abrupt and jagged boundaries, and irregular shape. Type 2 has a wood-grained texture, abrupt and jagged boundaries, and spheroidal shape. Type 3 displays homogeneous texture, abrupt and mostly smooth boundaries, spheroidal shape, and clearly defined rims. Type 4 is characterized by homogeneous texture, abrupt and smooth boundaries, irregular shape, coalescent, and branching distribution. Type 5 shows wood-grained texture, abrupt and smooth boundaries, and mostly spheroidal shape. Type 6 has a homogeneous

texture, gradual and jagged boundaries, irregular shape, and coalescent or isolated distribution. In decreasing order of abundance, the most common types of chert nodules are 6, 5, and 3.

3.3 Petrographic Analysis

The texture, composition, and paragenetic relations identified in the analyzed thin sections are discussed below. Tables 3.2 and 3.3 below summarize the main constituents. The complete description and quantification of the twenty thin sections is available in Appendices A and B.

3.3.1 Textures and Fabric

The thin sections comprise wackestones (micritic calcarenites) (Fig. 3.5a) *sensu* Grabau (1904) and Bramkamp & Powers, (1958) with mud fraction between 45% and 75% (av. 64% mud), sand between 28% and 54% (av. 33% sand), and gravel between 2% and 4% (av. 3% gravel) by volume of total sample. The nodular texture within samples was predominant compared to laminated and fractured textures in the thin section.

The bioclasts display chaotic orientation in all thin sections and loose grain packing (Fig. 3.5b). The particles were mainly supported by a combination of micritic matrix and matrix-replacive material, rarely by grain-replacive material and cement. Due to loose packing, point contacts prominenate, whereas longer grain boundary contacts are less abundant between grains.

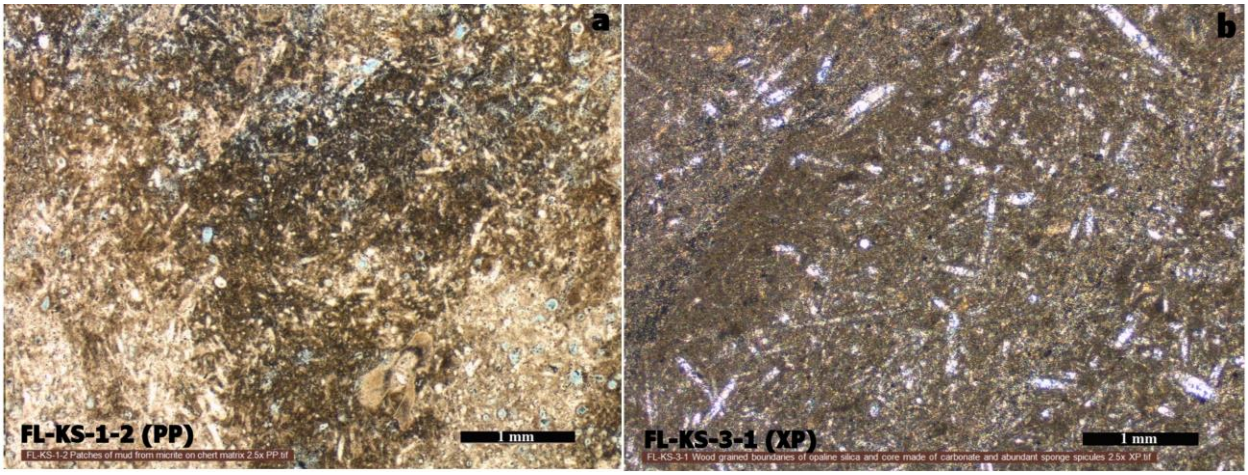

Figure 3.5- Common texture and fabric in studied thin sections:(a) wackestone (micritic calcarenite) and (b) loose grain packing with chaotic orientation of grains.

3.3.2 Primary Constituents

Syndepositional micrite matrix is the main primary constituent in thin sections, forming the original limestone that hosts the nodules. It originally accounted for up to 68% (av. 36%) (Tables 3.2 and 3.3). Original amounts were calculated by including the present and primary constituents replaced by any diagenetic constituent (e.g., radiolarian and radiolarian replaced by calcite).

Table 3.2- A summary of main constituents and their percentages (relative to total sample volume, based on counting of 300 points for each slide).

Thin Section	**FL-KS-1-1**	**FL-KS-1-2**	**FL-KS-2-1**	**FL-KS-2-2**	**FL-KS-3-1**	**FL-KS-3-2**	**FL-KS-4**	**FL-KS-5-1-1**	**FL-KS-5-1-2**	**FL-KS-5-2-1**
Constituents (%)										
Original carbonate matrix	9.35	32.00	12.78	49.71	64.36	33.33	31.72	29.27	21.54	16.20
Original carbonate bioclasts	39.00	43.33	43.00	22.67	19.67	26.67	26.67	19.00	32.67	39.00

Original siliceous bioclasts	2.67	3.67	7.67	3.00	6.99	8.34	2.67	9.67	10.00	1.33
Total opaline silica	0.00	1.30	0.00	0.00	11.70	0.00	0.00	10.30	1.00	1.70
Total chert	71.70	32.30	56.00	39.00	21.30	42.70	42.00	43.70	55.00	64.70
Total chalcedony	3.30	2.30	2.30	1.30	3.00	0.00	0.70	0.70	0.00	1.70
Total silica rosettes	2.00	4.70	2.30	6.00	0.00	17.00	10.30	1.00	10.00	9.00
Total silica	**77.00**	**40.60**	**60.70**	**46.30**	**36.00**	**59.70**	**53.00**	**55.70**	**66.00**	**77.00**
Total calcite	1.70	9.30	1.00	1.30	1.30	5.30	11.00	18.00	4.70	4.30
Total dolomite	0.00	0.00	0.00	0.00	0.00	0.00	3.70	2.00	0.70	1.30
Total iron oxide	1.70	1.30	5.00	1.70	2.00	1.00	2.00	1.70	3.30	2.00
Porosity	10.67	12.33	5.67	5.33	2.33	7.33	6.00	1.67	5.67	4.67

Thin Section	**FL-KS-5-2-2**	**FL-KS-5-2-3**	**FL-KS-5-3**	**FL-KS-6-1**	**FL-KS-6-2**	**FL-KS-6-3**	**FL-KS-7-1**	**FL-KS-7-2**	**FL-KS-7-3**	**FL-KS-8**
Constituents (%)										
Original carbonate matrix	26.03	49.64	68.28	15.00	41.24	59.40	39.51	50.51	34.66	27.71
Original carbonate bioclasts	35.33	22.00	15.33	11.33	17.67	27.33	32.67	32.67	38.33	40.00
Original siliceous bioclasts	0.33	0.66	3.33	1.00	1.33	1.00	1.67	1.33	2.33	3.67
Total opaline silica	6.70	7.00	5.30	5.30	8.00	4.70	3.30	17.70	8.30	2.00
Total chert	53.70	27.30	5.70	23.30	46.30	8.30	59.0	20.40	48.00	62.00
Total	1.30	0.70	1.70	22.00	1.70	1.00	1.00	0.70	3.00	4.00

chalcedony										
Total silica rosettes	18.70	17.00	0.00	0.00	16.70	0.00	4.30	1.00	2.00	5.70
Total silica	**80.30**	**52.00**	**12.70**	**50.70**	**72.70**	**14.00**	**67.70**	**39.70**	**61.30**	**73.70**
Total calcite	1.00	16.30	34.00	0.00	3.30	18.70	0.00	8.70	2.70	0.00
Total dolomite	0.00	1.70	8.00	0.00	0.00	0.30	0.00	0.00	0.00	0.00
Total iron oxide	0.30	0.00	1.00	2.30	2.00	0.30	2.00	0.70	0.70	1.70
Porosity	3.33	8.00	0.00	11.00	13.33	2.67	5.67	1.67	1.67	9.33

Table 3.3- A summary of major constituents in analyzed thin sections (n=20), showing the average and maximum percent volume (based on counting of 300 points for each slide) for relevant primary, diagenetic constituents and porosity.

Thin Section	Average	Maximum
Constituents (%)		
Original carbonate matrix	35.60	68.30
Original carbonate bioclasts	29.50	43.30
Original siliceous bioclasts	3.60	10.00
Total opaline silica	4.70	17.70
Total chert	41.10	71.70
Total chalcedony	2.60	22.00
Total silica rosettes	6.40	18.70
Total silica	**54.80**	**80.30**
Total calcite	7.10	34.00
Total dolomite	0.90	8.00
Total iron oxide	1.60	5.00
Porosity	5.90	13.30

Carbonate bioclasts, including brachiopods, calcispheres, gastropods, crinoids, and bryozoans (Fig. 3.6 a-b), are the second most abundant primary constituents, accounting for up to 43% (average of 30%) of total volume in samples. Siliceous bioclasts, dominantly sponge spicules, and subordinately radiolarians (Fig. 3.6 c-d) account for up to 10% (av. 4%) modally. All other allochems (carbonate peloids, glauconite grains, and phosphate bioclasts) occur in insignificant amounts (less than 1%) proportional to total sample volumes.

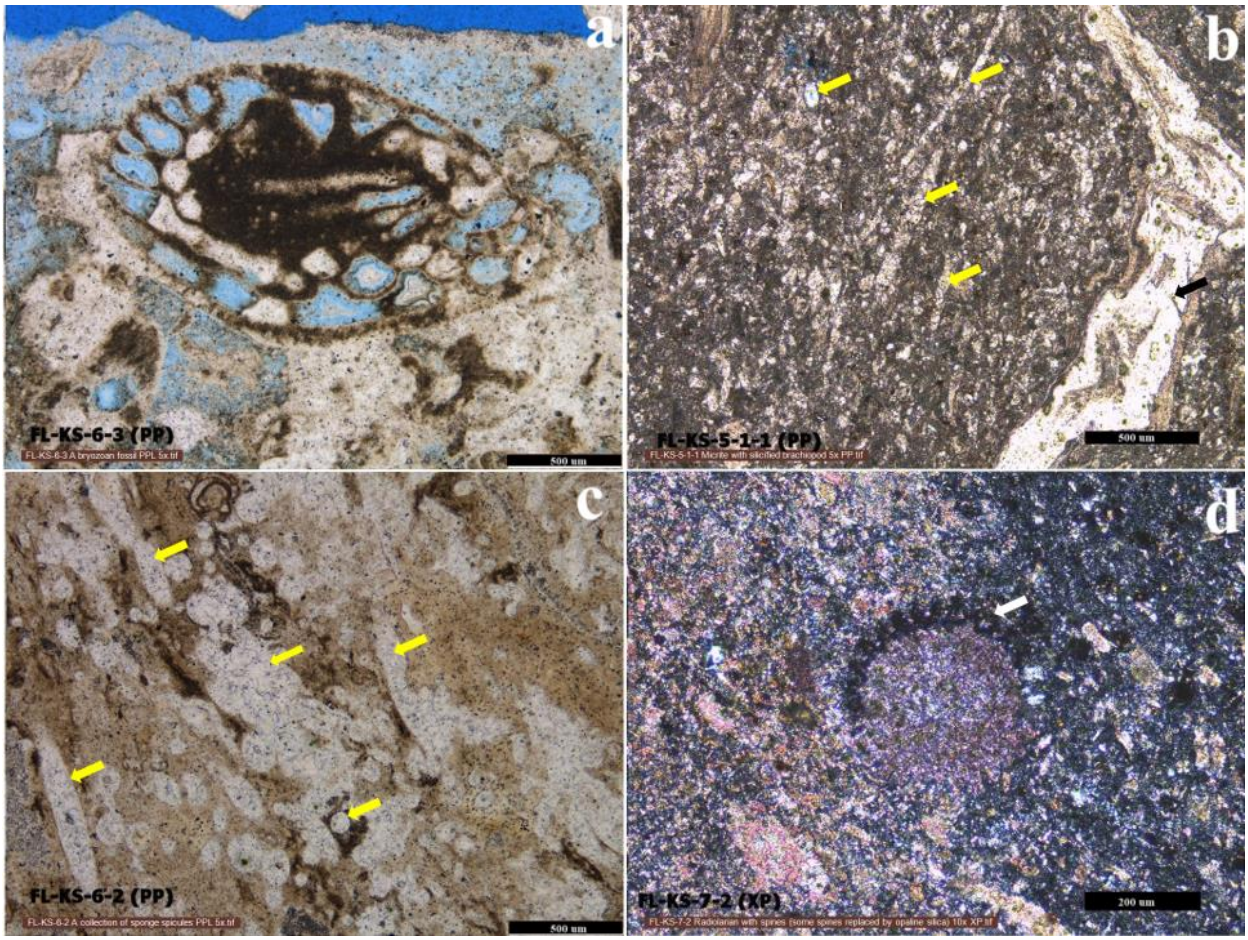

Figure 3.6- Different types of bioclasts in the studied thin sections: (a) a bryozoan with preserved primary porosity (plane polarized light, PP), (b) a silicified brachiopod (on the far right side shown by a black arrow) and sponge spicules (shown by yellow arrows) (PP), (c) an accumulation of sponge spicules (PP), (d) a rarely preserved radiolarian (shown by a white arrow in crossed polarized light, XP). The blue dye mark the pore spaces in the thin section, and pink color in calcite is due to staining with Alizarin Red.

3.3.3 Diagenetic Constituents

The main diagenetic constituent is silica, which accounts for up to 80% of the studied thin sections (av. 55%) (Table 3.3). It precipitated in different phases, discussed below. Calcite, dolomite, and Fe oxides are the other diagenetic minerals detected.

Four major diagenetic silica phases were identified. The most abundant silica phase was chert (av. 41%, max. 72%), followed by silica rosettes (av. 6%, max. 19%), opaline silica (av. 5%, max. 18%), and chalcedony (av. 3%, max. 22%) in total sample volumes (Figure 3.7). The mineralogy in each sample reflects the composition of the silica nodule, not of the host rock. Chert was the main silica phase in all thin sections observed. Opaline silica was observed replacing the micritic matrix and various bioclasts (Figure 3.7a). Chert is microcrystalline, with crystal sizes varying from 1µm to 10 µm (Figure 3.7b). It replaces the micritic matrix and bioclasts but also replaces opaline silica and fills interparticle, intraparticle, and fracture pores. Silica rosettes have a spherical/globular habit, with an average diameter of 20 µm (Figure 3.7c). Like chert, they replace the micritic matrix and bioclasts and fill interparticle, intraparticle, and fracture pores. The relationship between silica rosettes and opaline silica and chert was not observed in the thin sections that were studied. Chalcedony (fibrous silica) nodules vary from 50 µm to 200 µm (Figure 3.7d) and replace bioclasts and chert, rarely opaline silica.

The optical orientation of the above-mentioned fibrous silica indicates that both length-fast and length-slow orientations occur (Figure 3.8). Length-fast chalcedony is the ‘regular’ chalcedony, while length-slow chalcedony is called quartzine.

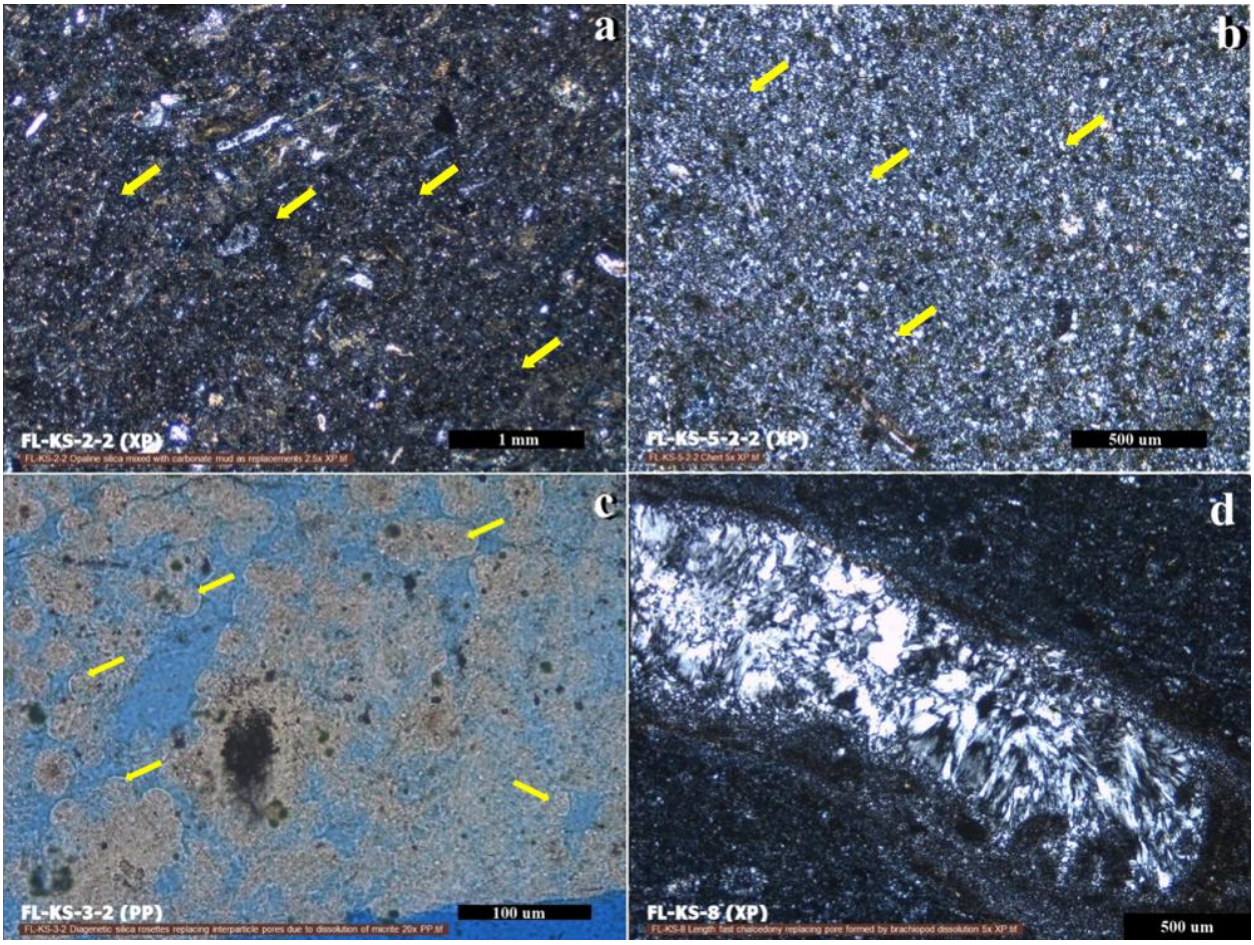

Figure 3.7- Four major silica phases: (a) opaline silica replacing micrite (indicated by yellow arrows, crossed polarized light, XP), (b) chert replacing micrite and sponge spicules (indicated by yellow arrows, XP), (c) silica rosettes (indicated by yellow arrows) filling interparticle and vug pores (plane polarized light, PP), and (d) chalcedony replacing bioclast.

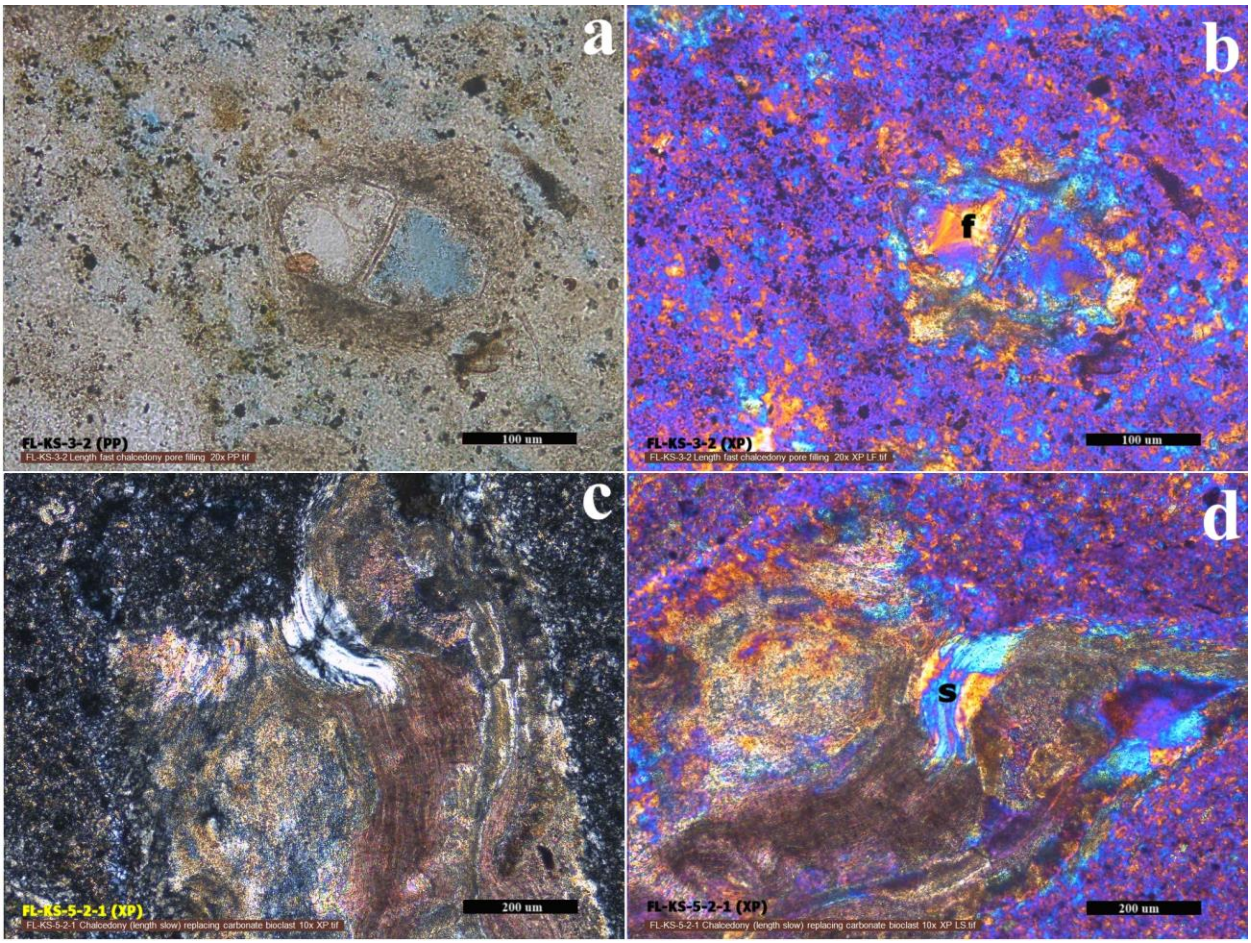

Figure 3.8- Different optical orientations of chalcedony fibers, indicating the occurrence of (a and b) length-fast chalcedony (f) within a bioclast and (c and d) length-slow (s) chalcedony (moganite) within a bioclast. (a) and (c) is the PP view, and (b) and (d) are the XP view with the addition of a gypsum plate.

In two thin sections, euhedral quartz crystals occur, either replacing and engulfing the micritic matrix or as drusiform filling of vug pores, with silica habits varying from spherulitic chalcedony to prismatic mega quartz crystals (Figure 3.9).

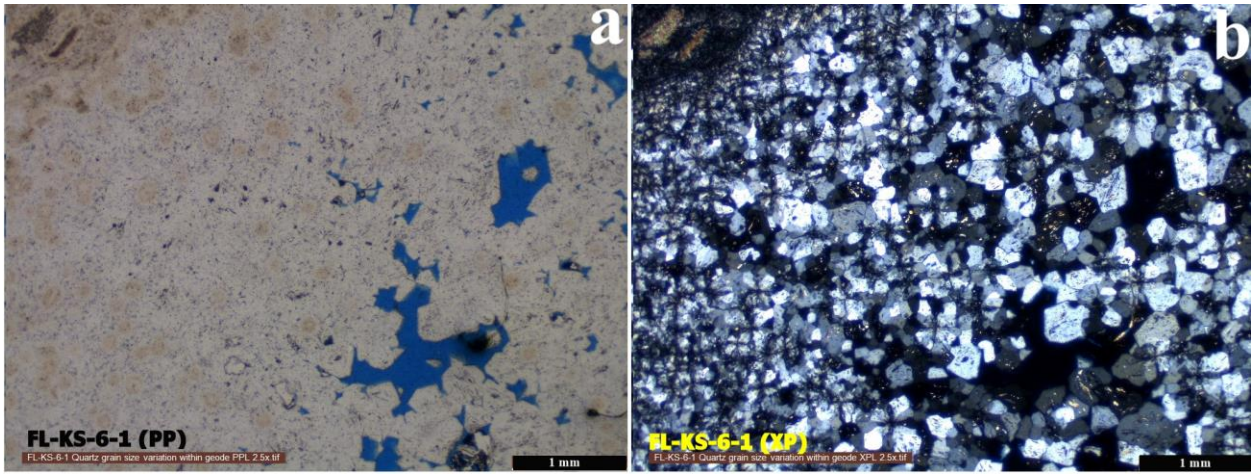

Figure 3.9- Spherulitic chalcedony (brownish color, abundant on the upper left corner) grading to euhedral quartz (more abundant toward the lower right) in a vug pore under (a) plane-polarized light (PP) and (b) crossed-polarized light (XP).

The paragenetic relations between different silica phases suggest a relative order of precipitation. Opaline silica is replaced by all the other silica phases, indicating that its precipitation predates the others. Chert extensively replaces opaline silica (Fig. 3.10a), and chalcedony replaces chert and opaline silica (Figure 3.10b-c). Although silica rosettes showed no direct paragenetic relation with other silica phases, they were predominantly found lining or filling secondary pores (Figure 3.10d).

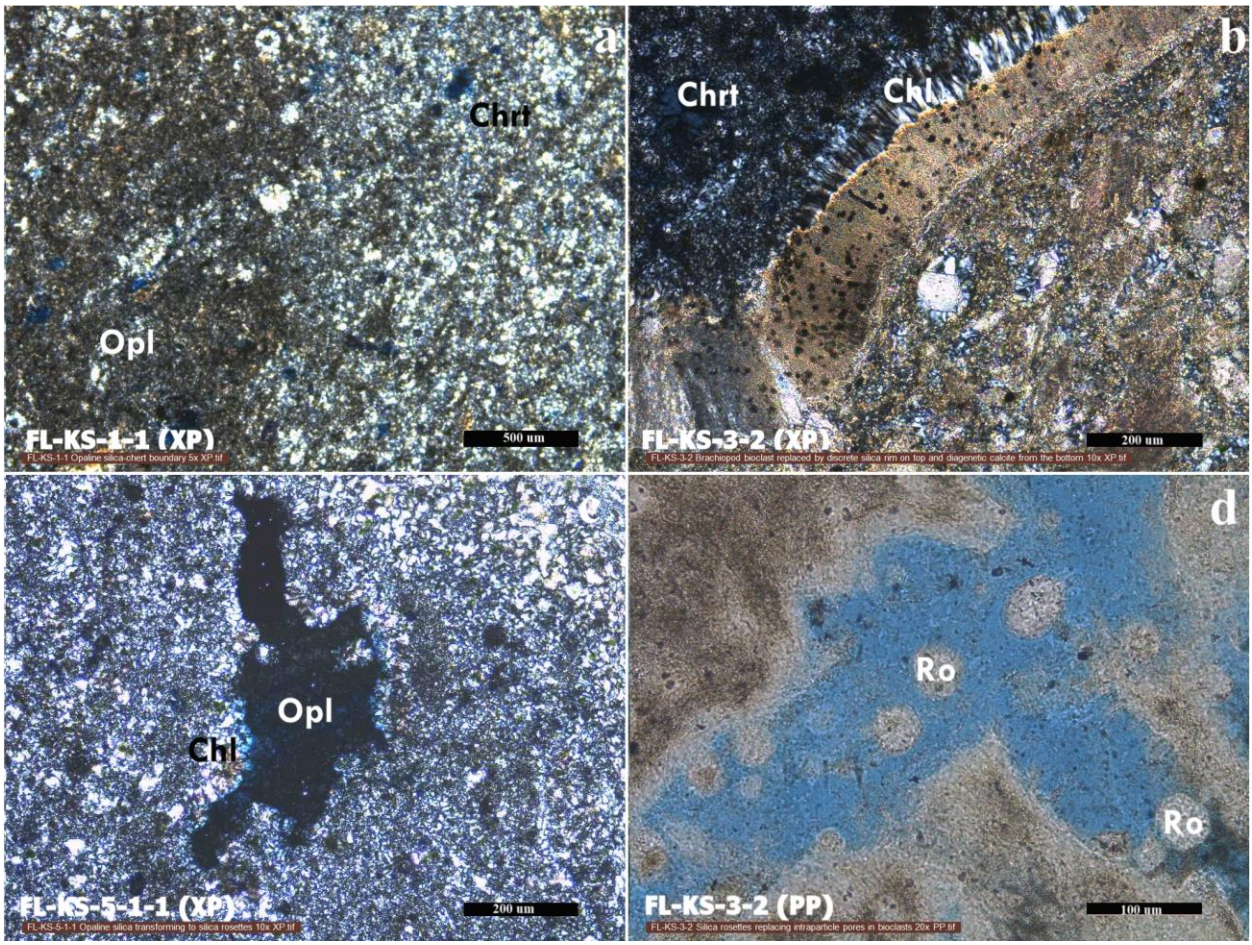

Figure 3.10- Paragenetic relations between silica phases. (a) Opaline silica (Opl) replaced by chert (Chrt), (b) chert replaced by chalcedony (Chl) along the margin of a bioclast, (c) opaline silica replaced by chalcedony, (d) silica rosettes (Ro) lining and filling dissolution pores.

Calcite is the second most abundant diagenetic mineral, accounting for up to 34% (av. 7%) of total sample volumes. It occurs as blocky crystals and small rhombs (rarely rims) replacing primary constituents (Fig. 3.11 a-b), opaline silica (Fig. 3.11c), chert and chalcedony (Fig. 3.11d), and filling intraparticle pores. Calcite is rarely replaced by dolomite.

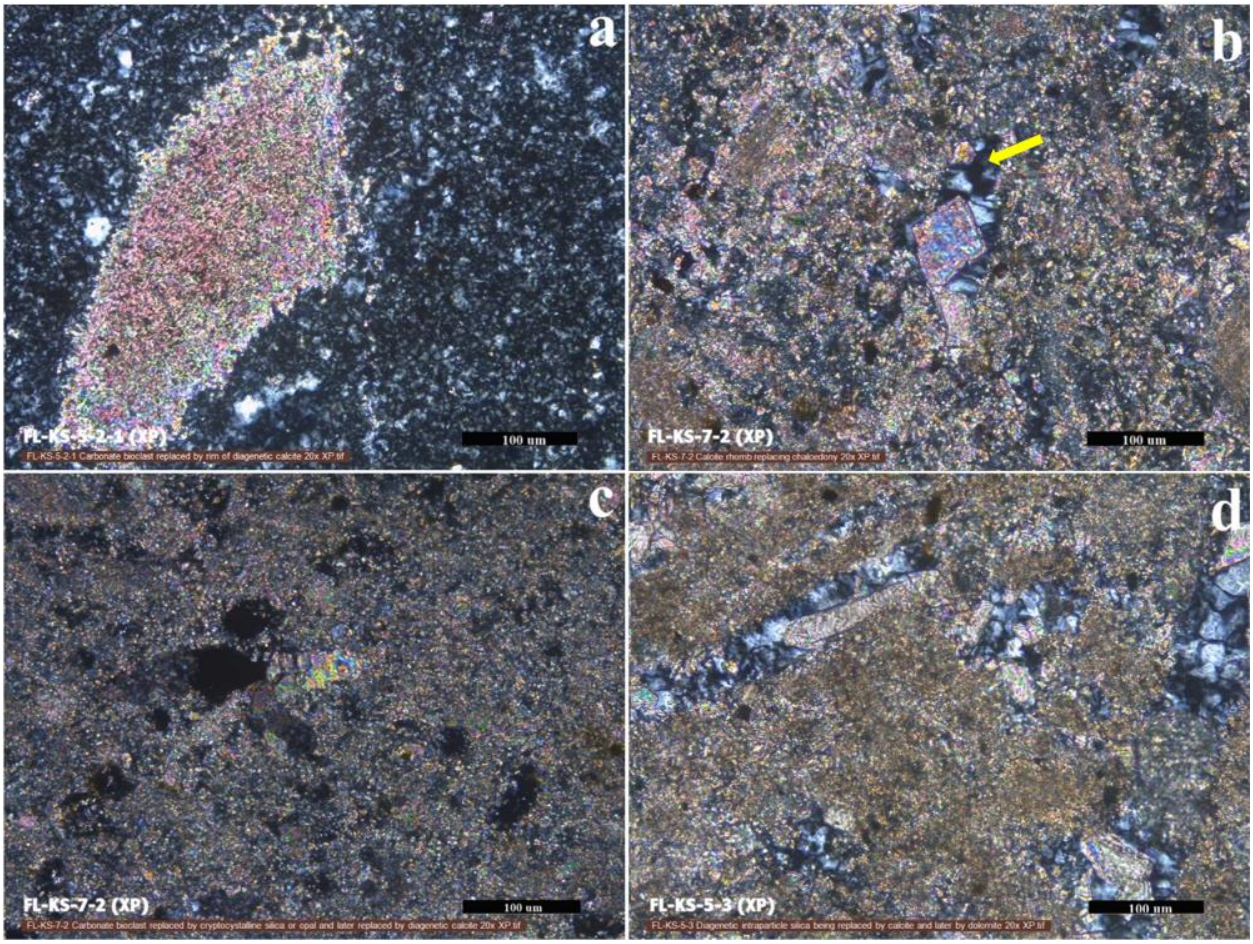

Figure 3.11- Calcite replacing (a) a carbonate bioclast, (b) a sponge spicule (shown in yellow arrow), (c) opaline silica, (d) chalcedony.

Dolomite (av. 1%, max. 8% of total sample volumes) occurs as blocky crystals, small rhombs, and microcrystalline habit, replacing primary constituents, calcite and silica.

Iron oxides (av. 2%, max. 5% of total sample volumes) with pelletoidal habit replace the micritic matrix and fill interparticle and intraparticle porosity.

Other rare diagenetic minerals include barite, precipitated as coarse (0.5 mm to 1 mm), hexagonal crystals (Fig. 3.12a) within dissolved anhydrite nodules (Figure 3.12b-c) and coarse (0.4 mm to 0.8 mm) spherulitic chalcedony with anhydrite inclusions (Fig. 3.12d).

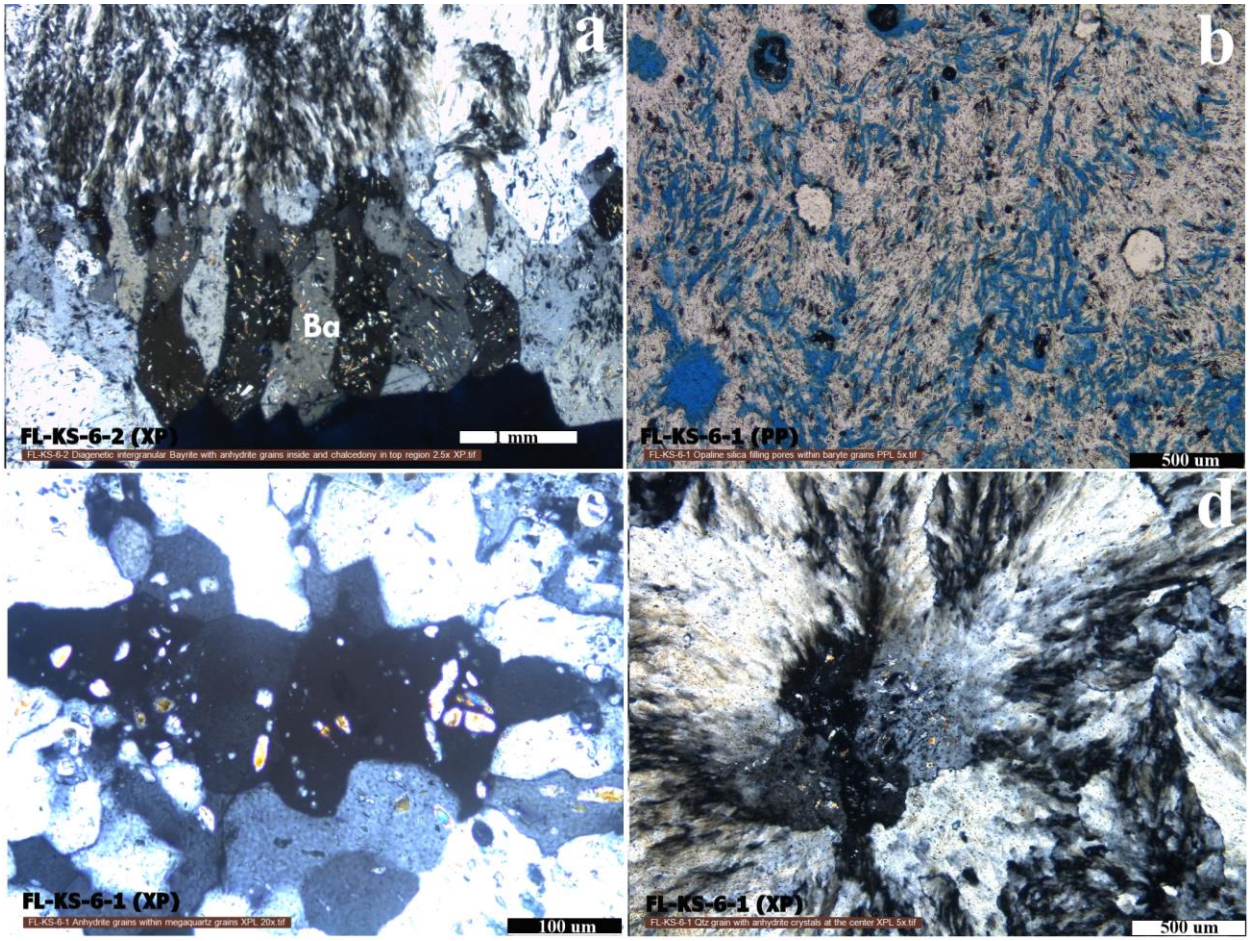

Figure 3.12- Other diagenetic minerals include (a) coarse barites replaced by chalcedony, precipitated within partially dissolved anhydrite nodules (b and c). The nodules are partially silicified by chalcedony, which contains anhydrite inclusions in the center (d).

3.3.4 Silica Nodule Mineralogy

The three main types of silica nodules contain different proportions of silica types (Table 3.4).

Table 3.4- Percentage of silica minerals in the different silica nodule types.

Thin Section	Type of Nodule	Silica Mineralogy (Averaged by the Number of Thin Sections)				
		Opaline Silica (%)	Chert (%)	Chalcedony (%)	Silica Rosettes (%)	Total Silica Content (%)
FL-KS-1-2 FL-KS-3-1 FL-KS-5-3 FL-KS-7-2	Wood-grained silica (Type 5)	9.0	20.0	2.0	1.4	32.2
FL-KS-4 FL-KS-5-1-1 FL-KS-5-1-2 FL-KS-7-1	Rimmed silica (Type 3)	3.7	50.0	1.8	6.4	60.6
FL-KS-1-1 FL-KS-2-1 FL-KS-2-2 FL-KS-3-2 FL-KS-5-2-1 FL-KS-5-2-3 FL-KS-6-2 FL-KS-7-3 FL-KS-8	Burrow/homogenous silica (Type 4)	1.5	52.0	2.0	8.4	63.7

As expected, chert accounts for the majority of the silica nodules, regardless of the nodule type. Wood-grained silica nodules (Type 5) preserved the highest percentage of opaline silica, while burrow/homogenous silica nodules contain higher percentage of chert and silica rosettes compared to other nodule types. The percentage of chalcedony is approximately the same in all three nodule types.

3.3.5 Porosity

Porosity in the studied thin sections varies from 0-13% (average 6%) of total sample volumes. Pore types included intraparticle pores within bioclasts (Figure 3.13a), interstitial pores due to the dissolution of micritic matrix and diagenetic silica (Figure 3.13b), and intraparticle and moldic pores due to the dissolution of bioclasts (Figure 3.13c). In addition, thin sections exhibited rare fracture pores (Figure 3.13d). Some of the moldic pores are partially filled by opaline silica.

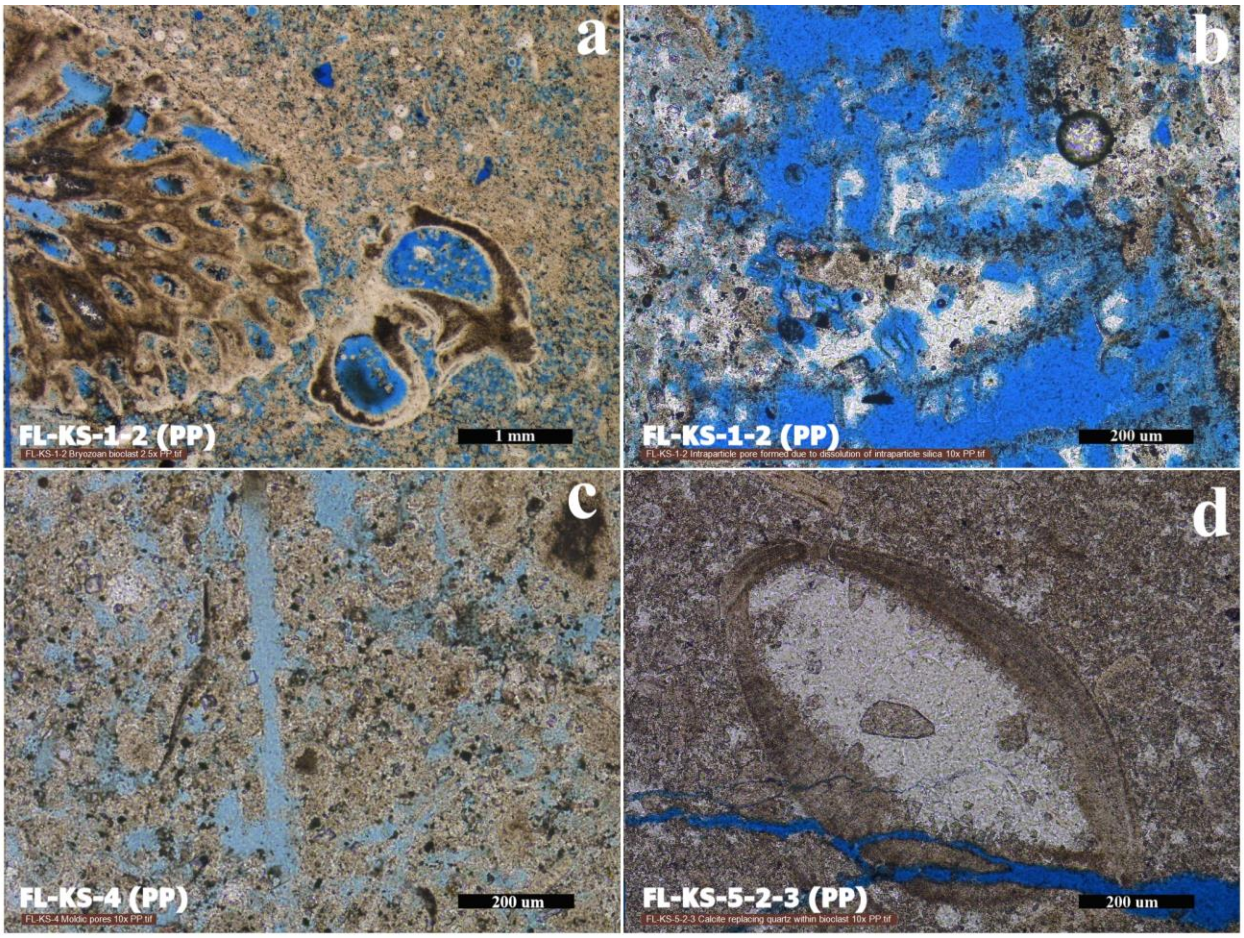

Figure 3.13- Porosity included (a) intraparticle pores within a bryozoan, (b) vug pores due to dissolution of micrite and chert, (c) moldic pores due to dissolution of bioclasts, (d) fracture pores.

3.3.6. Other petrographic features

Stylolites were observed in several thin sections. Along these structures, interparticle and moldic pores (Fig. 3.14a) and silica phases such as rosettes (Figure 3.14b-c) and opaline silica (Figure 3.14d) are common.

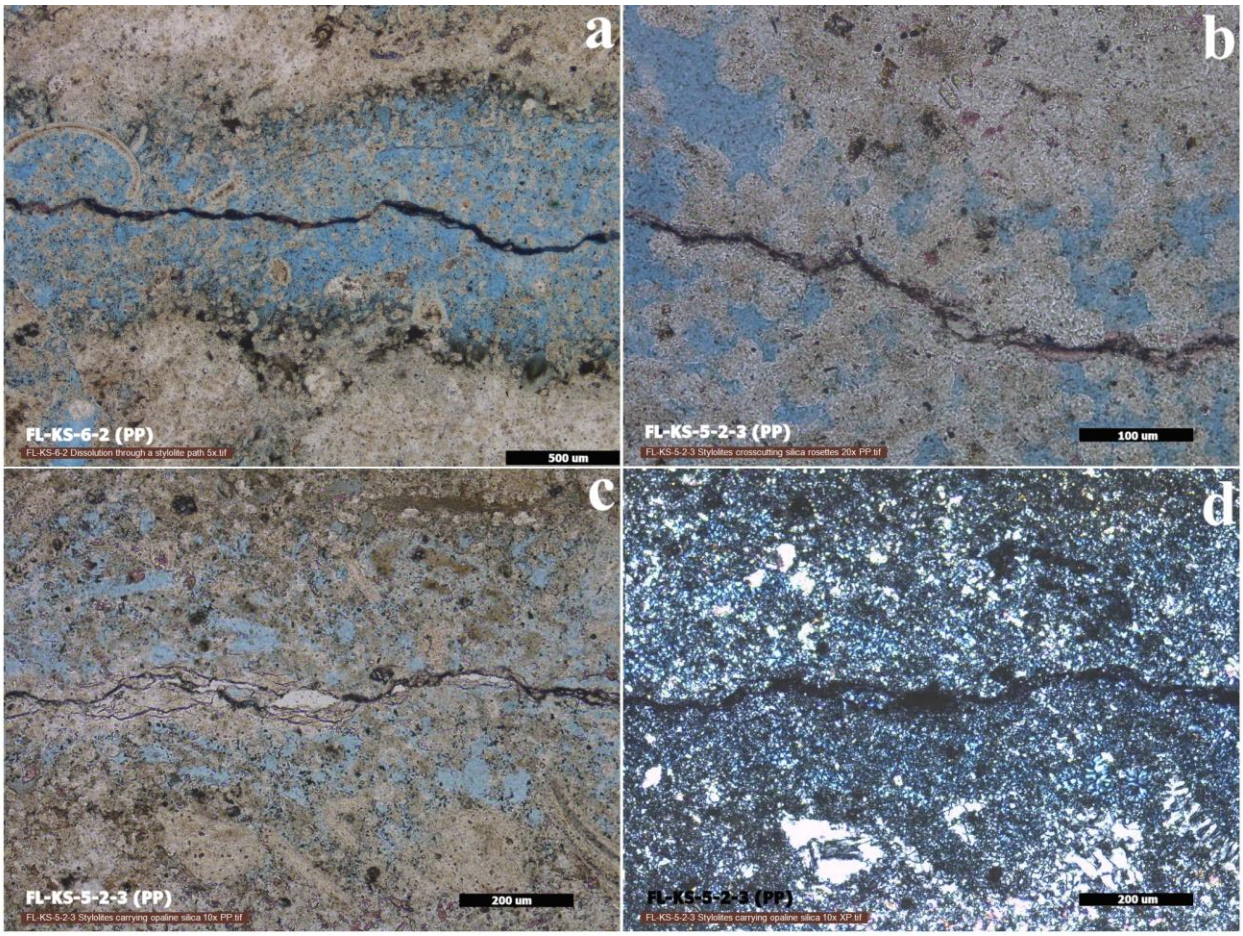

Figure 3.14- Stylolites are commonly accompanied by (a) interparticle and moldic pores, (b-c) silica rosettes, and (d) opaline silica precipitation. The preferential location of secondary pores (in blue) along stylolites suggests that the latter provided a pathway for the percolation of dissolving solutions that generated the pores, as well as late-stage solutions for the precipitation of silica rosettes and opaline silica during burial.

3.4 Cathodoluminescence Analysis

Cathodoluminescence facilitated distinguishing carbonate and silica, as a yellow-red luminescence is observed in carbonate particles (mostly visible in bioclasts), whereas no luminescence is observed in silica phases (Figure 3.15).

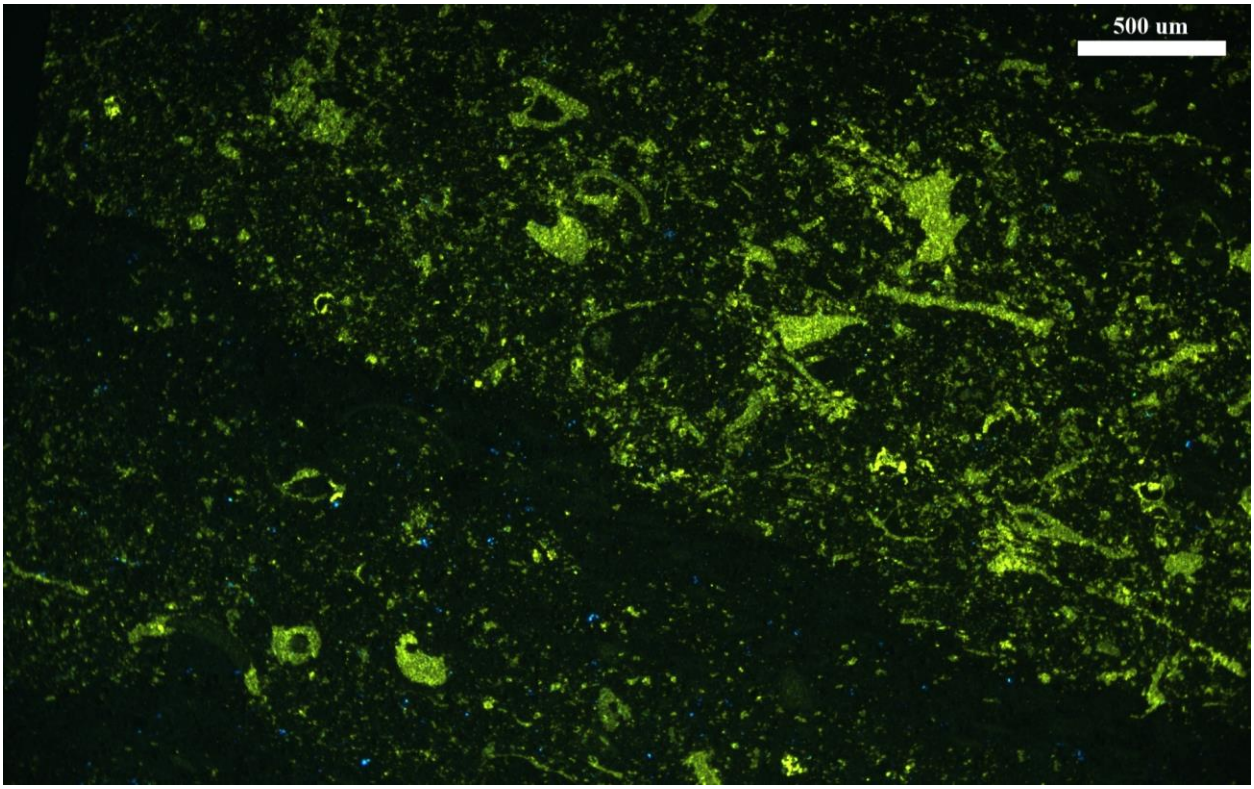

Figure 3.15- Luminescence observed on bioclasts in thin section FL-KS-7-2. The non-luminescent dark line in the middle is opaline silica in the wood-grained nodule. Dark spots surrounding luminescent carbonate particles are the chert replacements.

The different silica phases could not be distinguished by cathodoluminescence due to the small crystal sizes and lack of luminescence in the silica.

3.5 Raman Spectroscopy

This technique allowed the identification of α-quartz. In all nine samples, a prominent band around 464 cm^{-1} was observed (Table 3.5). This band corresponds to A_1 phonon of α-quartz, identified as chert (Figure 3.16).

Table 3.4- Peak and minor signals observed for each thin section analyzed. The uncertainity of the instrument was 2cm^{-1}.

Sample Name	Target in the thin section	Peak Signal (cm^{-1})	Other Signals (cm^{-1})
FK-KS-3-1	Sponge Spicule	464	1019
FL-KS-3-2	Silicified rims around bioclasts	463	1085
FL-KS-4	Chert matrix	464	-
FL-KS-5-1-1	Silicified bioclast	463	-
FL-KS-5-1-2	Opaline silica filling cracks Chert matrix	464 464	142
FL-KS-5-2-1	Silicified bioclast Chert matrix	463 464	126 205 263 353
FL-KS-5-2-2	Silica rosettes Pore-filling silica Chert matrix	464 464 464	-
FL-KS-5-3	Wood-grained silica boundary	464	127 206 1086
FL-KS-6-1	Chalcedony	464	127 206 267 354 393 501 503 1160

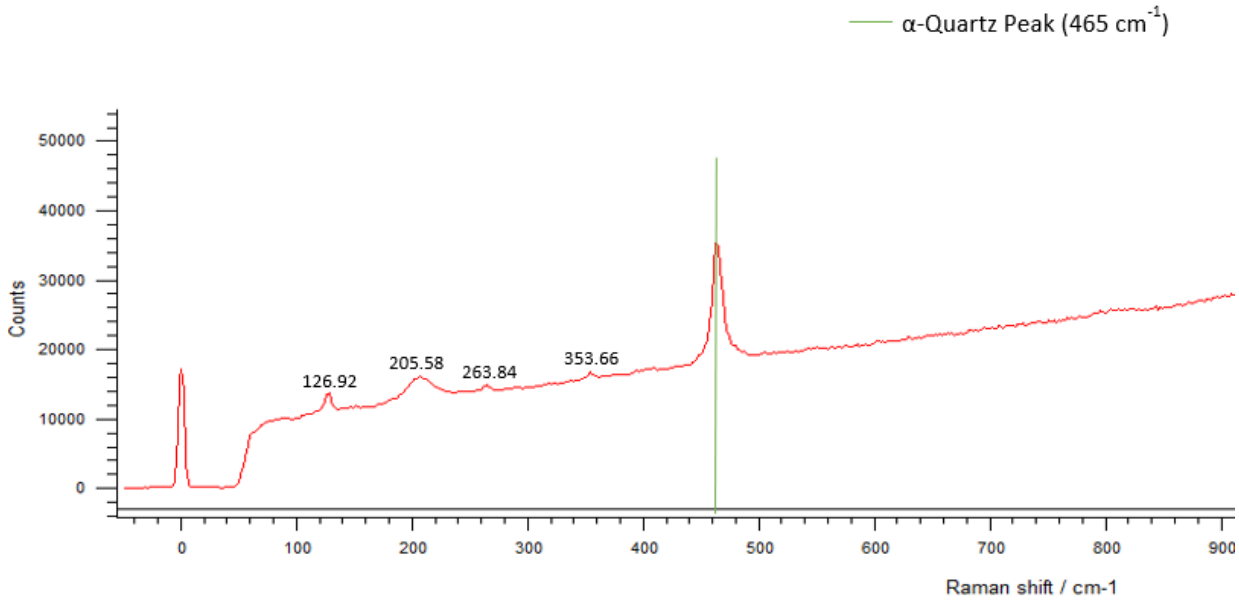

Figure 3.16- Raman shift corresponding to silica replacing a bioclast in sample FL-KS-3-1.

In addition to the α-quartz/chert band signal, two minor bands were observed in sample FL-KS-6-1. The Raman shift of ~501cm^{-1} is assigned as the A_g mode of moganite, and ~503 cm^{-1} signal can be assigned to silanol (SiO_3OH), a simple silica mineral formed through weathering of silica minerals (Figure 3.17).

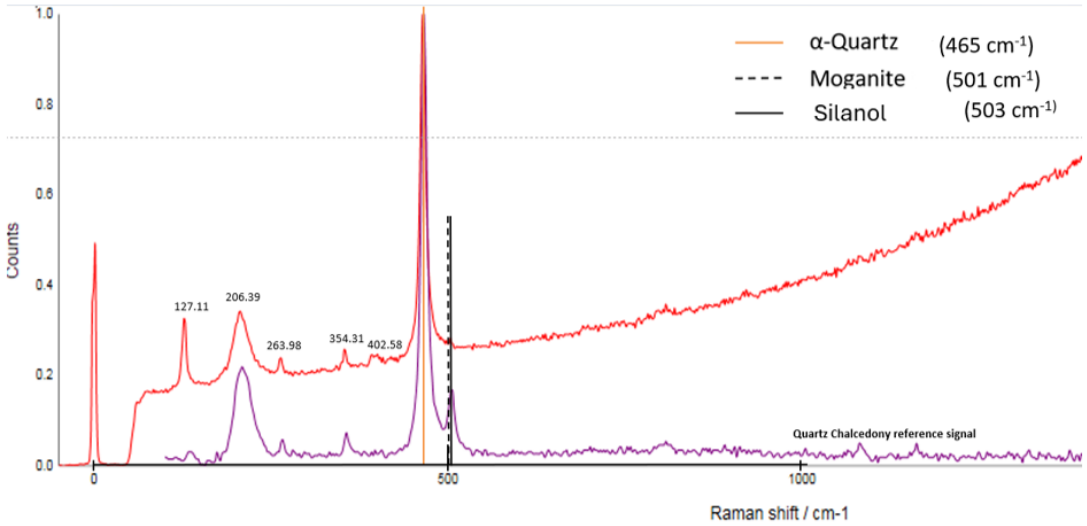

Figure 3.17- Raman shift signal for FL-KS-6-1, overlayed with the instrument's chalcedony reference signal (below).

3.6 X-Ray Diffraction

X-ray diffraction analysis indicates the presence of α-quartz, moganite-quartz associations, and calcite as the main minerals in sample FL-KS-7-1. No clear peak specifically for moganite was observed, but abundant signal peaks corresponding to moganite-quartz associations are present (Figure 3.18 and Figure 3.19).

Samples FL-KS-2-2, FL-KS-6-3, FL-KS-7-1, and FL-KS-7-2 show similar signal patterns, but with comparatively higher calcite proportions than the rest of the samples, while FL-KS-5-2-2 and FL-KS-6-2 displayed comparatively lower calcite proportions (lower peak).

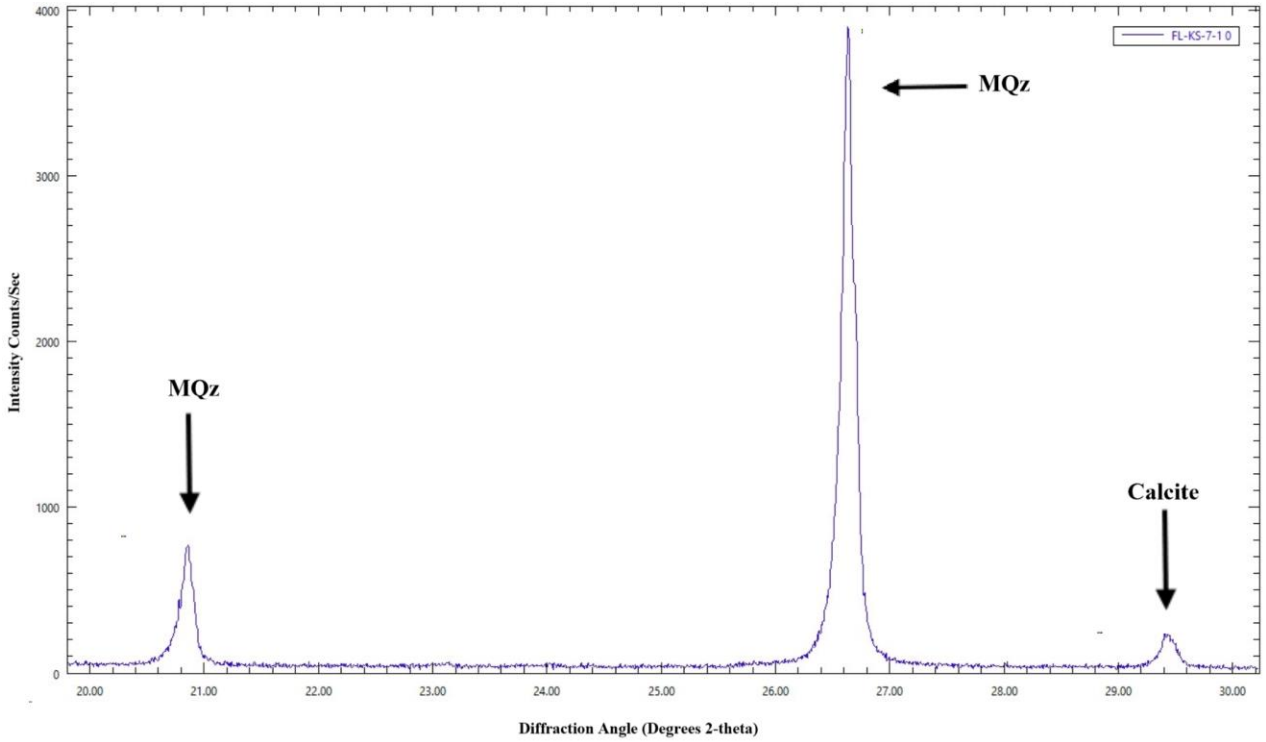

Figure 3.18- Diffractogram for FL-KS-7-1 showing Moganite-Quartz associations (MQz).

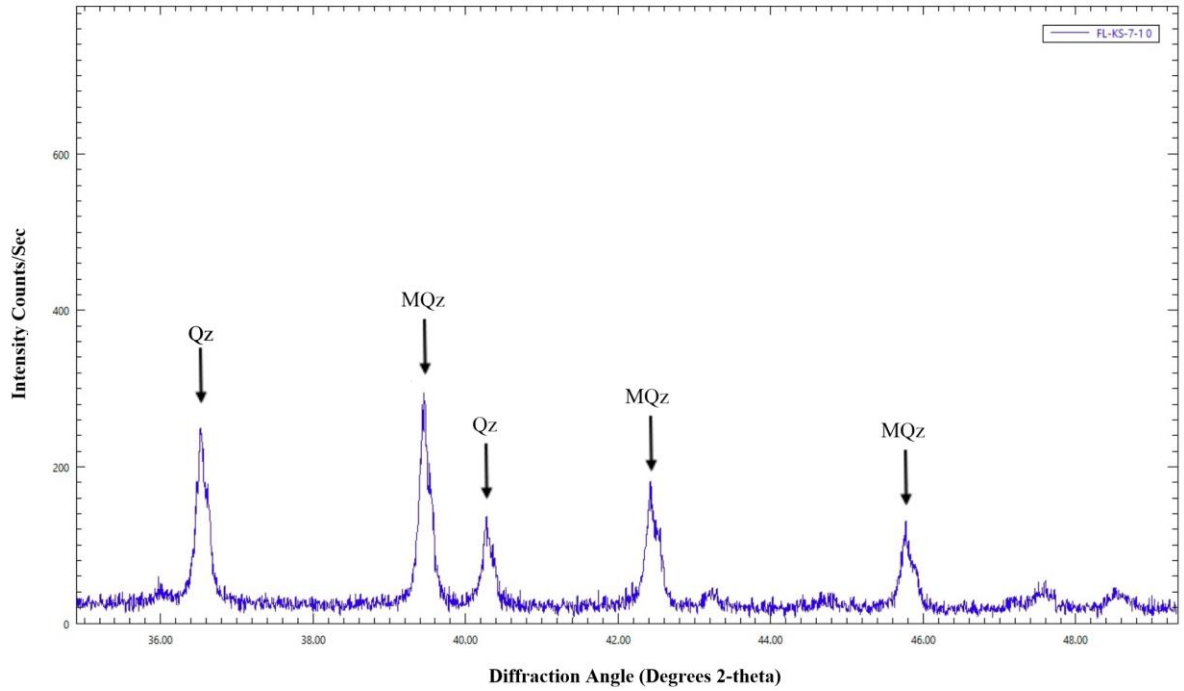

Figure 3.19- Diffractogram for FL-KS-7-1 showing Moganite-Quartz associations (MQz).

3.7 Oxygen Isotope Analysis

The values for oxygen isotope ratios in the six samples varied between 30.26‰ and 33.74 ‰ (VSMOW) (Table 3.6), which is remarkably constant. The precision of oxygen isotope values were 0.28‰ (1σ).

Table 3.5- Oxygen isotopic data of analyzed chert samples (1σ).

Sample	$\delta^{18}O$ VSMOW (‰)
FL-KS-2-2 opaline silica	30.2
FL-KS-6-2 chalcedony and megaquartz	32.4
FL-KS-6-3 opaline silica	32.6
FL-KS-5-2-2 chert	33.7
FL-KS-7-2 opaline silica	30.8
FL-KS-6-2 chalcedony and megaquartz duplicate	32.2
FL-KS-7-1 chert	30.6
FL-KS-7-2 opaline silica duplicate	30.8

No significant pattern was observed in relation to the type of silica and their respective oxygen isotope values (Figure 3.20).

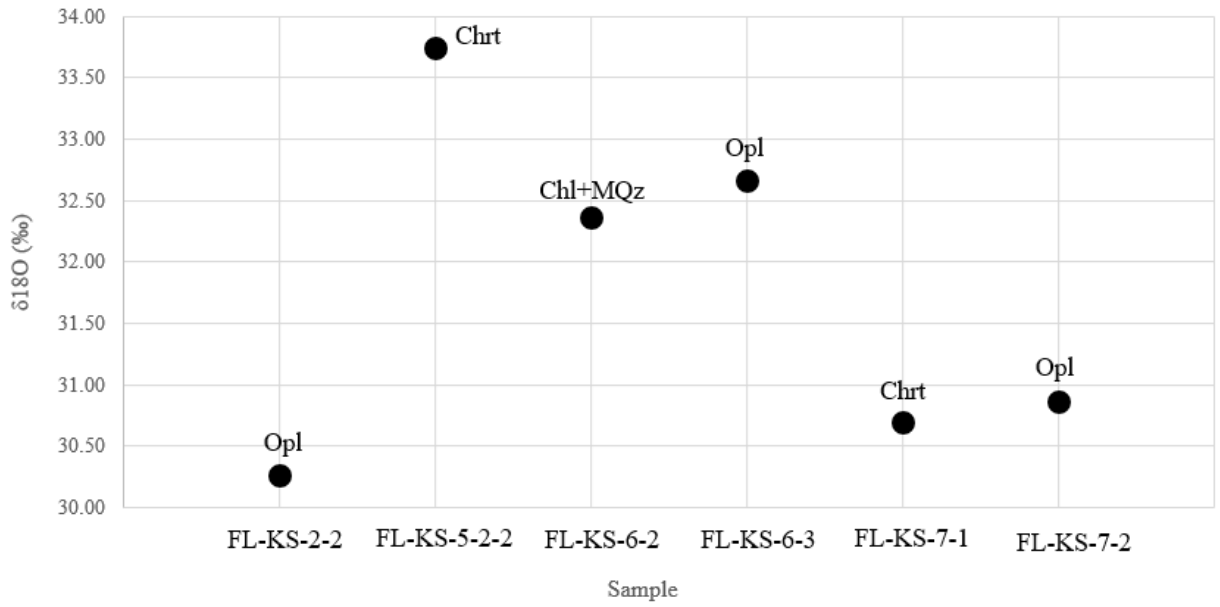

Figure 3.20- $\delta^{18}O$ values for the six samples analyzed, according to the major silica type (Opl- Opaline silica, Chrt- chert, Chl+MQz- Chalcedony with megaquartz). The markers (black circles) in the graph are larger than the analytical error of 0.28‰.

3.8 LA-ICP-MS Analysis

The samples analyzed by LA-ICPMS were assumed to contain 99.5% SiO_2, as explained in the Methods. Si concentration was calculated from the atomic weight fraction of Si in SiO_2, converted to parts per million (ppm). Ge concentrations (in ppm) were measured with LA-ICP-MS, and the Ge/Si ratio was calculated (Table 3.7). Ge/Si ($x10^6$) ratios range from 0.4 to 1.25 ($x10^6$).

Table 3.6- Si and Ge concentrations and the calculated Ge/Si ratios.

Sample	Si (ppm)	Ge (ppm)	Ge/Si ($x10^6$)
FL-KS-2-2	465163	0.58	1.25
FL-KS-5-2-2	465163	0.38	0.81
FL-KS-6-2	465163	0.23	0.5

FL-KS-6-3	465163	0.21	0.45
FL-KS-7-1	465163	0.39	0.85
FL-KS-7-2	465163	0.41	0.87

Like the oxygen isotope ratios, there is no trend in Ge/Si ratios in relation to the type of silica (Figure 3.21). However, Ge/Si ratios in chert are the same (~$0.8x10^6$), while opaline silica and chalcedony show slightly more variable ratios.

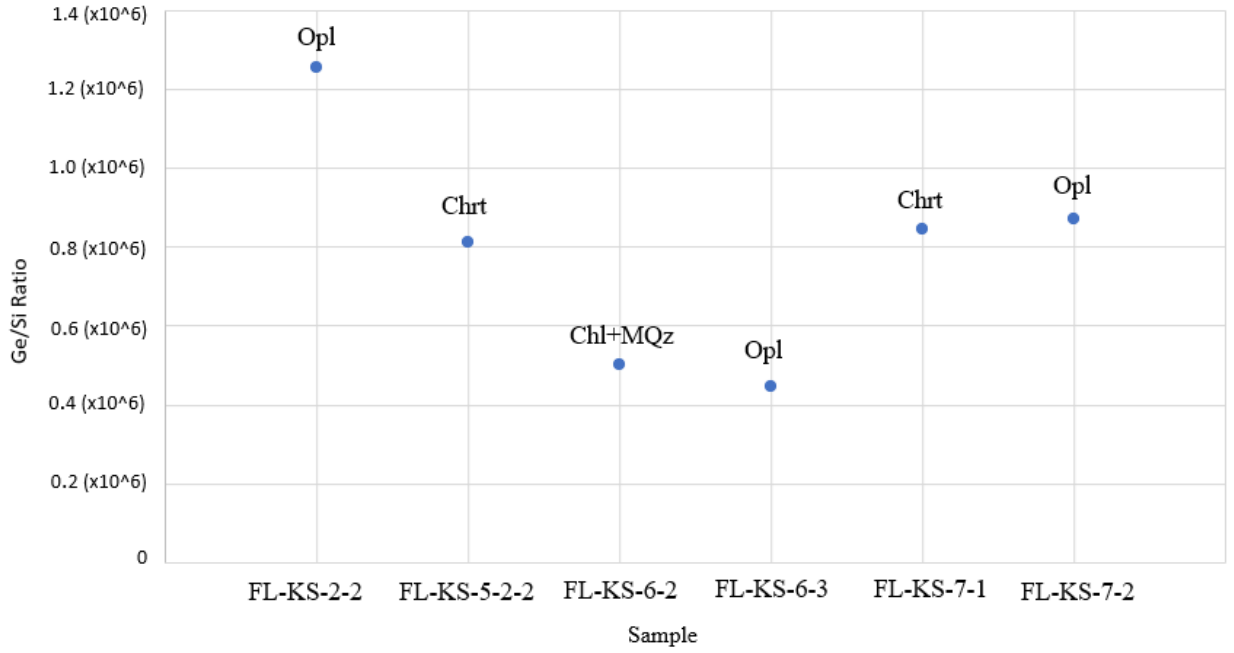

Figure 3.21- Ge/Si ($x10^6$) ratios analyzed in six samples with different types of silica (Opl- Opaline silica, Chrt- Chert, Chl+MQz- Chalcedony with megaquartz).

Chapter 4 - Discussion

4.1 Temperature of Silicification

The oxygen isotopic composition of ocean water is controlled by several factors, including temperature, evaporation-precipitation, continental and glacial runoff (Benway & Mix, 2004; Kiran Kumar et al., 2018, Yanchilina et al., 2020) to cite a few, but the temperature is a major control (Matheney & Knauth, 1993; Sharp & Kirschner, 1994; Tatzel et al., 2022). While increasing temperatures lead to negative or isotopically depleted $\delta^{18}O$ values in oceans, high evaporation in sabkha basinal conditions contributes to more positive or isotopically enriched $\delta^{18}O$ values in ocean water locally (Duane et al., 2004) due to isotopic fractionation. Silica precipitated at ocean surface conditions does not display isotopic fractionation, hence preserving the original oxygen isotope values of ocean water, but, this is true for silica which has undergone substantial diagenesis. For example, previous studies on chert subjected to burial indicate that oxygen isotope values is affected by silica phase transformation during diagenesis (Yanchilina et al., 2020; Tatzel et al., 2022) and ambient temperature of environment during silicification (Tatzel et al., 2022). Moreover, reseting of $\delta^{18}O$ values equilibrated with porewater can cause temperature estimations using oxygen isotope values of chert challenging (Tatzel et al., 2022).

The petrographic analysis shows evidence for deeper burial conditions during diagenesis of the Florence Limestone. The stylolites found in the studied samples are formed by pressure dissolution, and thus indicative of chemical compaction under mesodiagenetic conditions (Mazzullo & Harris, 2009; Moore & Wade, 2013). Previous studies indicate that stylolite formation can begin at ~550 m of burial and continue up to maximum depths of ~3500 m (Choquette & James, 1987; Sverdrup & Prestholm, 1990), associated with 100º C - 120º C

temperatures (Sverdrup & Prestholm, 1990; Moore & Wade, 2013). Therefore, the silica nodules were subjected to deeper burial conditions, reaching higher temperatures.

Furthermore, according to Yanchilina et al. (2020), Opal-A to Opal-CT transformation requires a minimum temperature of 43º C and Opal-CT to chert transformation requires at least 63º C of temperatures and estimated burial depth of above 450 m (Figure 4.1). Since chert is the most abundant silica type in the studied nodules (Table 3.3), they must have been subject to temperatures higher than 63º C. Therefore, the oxygen isotope values obtained for the six samples cannot be utilized to estimate temperatures of silicification, as they do not preserve the original signal.

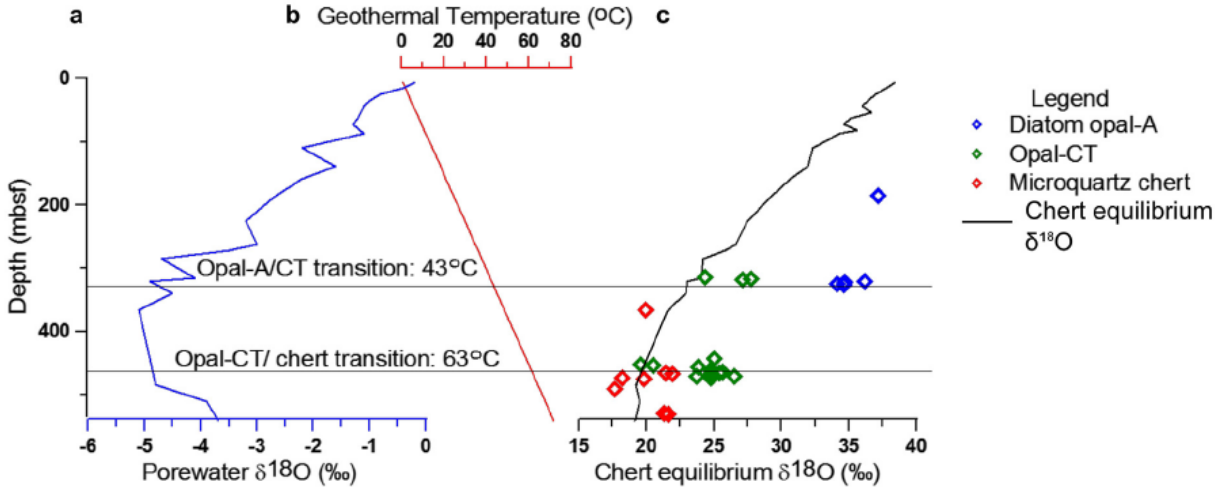

Figure 4.1- Measured oxygen isotope values of burial chert from ODP 795 from (Brumsack et al., 1992) vs depth of burial (Yanchilina et al, 2020). (mbsf = meters below the seafloor)

4.2 Paragenetic Sequence

Silica is the most abundant diagenetic mineral in the studied thin sections, with four main types/phases (opaline, chert, chalcedony, and quartz) identified through petrographic, X-ray diffraction, and Raman spectroscopy analyses (in addition to moganite or quartzine as a minor

phase). The petrographic study allowed the determination of the paragenesis and diagenetic evolution, emphasizing the timing of the different silica phases.

Eodiagenesis includes processes occurring under the influence of depositional fluids at depths less than about 2 km ($T < 70^{\circ}$ C), whereas mesodiagenesis includes processes occurring at depths $\geq$ 2 km ($T \geq 70^{\circ}$ C) and reactions involving chemically modified formation waters (Morad et al., 2000).

Interpreting diagenetic processes and products as eodiagenetic (pre-compactional) or mesodiagenetic (post-compactional) is based on paragenetic relations and mode of occurrence, such as replacement and/or engulfment relations between different diagenetic constituents; the presence of corroded borders (indicative of dissolution); and the relations between diagenetic constituents and porosity.

The main post-depositional and eodiagenetic processes were the burrowing of unconsolidated carbonate sediments. These formed preferential pathways for the percolation of silicifying solutions, precipitation of opaline silica, followed by chert and chalcedony (Figure 4.2). This is indicated by opaline silica cement replaces only carbonate sediments; chert replaces (and hence post-dates) opaline silica, and chalcedony replaces both opaline silica and chert. This leads us to propose the relative precipitation order of the different silica phases depicted in Figure 4.2. The interpretation that most silicification occurred during eodiagenesis is based on paragenetic relations, also in agreement with the shallow burial suggested by the oxygen isotopic data.

Carbonate precipitation was assumed to take place during mesodiagenesis because it replaces all eodiagenetic silica phases, but no direct petrographic evidence was observed between the carbonates and other mesodiagenetic products. Some dissolution occurred before

carbonate precipitation, as calcite and dolomite fill secondary pores, but carbonates are mostly replacive phases. Chemical compaction resulted in the formation of stylolites, along which mesodiagenetic fluids have percolated to generate secondary porosity. In these pores, silica rosettes precipitated. Since silica rosettes occur as pore-fills of the secondary pores generated during mesodiagenesis, it can be argued that percolation of late solutions formed silica rosettes under relatively deep burial conditions.

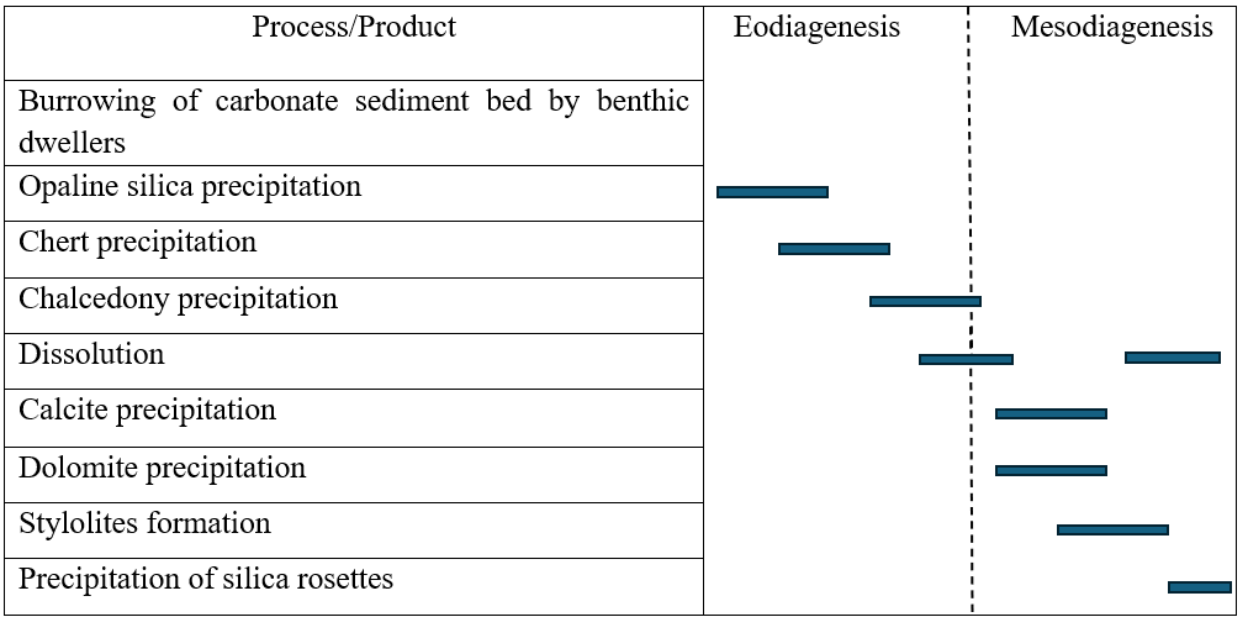

Figure 4.2 - Diagenetic processes and products observed during the formation of silica nodules in the Florence Limestone.

The gradual increase in crystallinity from opaline silica to megaquartz and chalcedony suggests that burial and diagenesis led to the formation of more stable quartz forms from meta-stable phases through a series of replacive reactions (Aoyagi & Kazama, 1980; Williams et al., 1985; Hesse & Schacht, 2011). Since silica rosettes occur in minor abundances, it was impossible to isolate this phase for isotopic analysis, and hence, the expected temperature of

precipitation of this phase remains speculative, but possibly be indicating even higher temperatures above 70º C during mesodiagenesis.

4.3 Sources of Silica

As discussed above, the bulk of silicification occurred at low temperatures (below or around 70º C), and therefore, a magmatic/volcanic silica source can be ruled out (except perhaps for the silica rosettes). The most compelling evidence for the silica source comes from the Ge/Si ratios (Table 3.6). Germanium and silicon have similar properties in the marine environment, and the former commonly substitutes for the latter in mineral phases forming in seawater, such as opal (Tribovillard et al., 2011). Since the Ge/Si ratios in biogenic silica, detrital and hydrothermal fluids have very characteristic Ge/Si ratios (Evans & Derry, 2002; Hammond et al., 2004; Tribovillard, 2013; Dong et al., 2015; Wang et al., 2022), this ratio allows the determination of silica sources.

The Ge/Si ratios for the six silica samples in this study are compared with the experimental data from Tribovillard et al. (2011) and Tribovillard (2013) in Figure 4.3. Ge/Si ratios in the studied silica nodules (ranging from 0.4×10^6 - 1.25×10^6) are similar to those of modern sponges and much lower than riverine (Wang et al., 2022) and hydrothermal-magmatic silica, the latter of which has Ge/Si ratios varying from 11 to 308 (Hammond et al., 2004; Dong et al., 2015; Wang et al., 2022). These data imply a biogenic origin for the silica, primarily sourced in sponge spicules.

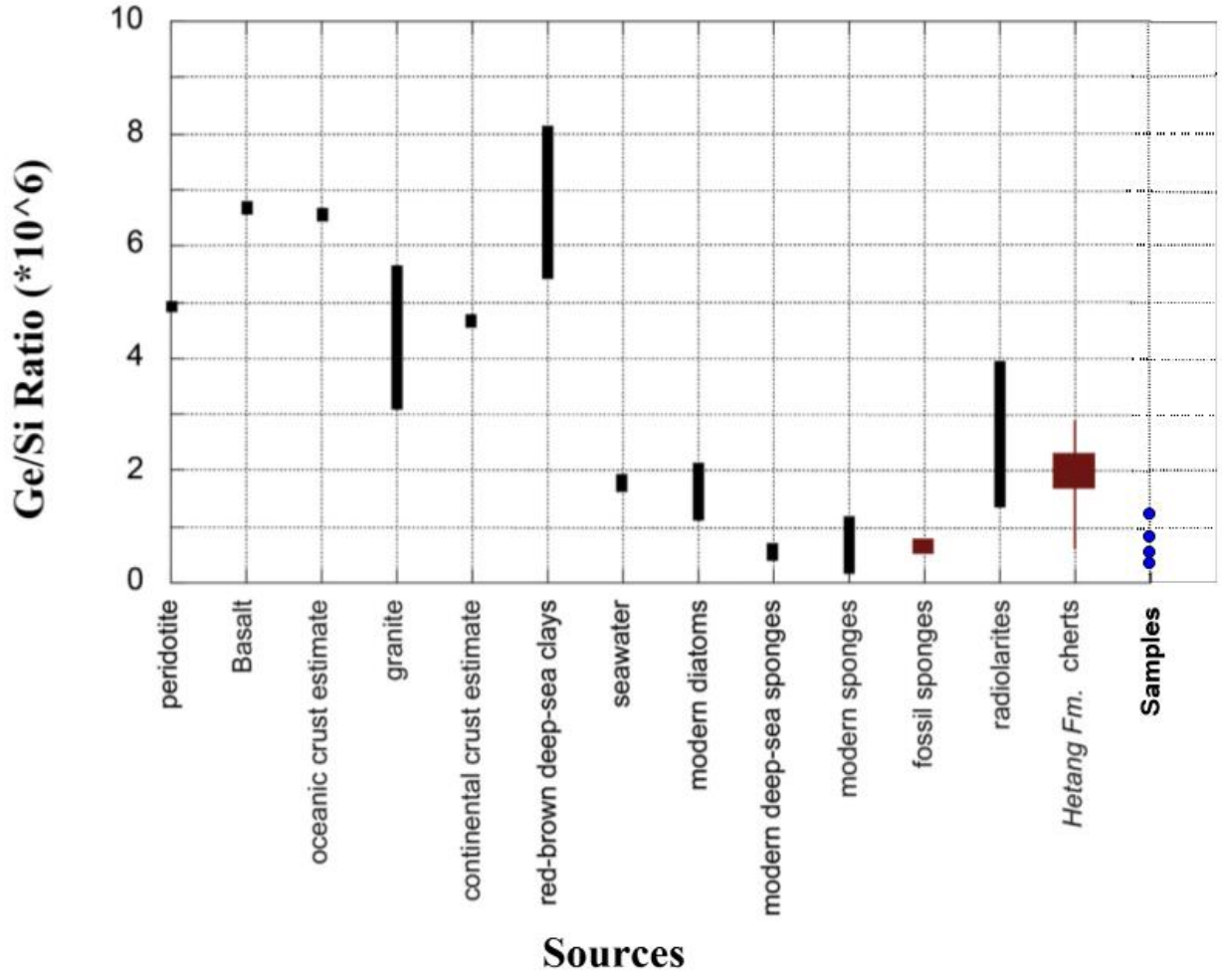

Figure 4.3 - Ge/Si ratios from this study (blue circles) compared with Ge/Si ratio from different sources of silica (Modified from Tribovillard et al., 2011; Tribovillard, 2013).

Furthermore, the biogenic origin of silica is supported by petrographic observations. Sponge spicules (individual and clustered bioclasts) and rare radiolarians were observed in thin sections (Figures 3.6-c and d), with siliceous bioclasts originally accounting for an average of 3.6% but up to 10% in one of the samples. It is possible that the original content of siliceous bioclasts in the Florence Limestone was much greater than the percentage observed since most bioclasts have been either recrystallized to different silica forms (what makes petrographic identification challenging) or dissolved (since silica dissolution is favored under higher pH).

In addition to the significant contribution of siliceous bioclasts as a silica source, climatically controlled evaporative conditions likely increased silica concentration. Evidence of the association between silica and evaporites is present in several thin sections, including a) anhydrite inclusions and barite within megaquartz crystals (Figure 3.12), forming centimetric nodules that displace the host sediment (Figure 4.4 below), and b) the occurrence of quartzine (length-slow chalcedony) spherulites. The formation of polyhalite and anhydrite is commonly associated with mineral precipitations in sabkhas (Folk & Pittman, 1971; Herrero et al., 2020), and Milliken (1979) dubbed the co-existence of quartzine and megaquartz as "silicified evaporite syndrome" since length-slow chalcedony almost exclusively occurs with sulfates and evaporites (Folk & Pittman, 1971). The presence of evaporative solutions was favored by the paleogeographic setting where the Permian sediments accumulated (discussed below).

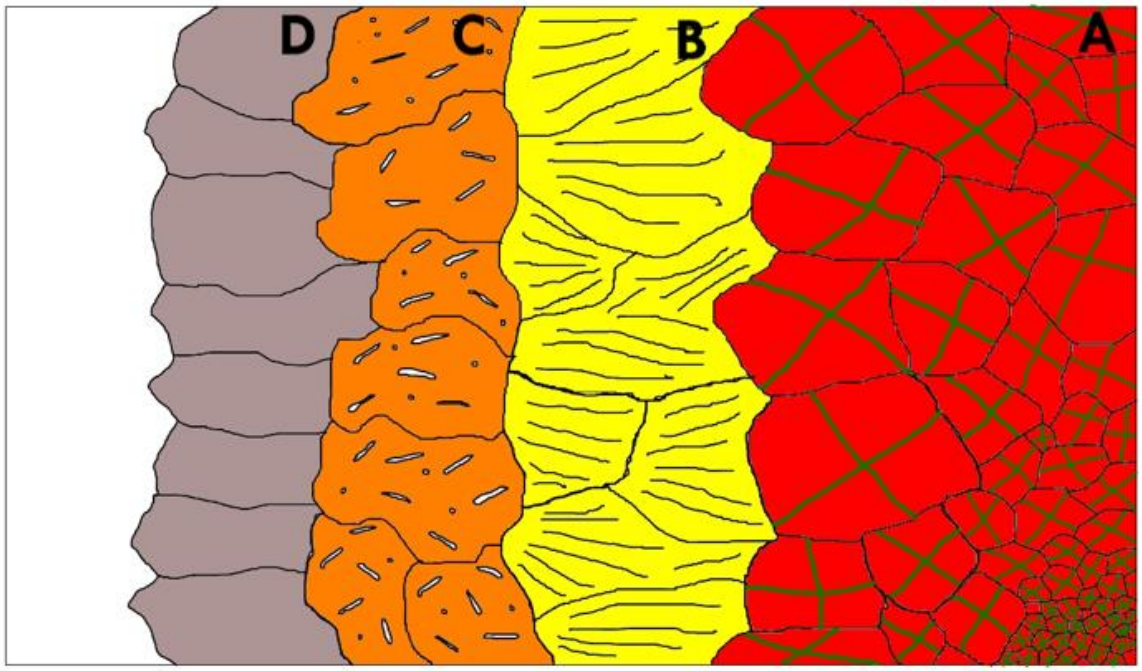

Figure 4.4 - Schematic illustration of an evaporite nodule observed in the studied thin sections. A- Quartzine spherulites of different sizes, B- Megaquartz with undulous extinction, C- Megaquartz with anhydrite inclusions, D- Prismatic barite crystals.

4.4 Permian Paleogeography

During the Wolfcampian, the North American midcontinent lay within the low-relief interior of the Pangeae supercontinent, which drifted towards higher latitudes with time (Rowley et al., 1985; Witzke, 1990). Kansas, along with a significant part of the present North American continent, was covered by an epicontinental sea during the Early Permian (Figure 4.5).

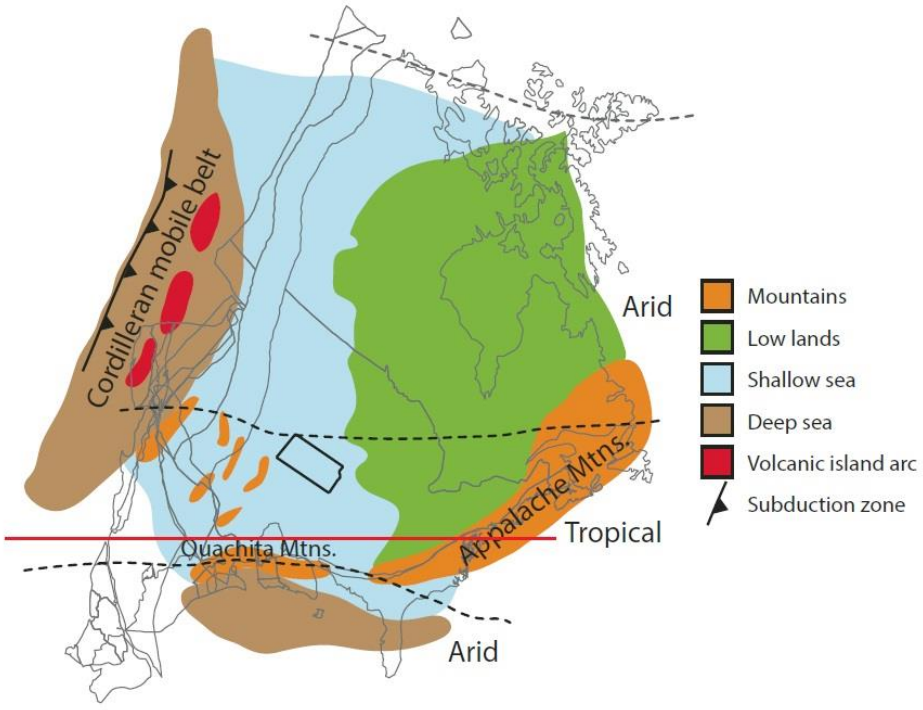

Figure 4.5 - Paleogeography of North America in the Early Permian. Kansas is marked by solid black margins and paleoequator is marked by a red solid line (Modified after Goldberg & Miller, 2019).

The Permian Midcontinent Basin experienced frequent sea level fluctuations that gave rise to cyclothems, repeated cycles of alternating clastic and carbonate deposits (Goldberg & Miller, 2019). Cyclothems are interpreted as driven by glacio-eustatic sea-level fluctuations

caused by Milankovich cycles, resulting in climate changes from arid to monsoonal (Miller et al., 1996). Globally, the widespread continental glaciation from the Pennsylvanian to the early Permian declined later towards the end of the Permian (Roscher & Schneider, 2006). The late Permian also marks the transition from humid to more arid climates in equatorial Pangea (Tabor & Poulsen, 2008).

The Permian Midcontinent Basin was located near the paleo-equator (Figure 4.6), where sufficient sunlight and warm waters favored primary productivity in the shallow ocean, sustaining a diverse, thriving marine community that included carbonate producers, sponges, and other marine fauna and flora (Rigby & Senowbari-Daryan, 1995; Murchey, 2004; Liu et al., 2008). Towards later stages, geologic records from Dongpan and Ma'anying sections, South China reveals 88% - 90% types and 88% - 92% forms of sponge spicules gradually extincted towards the end of Pemian period supplying sufficient silica to ocean water (Liu et al., 2008; Liu et al., 2014).

Figure 4.6 - Paleogeographic reconstruction of North America, with Kansas (red arrow) located close to the paleo equator (yellow line) (Blakey & Ranney, 2018).

In this shallow, oxygenated, warm and nutrient-rich environment where carbonate particles and the remains of pelagic siliceous organisms accumulated, a thriving benthic community was likely to exist, including infaunal organisms and deposit-feeders that reworked the sediments, ultimately forming burrows that fossilized as trace fossils such as Thalassinoides. These burrows may have provided a pathway for the percolation of silica-rich solutions that kicked off the precipitation of opaline silica as the initial silica phase, as discussed below. The low latitude position of this shallow marine engulfment may also favored the development of

evaporative conditions, similar to the modern-day Persian Gulf region, especially toward the middle Permian.

4.5 Mechanism of Nodule Formation

Integrating the results obtained from field observations, petrographic, isotopic, and other complementary analyses allows the portrait of the mechanism involved in nodule formation. As the first stage, high silica concentration in seawater was driven by the dissolution of siliceous bioclasts in the bottom levels of ocean (sponge spicules and radiolarians), augmented by evaporative solutions. These silica-rich solutions efficiently percolated burrow networks existing at (or near) the sediment-water interface, precipitating opaline silica along these permeable zones. This initial silicification occurred shortly after the deposition of the carbonate sediments that formed the Florence Limestone, both through cementation and replacement of allochems and micrite.

The precipitation of opaline silica along the burrows lowered silica activity in the ocean water, thereby prompting the nucleation of larger and more crystalline silica types. Concomitant with progressive burial, this allowed the successive precipitation of chert, chalcedony, and finally quartz at later stages. As the sediments were increasingly buried and compacted, the percolation of basinal fluids led to the partial dissolution of primary and eodiagenetic constituents (generating secondary porosity) and precipitation of diagenetic carbonates (Figure 3.11). As the final stage, minor phase of silicification, associated with the percolation of silica-rich (hydrothermal?) fluids along stylolitic surfaces, resulted in the localized formation of silica rosettes (Figure 3.14). The existence of a burrow network seems to be relevant for the

percolation of silicifying solutions even during later stages of diagenesis, as the highest percentages of chert and silica rosettes is found in burrow/homogeneous (Type 4) silica nodules.

Another finding of this study is the stratigraphic distribution of different types of silica nodules. Type 4 nodules (with morphologies resembling burrow networks) are more abundant in the lower sections. Type 5 (wood-grained) nodules occur in the middle section of the Florence Limestone, and type 3 (rimmed) nodules in the top section. The wood-grained texture expresses the alternation of micritic matrix and opaline silica (Figure 4.7). Maliva et al. (1999) suggested that this texture is formed by the late diagenetic replacement, with the lamination pattern strongly suggesting growth fronts. The wood-grained texture and the rims around the nodules are interpreted as secondary features. In other words, all the nodules were initially formed associated with burrow networks, aided by the high permeability of these conduits, but later on, they may or may not have been modified or differentiated by the percolation of late solutions (by replacement reactions). The fact that randomly branched ‘preserved’ nodules are found preferentially at the bottom of the succession suggests that these secondary solutions might have infiltrated from the top.

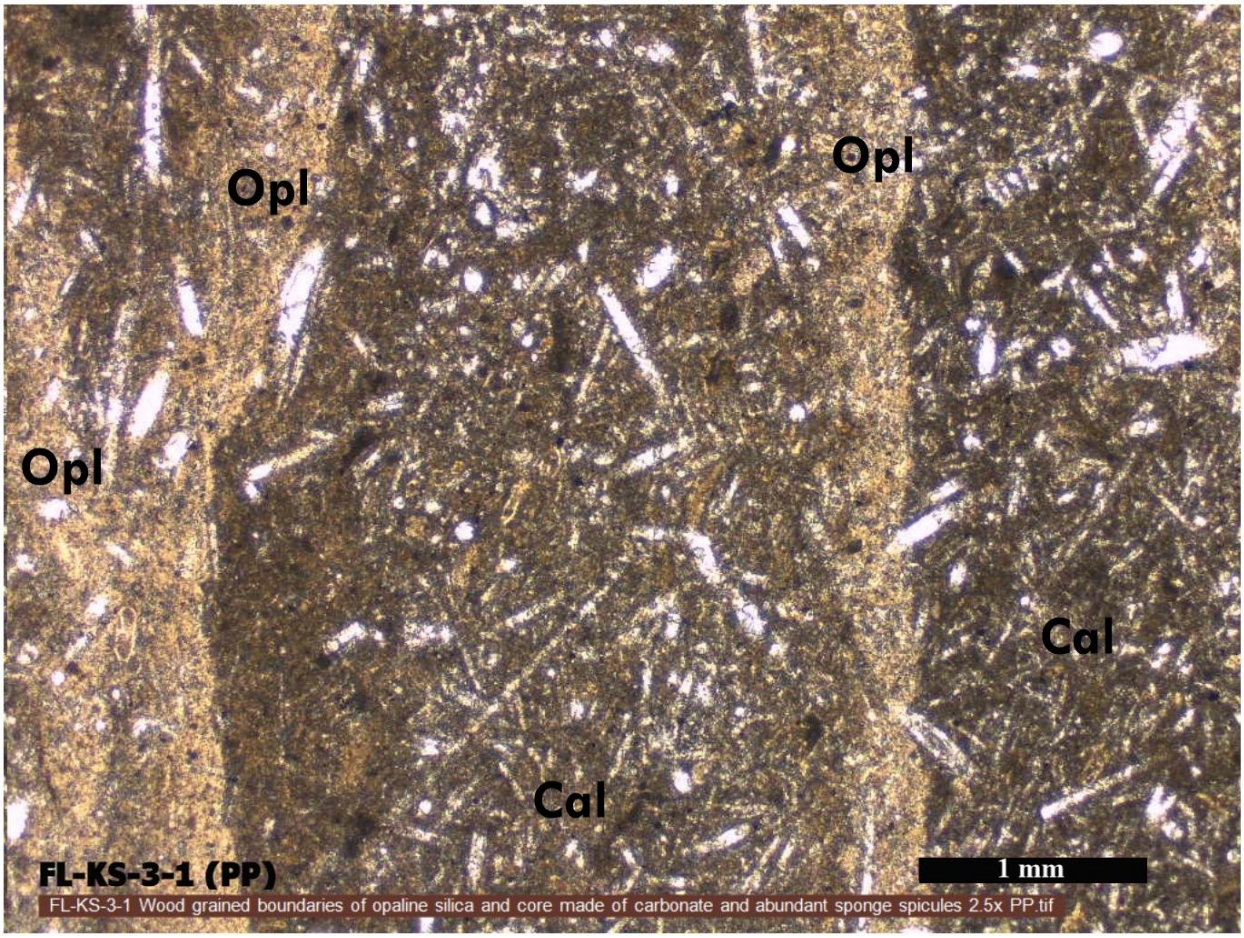

Figure 4.7 - Alternating opaline silica and micrite zones, forming the wood-grained texture. Note the abundant sponge spicules within the micrite matrix (Opl- opaline silica, Cal- micrite matrix).

Likewise, the rimmed nodules (Type 3; Figure 3.4) resemble a reaction around burrow-shaped Type 4 nodules. Therefore, it can be interpreted that other diagenetic minerals like rhombic calcite, dolomite and oxides later replaced the silica-filled burrows. These later solutions could be either basinal, percolating during mesodiagenesis, or even telodiagenetic, related to the overall sea-level fall and climate change toward arid conditions that characterized the Midcontinent Basin in Kansas during the Late Permian (West et al., 2010).

Sea-level and/or climate variations might also have controlled the occurrence of multiple "layers" of coalescing silica nodules in the Florence Limestone. The realization that these nodules were formed along burrow networks is indicative of the formation of hardgrounds, which are surfaces of synsedimentarily cemented carbonate layers that have been exposed on the seafloor (Wilson & Palmer, 1992), and hence a lithified seafloor. These surfaces represent stratigraphic discontinuities commonly developed under low sedimentation rates in starved basins, commonly marking the position of flooding surfaces. The relative position and frequency of these hardgrounds could have been controlled by Milankovitch cyclicity, but this requires further research to confirm.

Chapter 5 - Conclusions

By integrating field data with petrological, geochemical, and isotopic data, this study provides new insights into the origin and paragenetic relations of silica nodules in the Florence Limestone. Our main conclusions include the following:-

- Silicification occurred in multiple stages. The “chert nodules” comprise four main silica types: opaline silica, chert, chalcedony, and quartz, with minor silica rosettes and quartzine.
- Although chert is the major silica type in the nodules, the term “chert nodules” might mislead the original composition of nodules. Hence, the use of a broader term like “silica nodules” may be more representative of the actual silica mineralogy in the nodules.
- The silica for the nodules originated from a biogenic source (based on the Ge/Si ratios and petrographic evidence), through the dissolution of sponge spicules and subordinately radiolarians. A secondary source of silica derived from evaporitive solutions conditioned by the arid/semi-arid setting. No evidence was found for the contribution of hydrothermal-magmatic solutions; if the latter happened, it would possibly have been at later stages of silicification, associated with the precipitation of silica rosettes under mesodiagenetic conditions.
- The oxygen isotope composition of silica nodules was not effective for the calculation of silicification temperatures due to the overprint resulting from deeper burial of nodules. The transformation of opaline silica into chert indicates that the precipitation temperature must have been at least 63° C.
- The initial silicification was triggered by high silica activity in the ocean water, resulting from the dissolution of siliceous organic debris augmented by highly evaporative conditions.

Abundant bioturbation in the seafloor led to the development of burrow networks that provided preferential pathways for the percolation of silicifying solutions due to increased permeability in the burrows, which allowed the precipitation of opaline silica as the first silica phase. With increased burial, metastable silica phases gave rise to more stable ones, including chert, chalcedony, and quartz.

Bibliography

Adachi, M., Yamamoto, K., & Sugisaki, R. (1986). *Hydrothermal Chert and Associated Siliceous Rocks from the Northern Pacific: Their Geological Significance as Indication of Ocean Ridge Activity*. *Sedimentary Geology*, *47*(1-2), 125-148.

Allwood, A. C., Walter, M. R., & Marshall, C. P. (2006). Raman spectroscopy reveals thermal palaeoenvironments of c.3.5 billion-year-old organic matter. *Vibrational Spectroscopy*, *41*(2), 190–197. https://doi.org/10.1016/j.vibspec.2006.02.006

Aoyagi, K., & Kazama, T. (1980). Transformational changes of clay minerals, zeolites and silica minerals during diagenesis. *Sedimentology*, *27*(2), 179-188.

Banerjee, A., Patranabis-Deb, S., Saha, D., & Santosh, M. (2021). Inorganic silicification of ancient carbonate rocks. *Journal of Sedimentary Research*, *91*(2), 186–196. https://doi.org/10.2110/JSR.2020.099

Banks, N. G. (1970). Leadviller chert origin. *Geological Society of America Bulletin*, *81*, 3033–3048.

Behl, R. J. (2011). Chert spheroids of the Monterey Formation, California (USA): Early-diagenetic structures of bedded siliceous deposits. *Sedimentology*, *58*(2), 325–351. https://doi.org/10.1111/j.1365-3091.2010.01165.x

Behr Hans. (2002). Magadiite and Magadi chert - a critical analysis of the silica sediments in the Lake Magadi Basin Kenya. *SEPM Special Publication*, *No.73*, 257–273.

Benway, H. M., & Mix, A. C. (2004). Oxygen isotopes, upper-ocean salinity, and precipitation sources in the eastern tropical Pacific. *Earth and Planetary Science Letters*, *224*(3–4), 493–507. https://doi.org/10.1016/j.epsl.2004.05.014

Blakey, R. (2021). Paleotectonic and paleogeographic history of the arctic region. *Atlantic Geology*, *57*, 7–39. https://doi.org/10.4138/atlgeol.2021.002

Blakey, R. C., & Wong, T. E. (2003, August). Carboniferous–Permian paleogeography of the assembly of Pangaea. In *Proceedings of the XVth International Congress on Carboniferous and Permian Stratigraphy. Utrecht* (Vol. 10, p. 16).

Bohrmann, G., Abelmann, A., Gersonde, R., Hubberten, H., & Kuhn, G. (1994). Pure siliceous ooze, a diagenetic environment for early chert formation. *Geology*, *22*(3), 207-210.

Bosak, T., Moore, K. R., Gong, J., & Grotzinger, J. P. (2021). Searching for biosignatures in sedimentary rocks from early Earth and Mars. In *Nature Reviews Earth and Environment* (Vol. 2, Issue 7, pp. 490–506). Springer Nature. https://doi.org/10.1038/s43017-021-00169-5

Bramkamp, R. T., & Powers, R. W. (1958). Classification of Arabian carbonate rocks. *Geological Society of America Bulletin*, *69*(10), 1305-1318.

Brenna, B. L. (2016). *The chemical, physical, and microbial origins of Pleistocene cherts at Lake Magadi, Kenya Rift Valley* (Doctoral dissertation, University of Saskatchewan).

Brumsack, H. J., Zuleger, E., Gohn, E., & Murray, R. W. (1992). 36. Stable And Radiogenic Isotopes In Pore Waters From Leg 127, Japan Sea1.

Calvert, S. E. (1974). *Deposition and Diagenesis of Silica in Marine Sediments*. *Pelagic sediments: on land and under the sea*, 273-299.

Campbell, K. A., Guido, D. M., Gautret, P., Foucher, F., Ramboz, C., & Westall, F. (2015). Geyserite in hot-spring siliceous sinter: Window on Earth's hottest terrestrial (paleo)environment and its extreme life. In *Earth-Science Reviews* (Vol. 148, pp. 44–64). Elsevier B.V. https://doi.org/10.1016/j.earscirev.2015.05.009

Chanda, S. K., Bhattacharyya, A., & Sarkar, S. (1976). *Early Diagenetic Chert Nodules in Bhander Limestone, Maihar, Satna District, Madya Pradesh, India*. *The Journal of Geology*, *84*(2), 213-224. http://www.journals.uchicago.edu/t-and-c.

Chen, D., Qing, H., Yan, X., & Li, H. (2006). Hydrothermal venting and basin evolution (Devonian, South China): Constraints from rare earth element geochemistry of chert. *Sedimentary Geology*, *183*(3–4), 203–216. https://doi.org/10.1016/j.sedgeo.2005.09.020

Choquette, P. W., & James, N. P. (1987). DIAGENESIS #12. Diagenesis in Limestones-3. The Deep Burial Environment. *Geoscience Canada*, *14*(1), 3–35.

Clayton, R. N., & Epstein, S. (1961). *The Use of Oxygen Isotopes in High-Temperature Geological Thermometry*. *The Journal of Geology*, *69*(4), 447-452. http://www.journals.uchicago.edu/t-and-c.

Crerar, D. A., & Anderson, G. M. (1971). *Solubility and Solvation Reactions of Quartz in Dilute Hydrothermal Solutions*. *Chemical Geology*, *8*(2), 107-122.

Curtis, N. J., Gascooke, J. R., Johnston, M. R., & Pring, A. (2019). A review of the classification of opal with reference to recent new localities. *Minerals*, *9*(5). 299 https://doi.org/10.3390/min9050299

Dapples, E. C. (1967). Silica as an Agent in Diagenesis. *Developments in Sedimentology*, *8*(C), 323–342. https://doi.org/10.1016/S0070-4571(08)70845-8

David Zipser, H. P. E. (1967). *Hydrous Sodium Silicates from Lake Magadi, Kenya: Precursors of Bedded Chert*. *VOL. 157*(3793), 1177-1180.

Duane, M. J., Al-Zamel, A., & Eastoe, C. J. (2004). Stable isotope (chlorine, hydrogen and oxygen), geochemical and field evidence for continental fluid flow vectors in the Al-Khiran sabkha (Kuwait). *Journal of African Earth Sciences*, *40*(1–2), 49–60. https://doi.org/10.1016/j.jafrearsci.2004.07.004

Ekdale, A. A., & Bromley, R. G. (1984). Trace Fossils and Paleoenvironments: Marine Carbonate, Marginal Marine Terrigenous and Continental Terrigenous Settings. In *Source: Journal of Paleontology (Vol. 58, Issue 2) 283-284.* http://www.jstor.orgURL:http://www.jstor.org/stable/1304787

Elzea, J. M., & Rice, S. B. (1996). *Tem And X-Ray Diffraction Evidence For Cristobalite And Tridymite Stacking Sequences In Opal, Clays and Clay Minerals, (Vol. 44, Issue 4) 492-500*.

Götze, J., Plötze, M., & Habermann, D. (2001). Origin, spectral characteristics and practical applications of the cathodoluminescence (CL) of quartz–a review. *Mineralogy and petrology*, *71*, 225-250.

Evans, M. J., & Derry, L. A. (2002). Quartz control of high germanium/silicon ratios in geothermal waters. In *Geology* (Issue 11) *1019-1022*. www.geosociety.org/pubs/

Folk, R. L., & Pittman, A. J. S. (1971). Length-Slow Chalcedony: A New Testament For Vanished Evaporites 1. In *Journal Of Sedimentary Petrology* (Vol. 41, Issue 4) 1045-1058.

Fournier, R. O., & Rowe, J. J. (1966). Estimation of Underground Temperatures from the Silica Content of Water from Hot Springs and Wet-Steam Wells. *American Journal of Science*, *264*, 685–697.

Frelinger, S. N., Ledvina, M. D., Kyle, J. R., & Zhao, D. (2015). Scanning electron microscopy cathodoluminescence of quartz: Principles, techniques and applications in

ore geology. *Ore Geology Reviews*, *65*(P4), 840–852. https://doi.org/10.1016/j.oregeorev.2014.10.008

Frydenvang, J., Gasda, P. J., Hurowitz, J. A., Grotzinger, J. P., Wiens, R. C., Newsom, H. E., Edgett, K. S., Watkins, J., Bridges, J. C., Maurice, S., Fisk, M. R., Johnson, J. R., Rapin, W., Stein, N. T., Clegg, S. M., Schwenzer, S. P., Bedford, C. C., Edwards, P., Mangold, N., … Vasavada, A. R. (2017). Diagenetic silica enrichment and late-stage groundwater activity in Gale crater, Mars. *Geophysical Research Letters*, *44*(10), 4716–4724. https://doi.org/10.1002/2017GL073323

Füchtbauer, H., Leggewie, R., Gockeln, C., Heinemann, Chr., & Schröder, P. (1982). Methods of quartz investigations, applied to Mesozoic and Pleistocene sandstones and sands. *Neues Jahrbuch Für Geologie Und Paläontologie - Monatshefte*, *1982*(4), 193–210. https://doi.org/10.1127/njgpm/1982/1982/193

Gao, P., He, Z., Lash, G. G., Li, S., Xiao, X., Han, Y., & Zhang, R. (2020). Mixed seawater and hydrothermal sources of nodular chert in Middle Permian limestone on the eastern Paleo-Tethys margin (South China). *Palaeogeography, Palaeoclimatology, Palaeoecology*, *551*. https://doi.org/10.1016/j.palaeo.2020.109740

Goldberg, K., & Miller, K. B. (2019). Geology of the Flint Hills, Kansas: Sea-level and climate changes in the Permian. In *Exploring Extreme and Unusual Geology in the Stable Midcontinent: Field Excursions for the 2019 GSA South-Central, North-Central, and Rocky Mountain Sections Joint Meeting* (pp. 1–24). Geological Society of America. https://doi.org/10.1130/2019.0052(01)

Hart, M. B. (1993). Chert formation in the Portland Limestone Formation (Upper Jurassic) of the Dorset coast; a preliminary investigation. *Proceedings-Ussher Society*, *8*, *181-181*. https://www.researchgate.net/publication/267951583.

Hart, S. R., & Steinhart, J. S. (1965). Chert: Modern Inorganic Deposition in a Carbonate-Precipitating Locality. In *Cornell Univ. Agr. Exp. Sta* (Vol. 378, Issue 4).

Hatem, E., Tribovillard, N., Averbuch, O., Bout-Roumazeilles, V., Trentesaux, A., Deconinck, J. F., Baudin, F., & Adatte, T. (2017). Small-scaled lateral variations of an organic-rich formation in a ramp-type depositional environment (the Late Jurassic of the Boulonnais, France): impact of the clastic supply. *Bulletin de La Societe Geologique de France*, *188*(5). https://doi.org/10.1051/bsgf/2017193

Herrero, M. J., Marfil, R., Escavy, J. I., Al-Aasm, I., & Scherer, M. (2020). Diagenetic origin of bipyramidal quartz and hydrothermal aragonites within the upper triassic saline succession of the iberian basin: Implications for interpreting the burial–thermal evolution of the basin. *Minerals*, *10*(2). 177. https://doi.org/10.3390/min10020177

Hesse, R. (1988). Origin of chert: Diagenesis of Biogenic Siliceous Sediments. *The Geological Association of Canada*, *15*(3), 171–192.

Hesse, R. (1989). Silica diagenesis: origin of inorganic and replacement cherts. *Earth-Science Reviews*, *26*(1-3), 253-284.

Hesse, R., & Schacht, U. (2011a). *Early Diagenesis of Deep-Sea Sediments*. https://doi.org/10.1016/S0070-4571(11)63009-4

Hesse, R., & Schacht, U. (2011). Early diagenesis of deep-sea sediments. *Developments in Sedimentology*, *63*, 557-713.

Ilieva, A., Mihailova, B., Tsintsov, Z., & Petrov, O. (2007). Structural state of microcrystalline opals: A Raman spectroscopic study. *American Mineralogist*, *92*(8–9), 1325–1333. https://doi.org/10.2138/am.2007.2482

Jones, B. (2021). Siliceous sinters in thermal spring systems: Review of their mineralogy, diagenesis, and fabrics. In *Sedimentary Geology* (Vol. 413). Elsevier B.V. https://doi.org/10.1016/j.sedgeo.2020.105820

Jones, B., & Renautt, R. W. (1997). Formation of silica oncoids around geysers and hot springs at El Tatio, northern Chile. In *Sedimentology* (Vol. 44).

Jones, J. B., & Segnit, E. R. (1971). The nature of opal I. nomenclature and constituent phases. *Journal of the Geological Society of Australia*, *18*(1), 57–67. https://doi.org/10.1080/00167617108728743

Kimura, M., Weisberg, M. K., Lin, Y., Suzuki, A., Ohtani, E., & Okazaki, R. (2005). Thermal history of the enstatite chondrites from silica polymorphs. *Meteoritics and Planetary Science*, *40*(6), 855–868. https://doi.org/10.1111/j.1945-5100.2005.tb00159.x

Kiran Kumar, P., Singh, A., & Ramesh, R. (2018). Controls on δ18O, δD and δ18O-salinity relationship in the northern Indian Ocean. *Marine Chemistry*, *207*, 55–62. https://doi.org/10.1016/j.marchem.2018.10.010

Paul Knauth, L. (2005). Origin and diagenesis of cherts: an isotopic perspective. In *Isotopic signatures and sedimentary records* (pp. 123-152). Berlin, Heidelberg: Springer Berlin Heidelberg.

Knauth, L. P. (1979). A model for the origin of chert in limestone. *Geology*, *7*(6), 274-277.

Liu, G. C., Feng, Q. L., & Gu, S. Z. (2008). Extinction pattern and process of siliceous sponge spicules in deep-water during the latest Permian in South China. *Science in China, Series D: Earth Sciences*, *51*(11), 1623–1632. https://doi.org/10.1007/s11430-008-0124-2

Liu, G., Feng, Q., Shen, J., Yu, J., He, W., & Algeo, T. J. (2014). Decline of siliceous sponges and spicule miniaturization induced by marine productivity collapse and expanding anoxia during the permian-triassic crisis in South China. *Palaios*, *28*(8), 664–679. https://doi.org/10.2110/palo.2013.p13-035r

Maliva, R. G. *, Dickson, J. A. D., Schiovon, N., & Fallick, A. E. (1999). Self-organization origin of wood-grained chert, Portland Limestone Formation (Upper Jurassic), southern England. *Geol. Mag*, *136*(4), 413–421.

Maliva, R. G., Knoll, A. H., & Simonson, B. M. (2005). Secular change in the Precambrian silica cycle: Insights from chert petrology. In *Bulletin of the Geological Society of America* (Vol. 117, Issues 7–8, pp. 835–845). https://doi.org/10.1130/B25555.1

Maliva, R. G., & Siever, R. (1989). Chertification histories of some Late Mesozoic and Middle Palaeozoic platform carbonates. *Sedimentology*, *36*(5), 907–926. https://doi.org/10.1111/j.1365-3091.1989.tb01753.x

Marshall, A. O., Emry, J. R., & Marshall, C. P. (2012). Multiple generations of carbon in the apex chert and implications for preservation of microfossils. *Astrobiology*, *12*(2), 160–166. https://doi.org/10.1089/ast.2011.0729

Matheney, R. K., & Knauth, L. P. (1993). *New isotopic temperature estimates for early silica diagenesis in bedded cherts*. *Geology*, *21*(6), 519-522.

Matysik, M., Stemmerik, L., Olaussen, S., Rameil, N., Gianotten, I. P., & Brunstad, H. (2021). Cherts, spiculites, and collapse breccias – Porosity generation in upper Permian reservoir rocks, Gohta discovery, Loppa High, south-western Barents Sea. *Marine and Petroleum Geology*, *128*. https://doi.org/10.1016/j.marpetgeo.2021.105043

Mazzullo, S. J., & Harris, P. M. (1991). An overview of dissolution porosity development in the deep-burial environment, with examples from carbonate reservoirs in the Permian Basin. *West Texas Geological Society, Midland, TX*, 91-89.

Mccahon, T. J., & Miller, K. B. (1997). Climatic significance of natric horizons in Permian (Asselian) palaeosols of north-central Kansas, USA. In *Sedimentology* (Vol. 44).

Mclemore, V., & Barker, J. M. (1987). *Some Geological Applications of Cathodoluminescence Examples from the Lemitar Mountains and Riley Travertine, Socorro County, New Mexico*. *New Mexico Geology*, *9*, 37-40.

McManus, J., Hammond, D. E., Cummins, K., Klinkhammer, G. P., & Berelson, W. M. (2003). Diagenetic Ge-Si fractionation in continental margin environments: Further evidence for a nonopal Ge sink. *Geochimica et Cosmochimica Acta*, *67*(23), 4545–4557. https://doi.org/10.1016/S0016-7037(03)00385-5

Miller, K. B. (2001). *Geology of the Kansas Flint Hills: Ancient Ice Ages, Sea Levels, and Climate Change Fieldtrip Guidebook 2001 Meeting of the American Scientific Affiliation*.

Miller, K. B., McCahon, T. J., & West, R. R. (1996). Lower Permian (Wolfcampian) Paleosol-Bearing Cycles of the U.S. Midcontinent: Evidence of Climate Cyclicity. *Journal of Sedimentary Research*, *66*(1), 71–84.

Miller, Keith. B., & Twiss, Page. C. (1994). Rocks of the Milford Lake Spillway. *Kansas Geological Survey Open File Report*.

Milliken, K. Lou. (1979). The Silicified Evaporite Syndrome-Two Aspects Of Silicification History Of Former Evaporite Nodules From Southern Kentucky And Northern Tennessee. In *Journal Of Sedimentary Petrology* (Vol. 49, Issue 1). 245-256.

Mizutani, S. (1970). Silica Minerals in the Early Stage of Diagenesis. *Sedimentology*, *15*(3–4), 419–436. https://doi.org/10.1111/j.1365-3091.1970.tb02193.x

Moore, C. H., & Wade, W. J. (2013). Burial diagenetic environment. In *Developments in Sedimentology* (Vol. 67, pp. 239–284). Elsevier B.V. https://doi.org/10.1016/B978-0-444-53831-4.00010-0

Morad, S., Ketzer, J. M., & De Ros, L. R. (2000). Spatial and temporal distribution of diagenetic alterations in siliciclastic rocks: Implications for mass transfer in

sedimentary basins. In *Sedimentology* (Vol. 47, Issue SUPPL. 1, pp. 95–120). https://doi.org/10.1046/j.1365-3091.2000.00007.x

Murchey, B. L. (2004). Regional analysis of spiculite faunas in the Permian Phosphoria Basin: implications for paleoceanography. In *Handbook of Exploration and Environmental Geochemistry* (Vol. 8, pp. 111-135). Elsevier Science BV.

Murray, R. W., Jones, D. L., & Brink, M. R. B. T. (1992). Diagenetic formation of bedded chert: evidence from chemistry of the chert-shale couplet. *Geology*, *20*(3), 271-274.

Packard, J. J., Al-Aasm, I., Samson, I., Berger, Z., & Davies, J. (2001). A Devonian Hydrothermalchert Reservoir: The 225 bcf Parkland Field, British Columbia, Canada. *AAPG Bulletin*, *85*(1), 51–84.

Pandey, D. K., Fürsich, F. T., Alberti, M., Sharma, J. K., & Swami, N. (2018). Recurrent hardgrounds and their significance for intra-basinal correlations: a case study of upper Bathonian rocks from the western margin of the Indian craton. *Journal of Palaeogeography, 7*(1). 1-12. https://doi.org/10.1186/s42501-018-0013-3.

Peltonen, C., Marcussen, Ø., Bjørlykke, K., & Jahren, J. (2009). Clay mineral diagenesis and quartz cementation in mudstones: The effects of smectite to illite reaction on rock properties. *Marine and Petroleum Geology*, *26*(6), 887–898. https://doi.org/10.1016/j.marpetgeo.2008.01.021

Perry, E. C., & Lefticariu, L. (2007). *Formation and Geochemistry of Precambrian Cherts*. (Vol. 7, p. 407).

Pop, D., Constantina, C., Tătar, D., & Kiefer, W. (2004). *Raman Spectroscopy on Gem-Quality Microcrystalline and Amorphous Silica Varieties from Romania*. *Studia UBB Geologia*, *49*(1), 41-52.

Qiu, Z., & Wang, Q. C. (2011). Geochemical evidence for submarine hydrothermal origin of the Middle-Upper Permian chert in Laibin of Guangxi, China. *Science China Earth Sciences*, *54*(7), 1011–1023. https://doi.org/10.1007/s11430-011-4198-x

Raviolo, M. M., Barbosa, J. A., Neumann, V. H., & Leal, R. (2009). Characteristics, distribution and diagenetic stages of chert in the La Silla Formation (Lower Ordovician), Argentine Precordillera. *"Main" — 2009/10/20 — 20:07 — Page 781 — #1Anais Da Academia Brasileira de Ciências (2009) 81(4): 781-792(Annals of the Brazilian Academy of Scie*, *81*(4), 781–792. www.scielo.br/aabc

Renaut, R. W., Jones, B., & Rosen, M. R. (1996). Primary Silica Oncoids From Orakeikorako Hot Springs, North Island, New Zealand. In *Source: PALAIOS* (Vol. 11, Issue 5). 446-458.

Richiano, S., Schwarz, E., Veiga, G. D., & Trentini, G. Á. (2019). Non-depositional and erosional “offshore” bioeroded hardgrounds from the Lower Cretaceous of the Neuquén Basin, Argentina: Insights into their sequence-stratigraphic implications and controls. *Marine and Petroleum Geology*, *104*, 1–10. https://doi.org/10.1016/j.marpetgeo.2019.03.020

Rigby, K., & Senowbari-Daryan, B. (1995). Permian sponge biogeography and biostratigraphy. In *The Permian of Northern Pangea: Volume 1: Paleogeography, Paleoclimates, Stratigraphy* (pp. 153-166). Berlin, Heidelberg: Springer Berlin Heidelberg.

Rimstidt, J. D., & Cole, D. R. (1983). Geothermal mineralization-i-the mechanism of formation of the Beowawe Nevada siliceous sinter deposit. *American Journal of Science*, *283*, 861–875.

Roscher, M., & Schneider, J. W. (2006). Permo-Carboniferous climate: Early Pennsylvanian to Late Permian climate development of central Europe in a regional and global context. *Geological Society Special Publication*, *265*, 95–136. https://doi.org/10.1144/GSL.SP.2006.265.01.05

Rowley, D. B., Raymond, A., Parrish, J. T., Lottes, A. L., Scotese, C. R., & Ziegler, A. M. (1985). Carboniferous Paleogeographic, Phytogeographic and Paleoclimatic Reconstruction. *International Journal of Coal Geology*, *5*, 7–42.

Ruppert, L. F. (1986). Applications of Cathodoluminescence of Quartz and Feldspar to Sedimentary Petrology. In *Scanning Microscopy* (Vol. 1, Issue 1). https://digitalcommons.usu.edu/microscopyAvailableat:https://digitalcommons.usu.edu/microscopy/vol1/iss1/7

Schubev, K. A., & Simonson, B. M. (1990). *Petrography and Diagenesis of Cherts from Lake Magadi, Kenya*. *Journal of Sedimentary Research*, *60*(5), 761-776.

Scotese, C. R., & Langford, R. P. (1995). *Pangea and the Paleogeography of the Permian*. In *The Permian of Northern Pangea: Volume 1: Paleogeography, Paleoclimates, Stratigraphy* (pp. 3-19). Berlin, Heidelberg: Springer Berlin Heidelberg

Scotese, C. R., & Schettino, A. (2017). Late Permian-Early Jurassic Paleogeography of Western Tethys and the World. In *Permo-Triassic Salt Provinces of Europe, North Africa and the Atlantic Margins: Tectonics and Hydrocarbon Potential* (pp. 57–95). Elsevier. https://doi.org/10.1016/B978-0-12-809417-4.00004-5

Shanks, W. C. P., Morgan, L. A., Balistrieri, L., & Jeffrey, A. C. (2005). *Hydrothermal Vent Fluids, Siliceous Hydrothermal Deposits, and Hydrothermally Altered Sediments in Yellowstone Lake*. In *Thermal Biology Institute Workshop* (pp. 53-72).

Sharp, Z. D., Gibbons, J. A., Maltsev, O., Atudorei, V., Pack, A., Sengupta, S., Shock, E. L., & Knauth, L. P. (2016). A calibration of the triple oxygen isotope fractionation in the SiO2-H2O system and applications to natural samples. *Geochimica et Cosmochimica Acta*, *186*, 105–119. https://doi.org/10.1016/j.gca.2016.04.047

Shen, B., Ma, H., Ye, H., Lang, X., Pei, H., Zhou, C., Zhang, S., & Yang, R. (2018). Hydrothermal origin of syndepositional chert bands and nodules in the Mesoproterozoic Wumishan Formation: Implications for the evolution of Mesoproterozoic cratonic basin, North China. *Precambrian Research*, *310*, 213–228. https://doi.org/10.1016/j.precamres.2018.03.007

Stein, C. L., & Kirkpatrick, R. J. (1976). Experimental Porcelanite Recrystallization Kinetics: A Nucleation and Growth Model. *Journal of Sedimentary Petrology*, *46*(No.02), 430–435.

Sverdrup, E., & Prestholm, E. (1990). Synsedimentary deformation structures and their implications for stylolitization during deeper burial. *Sedimentary geology*, *68*(3), 201-210.

Tabor, N. J., & Poulsen, C. J. (2008). Palaeoclimate across the Late Pennsylvanian-Early Permian tropical palaeolatitudes: A review of climate indicators, their distribution, and relation to palaeophysiographic climate factors. *Palaeogeography, Palaeoclimatology, Palaeoecology*, *268*(3–4), 293–310. https://doi.org/10.1016/j.palaeo.2008.03.052

Tarhan, L. G., Hood, A. V. S., Droser, M. L., Gehling, J. G., & Briggs, D. E. G. (2016). Exceptional preservation of soft-bodied Ediacara Biota promoted by silica-rich oceans. *Geology*, *44*(11), 951–954. https://doi.org/10.1130/G38542.1

Tatzel, M., Frings, P. J., Oelze, M., Herwartz, D., Lünsdorf, N. K., & Wiedenbeck, M. (2022). Chert oxygen isotope ratios are driven by Earth's thermal evolution.

Proceedings of the National Academy of Sciences of the United States of America, *119*(51). https://doi.org/10.1073/pnas.2213076119

Theodor R. Walker. (1962). Reversible Nature of Chert-Carbonate Replacement in Sedimentary Rocks. *Geological Society of America Bulletin*, *73*, 237–242.

Thiry, M., & Millot, G. (1987). Mineralogical forms of silica and their sequence of formation in silcretes. *Journal of Sedimentary Research*, *57*(2), 343-352.

Trewin N H, & Fallick A E. (2009). *Quartz cement origins and budget in the Tumblagooda Sandstone, Western Australia*. John Wiley & Sons.

Tribovillard, N. (2013). The Ge/Si ratio as a tool to recognize biogenic silica in chert. *Comptes Rendus - Geoscience*, *345*(3), 160–165. https://doi.org/10.1016/j.crte.2013.02.005

Tribovillard, N., Bout-Roumazeilles, V., Riboulleau, A., Baudin, F., Danelian, T., & Riquier, L. (2011). Transfer of germanium to marine sediments: Insights from its accumulation in radiolarites and authigenic capture under reducing conditions. Some examples through geological ages. *Chemical Geology*, *282*(3–4), 120–130. https://doi.org/10.1016/j.chemgeo.2011.01.015.

Van Cappellen, P., & Qiu, L. (1997). *Biogenic silica dissolution in sediments of the Southern Ocean. II. Kinetics* (Vol. 44, Issue 5). 1129-1150.

van den Boorn, S. H. J. M., van Bergen, M. J., Nijman, W., & Vroon, P. Z. (2007). Dual role of seawater and hydrothermal fluids in Early Archean chert formation: Evidence from silicon isotopes. *Geology*, *35*(10), 939–942. https://doi.org/10.1130/G24096A.1

Varkouhi, S., & Wells, J. (2020). The relation between temperature and silica benthic exchange rates and implications for near-seabed formation of diagenetic opal. *Results in Geophysical Sciences*, *1–4*, 100002. https://doi.org/10.1016/j.ringps.2020.100002

Wachs, D., & Hein, J. R. (1974). *Petrography and Diagenesis of Franciscan Limestones* (Vol. 44, Issue 4).

Walther, John. V., & Harold, Helgeson. C. (1977). Calculation of the Thermodynamic Properties of Aqueous Silica and the Solubility of Quartz and its Polymorphs at High Pressure and Temperatures. *American Journal of Science*, *277*, 1315–1351.

Wang, Y., Zhao, T., Xu, Z., Sun, H., & Zhang, J. (2022). Ge/Si Ratio of River Water in the Yarlung Tsangpo: Implications for Hydrothermal Input and Chemical Weathering. *Water (Switzerland)*, *14*(2). 181. https://doi.org/10.3390/w14020181

West, R. R., Miller, K. B., & Watney, W. L. (2010). *The Permian System in Kansas*. *Bulletin (Kansas Geological Survey)*, (257), 1-82.

Wheat, C. G., & McManus, J. (2005). The potential role of ridge-flank hydrothermal systems on oceanic germanium and silicon balances. *Geochimica et Cosmochimica Acta*, *69*(8), 2021–2029. https://doi.org/10.1016/j.gca.2004.05.046

White, D. E., Rrannock, W. W., & Murata, K. J. (1956). *Silica in Hot-Spring Water* (Vol. 10). Pcrgamon Preaa Ltd.

Willey, J. D. (1974). The Effect of Pressure on the Solubility of Amorphous Silica in Seawater at 0°C. In *Marine Chemistry* (Vol. 2). 239-250.

Williams, L. A., Crerar, D. A., & Hall, G. (1985). *Silica Diagenesis, II. General Mechanisms 1*. *Journal of Sedimentary Research*, *55*(3), 312-321.

Williams, L. A., Parks, G. A., & Crerar, D. A. (1985). *Silica Diagenesis, I. Solubility Controls*. *Journal of Sedimentary Research*, *55*(3), 301-311.

Wilson, M.A.; Palmer, T.J. (1992). "Hardgrounds and hardground faunas". *University of Wales, Aberystwyth, Institute of Earth Studies Publications.* ***9: 1–131.***

Winter, B. L., & Knauth, L. P. (1992). Stable isotope geochemistry of cherts and carbonates from the 2.0 Ga Gunflint Iron Formation: implications for the depositional setting, and the effects of diagenesis and metamorphism. In *Precambrian Research* (Vol. 59). 283-313.

Wistort, Z. P., Ritterbush, K. A., & Ekdale, A. A. (2019). Trace fossils of problematic origin: Assessing silicified trace fossils from the Permian of Utah, U.S.A. *Palaios*, *34*(12), 631–638. https://doi.org/10.2110/palo.2019.011.

Wistort, Z. P., Ritterbush, K. A., & Ekdale, A. A. (2019). Trace fossils of problematic origin: Assessing silicified trace fossils from the Permian of Utah, U.S.A. *Palaios*, *34*(12), 631–638. https://doi.org/10.2110/palo.2019.011.

Witzke, B. J. (1990). *Palaeoclimatic constraints for Palaeozoic Palaeolatitudes of Laurentia and Euramerica*. *Geological Society, London, Memoirs*, *12*(1), 57-73. http://mem.lyellcollection.org/.

Yao, X., Su, L. I., Zhou, Y., & Hinnov, L. A. (2021). Hydrothermal Origin of Early Permian Chert Nodules in the Central North China Craton Linked to Northern Margin Cratonic Activation. *Acta Geologica Sinica (English Edition)*, *95*(2), 541–557. https://doi.org/10.1111/1755-6724.14649.

Appendix A - Petrographic Descriptions

Thin section ID: **FL-KS-1-1**

Summary

Peloidal-bioclastic packstone was extensively replaced by chert (subordinately chalcedony spherulites). Localized areas with intense dissolution of micrite and carbonate particles form moldic pores. Partial replacement of diagenetic silica by Fe oxides.

Microscopic textural features

Structure(s):	Nodular (10.0-40.0µm), Fractured (0.0-0.0)
Texture	
Grain size range:	Clay (0.0 mm) to Pebble (6.0 mm)
Modal grain size:	Silt (0.0 mm)
Gravel:	4.0%
Sand:	31.0%
Mud:	65.0%
Sorting:	Moderately sorted(0.6)
Sphericity:	Medium
Fabric	
Orientation(s):	Without orientation
Support:	Supported by grain-replacive material and by the cement
Packing:	Loose (0)
Point contacts:	Abundant
Long contacts:	Rare

Intrabasinal grains

2.7% Sponge spicule, As intrabasinal constituent;
2.0% Brachiopod bioclast, As intrabasinal constituent;
1.3% Carbonate bioclast undifferentiated, As intrabasinal constituent;
1.0% Crinoid bioclast, As intrabasinal constituent;
1.0% Bryozoan bioclast, As intrabasinal constituent;
1.0% Gastropod bioclast, As intrabasinal constituent;

Diagenetic Composition

44.7% Diagenetic silica, Microcrystalline, Interparticle replacive, Replacing <Primary-Constituent>, Micritic matrix syndepositional, As intrabasinal constituent;

17.0% Diagenetic silica, Microcrystalline, Intraparticle replacive, Replacing <Primary-Constituent>, Carbonate bioclast undifferentiated, As intrabasinal constituent;

3.3% Diagenetic silica, Microcrystalline, Intraparticle replacive, Replacing <Primary-Constituent>, Brachiopod bioclast, As intrabasinal constituent;

3.3% Chalcedony, Spherulite, Intraparticle replacive, Replacing <Primary-Constituent>, Carbonate bioclast undifferentiated, As intrabasinal constituent;

2.0% Diagenetic silica, Microcrystalline, Filling intraparticle pore, Within <Primary-Constituent>, Bryozoan bioclast, As intrabasinal constituent;

2.0% Diagenetic silica, Rosette, Intraparticle pore-lining, Within <pore>, Moldic pore, Framework;

1.7% Calcite, Blocky, Intraparticle replacive, Replacing <Diagenetic-Constituent>, Chalcedony, Intraparticle replacive;

1.7% Diagenetic iron oxide/hydroxide, Pelletoid, Interparticle replacive, Replacing <Primary-Constituent>, Micritic matrix syndepositional, As intrabasinal constituent;

1.3% Diagenetic silica, Microcrystalline, Filling interparticle pore, Within pore from dissolution of <Primary-Constituent>, Micritic matrix syndepositional, As intrabasinal constituent;

1.3% Diagenetic silica, Coarsely-crystalline, Intraparticle replacive, Within <Primary-Constituent>, Carbonate bioclast undifferentiated, As intrabasinal constituent;

1.0% Diagenetic silica, Microcrystalline, Filling intraparticle pore, Within <pore>, Moldic pore, Framework;

1.0% Diagenetic silica, Rim, Intraparticle replacive, Replacing <Primary-Constituent>, Carbonate bioclast undifferentiated, As intrabasinal constituent, The particle is Iron oxide since balck colored lining observed within pore of particle. Has a cubic outline;

Porosity

4.3% Interparticle pore, Interstitial, Dissolution of <Primary-Constituent>, Micritic matrix syndepositional, As intrabasinal constituent;

3.0% Moldic pore, Framework, Dissolution of <Primary-Constituent>, Carbonate bioclast undifferentiated, As intrabasinal constituent;

1.7% Rock fracture pore, Framework and interstitial;

1.7% Intraparticle pore, Framework, Within <Primary-Constituent>, Carbonate bioclast undifferentiated, As intrabasinal constituent;

Carbonate Classification:

Name of classification's method:	Grabau, Brankamp, Powers and Folk
Classification result:	Micritic calcarenite

Photomicrographs

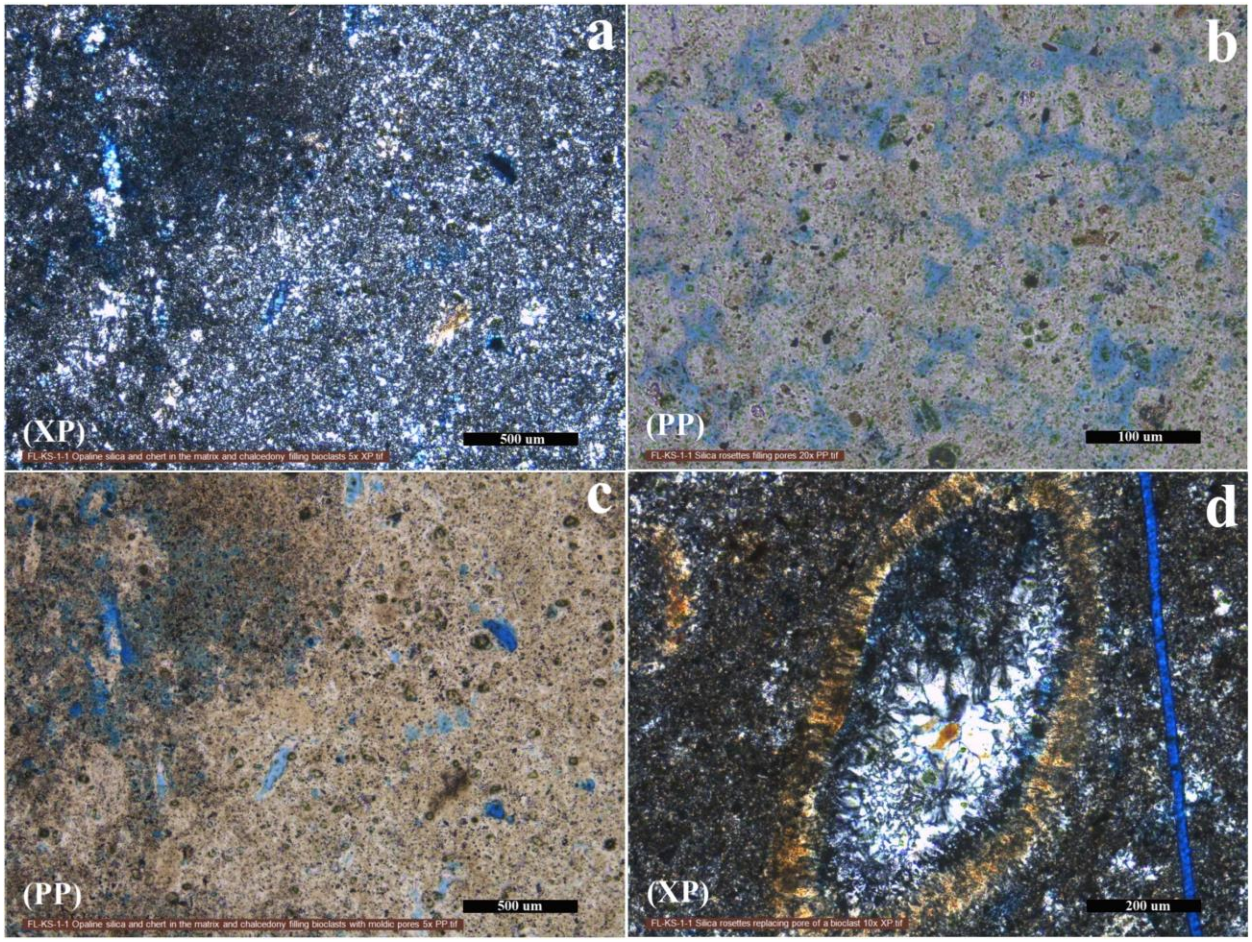

Figure A.1- (a) Opaline silica replaced by chert (b) Silica rosettes filling dissolution pores (c) Abundant moldic pores (d) Brachiopod intraparticle pore filled by chalcedony.

Thin section ID: **FL-KS-1-2**

Summary

Wackestone (=micritic calcarenite) with peloids and bioclasts (brachiopods, bryozoans, bivalves, and radiolarians) with about 40% micrite extensively replaced by chert. Most peloids and micrite are replaced by diagenetic silica. Moldic and interparticle dissolution pores. Wood grain margins are carbonate-rich, while the core is mostly silicified, with spots with remnants of carbonate matrix.

Microscopic textural features

Structure(s):	Lamination (0.028-0.319mm)
Texture	
Grain size range:	Clay (0.0 mm) to Granule (2.4 mm)
Modal grain size:	Silt (0.1 mm)
Gravel:	1.0%
Sand:	54.0%
Mud:	45.0%
Sorting:	Moderately sorted(0.6)

Sphericity: Medium

Fabric

Orientation(s): Chaotic
Support: Matrix and matrix-replacive phase supported
Packing: Loose (30)
Point contacts: Common (90.0 %)
Long contacts: Rare (10.0 %)

Intrabasinal grains

11.3% Carbonate bioclast undifferentiated, As intrabasinal constituent;
3.7% Radiolarian, As intrabasinal constituent, Spherulitic in structure;
1.7% Sponge spicule, As intrabasinal constituent;
1.3% Calcisphere bioclast, As intrabasinal constituent;
1.0% Bryozoan bioclast, As intrabasinal constituent;
1.0% Brachiopod bioclast, As intrabasinal constituent;

Matrix

17.0% Micritic matrix syndepositional, As intrabasinal constituent;

Diagenetic Composition

15.3% Diagenetic silica, Microcrystalline, Interparticle replacive, Replacing <Primary-Constituent>, Micritic matrix syndepositional, As intrabasinal constituent;
12.7% Diagenetic silica, Microcrystalline, Intraparticle replacive, Replacing <Primary-Constituent>, Carbonate bioclast undifferentiated, As intrabasinal constituent;
3.7% Calcite, Small rhomb, Intraparticle replacive, Replacing <Diagenetic-Constituent>, Diagenetic silica, Intraparticle replacive;
2.3% Chalcedony, Spherulite, Intraparticle replacive, Within <Primary-Constituent>, Carbonate bioclast undifferentiated, As intrabasinal constituent;
2.3% Calcite, Blocky, Interparticle replacive, Replacing <Diagenetic-Constituent>, Diagenetic silica, Interparticle replacive;
2.0% Diagenetic silica, Rosette, Interparticle replacive, Within <Primary-Constituent>, Micritic matrix syndepositional, As intrabasinal constituent;
1.7% Diagenetic silica, Rosette, Filling interparticle pore, Within <Primary-Constituent>, Micritic matrix syndepositional, As intrabasinal constituent;
1.3% Opal, Cryptocrystalline, Interparticle replacive, Replacing <Primary-Constituent>, Micritic matrix syndepositional, As intrabasinal constituent;
1.3% Diagenetic silica, Microcrystalline, Intraparticle replacive, Replacing <Primary-Constituent>, Calcisphere bioclast, As intrabasinal constituent;
1.3% Calcite, Small rhomb, Intraparticle replacive, Replacing <Primary-Constituent>, Carbonate bioclast undifferentiated, As intrabasinal constituent;
1.0% Diagenetic silica, Microcrystalline, Intraparticle replacive, Within <Primary-Constituent>, Brachiopod bioclast, As intrabasinal constituent;
1.0% Diagenetic silica, Rosette, Moldic pore-lining, Within <pore>, Moldic pore, Framework;
1.0% Calcite, Small rhomb, Intraparticle replacive, Replacing <Diagenetic-Constituent>, Chalcedony, Intraparticle replacive;
1.0% Calcite, Small rhomb, Filling interparticle pore, Within <Primary-Constituent>, Micritic matrix syndepositional, As intrabasinal constituent;
0.7% Diagenetic iron oxide/hydroxide, Pelletoid, Filling intraparticle pore, Within <pore>, Moldic pore, Framework;
0.7% Diagenetic iron oxide/hydroxide, Pelletoid, Interparticle replacive, Replacing <Primary-Constituent>, Micritic matrix syndepositional, As intrabasinal constituent;
0.3% Diagenetic silica, Microcrystalline, Filling intraparticle pore, Within <Primary-Constituent>,

Bryozoan bioclast, As intrabasinal constituent;
0.3% Diagenetic silica, Microcrystalline, Filling intraparticle pore, Within <pore>, Moldic pore, Framework;
0.3% Diagenetic silica, Rim, Interparticle continous pore-lining, Covering <Primary-Constituent>, Bivalve bioclast, As intrabasinal constituent;
0.3% Diagenetic titanium mineral, Small rhomb, Interparticle replacive, Replacing <Primary-Constituent>, Micritic matrix syndepositional, As intrabasinal constituent;

Porosity

6.0% Moldic pore, Framework, Dissolution of <Primary-Constituent>, Carbonate bioclast undifferentiated, As intrabasinal constituent;
4.3% Interparticle pore, Interstitial, Dissolution of <Primary-Constituent>, Micritic matrix syndepositional, As intrabasinal constituent;
2.0% Intraparticle pore, Framework, Dissolution of <Primary-Constituent>, Carbonate bioclast undifferentiated, As intrabasinal constituent;

Carbonate Classification:

Name of classification's method:	Grabau, Brankamp, Powers and Folk
Classification result:	Micritic calcarenite

Total Volumes

Framework:	53.666
Interstitial:	46.333
Cement:	7.333
Matrix:	17.000
Porosity:	12.333
Microporosity:	Not calculated
Total diagenetic constituents:	50.666
Rigid grains:	20.000

Intrabasinal constituents

Intrabasinal constituents:	72.333
Present primary carbonate constituents:	31.666
Original primary carbonate constituents:	65.000
Intrabasinal grains:	51.000
Present carbonate allochems:	14.666
Original carbonate allochems:	43.666
Primary proportion of original carbonate allochems:	67.179
Present Carbonate bioclasts:	14.666
Original Carbonate bioclasts:	41.666
Present carbonate matrix:	17.000
Original carbonate matrix:	21.333
Primary proportion of original carbonate matrix:	32.820
Carbonate cement:	3.333
Present intrabasinal non-carbonate grains:	5.333
Original intrabasinal non-carbonate grains:	7.333

Photomicrographs

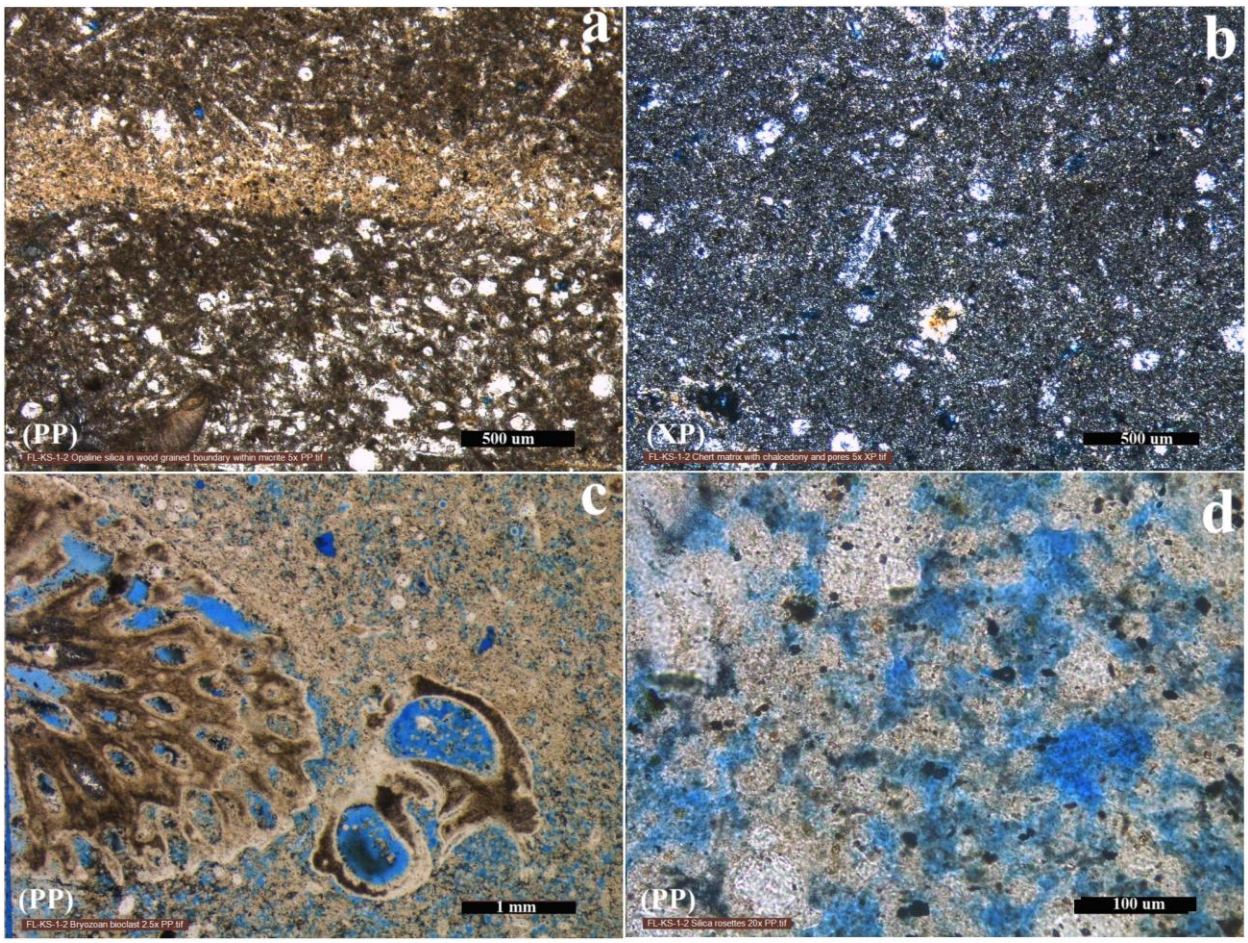

Figure A.2- Wood-grained nodule boundary with opaline silica and chert (b) Opaline silica with bioclasts replaced by chalcedony (c) A bryozoan bioclast with abundant intraparticular pores (d) Silica rosettes filling dissolution pores.

Description identification: FL-KS-2-1

Summary

Wackestone (=micritic calcarenite) with abundant bioclasts (brachiopods, bryozoans, sponge spicules, calcispheres) about 40%, extensively replaced by chert. Micrite is replaced by diagenetic silica. Moldic and interparticle dissolution pores from the dissolution of peloids and micrite. Abundant sponge spicules or elongated bioclasts within silica were observed.

Microscopic textural features

Structure(s):	Nodular (0.017-0.059mm)
Texture	
Grain size range:	Clay (0.0 mm) to Pebble (23.0 mm)
Modal grain size:	Silt (0.0 mm)
Gravel:	2.0%
Sand:	30.0%
Mud:	68.0%
Sorting:	Moderately sorted(0.66)

Sphericity:	Medium

Fabric

Orientation(s):	Chaotic
Support:	Matrix and matrix-replacive phase supported
Packing:	Loose (40)
Point contacts:	Common (85.0 %)
Long contacts:	Common (15.0 %)

Intrabasinal grains

5.3% Carbonate bioclast undifferentiated, As intrabasinal constituent;
5.3% Calcisphere bioclast, As intrabasinal constituent;
4.0% Brachiopod bioclast, As intrabasinal constituent;
3.0% Carbonate peloid, As intrabasinal constituent;
2.7% Sponge spicule, As intrabasinal constituent, Spherulitic in structure;
1.0% Bryozoan bioclast, As intrabasinal constituent;

Matrix

6.0% Micritic matrix syndepositional, As intrabasinal constituent;

Diagenetic Composition

29.0% Diagenetic silica, Microcrystalline, Interparticle replacive, Replacing <Primary-Constituent>, Micritic matrix syndepositional, As intrabasinal constituent;

16.0% Diagenetic silica, Microcrystalline, Intraparticle replacive, Replacing <Primary-Constituent>, Carbonate bioclast undifferentiated, As intrabasinal constituent;

4.3% Diagenetic silica, Microcrystalline, Intraparticle replacive, Replacing <Primary-Constituent>, Calcisphere bioclast, As intrabasinal constituent;

3.0% Diagenetic silica, Microcrystalline, Intraparticle replacive, Replacing <Primary-Constituent>, Sponge spicule, As intrabasinal constituent;

3.0% Diagenetic iron oxide/hydroxide, Pelletoid, Filling intraparticle pore, Within <pore>, Moldic pore, Framework;

2.3% Diagenetic silica, Rosette, Moldic pore-lining, Within <pore>, Moldic pore, Framework;

2.3% Chalcedony, Spherulite, Intraparticle replacive, Replacing <Primary-Constituent>, Carbonate bioclast undifferentiated, As intrabasinal constituent;

1.7% Diagenetic silica, Coarsely-crystalline, Intraparticle replacive, Replacing <Primary-Constituent>, Carbonate bioclast undifferentiated, As intrabasinal constituent;

1.0% Diagenetic silica, Microcrystalline, Filling intraparticle pore, Within <Primary-Constituent>, Bryozoan bioclast, As intrabasinal constituent;

1.0% Diagenetic silica, Microcrystalline, Filling intraparticle pore, Within <pore>, Moldic pore, Framework;

1.0% Calcite, Blocky, Intraparticle replacive, Replacing <Diagenetic-Constituent>, Diagenetic silica, Intraparticle replacive;

1.0% Diagenetic iron oxide/hydroxide, Pelletoid, Interparticle replacive, Replacing <Primary-Constituent>, Micritic matrix syndepositional, As intrabasinal constituent;

1.0% Diagenetic iron oxide/hydroxide, Pelletoid, Filling vugular pore, Within pore from dissolution of <Primary-Constituent>, Micritic matrix syndepositional, As intrabasinal constituent;

0.3% Diagenetic titanium mineral, Small rhomb, Interparticle replacive, Replacing <Primary-Constituent>, Micritic matrix syndepositional, As intrabasinal constituent;

Porosity

4.0% Moldic pore, Framework, Dissolution of <Primary-Constituent>, Carbonate bioclast undifferentiated, As intrabasinal constituent;

1.7% Interparticle pore, Interstitial, Dissolution of <Primary-Constituent>, Micritic matrix syndepositional, As intrabasinal constituent;

Carbonate Classification:

Name of classification's method:	Grabau, Brankamp, Powers, and Folk
Classification result:	Micritic calcarenite

Total Volumes

Framework:	62.000
Interstitial:	38.000
Cement:	0.000
Matrix:	6.000
Porosity:	5.666
Microporosity:	Not calculated
Total diagenetic constituents:	67.000
Rigid grains:	18.333
Ductile grains:	3.000

Intrabasinal constituents

Intrabasinal constituents:	73.999
Present primary carbonate constituents:	24.666
Original primary carbonate constituents:	62.000
Intrabasinal grains:	66.333
Present carbonate allochems:	18.666
Original carbonate allochems:	54.333
Primary proportion of original carbonate allochems:	87.634
Present Carbonate bioclasts:	15.666
Original Carbonate bioclasts:	45.000
Present carbonate matrix:	6.000
Original carbonate matrix:	7.666
Primary proportion of original carbonate matrix:	12.365
Carbonate cement:	0.000
Present intrabasinal non-carbonate grains:	2.666
Original intrabasinal non-carbonate grains:	12.000

Photomicrographs

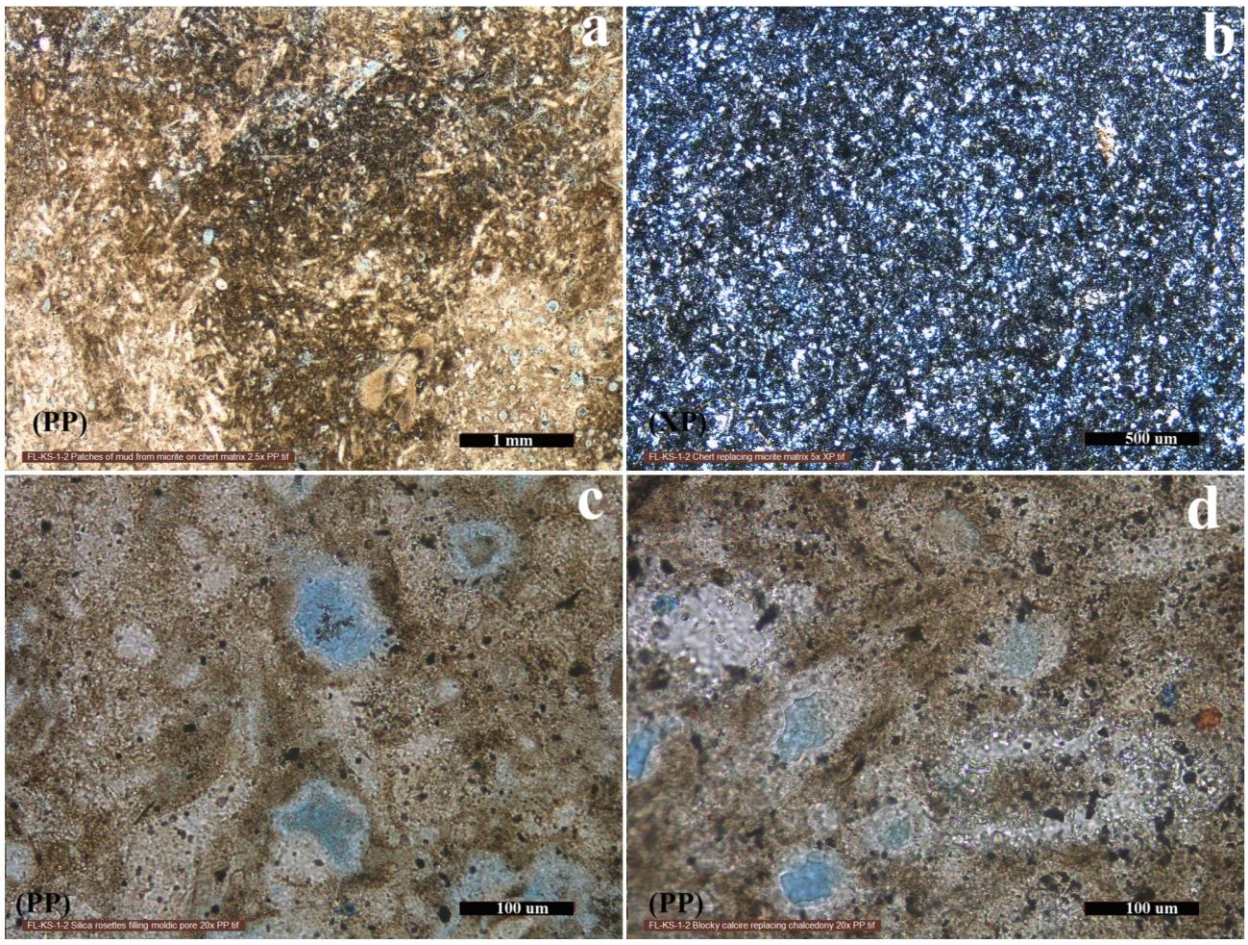

Figure A.3- (a) Wackestone with abundant bioclasts (including sponge spicules) (b) Chert replacing micrite matrix (c) Silica rosettes lining moldic pores (d) Blocky calcite replacing chalcedony.

Thin section ID: **FL-KS-2-2**

Summary

Wackestone (=micritic calcarenite) with abundant peloids and bioclasts (brachiopods, gastropods, bryozoans, sponge spicules) about 23% in composition. The sample contains abundant micrite as the matrix, and the matrix is replaced by silica. The thin section is layered, with alternate zones of preserved original rock (only partially silicified), completely silicified, and porous layers. Interparticular pores and moldic pores due to dissolution of micrite and bioclasts.

Microscopic textural features

Structure(s):	Nodular (0.017-0.059mm), Lamination (0.0-0.0)
Texture	
Grain size range:	Clay (0.0 mm) to Granule (2.2 mm)
Modal grain size:	Silt (0.0 mm)
Gravel:	4.0%
Sand:	24.0%
Mud:	72.0%
Sorting:	Moderately sorted(0.7)

Sphericity:	Medium

Fabric

Orientation(s):	Chaotic
Support:	Matrix and matrix-replacive phase supported
Packing:	Loose (40)
Point contacts:	Common (85.0 %)
Long contacts:	Common (15.0 %)

Intrabasinal grains

5.3% Carbonate bioclast undifferentiated, As intrabasinal constituent;
5.3% Carbonate peloid, As intrabasinal constituent;
3.7% Brachiopod bioclast, As intrabasinal constituent;
1.7% Sponge spicule, As intrabasinal constituent;
1.7% Gastropod bioclast, As intrabasinal constituent;
1.0% Bryozoan bioclast, As intrabasinal constituent;
1.0% Coral bioclast, As intrabasinal constituent;

Matrix

25.0% Micritic matrix syndepositional, As intrabasinal constituent;

Diagenetic Composition

32.3% Diagenetic silica, Microcrystalline, Interparticle replacive, Replacing <Primary-Constituent>, Micritic matrix syndepositional, As intrabasinal constituent;
4.7% Diagenetic silica, Microcrystalline, Intraparticle replacive, Replacing <Primary-Constituent>, Carbonate bioclast undifferentiated, As intrabasinal constituent;
3.3% Diagenetic silica, Rosette, Interparticle replacive, Replacing <Primary-Constituent>, Micritic matrix syndepositional, As intrabasinal constituent;
2.7% Diagenetic silica, Rosette, Moldic pore-lining, Within <pore>, Moldic pore, Framework;
1.7% Diagenetic iron oxide/hydroxide, Peloidal, Interparticle replacive, Replacing <Primary-Constituent>, Micritic matrix syndepositional, As intrabasinal constituent;
1.3% Chalcedony, Spherulite, Intraparticle replacive, Within <Primary-Constituent>, Carbonate bioclast undifferentiated, As intrabasinal constituent;
1.3% Calcite, Blocky, Intraparticle replacive, Replacing <Diagenetic-Constituent>, Diagenetic silica, Intraparticle replacive;
1.0% Diagenetic silica, Microcrystalline, Filling intraparticle pore, Within <Primary-Constituent>, Bryozoan bioclast, As intrabasinal constituent;
1.0% Diagenetic silica, Microcrystalline, Intraparticle replacive, Replacing <Primary-Constituent>, Calcisphere bioclast, As intrabasinal constituent;
0.7% Diagenetic titanium mineral, Small rhomb, Interparticle replacive, Replacing <Primary-Constituent>, Micritic matrix syndepositional, As intrabasinal constituent;

Porosity

3.7% Interparticle pore, Interstitial, Dissolution of <Primary-Constituent>, Micritic matrix syndepositional, As intrabasinal constituent;
1.7% Moldic pore, Framework, Dissolution of <Primary-Constituent>, Carbonate bioclast undifferentiated, As intrabasinal constituent;

Carbonate Classification:

Name of classification's method:	Grabau, Brankamp, Powers and Folk
Classification result:	Micritic calcarenite

Total Volumes

Framework:	33.333

Interstitial:	66.666
Cement:	0.000
Matrix:	25.000
Porosity:	5.333
Microporosity:	Not calculated
Total diagenetic constituents:	50.000
Rigid grains:	14.333
Ductile grains:	5.333

Intrabasinal constituents

Intrabasinal constituents:	63.333
Present primary carbonate constituents:	43.000
Original primary carbonate constituents:	59.000
Intrabasinal grains:	34.666
Present carbonate allochems:	18.000
Original carbonate allochems:	30.333
Primary proportion of original carbonate allochems:	51.412
Present Carbonate bioclasts:	12.666
Original Carbonate bioclasts:	22.333
Present carbonate matrix:	25.000
Original carbonate matrix:	28.666
Primary proportion of original carbonate matrix:	48.587
Carbonate cement:	0.000
Present intrabasinal non-carbonate grains:	1.666
Original intrabasinal non-carbonate grains:	4.333

Photomicrographs

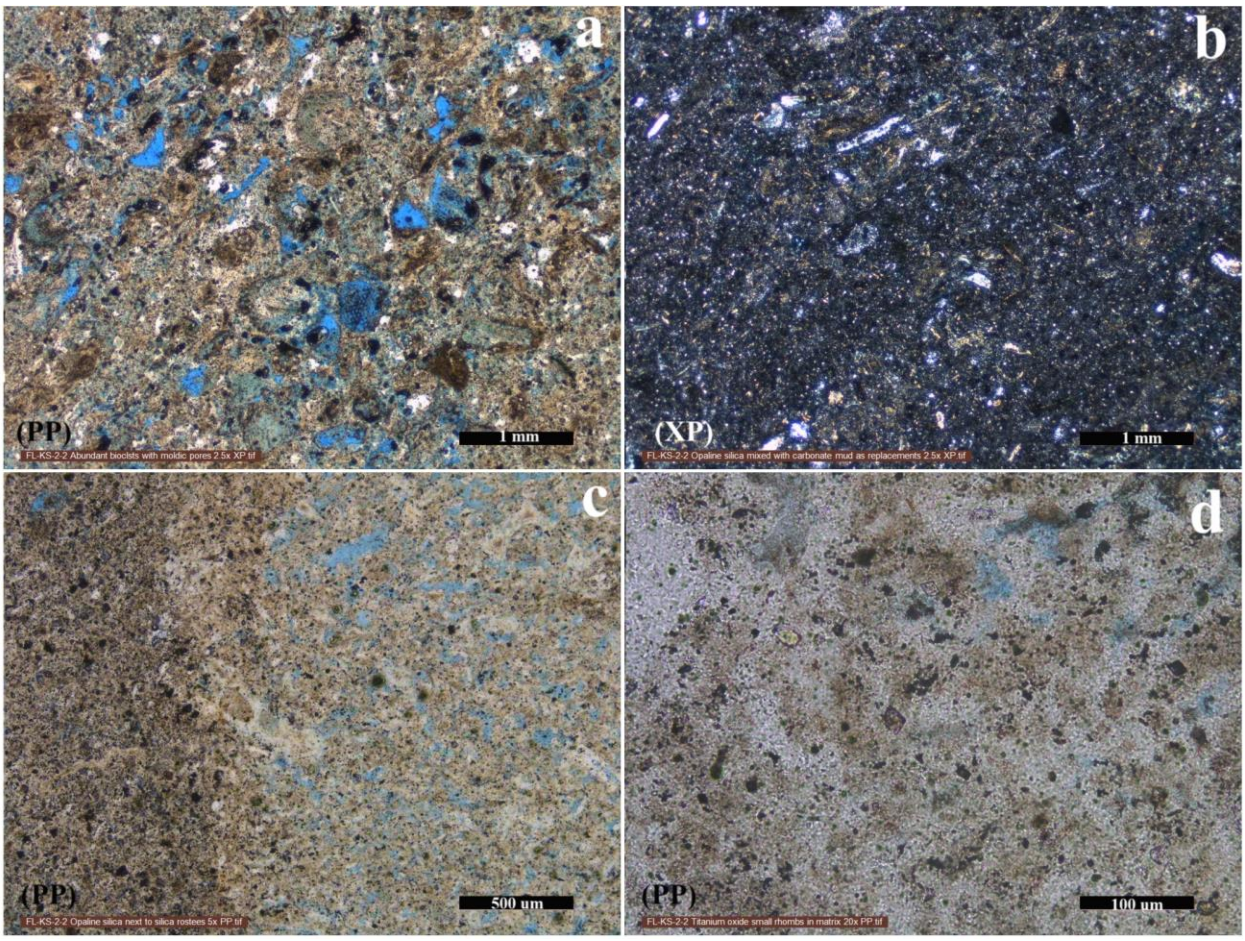

Figure A.4- (a) Abundant bioclasts with moldic pores within micrite (b) Remains of micritic mud replaced by chert (c) Opaline silica formations adjacent to silica rosettes (d) Titanium oxide rhombs(secondary) in micrite matrix.

Thin section ID: **FL-KS-3-1**

Summary

Wackestone (=micritic calcarenite) with abundant peloids and bioclasts (brachiopods, sponge spicules) about 20%. Matrix is mainly micritic, while wood-grained boundaries have opaline silica replacing micrite. Outside of the nodule, intraparticle, interparticle, and oversized pores due to dissolution of micrite and allochems. Blocky calcite partially replacing sponge spicules (siliceous). Very thin silica veins across lamination.

Microscopic textural features

Structure(s):	Nodular (0.028-0.059mm), Irregular lamination (0.0-0.0)
Texture	
Grain size range:	Clay (0.0 mm) to Pebble (7.0 mm)
Modal grain size:	Clay (0.0 mm)
Gravel:	4.0%
Sand:	26.0%
Mud:	70.0%

Sorting:	Moderately sorted(0.7)
Sphericity:	Medium

Fabric

Orientation(s):	Chaotic
Support:	Matrix and matrix-replacive phase supported
Packing:	Loose (40)
Point contacts:	Common (80.0 %)
Long contacts:	Common (20.0 %)

Intrabasinal grains

7.7% Carbonate bioclast undifferentiated, As intrabasinal constituent;
5.7% Sponge spicule, As intrabasinal constituent;
2.7% Brachiopod bioclast, As intrabasinal constituent;
1.7% Bryozoan bioclast, As intrabasinal constituent;
1.7% Carbonate peloid, As intrabasinal constituent;
1.3% Gastropod bioclast, As intrabasinal constituent;

Matrix

37.7% Micritic matrix syndepositional, As intrabasinal constituent;

Diagenetic Composition

17.7% Diagenetic silica, Microcrystalline, Interparticle replacive, Replacing <Primary-Constituent>, Micritic matrix syndepositional, As intrabasinal constituent;

11.7% Opal, Cryptocrystalline, Interparticle replacive, Replacing <Primary-Constituent>, Micritic matrix syndepositional, As intrabasinal constituent;

3.0% Chalcedony, Spherulite, Intraparticle replacive, Replacing <Primary-Constituent>, Carbonate bioclast undifferentiated, As intrabasinal constituent;

2.7% Diagenetic silica, Microcrystalline, Intraparticle replacive, Replacing <Primary-Constituent>, Carbonate bioclast undifferentiated, As intrabasinal constituent;

1.3% Calcite, Blocky, Intraparticle replacive, Replacing <Primary-Constituent>, Sponge spicule, As intrabasinal constituent;

1.0% Diagenetic silica, Coarsely-crystalline, Filling intraparticle pore, Replacing <Primary-Constituent>, Carbonate bioclast undifferentiated, As intrabasinal constituent;

1.0% Diagenetic iron oxide/hydroxide, Pelletoid, Interparticle replacive, Replacing <Primary-Constituent>, Micritic matrix syndepositional, As intrabasinal constituent;

1.0% Diagenetic iron oxide/hydroxide, Pelletoid, Filling intraparticle pore, Within <pore>, Moldic pore, Framework;

Porosity

2.3% Interparticle pore, Interstitial, Dissolution of <Primary-Constituent>, Micritic matrix syndepositional, As intrabasinal constituent;

Carbonate Classification:

Name of classification's method:	Grabau, Brankamp, Powers and Folk
Classification result:	Micritic calcarenite

Total Volumes

Framework:	29.666
Interstitial:	70.333
Cement:	0.000
Matrix:	37.666
Porosity:	2.333
Microporosity:	Not calculated

Total diagenetic constituents:	39.333
Rigid grains:	19.000
Ductile grains:	1.666
Intrabasinal constituents	
Intrabasinal constituents:	70.666
Present primary carbonate constituents:	52.666
Original primary carbonate constituents:	62.666
Intrabasinal grains:	30.666
Present carbonate allochems:	15.000
Original carbonate allochems:	22.666
Primary proportion of original carbonate allochems:	36.170
Present Carbonate bioclasts:	13.333
Original Carbonate bioclasts:	20.000
Present carbonate matrix:	37.666
Original carbonate matrix:	40.000
Primary proportion of original carbonate matrix:	63.829
Carbonate cement:	0.000
Present intrabasinal non-carbonate grains:	5.666
Original intrabasinal non-carbonate grains:	8.000

Photomicrographs

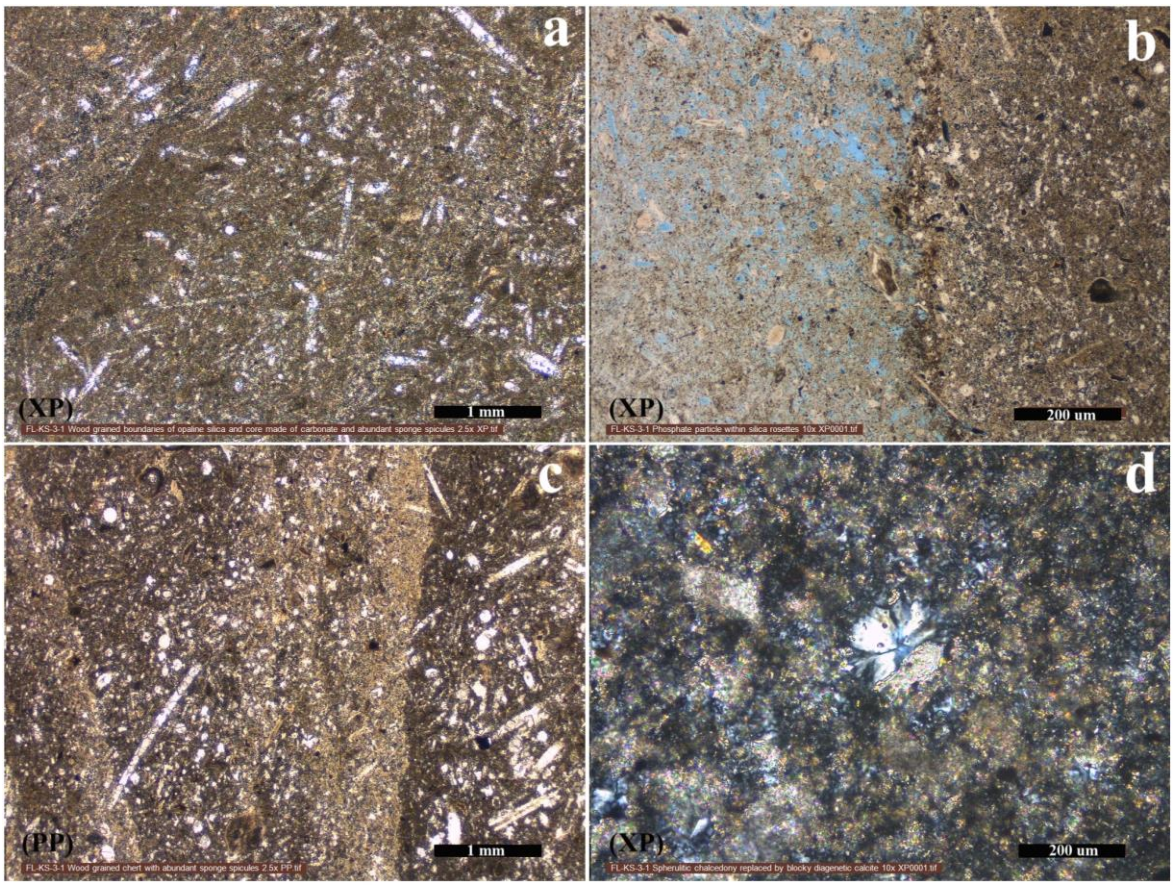

Figure A.5- (a) Abundant sponge spicules close to wood-grained chert boundary (b) Silica rosettes bordering with wood-grained chert (c) Possible "growth front" looking wood-grained chert boundaries (d) Spherulitic chalcedony replaced by blocky calcite.

Thin section ID: **FL-KS-3-2**

Summary

Wackestone (=micritic calcarenite) with abundant bioclasts (brachiopods, bryozoans, corals, sponge spicules) and some peloids, about 22%. Micrite is extensively replaced by chert, and matrix accounts for about 60%. Bioclasts are partially silicified and covered by diagenetic silica rims. Abundant interparticle and moldic pores due to the dissolution of micrite with some intraparticle pores within corals and bryozoans. Intraparticle and interparticle pores lined with silica rims were observed. Silica rosettes partially fill interparticle pores. Blocky calcite partially replaces sponge spicules and silicified carbonate bioclasts. Stylolites.

Microscopic textural features

Structure(s):	Nodular (0.002-0.006mm), Stylolite (0.0-0.0)
Texture	
Grain size range:	Clay (0.0 mm) to Pebble (8.4 mm)
Modal grain size:	Clay (0.0 mm)
Gravel:	5.0%
Sand:	35.0%
Mud:	60.0%

Sorting:	Poorly sorted(2.0)
Sphericity:	Medium

Fabric

Orientation(s):	Chaotic
Support:	Matrix and matrix-replacive phase supported
Packing:	Loose (40)
Point contacts:	Common (85.0 %)
Long contacts:	Common (15.0 %)

Intrabasinal grains

5.7% Sponge spicule, As intrabasinal constituent;
4.3% Carbonate bioclast undifferentiated, As intrabasinal constituent;
2.3% Coral bioclast, As intrabasinal constituent;
1.3% Glauconite grain, As intrabasinal constituent;
1.0% Brachiopod bioclast, As intrabasinal constituent;
1.0% Bryozoan bioclast, As intrabasinal constituent;

Matrix

10.0% Micritic matrix syndepositional, As intrabasinal constituent;

Diagenetic Composition

26.7% Diagenetic silica, Microcrystalline, Interparticle replacive, Replacing <Primary-Constituent>, Micritic matrix syndepositional, As intrabasinal constituent;
9.3% Diagenetic silica, Microcrystalline, Intraparticle replacive, Replacing <Primary-Constituent>, Carbonate bioclast undifferentiated, As intrabasinal constituent;
8.7% Diagenetic silica, Rosette, Interparticle replacive, Replacing <Primary-Constituent>, Micritic matrix syndepositional, As intrabasinal constituent;
6.3% Diagenetic silica, Rosette, Filling interparticle pore, Within <Primary-Constituent>, Micritic matrix syndepositional, As intrabasinal constituent;
3.3% Calcite, Blocky, Intraparticle replacive, Replacing <Diagenetic-Constituent>, Diagenetic silica, Intraparticle replacive;
2.0% Diagenetic silica, Rosette, Moldic pore-lining, Within <pore>, Moldic pore, Framework;
1.3% Diagenetic silica, Rim, Intraparticle replacive, Covering <Primary-Constituent>, Carbonate bioclast undifferentiated, As intrabasinal constituent;
1.0% Diagenetic silica, Coarsely-crystalline, Intraparticle replacive, Replacing <Primary-Constituent>, Carbonate bioclast undifferentiated, As intrabasinal constituent;
1.0% Diagenetic silica, Rim, Intraparticle pore-lining, Replacing <Primary-Constituent>, Coral bioclast, As intrabasinal constituent;
1.0% Diagenetic silica, Rim, Interparticle continous pore-lining, Covering <Primary-Constituent>, Coral bioclast, As intrabasinal constituent;
1.0% Diagenetic silica, Rosette, Filling intraparticle pore, Within <Primary-Constituent>, Coral bioclast, As intrabasinal constituent;
1.0% Diagenetic iron oxide/hydroxide, Pelletoid, Interparticle replacive, Replacing <Primary-Constituent>, Micritic matrix syndepositional, As intrabasinal constituent;
0.7% Diagenetic silica, Microcrystalline, Intraparticle replacive, Replacing <Primary-Constituent>, Coral bioclast, As intrabasinal constituent;
0.7% Diagenetic silica, Rim, Interparticle replacive, Covering <Primary-Constituent>, Sponge spicule, As intrabasinal constituent;
0.7% Diagenetic silica, Rim, Intraparticle replacive, Covering <Primary-Constituent>, Bryozoan bioclast, As intrabasinal constituent;
0.7% Calcite, Blocky, Intraparticle replacive, Replacing <Primary-Constituent>, Carbonate bioclast undifferentiated, As intrabasinal constituent;

0.3% Diagenetic silica, Microcrystalline, Filling intraparticle pore, Within <Primary-Constituent>, Coral bioclast, As intrabasinal constituent;
0.3% Diagenetic silica, Rim, Intraparticle pore-lining, Replacing <Primary-Constituent>, Brachiopod bioclast, As intrabasinal constituent;
0.3% Diagenetic silica, Rim, Interparticle continous pore-lining, Covering <Primary-Constituent>, Carbonate bioclast undifferentiated;
0.3% Diagenetic silica, Rim, Intraparticle pore-lining, Replacing <Primary-Constituent>, Bryozoan bioclast, As intrabasinal constituent;
0.3% Calcite, Blocky, Intraparticle replacive, Replacing <Primary-Constituent>, Sponge spicule, As intrabasinal constituent;

Porosity

4.3% Interparticle pore, Interstitial, Dissolution of <Primary-Constituent>, Micritic matrix syndepositional, As intrabasinal constituent;
3.0% Intraparticle pore, Framework, Within <Primary-Constituent>, Coral bioclast, As intrabasinal constituent;

Carbonate Classification:

Name of classification's method:	Grabau, Brankamp, Powers and Folk
Classification result:	Micritic calcarenite

Total Volumes

Framework:	41.000
Interstitial:	59.000
Cement:	8.333
Matrix:	10.000
Porosity:	7.333
Microporosity:	Not calculated
Total diagenetic constituents:	67.000
Rigid grains:	14.333
Ductile grains:	1.333
Intrabasinal constituents:	52.000
Present primary carbonate constituents:	18.666
Original primary carbonate constituents:	42.666
Intrabasinal grains:	37.666
Present carbonate allochems:	8.666
Original carbonate allochems:	28.333
Primary proportion of original carbonate allochems:	66.406
Present Carbonate bioclasts:	8.666
Original Carbonate bioclasts:	26.333
Present carbonate matrix:	10.000
Original carbonate matrix:	14.333
Primary proportion of original carbonate matrix:	33.593
Carbonate cement:	0.000
Present intrabasinal non-carbonate grains:	7.000
Original intrabasinal non-carbonate grains:	9.333

Photomicrographs

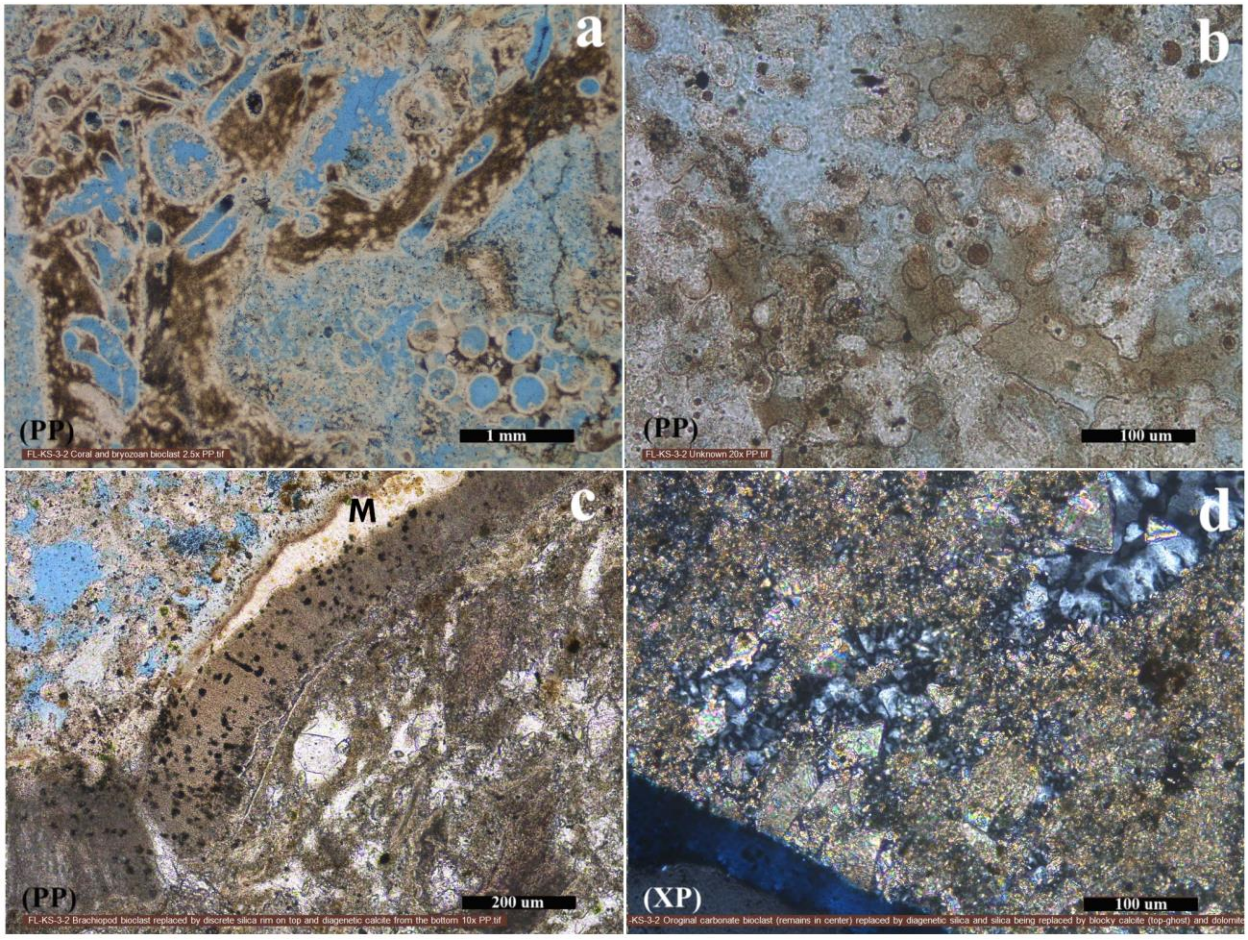

Figure A.6- Intraparticle pores of corals and bryozoans partially filled by silica rosettes (b) Abundant calcispheres (c) Brachiopod shell replaced by Moganite (M) (d) Undifferentiated carbonate bioclast replaced by chalcedony and chalcedony replaced by diagenetic calcite rhombs.

Thin section ID: **FL-KS-4**

Summary

Wackestone (=micritic calcarenite) with abundant bioclasts (brachiopods, bryozoans, corals, sponge spicules, calcispheres) making about 13%. Micrite and micrite replacing silica and blocky calcite/dolomite are predominant, with about 65%. Moldic and intraparticle pores resulting from the dissolution of micrite were observed. Most calcipheres were silicified, and silica rosettes were observed in regions with higher porosity.

Microscopic textural features

Structure(s):	Nodular (0.002-0.006mm)
Texture	
Grain size range:	Clay (0.0 mm) to Pebble (5.4 mm)
Modal grain size:	Clay (0.0 mm)
Gravel:	7.0%
Sand:	38.0%

Mud:	55.0%
Sorting:	Poorly sorted(2.0)
Sphericity:	Medium

Fabric

Orientation(s):	Chaotic
Support:	Matrix and matrix-replacive phase supported
Packing:	Loose (40)
Point contacts:	Common (85.0 %)
Long contacts:	Common (15.0 %)

Intrabasinal grains

3.7% Carbonate bioclast undifferentiated, As intrabasinal constituent;
3.0% Brachiopod bioclast, As intrabasinal constituent;
2.7% Calcisphere bioclast, As intrabasinal constituent;
2.0% Sponge spicule, As intrabasinal constituent;
1.3% Coral bioclast, As intrabasinal constituent;
0.3% Bryozoan bioclast, As intrabasinal constituent;

Matrix

10.3% Micritic matrix syndepositional, As intrabasinal constituent;

Diagenetic Composition

21.7% Diagenetic silica, Microcrystalline, Interparticle replacive, Replacing <Primary-Constituent>, Micritic matrix syndepositional, As intrabasinal constituent;
8.3% Diagenetic silica, Microcrystalline, Intraparticle replacive, Replacing <Primary-Constituent>, Calcisphere bioclast, As intrabasinal constituent;
6.0% Diagenetic silica, Microcrystalline, Intraparticle replacive, Replacing <Primary-Constituent>, Carbonate bioclast undifferentiated, As intrabasinal constituent;
5.3% Diagenetic silica, Rosette, Interparticle replacive, Replacing <Primary-Constituent>, Micritic matrix syndepositional, As intrabasinal constituent;
5.0% Calcite, Blocky, Interparticle replacive, Replacing <Diagenetic-Constituent>, Diagenetic silica, Interparticle replacive;
4.3% Diagenetic silica, Rosette, Filling interparticle pore, Within <Primary-Constituent>, Micritic matrix syndepositional, As intrabasinal constituent;
4.3% Calcite, Blocky, Intraparticle replacive, Replacing <Diagenetic-Constituent>, Diagenetic silica, Intraparticle replacive;
2.3% Dolomite, Microcrystalline, Intraparticle replacive, Replacing <Diagenetic-Constituent>, Diagenetic silica, Intraparticle replacive;
1.7% Diagenetic silica, Microcrystalline, Intraparticle replacive, Replacing <Primary-Constituent>, Brachiopod bioclast, As intrabasinal constituent;
1.7% Diagenetic iron oxide/hydroxide, Pelletoid, Interparticle replacive, Replacing <Primary-Constituent>, Micritic matrix syndepositional, As intrabasinal constituent;
1.3% Diagenetic silica, Coarsely-crystalline, Intraparticle replacive, Replacing <Primary-Constituent>, Carbonate bioclast undifferentiated, As intrabasinal constituent;
1.3% Diagenetic silica, Rim, Interparticle continous pore-lining, Covering <Primary-Constituent>, Brachiopod bioclast, As intrabasinal constituent;
0.7% Diagenetic silica, Microcrystalline, Filling intraparticle pore, Within <Primary-Constituent>, Bryozoan bioclast, As intrabasinal constituent;
0.7% Diagenetic silica, Microcrystalline, Filling interparticle pore, Within <Primary-Constituent>, Micritic matrix syndepositional, As intrabasinal constituent;
0.7% Diagenetic silica, Rim, Interparticle continous pore-lining, Covering <Primary-Constituent>, Coral bioclast, As intrabasinal constituent;

0.7% Diagenetic silica, Rosette, Moldic pore-lining, Within <pore>, Moldic pore, Framework;
0.7% Chalcedony, Spherulite, Intraparticle replacive, Replacing <Primary-Constituent>, Carbonate bioclast undifferentiated, As intrabasinal constituent;
0.7% Calcite, Blocky, Filling intraparticle pore, Within <Primary-Constituent>, Brachiopod bioclast, As intrabasinal constituent;
0.7% Calcite, Blocky, Intraparticle replacive, Replacing <Primary-Constituent>, Carbonate bioclast undifferentiated, As intrabasinal constituent;
0.7% Dolomite, Microcrystalline, Filling interparticle pore, Within pore from dissolution of <Primary-Constituent>, Micritic matrix syndepositional, As intrabasinal constituent;
0.3% Diagenetic silica, Rim, Intraparticle pore-lining, Within <Primary-Constituent>, Brachiopod bioclast, As intrabasinal constituent;
0.3% Calcite, Blocky, Intraparticle replacive, Replacing <Diagenetic-Constituent>, Diagenetic silica, Intraparticle replacive;
0.3% Dolomite, Small rhomb, Intraparticle replacive, Replacing <Diagenetic-Constituent>, Calcite, Intraparticle replacive;
0.3% Dolomite, Microcrystalline, Intraparticle replacive, Replacing <Primary-Constituent>, Calcisphere bioclast, As intrabasinal constituent;
0.3% Diagenetic iron oxide/hydroxide, Pelletoid, Filling intraparticle pore, Within <pore>, Moldic pore, Framework;
0.3% Diagenetic titanium mineral, Small rhomb, Interparticle replacive, Replacing <Primary-Constituent>, Micritic matrix syndepositional, As intrabasinal constituent;

Porosity

5.0% Interparticle pore, Interstitial, Dissolution of <Primary-Constituent>, Micritic matrix syndepositional, As intrabasinal constituent;
1.0% Moldic pore, Framework, Dissolution of <Primary-Constituent>, Carbonate bioclast undifferentiated, As intrabasinal constituent;

Carbonate Classification:

Name of classification's method:	Grabau, Brankamp, Powers and Folk
Classification result:	Micritic/spathic calcarenite

Total Volumes

Framework:	43.000
Interstitial:	57.000
Cement:	12.666
Matrix:	10.333
Porosity:	6.000
Microporosity:	Not calculated
Total diagenetic constituents:	70.666
Rigid grains:	12.999

Intrabasinal constituents

Intrabasinal constituents:	51.999
Present primary carbonate constituents:	21.333
Original primary carbonate constituents:	48.999
Intrabasinal grains:	36.666
Present carbonate allochems:	11.000
Original carbonate allochems:	33.666
Primary proportion of original carbonate allochems:	68.707
Present Carbonate bioclasts:	11.000
Original Carbonate bioclasts:	32.666
Present carbonate matrix:	10.333

Original carbonate matrix:	15.333
Primary proportion of original carbonate matrix:	31.292
Carbonate cement:	5.666
Present intrabasinal non-carbonate grains:	2.000
Original intrabasinal non-carbonate grains:	3.000
Dolomite/Calcite ratio:	0.333

Photomicrographs

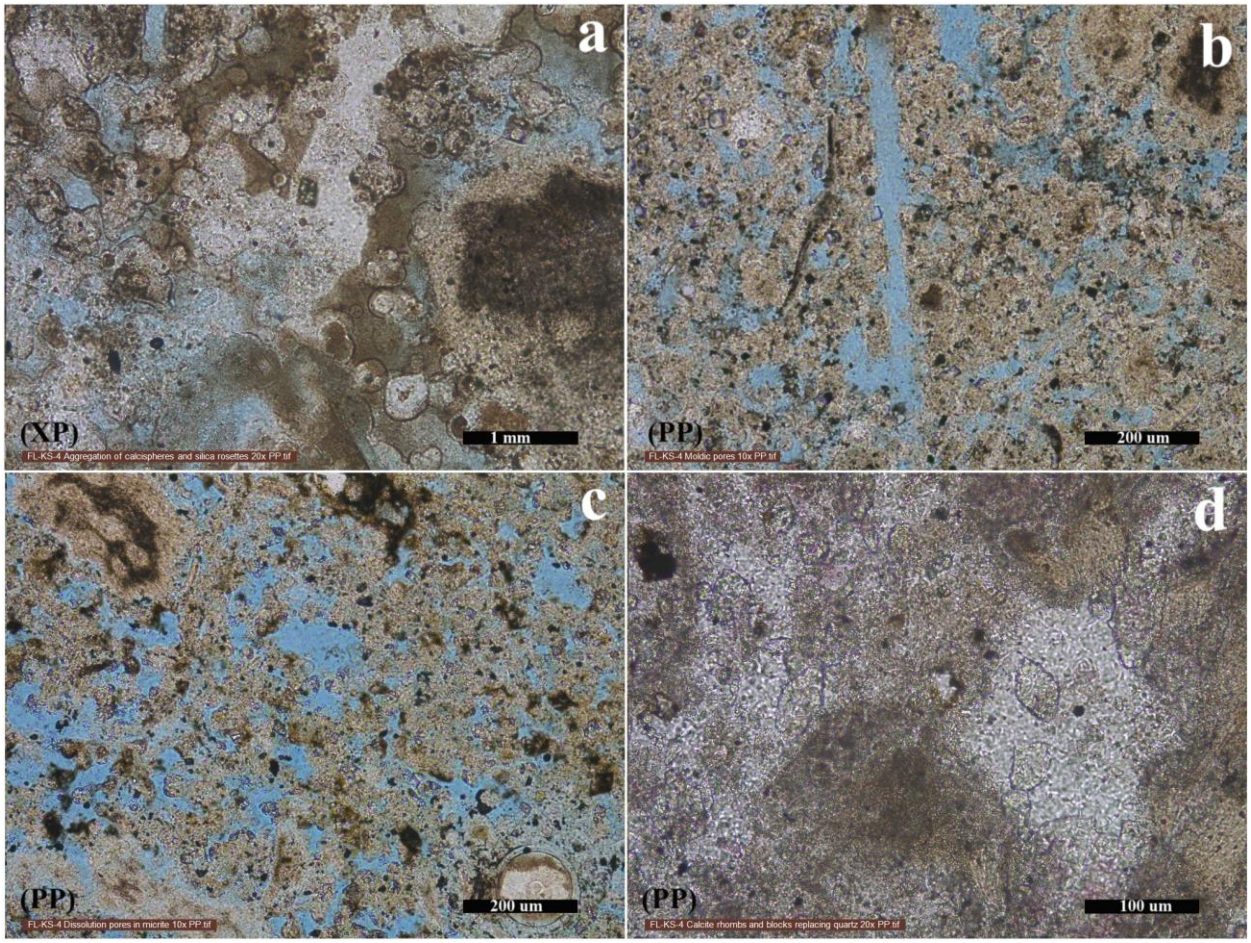

Figure A.7- (a) Calcisphere bioclasts embedded within micritic matrix (b and c) Moldic and dissolution pores within chert (d) Calcite rhombs replacing chert.

Thin section ID: **FL-KS-5-1-1**

Summary

Wackestone (=micritic calcarenite) with abundant bioclasts (brachiopods, corals, sponge spicules, gastropods) making about 25%. Micrite and micrite-replacive silica and blocky calcite/dolomite are predominant, with about 60%. Moldic and intraparticle pores were resulted from the dissolution of micrite. Interparticle opaline silica was observed at diffused boundaries of silica-rich and carbonate-rich

zones. Opaline silica seems to be replaced by chert, which is replaced by chalcedony-calcite-dolomite.

Microscopic textural features

Structure(s):	Lamination (0.002-0.006mm), Fractured (0.0-0.0)
Texture	
Grain size range:	Clay (0.0 mm) to Pebble (9.6 mm)
Modal grain size:	Clay (0.0 mm)
Gravel:	2.0%
Sand:	38.0%
Mud:	60.0%
Sorting:	Poorly sorted(2.0)
Sphericity:	Medium
Fabric	
Orientation(s):	Chaotic
Support:	Matrix and matrix-replacive phase supported
Packing:	Loose (40)
Point contacts:	Common (85.0 %)
Long contacts:	Common (15.0 %)

Intrabasinal grains

9.7% Sponge spicule, As intrabasinal constituent;
1.3% Carbonate bioclast undifferentiated, As intrabasinal constituent;
1.3% Brachiopod bioclast, As intrabasinal constituent;
0.3% Coral bioclast, As intrabasinal constituent;
0.3% Gastropod bioclast, As intrabasinal constituent;

Matrix

7.0% Micritic matrix syndepositional, As intrabasinal constituent;

Diagenetic Composition

31.0% Diagenetic silica, Microcrystalline, Interparticle replacive, Replacing <Primary-Constituent>, Micritic matrix syndepositional, As intrabasinal constituent;

10.7% Diagenetic silica, Microcrystalline, Intraparticle replacive, Replacing <Primary-Constituent>, Carbonate bioclast undifferentiated, As intrabasinal constituent;

10.7% Calcite, Blocky, Interparticle replacive, Replacing <Diagenetic-Constituent>, Diagenetic silica, Interparticle replacive;

9.7% Opal, Cryptocrystalline, Interparticle replacive, Replacing <Primary-Constituent>, Micritic matrix syndepositional, As intrabasinal constituent;

3.7% Calcite, Blocky, Interparticle replacive, Replacing <Primary-Constituent>, Micritic matrix syndepositional, As intrabasinal constituent;

2.0% Calcite, Blocky, Intraparticle replacive, Replacing <Diagenetic-Constituent>, Diagenetic silica, Intraparticle replacive;

1.7% Diagenetic iron oxide/hydroxide, Pelletoid, Interparticle replacive, Replacing <Primary-Constituent>, Micritic matrix syndepositional, As intrabasinal constituent;

1.0% Diagenetic silica, Coarsely-crystalline, Intraparticle replacive, Replacing <Primary-Constituent>, Carbonate bioclast undifferentiated, As intrabasinal constituent;

1.0% Dolomite, Small rhomb, Intraparticle replacive, Replacing <Diagenetic-Constituent>, Calcite, Intraparticle replacive;

1.0% Dolomite, Small rhomb, Interparticle replacive, Replacing <Primary-Constituent>, Micritic matrix syndepositional, As intrabasinal constituent;

0.7% Diagenetic silica, Fibrous, Intraparticle replacive, Replacing <Primary-Constituent>, Carbonate bioclast undifferentiated, As intrabasinal constituent;

0.7% Chalcedony, Spherulite, Intraparticle replacive, Replacing <Primary-Constituent>, Carbonate bioclast undifferentiated, As intrabasinal constituent;
0.7% Calcite, Blocky, Filling intraparticle pore, Within <Diagenetic-Constituent>, Diagenetic silica, Intraparticle replacive;
0.7% Calcite, Blocky, Intraparticle replacive, Replacing <Primary-Constituent>, Carbonate bioclast undifferentiated, As intrabasinal constituent;
0.3% Opal, Cryptocrystalline, Filling intraparticle pore, Within <Primary-Constituent>, Brachiopod bioclast, Framework;
0.3% Opal, Cryptocrystalline, Interparticle replacive, Replacing <Diagenetic-Constituent>, Dolomite, Interparticle replacive;
0.3% Diagenetic silica, Microcrystalline, Intraparticle replacive, Replacing <Primary-Constituent>, Brachiopod bioclast, As intrabasinal constituent;
0.3% Diagenetic silica, Microcrystalline, Intraparticle pore-lining, Within <Primary-Constituent>, Carbonate bioclast undifferentiated, As intrabasinal constituent;
0.3% Diagenetic silica, Rim, Interparticle replacive, Covering <Primary-Constituent>, Brachiopod bioclast, As intrabasinal constituent;
0.3% Diagenetic silica, Rosette, Interparticle replacive, Replacing <Primary-Constituent>, Micritic matrix syndepositional, As intrabasinal constituent;
0.3% Diagenetic silica, Rosette, Moldic pore-lining, Within <pore>, Moldic pore, Framework;
0.3% Diagenetic silica, Rosette, Filling interparticle pore, Within <Primary-Constituent>, Micritic matrix syndepositional, As intrabasinal constituent;
0.3% Calcite, Blocky, Filling intraparticle pore, Within <Primary-Constituent>, Brachiopod bioclast, As intrabasinal constituent;
0.3% Diagenetic titanium mineral, Small rhomb, Interparticle replacive, Replacing <Primary-Constituent>, Micritic matrix syndepositional, As intrabasinal constituent;

Porosity

1.0% Interparticle pore, Interstitial, Dissolution of <Primary-Constituent>, Micritic matrix syndepositional, As intrabasinal constituent;
0.7% Moldic pore, Framework, Dissolution of <Primary-Constituent>, Carbonate bioclast undifferentiated, As intrabasinal constituent;

Carbonate Classification:

Name of classification's method:	Grabau, Brankamp, Powers and Folk
Classification result:	Spathic/micritic calcarenite

Total Volumes

Framework:	32.666
Interstitial:	67.333
Cement:	11.666
Matrix:	7.000
Porosity:	1.666
Microporosity:	Not calculated
Total diagenetic constituents:	78.333
Rigid grains:	12.999
Intrabasinal constituents	
Intrabasinal constituents:	36.999
Present primary carbonate constituents:	10.333
Original primary carbonate constituents:	26.999
Intrabasinal grains:	28.999
Present carbonate allochems:	3.333
Original carbonate allochems:	18.999

Primary proportion of original carbonate allochems:	70.370
Present Carbonate bioclasts:	3.333
Original Carbonate bioclasts:	18.666
Present carbonate matrix:	7.000
Original carbonate matrix:	8.000
Primary proportion of original carbonate matrix:	29.629
Carbonate cement:	10.666
Present intrabasinal non-carbonate grains:	9.666
Original intrabasinal non-carbonate grains:	9.999
Dolomite/Calcite ratio:	0.111

Photomicrographs

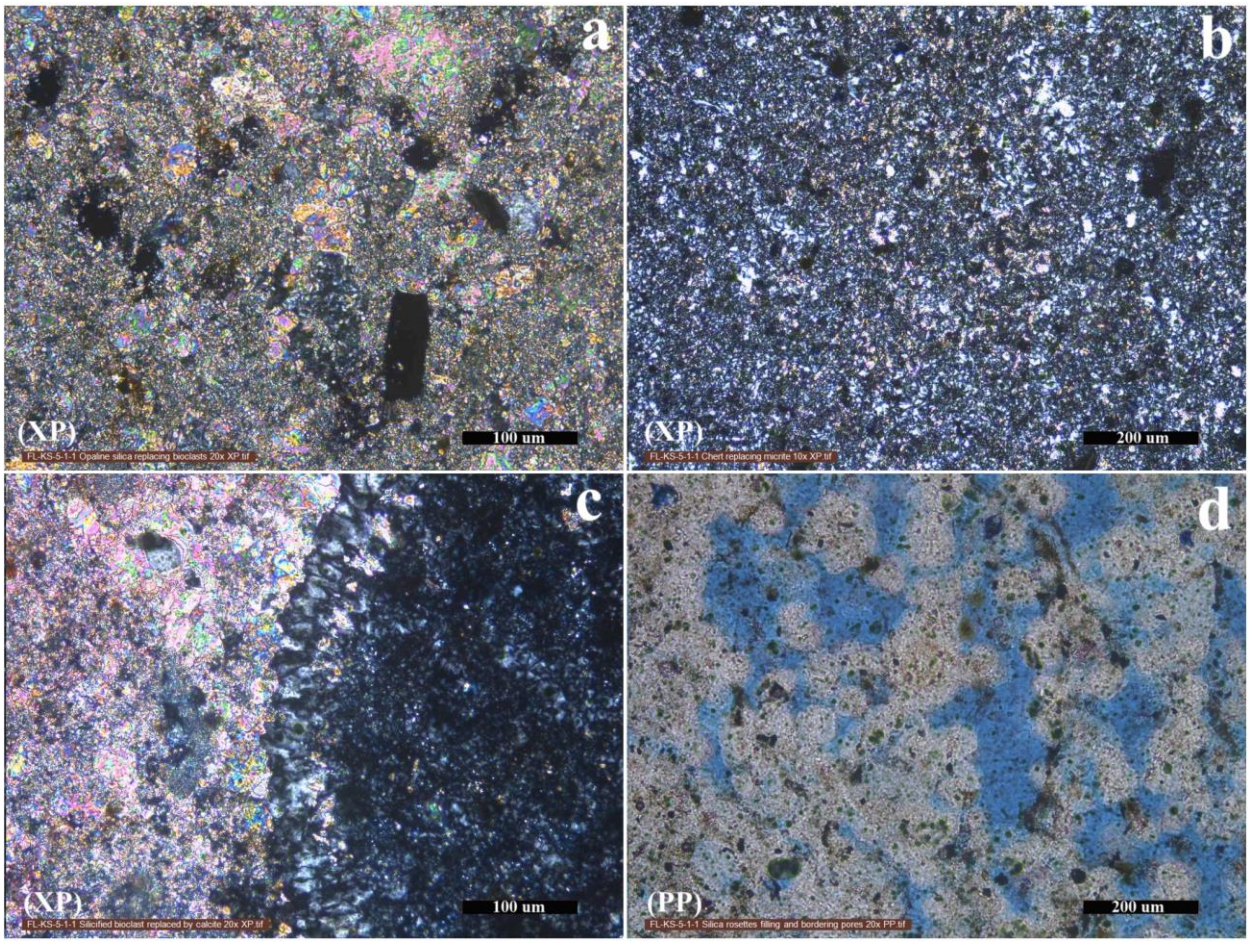

Figure A.8- (a) Moldic pores within micrite filled by opaline silica (b) Chert replacing micrite (c) Carbonate bioclast replaced by chalcedony and chalcedony later replaced by blocky calcite (d) Well-formed/spherical silica rosettes filling dissolution pores.

Thin section ID: **FL-KS-5-1-2**

Summary

Wackestone (=micritic calcarenite) with abundant bioclasts (brachiopods, sponge spicules, gastropods,calcispheres) making about 13%. Micrite and micrite-replacive silica are predominant, accounting for about 50%. Many undifferentiated carbonate bioclasts were replaced by diagenetic silica, making about 25%. Moldic and intraparticle pores resulted from the dissolution of micrite. Opaline silica was observed at diffused boundaries of silica-rich and carbonate-rich zones. Fractures were seen.

Microscopic textural features

Structure(s):	Lamination (0.002-0.006mm), Fractured (0.0-0.0)
Texture	
Grain size range:	Clay (0.0 mm) to Pebble (4.8 mm)
Modal grain size:	Clay (0.0 mm)
Gravel:	2.0%
Sand:	38.0%
Mud:	60.0%
Sorting:	Poorly sorted(2.0)
Sphericity:	Medium
Fabric	
Orientation(s):	Chaotic
Support:	Matrix and matrix-replacive phase supported
Packing:	Loose (40)
Point contacts:	Common (85.0 %)
Long contacts:	Common (15.0 %)

Intrabasinal grains

10.0% Sponge spicule, As intrabasinal constituent;
1.3% Carbonate bioclast undifferentiated, As intrabasinal constituent;
1.0% Brachiopod bioclast, As intrabasinal constituent;
0.7% Carbonate peloid, As intrabasinal constituent;
0.3% Calcisphere bioclast, As intrabasinal constituent;

Matrix

5.7% Micritic matrix syndepositional, As intrabasinal constituent;

Diagenetic Composition

27.3% Diagenetic silica, Microcrystalline, Interparticle replacive, Replacing <Primary-Constituent>, Micritic matrix syndepositional, As intrabasinal constituent;

14.0% Diagenetic silica, Coarsely-crystalline, Intraparticle replacive, Replacing <Primary-Constituent>, Carbonate bioclast undifferentiated, As intrabasinal constituent;

11.0% Diagenetic silica, Microcrystalline, Intraparticle replacive, Replacing <Primary-Constituent>, Carbonate bioclast undifferentiated, As intrabasinal constituent;

6.0% Diagenetic silica, Rosette, Interparticle replacive, Replacing <Primary-Constituent>, Micritic matrix syndepositional, As intrabasinal constituent;

3.3% Diagenetic silica, Rosette, Filling interparticle pore, Within <Primary-Constituent>, Micritic matrix syndepositional, As intrabasinal constituent;

3.3% Calcite, Blocky, Interparticle replacive, Replacing <Diagenetic-Constituent>, Diagenetic silica, Interparticle replacive;

3.3% Diagenetic iron oxide/hydroxide, Pelletoid, Interparticle replacive, Replacing <Primary-Constituent>, Micritic matrix syndepositional, As intrabasinal constituent;

1.3% Diagenetic silica, Microcrystalline, Intraparticle replacive, Replacing <Primary-Constituent>,

Calcisphere bioclast, As intrabasinal constituent;
1.0% Opal, Cryptocrystalline, Interparticle replacive, Replacing <Primary-Constituent>, Micritic matrix syndepositional, As intrabasinal constituent;
0.7% Diagenetic silica, Microcrystalline, Intraparticle replacive, Replacing <Primary-Constituent>, Brachiopod bioclast, As intrabasinal constituent;
0.7% Diagenetic silica, Rosette, Moldic pore-lining, Within <pore>, Moldic pore, Framework;
0.7% Calcite, Blocky, Interparticle replacive, Replacing <Primary-Constituent>, Micritic matrix syndepositional, As intrabasinal constituent;
0.7% Diagenetic titanium mineral, Small rhomb, Interparticle replacive, Replacing <Primary-Constituent>, Micritic matrix syndepositional, As intrabasinal constituent;
0.3% Diagenetic silica, Fibrous, Intraparticle replacive, Replacing <Primary-Constituent>, Carbonate bioclast undifferentiated, As intrabasinal constituent;
0.3% Diagenetic silica, Rim, Intraparticle replacive, Replacing <Primary-Constituent>, Brachiopod bioclast, As intrabasinal constituent;
0.3% Calcite, Blocky, Intraparticle replacive, Replacing <Diagenetic-Constituent>, Diagenetic silica, Intraparticle replacive;
0.3% Calcite, Blocky, Intraparticle replacive, Replacing <Primary-Constituent>, Carbonate bioclast undifferentiated, As intrabasinal constituent;
0.3% Dolomite, Small rhomb, Intraparticle replacive, Replacing <Diagenetic-Constituent>, Calcite, Intraparticle replacive;
0.3% Dolomite, Small rhomb, Interparticle replacive, Replacing <Primary-Constituent>, Micritic matrix syndepositional, As intrabasinal constituent;

Porosity

3.7% Interparticle pore, Interstitial, Dissolution of <Primary-Constituent>, Micritic matrix syndepositional, As intrabasinal constituent;
2.0% Moldic pore, Framework, Dissolution of <Primary-Constituent>, Carbonate bioclast undifferentiated, As intrabasinal constituent;

Carbonate Classification:

Name of classification's method:	Grabau, Brankamp, Powers and Folk
Classification result:	Micritic/spathic calcarenite

Total Volumes

Framework:	44.666
Interstitial:	55.333
Cement:	6.666
Matrix:	5.666
Porosity:	5.666
Microporosity:	Not calculated
Total diagenetic constituents:	75.333
Rigid grains:	12.666
Ductile grains:	0.666

Intrabasinal constituents

Intrabasinal constituents:	54.000
Present primary carbonate constituents:	9.000
Original primary carbonate constituents:	43.333
Intrabasinal grains:	44.666
Present carbonate allochems:	3.333
Original carbonate allochems:	34.000
Primary proportion of original carbonate allochems:	78.461
Present Carbonate bioclasts:	2.666

Original Carbonate bioclasts:	32.666
Carbonate peloids/pellets:	0.666
Present carbonate matrix:	5.666
Original carbonate matrix:	9.333
Primary proportion of original carbonate matrix:	21.538
Carbonate cement:	3.333
Present intrabasinal non-carbonate grains:	10.000
Original intrabasinal non-carbonate grains:	10.666
Dolomite/Calcite ratio:	0.142

Photomicrographs

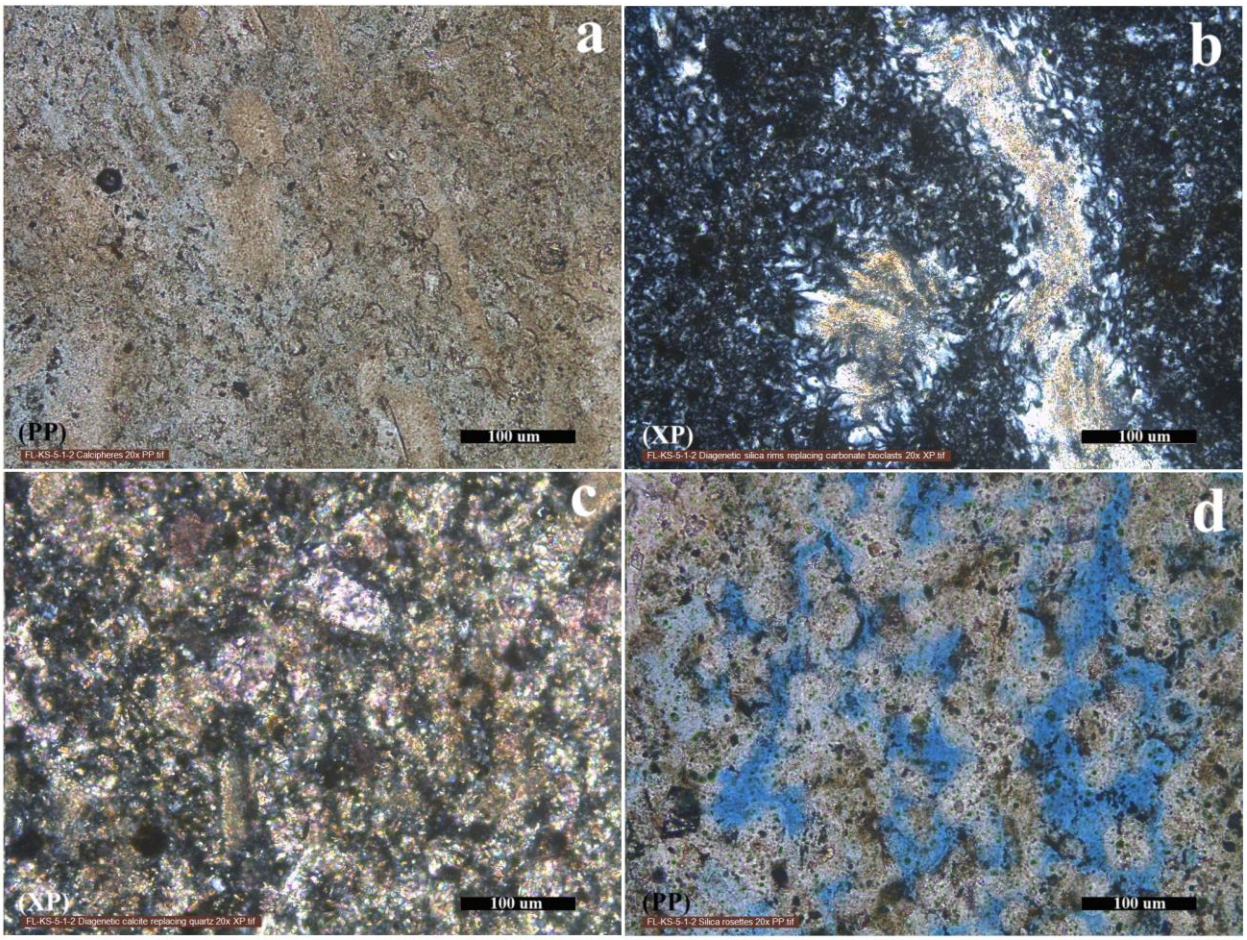

Figure A.9- (a) Abundant calcisphere bioclasts (b) Diagenetic silica rims replacing carbonate bioclast indicating a replacive reaction (c) Blocky calcite replacing chert (d) Silica rosettes filling dissolution pores.

Thin section ID: **FL-KS-5-2-1**

Summary

Wackestone (=micritic calcarenite) with abundant bioclasts (brachiopods, sponge spicules, corals,calcispheres) making about 15%. Micrite and micrite-replacive silica are predominant, accounting for about 35%. Many undifferentiated carbonate bioclasts were replaced by diagenetic silica, making about 25%. Moldic and intraparticle pores resulted from the dissolution of micrite. Opaline silica was observed at diffused boundaries of silica-rich and carbonate-rich zones. Micrite was replaced by calcite, and calcite was replaced by dolomite. Fractures were observed.

Microscopic textural features

Structure(s):	Nodular (0.002-0.006mm), Fractured (0.0-0.0)
Texture	
Grain size range:	Clay (0.0 mm) to Pebble (14.0 mm)
Modal grain size:	Clay (0.0 mm)
Gravel:	2.0%
Sand:	28.0%
Mud:	70.0%
Sorting:	Poorly sorted(2.0)
Sphericity:	Medium
Fabric	
Orientation(s):	Chaotic
Support:	Matrix and matrix-replacive phase supported
Packing:	Loose (40)
Point contacts:	Common (85.0 %)
Long contacts:	Common (15.0 %)

Intrabasinal grains

1.7% Carbonate bioclast undifferentiated, As intrabasinal constituent;
1.3% Sponge spicule, As intrabasinal constituent;
1.3% Brachiopod bioclast, As intrabasinal constituent;

Matrix

5.7% Micritic matrix syndepositional, As intrabasinal constituent;

Diagenetic Composition

30.3% Diagenetic silica, Microcrystalline, Interparticle replacive, Replacing <Primary-Constituent>, Micritic matrix syndepositional, As intrabasinal constituent;

21.0% Diagenetic silica, Coarsely-crystalline, Intraparticle replacive, Replacing <Primary-Constituent>, Carbonate bioclast undifferentiated, As intrabasinal constituent;

7.0% Diagenetic silica, Microcrystalline, Intraparticle replacive, Replacing <Primary-Constituent>, Calcisphere bioclast, As intrabasinal constituent;

5.3% Diagenetic silica, Rosette, Interparticle replacive, Replacing <Primary-Constituent>, Micritic matrix syndepositional, As intrabasinal constituent;

2.7% Diagenetic silica, Microcrystalline, Intraparticle replacive, Replacing <Primary-Constituent>, Carbonate bioclast undifferentiated, As intrabasinal constituent;

2.7% Diagenetic silica, Rosette, Filling interparticle pore, Within <Primary-Constituent>, Micritic matrix syndepositional, As intrabasinal constituent;

2.3% Calcite, Blocky, Intraparticle replacive, Replacing <Diagenetic-Constituent>, Diagenetic silica, Intraparticle replacive;

1.7% Opal, Cryptocrystalline, Interparticle replacive, Replacing <Primary-Constituent>, Micritic matrix syndepositional, As intrabasinal constituent;

1.7% Diagenetic silica, Microcrystalline, Intraparticle replacive, Replacing <Primary-Constituent>, Brachiopod bioclast, As intrabasinal constituent;

1.7% Chalcedony, Spherulite, Intraparticle replacive, Replacing <Diagenetic-Constituent>, Diagenetic

silica, Intraparticle replacive;
1.7% Diagenetic iron oxide/hydroxide, Pelletoid, Interparticle replacive, Replacing <Primary-Constituent>, Micritic matrix syndepositional, As intrabasinal constituent;
1.3% Diagenetic silica, Rim, Intraparticle replacive, Replacing <Primary-Constituent>, Brachiopod bioclast, As intrabasinal constituent;
1.0% Calcite, Blocky, Interparticle replacive, Replacing <Primary-Constituent>, Micritic matrix syndepositional, As intrabasinal constituent;
0.7% Diagenetic silica, Rosette, Moldic pore-lining, Within <pore>, Moldic pore, Framework;
0.7% Dolomite, Small rhomb, Intraparticle replacive, Replacing <Diagenetic-Constituent>, Calcite, Intraparticle replacive;
0.7% Dolomite, Small rhomb, Interparticle replacive, Replacing <Primary-Constituent>, Micritic matrix syndepositional, As intrabasinal constituent;
0.7% Diagenetic titanium mineral, Small rhomb, Interparticle replacive, Replacing <Primary-Constituent>, Micritic matrix syndepositional, As intrabasinal constituent;
0.3% Diagenetic silica, Microcrystalline, Intraparticle pore-lining, Replacing <Primary-Constituent>, Bryozoan bioclast, As intrabasinal constituent;
0.3% Diagenetic silica, Rim, Intraparticle replacive, Replacing <Primary-Constituent>, Carbonate bioclast undifferentiated, As intrabasinal constituent;
0.3% Diagenetic silica, Rosette, Rock fracture-lining, Within <pore>, Fracture pore, Framework and interstitial;
0.3% Calcite, Blocky, Intraparticle replacive, Replacing <Primary-Constituent>, Carbonate bioclast undifferentiated, As intrabasinal constituent;
0.3% Calcite, Blocky, Interparticle replacive, Replacing <Diagenetic-Constituent>, Diagenetic silica, Interparticle replacive;
0.3% Calcite, Rim, Intraparticle replacive, Replacing <Primary-Constituent>, Carbonate bioclast undifferentiated, As intrabasinal constituent;
0.3% Diagenetic iron oxide/hydroxide, Pelletoid, Filling intraparticle pore, Within <Primary-Constituent>, Micritic matrix syndepositional, As intrabasinal constituent;

Porosity

2.0% Interparticle pore, Interstitial, Dissolution of <Primary-Constituent>, Micritic matrix syndepositional, As intrabasinal constituent;
1.7% Fracture pore, Framework and interstitial;
1.0% Moldic pore, Framework, Dissolution of <Primary-Constituent>, Carbonate bioclast undifferentiated, As intrabasinal constituent;

Carbonate Classification:

Name of classification's method:	Grabau, Brankamp, Powers and Folk
Classification result:	Micritic/spathic calcarenite

Diagenetic environments with some evidences

Siliciclastic environment of eodiagenesis under marine conditions

Total Volumes

Framework:	47.999
Interstitial:	52.000
Cement:	3.000
Matrix:	5.666
Porosity:	4.666
Microporosity:	Not calculated
Total diagenetic constituents:	85.333
Rigid grains:	4.333

Intrabasinal constituents

Intrabasinal constituents:	49.333
Present primary carbonate constituents:	8.666
Original primary carbonate constituents:	47.333
Intrabasinal grains:	41.666
Present carbonate allochems:	3.000
Original carbonate allochems:	39.666
Primary proportion of original carbonate allochems:	83.802
Present Carbonate bioclasts:	3.000
Original Carbonate bioclasts:	38.999
Present carbonate matrix:	5.666
Original carbonate matrix:	7.666
Primary proportion of original carbonate matrix:	16.197
Carbonate cement:	0.333
Present intrabasinal non-carbonate grains:	1.333
Original intrabasinal non-carbonate grains:	2.000
Dolomite/Calcite ratio:	0.307

Photomicrographs

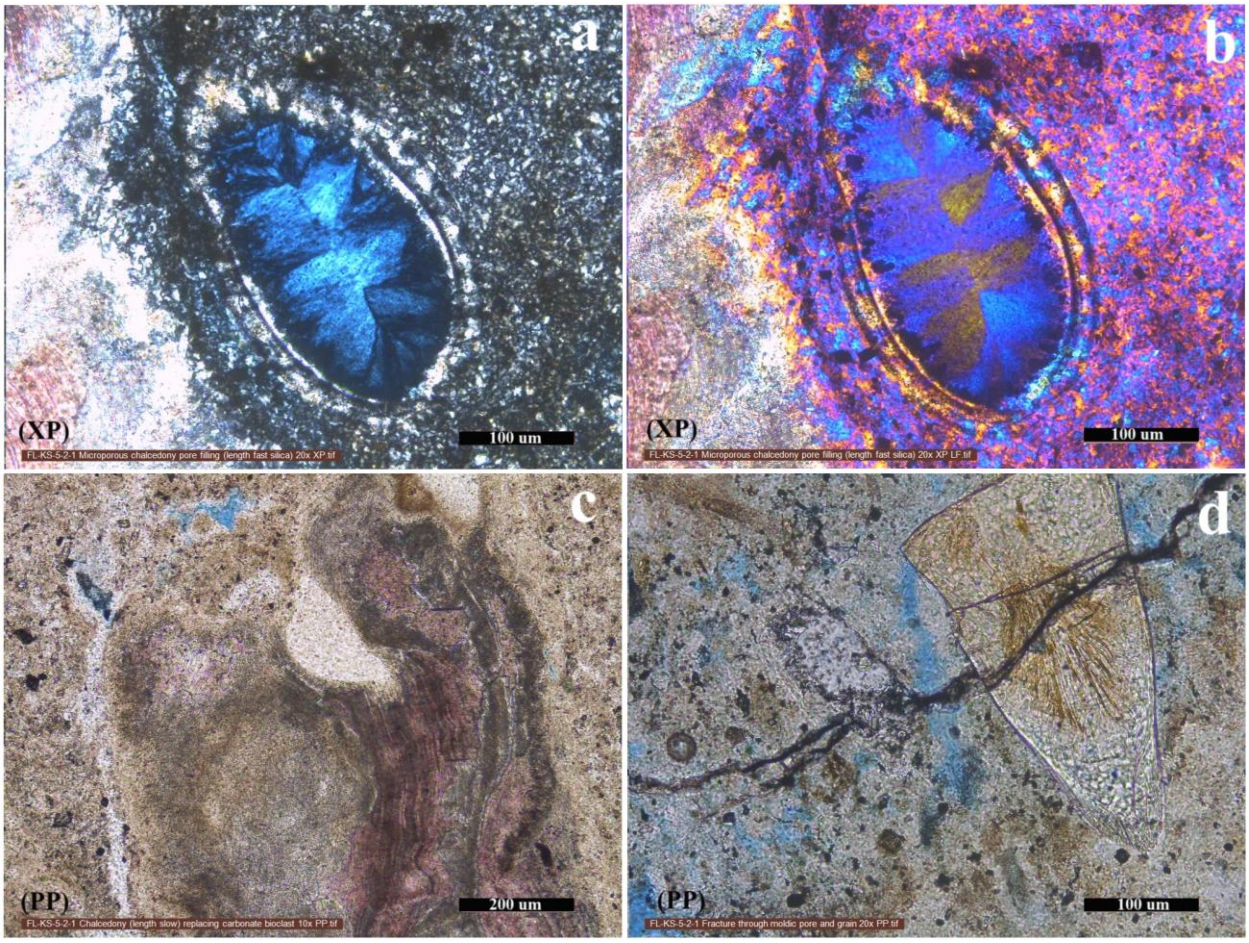

Figure A.10- (a and b) Intraparticular pore of a brachiopod shell filled by length fast chalcedony (a = XPL and b = XPL with gypsum plate). Note the surrounding chert matrix with some parts of bioclast replaced by calcite (c) Chalcedony replacing carbonate bioclast (d) Stylolite formed through a phosphate grain.

Thin section ID: **FL-KS-5-2-2**

Summary

Wackestone (=micritic calcarenite) with abundant bioclasts (brachiopods, sponge spicules, calcispheres, bryozoans), about 5%-6% still preserved. Micrite and micrite-replacive silica are predominant, accounting for about 70%. Many carbonate bioclasts were replaced by diagenetic silica, making up about 30%. Moldic and interparticle pores resulted from the dissolution of micrite. Opaline silica replacing interparticle micrite and intraparticle carbonate. Micrite and bioclasts were partially replaced by calcite. Fractures and stylolites observed.

Microscopic textural features

Structure(s): Nodular (0.002-0.006mm), Fractured (0.0-0.0), Stylolite (0.0-0.0)

Texture

Grain size range: Clay (0.0 mm) to Pebble (14.0 mm)

Modal grain size: Clay (0.0 mm)

Gravel:	2.0%
Sand:	33.0%
Mud:	65.0%
Sorting:	Moderately sorted(0.7)
Sphericity:	Medium

Fabric

Orientation(s):	Chaotic
Support:	Matrix and matrix-replacive phase supported
Packing:	Loose (40)
Point contacts:	Common (85.0 %)
Long contacts:	Common (15.0 %)

Intrabasinal grains

1.0% Carbonate bioclast undifferentiated, As intrabasinal constituent;
1.0% Brachiopod bioclast, As intrabasinal constituent;
1.0% Calcisphere bioclast, As intrabasinal constituent;
0.3% Sponge spicule, As intrabasinal constituent;
0.3% Phosphate bioclast undifferentiated, As intrabasinal constituent;

Matrix

10.7% Micritic matrix syndepositional, As intrabasinal constituent;

Diagenetic Composition

24.7% Diagenetic silica, Microcrystalline, Interparticle replacive, Replacing <Primary-Constituent>, Micritic matrix syndepositional, As intrabasinal constituent;

20.3% Diagenetic silica, Microcrystalline, Intraparticle replacive, Replacing <Primary-Constituent>, Carbonate bioclast undifferentiated, As intrabasinal constituent;

12.7% Diagenetic silica, Rosette, Interparticle replacive, Replacing <Primary-Constituent>, Micritic matrix syndepositional, As intrabasinal constituent;

7.7% Diagenetic silica, Microcrystalline, Intraparticle replacive, Replacing <Primary-Constituent>, Calcisphere bioclast, As intrabasinal constituent;

6.7% Opal, Cryptocrystalline, Interparticle replacive, Replacing <Primary-Constituent>, Micritic matrix syndepositional, As intrabasinal constituent;

3.3% Diagenetic silica, Rosette, Lining interparticle pore, Within <Primary-Constituent>, Micritic matrix syndepositional, As intrabasinal constituent;

1.7% Diagenetic silica, Rosette, Moldic pore-filling, Within <Primary-Constituent>, Carbonate bioclast undifferentiated, In intrabasinal constituent;

1.3% Chalcedony, Spherulite, Intraparticle replacive, Replacing <Diagenetic-Constituent>, Diagenetic silica, Intraparticle replacive;

1.0% Diagenetic silica, Rim, Intraparticle replacive, Replacing <Primary-Constituent>, Brachiopod bioclast, As intrabasinal constituent;

0.7% Diagenetic silica, Rosette, Moldic pore-lining, Within <pore>, Moldic pore, Framework;

0.7% Calcite, Blocky, Intraparticle replacive, Replacing <Diagenetic-Constituent>, Diagenetic silica, Intraparticle replacive;

0.7% Diagenetic titanium mineral, Small rhomb, Interparticle replacive, Replacing <Primary-Constituent>, Micritic matrix syndepositional, As intrabasinal constituent;

0.3% Diagenetic silica, Rosette, Filling intraparticle pore, Within <Primary-Constituent>, Brachiopod bioclast, As intrabasinal constituent;

0.3% Calcite, Blocky, Filling intraparticle pore, Within <Primary-Constituent>, Calcisphere bioclast, Framework;

0.3% Diagenetic iron oxide/hydroxide, Pelletoid, Interparticle replacive, Replacing <Primary-Constituent>, Micritic matrix syndepositional, As intrabasinal constituent;

Porosity

2.0% Interparticle pore, Interstitial, Dissolution of <Primary-Constituent>, Micritic matrix syndepositional, As intrabasinal constituent;

1.3% Moldic pore, Framework, Dissolution of <Primary-Constituent>, Carbonate bioclast undifferentiated, As intrabasinal constituent;

Carbonate Classification:

Name of classification's method:	Grabau, Brankamp, Powers and Folk
Classification result:	Micritic calcarenite

Total Volumes

Framework:	39.000
Interstitial:	60.999
Cement:	3.333
Matrix:	10.666
Porosity:	3.333
Microporosity:	Not calculated
Total diagenetic constituents:	82.333
Rigid grains:	3.666
Intrabasinal constituents	
Intrabasinal constituents:	48.333
Present primary carbonate constituents:	13.666
Original primary carbonate constituents:	47.000
Intrabasinal grains:	35.666
Present carbonate allochems:	3.000
Original carbonate allochems:	34.333
Primary proportion of original carbonate allochems:	73.049
Present Carbonate bioclasts:	3.000
Original Carbonate bioclasts:	33.666
Present carbonate matrix:	10.666
Original carbonate matrix:	12.666
Primary proportion of original carbonate matrix:	26.950
Present intrabasinal non-carbonate grains:	0.666
Original intrabasinal non-carbonate grains:	1.333

Photomicrographs

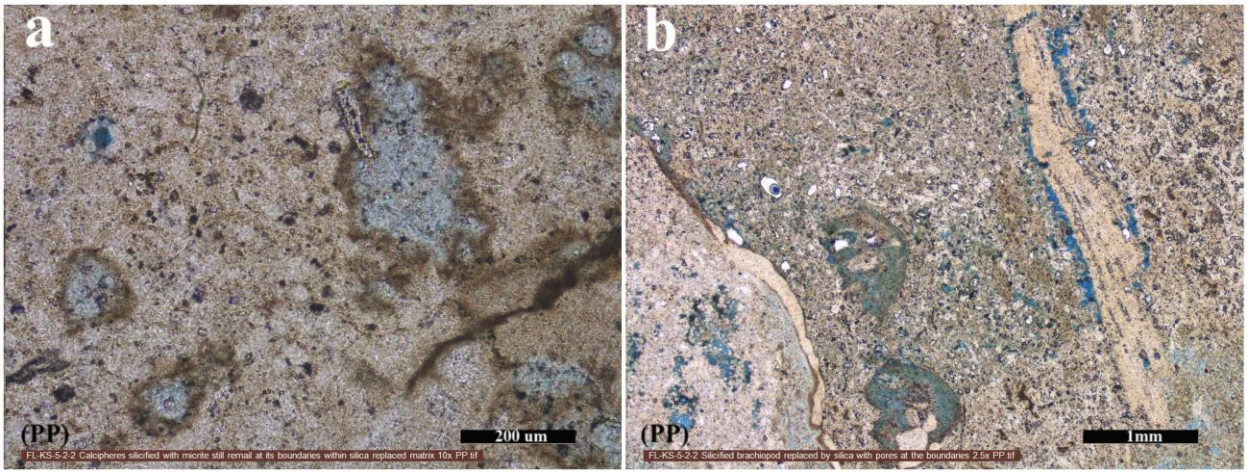

Figure A.11- (a) Calcispheres silicified with some micrite remnants within the silica-replaced matrix (b) Silicified brachiopod shell replaced by chalcedony with dissolution pores at the boundaries of fossil.

Thin section ID: **FL-KS-5-2-3**

Summary

Wackestone (=micritic calcarenite) with abundant bioclasts (brachiopods, sponge spicules, bryozoans,calcispheres) making about 25%. Micrite and micrite-replacive silica are predominant, accounting for about 45%. Many undifferentiated carbonate bioclasts are replaced by diagenetic silica, making about 10%, while diagenetic calcite replaces about 20% of diagenetic silica. Moldic and intraparticle pores resulted from the dissolution of micrite. Opaline silica was observed in wood-grained and adjacent regions. Stylolites and fractures were observed.

Microscopic textural features

Structure(s): Lamination (0.002-0.006mm), Fractured (0.0-0.0), Stylolite (0.0-0.0)

Texture

Grain size range:	Clay (0.0 mm) to Very coarse sand (2.0 mm)
Modal grain size:	Clay (0.0 mm)
Sand:	25.0%
Mud:	75.0%
Sorting:	Poorly sorted(2.0)
Sphericity:	Medium

Fabric

Orientation(s):	Chaotic
Support:	Matrix and matrix-replacive phase supported
Packing:	Loose (40)
Point contacts:	Common (85.0 %)
Long contacts:	Common (15.0 %)

Intrabasinal grains

2.0% Carbonate bioclast undifferentiated, As intrabasinal constituent;
1.0% Brachiopod bioclast, As intrabasinal constituent;
0.3% Sponge spicule, As intrabasinal constituent;

0.3% Bryozoan bioclast, As intrabasinal constituent;

Matrix

17.7% Micritic matrix syndepositional, As intrabasinal constituent;

Diagenetic Composition

13.7% Diagenetic silica, Microcrystalline, Interparticle replacive, Replacing <Primary-Constituent>, Micritic matrix syndepositional, As intrabasinal constituent;

10.0% Diagenetic silica, Rosette, Interparticle replacive, Replacing <Primary-Constituent>, Micritic matrix syndepositional, As intrabasinal constituent;

8.7% Calcite, Blocky, Intraparticle replacive, Replacing <Diagenetic-Constituent>, Diagenetic silica, Intraparticle replacive;

8.0% Diagenetic silica, Coarsely-crystalline, Intraparticle replacive, Replacing <Primary-Constituent>, Carbonate bioclast undifferentiated, As intrabasinal constituent;

7.0% Opal, Cryptocrystalline, Interparticle replacive, Replacing <Primary-Constituent>, Micritic matrix syndepositional, As intrabasinal constituent;

5.7% Diagenetic silica, Rosette, Interparticle continous pore-lining, Within <Primary-Constituent>, Micritic matrix syndepositional, As intrabasinal constituent;

4.0% Calcite, Blocky, Interparticle replacive, Replacing <Primary-Constituent>, Micritic matrix syndepositional, As intrabasinal constituent;

3.0% Calcite, Blocky, Intraparticle replacive, Replacing <Primary-Constituent>, Carbonate bioclast undifferentiated, Framework;

2.7% Diagenetic silica, Rim, Intraparticle replacive, Replacing <Primary-Constituent>, Brachiopod bioclast, As intrabasinal constituent;

2.3% Diagenetic silica, Microcrystalline, Intraparticle replacive, Replacing <Primary-Constituent>, Carbonate bioclast undifferentiated, As intrabasinal constituent;

1.3% Diagenetic silica, Rosette, Moldic pore-lining, Within <pore>, Moldic pore, Framework;

1.3% Dolomite, Small rhomb, Interparticle replacive, Replacing <Diagenetic-Constituent>, Calcite, Interparticle replacive;

0.7% Chalcedony, Spherulite, Intraparticle replacive, Replacing <Diagenetic-Constituent>, Diagenetic silica, Intraparticle replacive;

0.7% Diagenetic titanium mineral, Small rhomb, Interparticle replacive, Replacing <Primary-Constituent>, Micritic matrix syndepositional, As intrabasinal constituent;

0.3% Diagenetic silica, Microcrystalline, Intraparticle replacive, Replacing <Primary-Constituent>, Calcisphere bioclast, As intrabasinal constituent;

0.3% Diagenetic silica, Microcrystalline, Intraparticle pore-lining, Within <Primary-Constituent>, Micritic matrix syndepositional, As intrabasinal constituent;

0.3% Calcite, Blocky, Intraparticle replacive, Replacing <Primary-Constituent>, Brachiopod bioclast, As intrabasinal constituent;

0.3% Calcite, Rim, Intraparticle replacive, Replacing <Primary-Constituent>, Sponge spicule, As intrabasinal constituent;

0.3% Dolomite, Small rhomb, Intraparticle replacive, Replacing <Diagenetic-Constituent>, Diagenetic silica, Intraparticle replacive;

Porosity

5.3% Interparticle pore, Interstitial, Dissolution of <Primary-Constituent>, Micritic matrix syndepositional, As intrabasinal constituent;

2.0% Moldic pore, Framework, Dissolution of <Primary-Constituent>, Carbonate bioclast undifferentiated, As intrabasinal constituent;

0.7% Fracture pore, Framework and interstitial, Stylolite;

Carbonate Classification:

Name of classification's method: Grabau, Brankamp, Powers and Folk

Classification result: Micritic/spathic calcarenite

Diagenetic environments with some evidences

Siliciclastic environment of eodiagenesis under marine conditions

Total Volumes

Framework:	34.666
Interstitial:	65.333
Cement:	7.000
Matrix:	17.666
Porosity:	8.000
Microporosity:	Not calculated
Total diagenetic constituents:	70.666
Rigid grains:	3.666

Intrabasinal constituents

Intrabasinal constituents:	45.333
Present primary carbonate constituents:	21.000
Original primary carbonate constituents:	43.333
Intrabasinal grains:	22.333
Present carbonate allochems:	3.333
Original carbonate allochems:	20.333
Primary proportion of original carbonate allochems:	46.923
Present Carbonate bioclasts:	3.333
Original Carbonate bioclasts:	19.000
Present carbonate matrix:	17.666
Original carbonate matrix:	23.000
Primary proportion of original carbonate matrix:	53.076
Carbonate cement:	1.333
Present intrabasinal non-carbonate grains:	0.333
Original intrabasinal non-carbonate grains:	2.000
Dolomite/Calcite ratio:	0.102

Photomicrographs

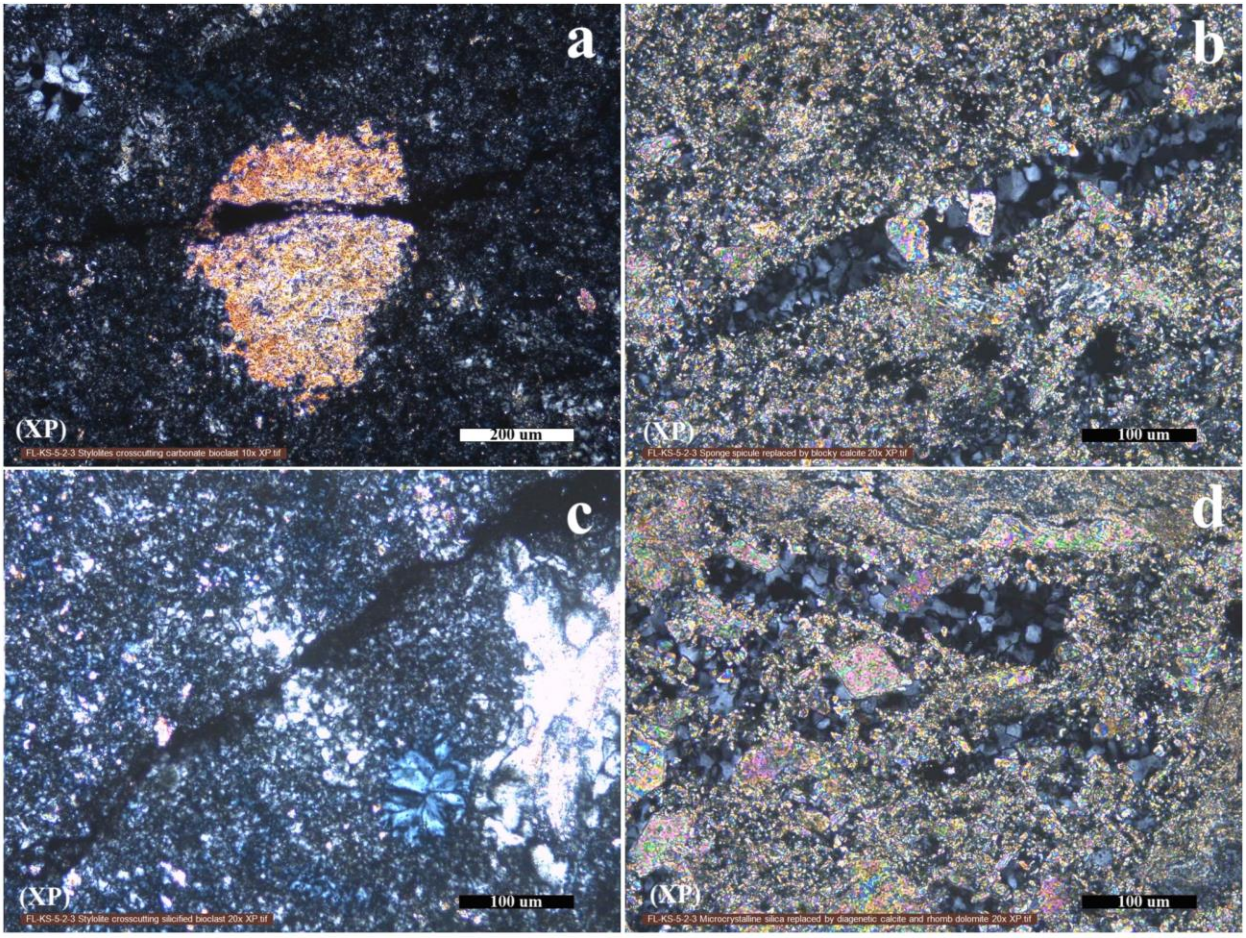

Figure A.12- (a) Opaline silica precipitated within a stylolite cutting an undifferentiated carbonate bioclast (b) Blocky calcite replacing a recrystalized sponge spicule (c) Spherulitic chalcedony replacing a brachiopod spine (d) Dolomite rhomb replacing chert.

Thin section ID: **FL-KS-5-3**

Summary

Wackestone (=micritic calcarenite) with abundant bioclasts (brachiopods, sponge spicules, bryozoans,calcispheres, corals, undifferentiated bioclasts) making about 10% of pristine bioclasts. Micrite and micrite-replacive silica are predominant, accounting for about 65%. ~25% of undifferentiated bioclasts were replaced by diagenetic silica and calcite. Dolomite rhombs replacing calcite. Opaline silica along lines replacing micrite. Opaline silica was replaced by diagenetic quartz and calcite.

Microscopic textural features

Structure(s):	Lamination (0.002-0.006mm)
Texture	
Grain size range:	Clay (0.0 mm) to Pebble (6.1 mm)
Modal grain size:	Clay (0.0 mm)
Sand:	35.0%
Mud:	65.0%
Sorting:	Poorly sorted(2.0)

Sphericity:	Medium

Fabric

Orientation(s):	Chaotic
Support:	Supported by grain-replacive material and by the cement
Packing:	Loose (40)
Point contacts:	Common (85.0 %)
Long contacts:	Common (15.0 %)

Intrabasinal grains

3.7% Brachiopod bioclast, As intrabasinal constituent;
3.3% Carbonate bioclast undifferentiated, As intrabasinal constituent;
1.0% Sponge spicule, As intrabasinal constituent;
0.7% Bryozoan bioclast, As intrabasinal constituent;
0.3% Calcisphere bioclast, As intrabasinal constituent;
0.3% Coral bioclast, As intrabasinal constituent;

Matrix

35.0% Micritic matrix syndepositional, As intrabasinal constituent;

Diagenetic Composition

20.0% Calcite, Blocky, Intraparticle replacive, Replacing <Diagenetic-Constituent>, Diagenetic silica, Intraparticle replacive;
12.3% Calcite, Blocky, Interparticle replacive, Replacing <Primary-Constituent>, Micritic matrix syndepositional, As intrabasinal constituent;
6.0% Dolomite, Small rhomb, Intraparticle replacive, Replacing <Diagenetic-Constituent>, Diagenetic silica, Intraparticle replacive;
5.3% Opal, Cryptocrystalline, Interparticle replacive, Replacing <Primary-Constituent>, Micritic matrix syndepositional, As intrabasinal constituent;
3.3% Diagenetic silica, Coarsely-crystalline, Intraparticle replacive, Replacing <Primary-Constituent>, Carbonate bioclast undifferentiated, As intrabasinal constituent;
1.3% Diagenetic silica, Microcrystalline, Intraparticle replacive, Replacing <Primary-Constituent>, Carbonate bioclast undifferentiated, As intrabasinal constituent;
1.0% Chalcedony, Spherulite, Intraparticle replacive, Replacing <Diagenetic-Constituent>, Diagenetic silica, Intraparticle replacive;
1.0% Calcite, Blocky, Intraparticle replacive, Replacing <Primary-Constituent>, Carbonate bioclast undifferentiated, Framework;
1.0% Dolomite, Small rhomb, Interparticle replacive, Replacing <Diagenetic-Constituent>, Calcite, Interparticle replacive;
1.0% Dolomite, Blocky, Intraparticle replacive, Replacing <Diagenetic-Constituent>, Calcite, Intraparticle replacive;
1.0% Diagenetic iron oxide/hydroxide, Pelletoid, Replacing <Primary-Constituent>, Micritic matrix syndepositional, As intrabasinal constituent;
0.7% Diagenetic silica, Microcrystalline, Interparticle replacive, Replacing <Primary-Constituent>, Micritic matrix syndepositional, As intrabasinal constituent;
0.7% Chalcedony, Spherulite, Intraparticle replacive, Replacing <Primary-Constituent>, Brachiopod bioclast, As intrabasinal constituent;
0.3% Diagenetic silica, Rim, Intraparticle replacive, Replacing <Primary-Constituent>, Brachiopod bioclast, As intrabasinal constituent;
0.3% Calcite, Blocky, Intraparticle replacive, Replacing <Primary-Constituent>, Calcisphere bioclast, As intrabasinal constituent;
0.3% Calcite, Rim, Intraparticle replacive, Replacing <Primary-Constituent>, Sponge spicule, As intrabasinal constituent;

Carbonate Classification:

Name of classification's method:	Grabau, Brankamp, Powers and Folk
Classification result:	Micritic/spathic calcarenite

Diagenetic environments with some evidences

Siliciclastic environment of eodiagenesis under marine conditions

Total Volumes

Framework:	45.666
Interstitial:	54.333
Cement:	1.000
Matrix:	35.000
Porosity:	0.000
Microporosity:	Not calculated
Total diagenetic constituents:	55.666
Rigid grains:	9.333
Intrabasinal constituents:	50.666
Present primary carbonate constituents:	43.333
Original primary carbonate constituents:	49.333
Intrabasinal grains:	15.666
Present carbonate allochems:	8.333
Original carbonate allochems:	14.333
Primary proportion of original carbonate allochems:	29.054
Present Carbonate bioclasts:	8.333
Original Carbonate bioclasts:	14.333
Present carbonate matrix:	35.000
Original carbonate matrix:	35.000
Primary proportion of original carbonate matrix:	70.945
Carbonate cement:	1.000
Present intrabasinal non-carbonate grains:	1.000
Original intrabasinal non-carbonate grains:	1.333
Dolomite/Calcite ratio:	0.235

Photomicrographs

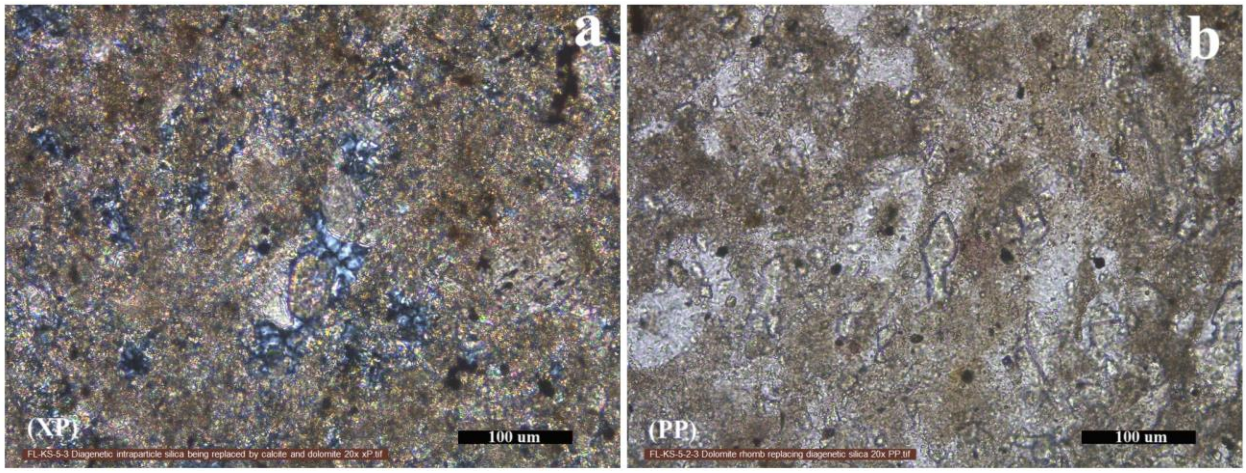

Figure A.13- (a and b) Diagenetic calcite and dolomite rhombs replacing chert.

Thin section ID: **FL-KS-6-1**

Summary

Wackestone (=micritic calcarenite) with bioclasts (brachiopods, sponge spicules, calcispheres, crinoids, ostracods) making about 10%. About 50% of the thin section is occupied by a geode partially filled with sulfate (baryite?) or quartz?, which replaced anhydrite, and later baryite/quartz is replaced by chalcedony rosettes (with ghosts of prismatic crystals within). Abundant moldic pores within baryte/quartz due to the dissolution of anhydrite acicular crystals. The rest of the thin section is made of chert, replacing micrite and bioclasts.

Microscopic textural features

Structure(s):	Nodular (0.002-0.006mm)
Texture	
Grain size range:	Clay (0.0 mm) to Pebble (5.6 mm)
Modal grain size:	Clay (0.0 mm)
Gravel:	4.0%
Sand:	35.0%
Mud:	61.0%
Sorting:	Poorly sorted(2.0)
Sphericity:	Medium
Fabric	
Orientation(s):	Chaotic
Support:	Matrix-replacive phase supported
Packing:	Loose (40)
Point contacts:	Common (85.0 %)
Long contacts:	Common (15.0 %)

Intrabasinal grains

1.3% Brachiopod bioclast, As intrabasinal constituent;
1.0% Sponge spicule, As intrabasinal constituent;
0.3% Calcisphere bioclast, As intrabasinal constituent;
0.3% Crinoid bioclast, As intrabasinal constituent;

Matrix

1.3% Micritic matrix syndepositional, As intrabasinal constituent;

Diagenetic Composition

20.3% Baryte, Coarsely-crystalline, Interparticle replacive, Replacing <Diagenetic-Constituent>, Anhydrite, Concretions/nodules, Or quartz?;

20.0% Chalcedony, Spherulite, Interparticle replacive, Replacing <Diagenetic-Constituent>, Baryte, Interparticle replacive, Replacing baryte that replaces anhydrite nodule;

14.7% Diagenetic silica, Microcrystalline, Interparticle replacive, Replacing <Primary-Constituent>, Micritic matrix syndepositional, As intrabasinal constituent;

9.7% Baryte, Prismatic, Interparticle replacive, Replacing <Diagenetic-Constituent>, Anhydrite, Concretions/nodules, Or quartz?;

5.3% Opal, Microcrystalline, Interparticle replacive, Replacing <Primary-Constituent>, Micritic matrix syndepositional, As intrabasinal constituent;

5.3% Diagenetic silica, Microcrystalline, Intraparticle replacive, Replacing <Primary-Constituent>, Carbonate bioclast undifferentiated, As intrabasinal constituent;

2.7% Diagenetic silica, Microcrystalline, Intraparticle replacive, Replacing <Primary-Constituent>, Brachiopod bioclast, As intrabasinal constituent;

2.3% Diagenetic iron oxide/hydroxide, Pelletoid, Interparticle replacive, Replacing <Diagenetic-Constituent>, Baryte, Interparticle replacive;

1.7% Anhydrite, Prismatic, Interparticle displacive, Displacing <Primary-Constituent>, Micritic matrix syndepositional, As intrabasinal constituent, Inclusions;

1.3% Chalcedony, Rim, Interparticle replacive, Replacing <Diagenetic-Constituent>, Baryte, Interparticle replacive, Replacing baryte that replaces anhydrite nodule;

0.7% Chalcedony, Rim, Intraparticle replacive, Replacing <Primary-Constituent>, Brachiopod bioclast, As intrabasinal constituent;

0.3% Diagenetic silica, Microcrystalline, Interparticle replacive, Replacing <Diagenetic-Constituent>, Baryte, Interparticle replacive, Replacing baryte that replaces anhydrite nodule;

0.3% Diagenetic silica, Microcrystalline, Intraparticle replacive, Replacing <Primary-Constituent>, Calcisphere bioclast, As intrabasinal constituent;

Porosity

9.7% Moldic pore, Framework, Dissolution of <Diagenetic-Constituent>, Anhydrite, Interparticle displacive;

0.7% Interparticle pore, Interstitial, Dissolution of <Primary-Constituent>, Micritic matrix syndepositional, As intrabasinal constituent;

0.3% Moldic pore, Framework, Dissolution of <Primary-Constituent>, Bivalve bioclast, As intrabasinal constituent;

0.3% Vug pore, Framework and interstitial, Within <Diagenetic-Constituent>, Baryte, Interparticle replacive, Remaining pore space within geode;

Carbonate Classification:

Name of classification's method:	Grabau, Brankamp, Powers and Folk
Classification result:	Micritic calcarenite

Interpreted diagenetic environments

Siliciclastic environment of continental meteoric eodiagenesis under dry climate

Total Volumes

Framework:	22.333
Interstitial:	77.666
Cement:	55.666

Matrix:	1.333
Porosity:	10.999
Microporosity:	Not calculated
Total diagenetic constituents:	84.666
Rigid grains:	3.000
Intrabasinal constituents	
Intrabasinal constituents:	14.333
Present primary carbonate constituents:	3.333
Original primary carbonate constituents:	13.333
Intrabasinal grains:	12.333
Present carbonate allochems:	2.000
Original carbonate allochems:	11.333
Primary proportion of original carbonate allochems:	85.000
Present Carbonate bioclasts:	2.000
Original Carbonate bioclasts:	11.333
Present carbonate matrix:	1.333
Original carbonate matrix:	2.000
Primary proportion of original carbonate matrix:	14.999
Carbonate cement:	0.000
Present intrabasinal non-carbonate grains:	1.000
Original intrabasinal non-carbonate grains:	1.000

Photomicrographs

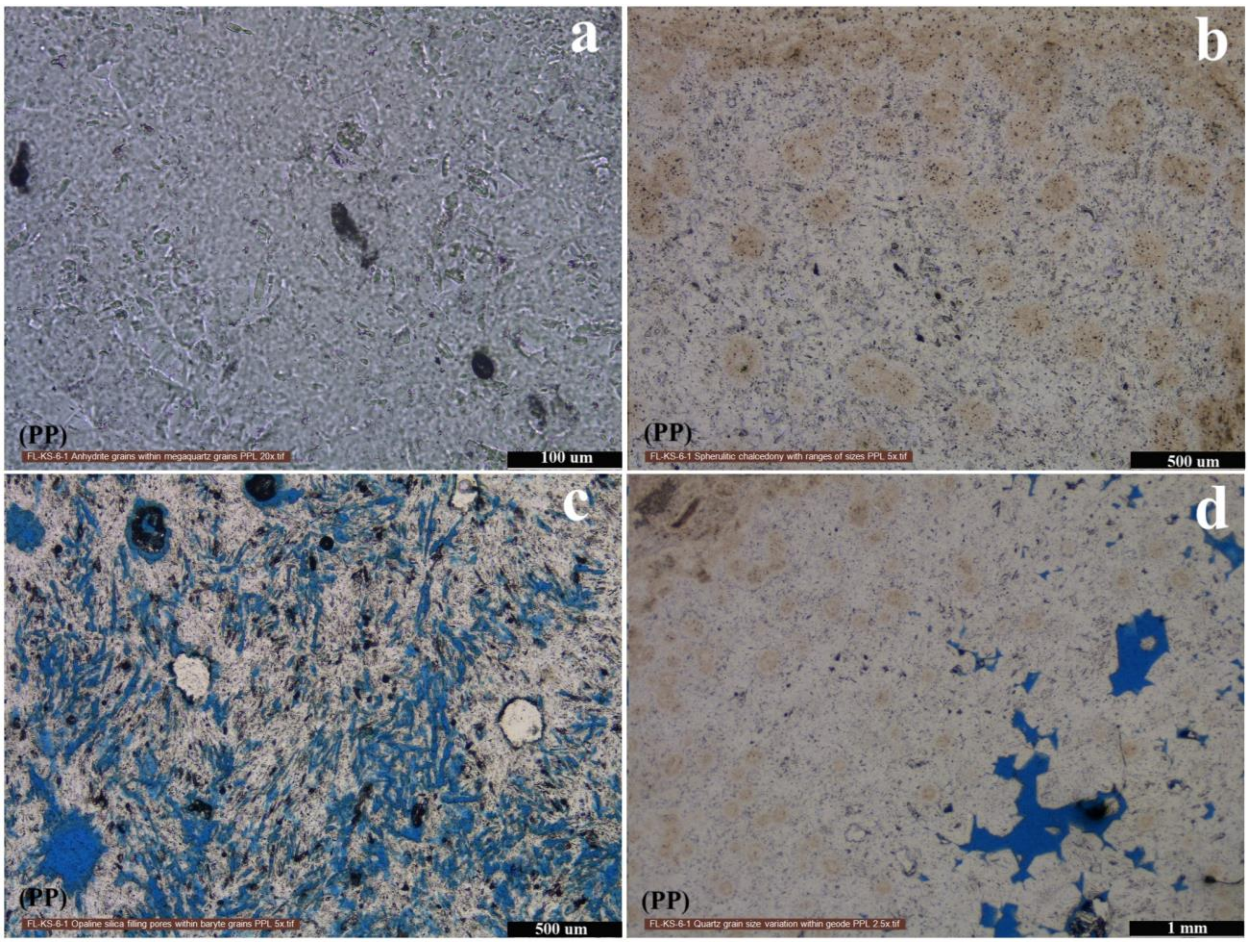

Figure A.14- (a) Abundant anhydrite crystals within megaquartz (b) Varying sizes of spherulitic chalcedony (c) Opaline silica filling pores within baryte grains (d) Subhedral megaquartz filling a vuggy pore.

Thin section ID: **FL-KS-6-2**

Summary

Wackestone (=micritic calcarenite) with abundant bioclasts (brachiopods, sponge spicules, bryozoans) making about 10%. Micrite and micrite-replacive silica are predominant, accounting for about 50%. Undifferentiated carbonate bioclasts were replaced by diagenetic silica, making about 10%. Moldic and interparticle pores resulting from the dissolution of bioclasts and micrites are abundant. Opaline silica, replacing micrite, is replaced by chert. Silica rosettes partially fill dissolution pores. Chalcedony is filling shelter pores and replacing bioclasts. Stylolites and fractures (some filled by chert). Oil stains (?) concentrated along some dissolved areas.

Microscopic textural features

Structure(s): Lamination (0.002-0.006mm), Fractured (0.0-0.0), Stylolite (0.0-0.0)

Texture

Grain size range: Clay (0.0 mm) to Granule (2.8 mm)

Modal grain size:	Clay (0.0 mm)
Gravel:	3.0%
Sand:	32.0%
Mud:	65.0%
Sorting:	Poorly sorted(2.0)
Sphericity:	Medium

Fabric

Orientation(s):	Chaotic
Support:	Matrix and matrix-replacive phase supported
Packing:	Loose (40)
Point contacts:	Common (85.0 %)
Long contacts:	Common (15.0 %)

Intrabasinal grains

2.3% Brachiopod bioclast, As intrabasinal constituent;
1.3% Sponge spicule, As intrabasinal constituent;
1.0% Carbonate bioclast undifferentiated, As intrabasinal constituent;
0.7% Bryozoan bioclast, As intrabasinal constituent;

Matrix

3.3% Micritic matrix syndepositional, As intrabasinal constituent;

Diagenetic Composition

34.7% Diagenetic silica, Microcrystalline, Interparticle replacive, Replacing <Primary-Constituent>, Micritic matrix syndepositional, As intrabasinal constituent;
9.7% Diagenetic silica, Rosette, Filling interparticle pore, Within <Primary-Constituent>, Micritic matrix syndepositional, As intrabasinal constituent;
8.0% Opal, Cryptocrystalline, Interparticle replacive, Replacing <Primary-Constituent>, Micritic matrix syndepositional, As intrabasinal constituent;
5.7% Diagenetic silica, Rosette, Interparticle replacive, Replacing <Primary-Constituent>, Micritic matrix syndepositional, As intrabasinal constituent;
5.3% Diagenetic silica, Coarsely-crystalline, Intraparticle replacive, Replacing <Primary-Constituent>, Carbonate bioclast undifferentiated, As intrabasinal constituent;
2.0% Diagenetic iron oxide/hydroxide, Pelletoid, Interparticle replacive, Replacing <Primary-Constituent>, Micritic matrix syndepositional, As intrabasinal constituent;
1.7% Diagenetic silica, Microcrystalline, Intraparticle replacive, Replacing <Primary-Constituent>, Carbonate bioclast undifferentiated, As intrabasinal constituent;
1.7% Diagenetic silica, Microcrystalline, Filling interparticle pore, Within <Primary-Constituent>, Micritic matrix syndepositional, As intrabasinal constituent;
1.7% Chalcedony, Spherulite, Intraparticle replacive, Replacing <Diagenetic-Constituent>, Diagenetic silica, Intraparticle replacive;
1.7% Calcite, Blocky, Intraparticle replacive, Replacing <Diagenetic-Constituent>, Diagenetic silica, Intraparticle replacive;
1.7% Calcite, Blocky, Intraparticle replacive, Replacing <Primary-Constituent>, Carbonate bioclast undifferentiated, As intrabasinal constituent;
1.3% Diagenetic silica, Rosette, Moldic pore-lining, Within <pore>, Moldic pore, Framework;
1.3% Diagenetic silica, Rim, Intraparticle replacive, Replacing <Primary-Constituent>, Carbonate bioclast undifferentiated, As intrabasinal constituent;
0.7% Diagenetic silica, Rim, Intraparticle replacive, Replacing <Primary-Constituent>, Brachiopod bioclast, As intrabasinal constituent;
0.3% Diagenetic silica, Microcrystalline, Intraparticle replacive, Replacing <Primary-Constituent>, Brachiopod bioclast, As intrabasinal constituent;

0.3% Diagenetic silica, Microcrystalline, Intraparticle pore-lining, Within <Primary-Constituent>, Carbonate bioclast undifferentiated, As intrabasinal constituent;
0.3% Diagenetic silica, Rim, Rock fracture-lining, Within <pore>, Fracture pore, Framework and interstitial;

Porosity

10.0% Interparticle pore, Interstitial, Dissolution of <Primary-Constituent>, Micritic matrix syndepositional, As intrabasinal constituent;
2.3% Moldic pore, Framework, Dissolution of <Primary-Constituent>, Carbonate bioclast undifferentiated, As intrabasinal constituent;
0.7% Fracture pore, Framework and interstitial, Stylolite;
0.3% Vug pore, Framework and interstitial, Enlarged by dissolution;

Carbonate Classification:

Name of classification's method:	Grabau, Brankamp, Powers and Folk
Classification result:	Micritic/spathic calcarenite

Total Volumes

Framework:	25.000
Interstitial:	75.000
Cement:	11.333
Matrix:	3.333
Porosity:	13.333
Microporosity:	Not calculated
Total diagenetic constituents:	77.999
Rigid grains:	5.333
Intrabasinal constituents	
Intrabasinal constituents:	35.000
Present primary carbonate constituents:	7.333
Original primary carbonate constituents:	32.333
Intrabasinal grains:	21.666
Present carbonate allochems:	4.000
Original carbonate allochems:	19.000
Primary proportion of original carbonate allochems:	58.762
Present Carbonate bioclasts:	4.000
Original Carbonate bioclasts:	17.666
Present carbonate matrix:	3.333
Original carbonate matrix:	13.333
Primary proportion of original carbonate matrix:	41.237
Carbonate cement:	0.000
Present intrabasinal non-carbonate grains:	1.333
Original intrabasinal non-carbonate grains:	2.666

Photomicrographs

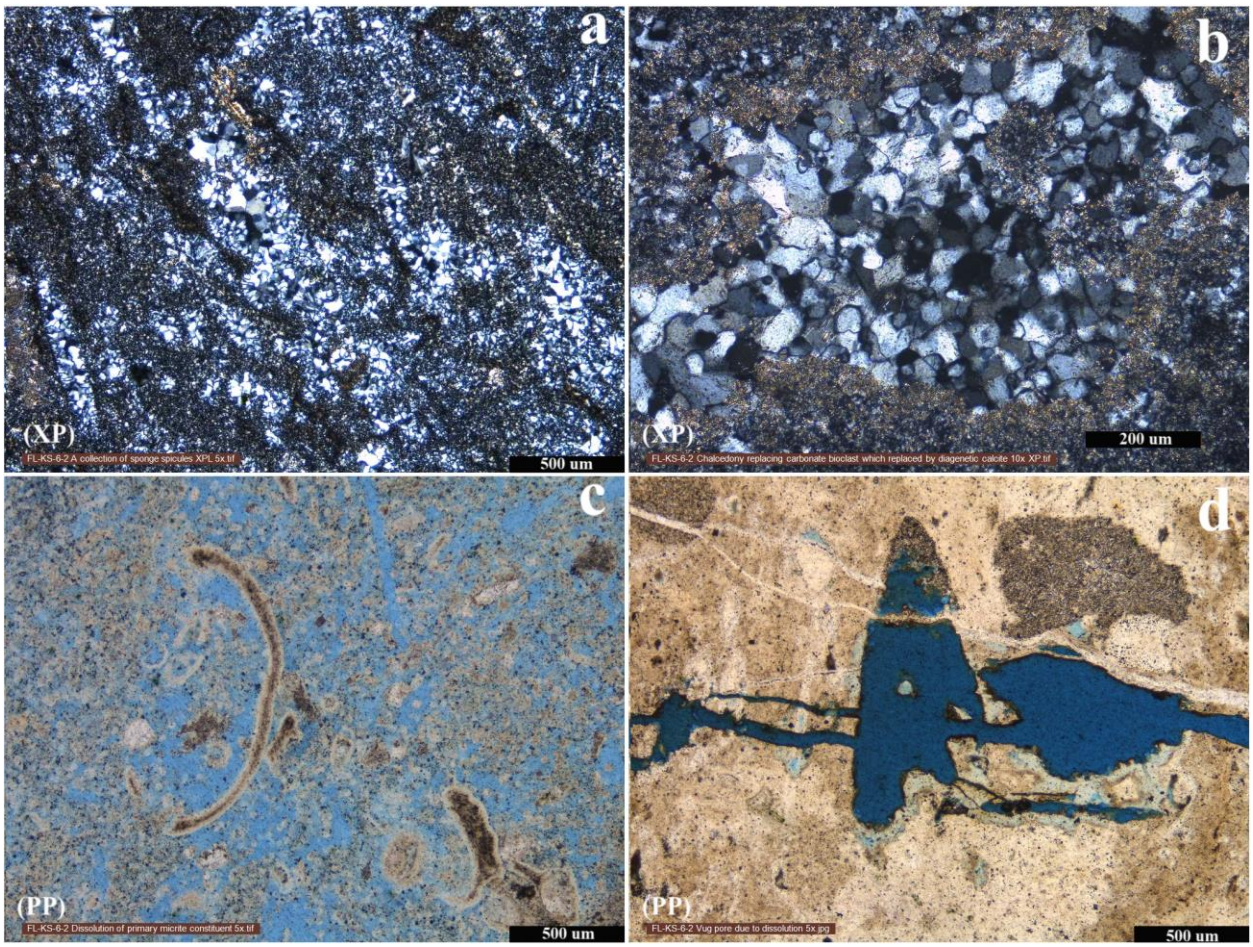

Figure A.15- (a) Aggregate of sponge spicules (b) Chalcedony and megaquartz replacing an undifferentiated carbonate bioclast (c) Dissolution of micrite forming abundant pores (d) A vuggy pore.

Thin section ID: **FL-KS-6-3**

Summary

Wackestone (=micritic calcarenite) with abundant bioclasts (brachiopods, sponge spicules, bryozoans, gastropods, and calcispheres) making about 25%. Micrite and micrite-replacive silica are predominant, accounting for about 65%. The nodule is composed of three zones: the outer rim is chert-rich, and inside, there is a micrite-rich and another zone with micrite partially engulfed by small, euhedral bipyramidal quartz crystals. The latter are especially abundant at the boundary between micrite-rich and inner micrite-quartz zones. Moldic and interparticle pores resulted from the dissolution of bioclasts and micrite. Calcite appears to replace micrite and silica. Chalcedony replacing bioclasts.

Microscopic textural features

Structure(s): Nodular (0.002-0.006mm)

Texture

Grain size range:	Clay (0.0 mm) to Granule (2.8 mm)
Modal grain size:	Clay (0.0 mm)
Gravel:	3.0%

Sand:	32.0%
Mud:	65.0%
Sorting:	Poorly sorted(2.0)
Sphericity:	Medium

Fabric

Orientation(s):	Chaotic
Support:	Matrix and matrix-replacive phase supported
Packing:	Loose (40)
Point contacts:	Common (85.0 %)
Long contacts:	Common (15.0 %)

Intrabasinal grains

5.7% Brachiopod bioclast, As intrabasinal constituent;
4.7% Carbonate bioclast undifferentiated, As intrabasinal constituent;
1.7% Gastropod bioclast, As intrabasinal constituent;
1.3% Calcisphere bioclast, As intrabasinal constituent;
1.0% Sponge spicule, As intrabasinal constituent;
1.0% Bryozoan bioclast, As intrabasinal constituent;

Matrix

38.0% Micritic matrix syndepositional, As intrabasinal constituent;

Diagenetic Composition

9.0% Calcite, Blocky, Interparticle replacive, Replacing <Primary-Constituent>, Micritic matrix syndepositional, As intrabasinal constituent;
6.7% Quartz, Prismatic, Interparticle replacive, Replacing <Primary-Constituent>, Micritic matrix syndepositional, As intrabasinal constituent, Euhedral, bipyramidal crystals engulfing micrite;
4.7% Opal, Cryptocrystalline, Interparticle replacive, Replacing <Primary-Constituent>, Micritic matrix syndepositional, As intrabasinal constituent;
4.3% Diagenetic silica, Microcrystalline, Interparticle replacive, Replacing <Primary-Constituent>, Micritic matrix syndepositional, As intrabasinal constituent;
4.0% Calcite, Blocky, Intraparticle replacive, Replacing <Diagenetic-Constituent>, Diagenetic silica, Intraparticle replacive;
3.7% Quartz, Prismatic, Intraparticle replacive, Replacing <Primary-Constituent>, Carbonate bioclast undifferentiated, As intrabasinal constituent;
3.7% Calcite, Blocky, Intraparticle replacive, Replacing <Primary-Constituent>, Carbonate bioclast undifferentiated, As intrabasinal constituent;
2.7% Diagenetic silica, Coarsely-crystalline, Intraparticle replacive, Replacing <Primary-Constituent>, Carbonate bioclast undifferentiated, As intrabasinal constituent;
2.0% Quartz, Prismatic, Intraparticle replacive, Replacing <Diagenetic-Constituent>, Calcite, Intraparticle replacive;
1.3% Diagenetic silica, Microcrystalline, Intraparticle replacive, Replacing <Primary-Constituent>, Carbonate bioclast undifferentiated, As intrabasinal constituent;
1.0% Chalcedony, Spherulite, Intraparticle replacive, Replacing <Primary-Constituent>, Carbonate bioclast undifferentiated, As intrabasinal constituent;
0.3% Dolomite, Blocky, Intraparticle replacive, Replacing <Diagenetic-Constituent>, Diagenetic silica, Intraparticle replacive;
0.3% Diagenetic iron oxide/hydroxide, Pelletoid, Interparticle replacive, Replacing <Primary-Constituent>, Micritic matrix syndepositional, As intrabasinal constituent;
0.3% Diagenetic titanium mineral, Small rhomb, Interparticle replacive, Replacing <Primary-Constituent>, Micritic matrix syndepositional, As intrabasinal constituent;

Porosity

2.0% Interparticle pore, Interstitial, Dissolution of <Primary-Constituent>, Micritic matrix syndepositional, As intrabasinal constituent;
0.7% Moldic pore, Framework, Dissolution of <Primary-Constituent>, Carbonate bioclast undifferentiated, As intrabasinal constituent;

Carbonate Classification:

Name of classification's method:	Grabau, Brankamp, Powers and Folk
Classification result:	Micritic/spathic calcarenite

Total Volumes

Framework:	34.666
Interstitial:	65.333
Cement:	0.000
Matrix:	38.000
Porosity:	2.666
Microporosity:	Not calculated
Total diagenetic constituents:	43.999
Rigid grains:	15.333

Intrabasinal constituents

Intrabasinal constituents:	68.333
Present primary carbonate constituents:	52.333
Original primary carbonate constituents:	67.333
Intrabasinal grains:	28.333
Present carbonate allochems:	14.333
Original carbonate allochems:	27.333
Primary proportion of original carbonate allochems:	40.594
Present Carbonate bioclasts:	14.333
Original Carbonate bioclasts:	27.333
Present carbonate matrix:	38.000
Original carbonate matrix:	40.000
Primary proportion of original carbonate matrix:	59.405
Present intrabasinal non-carbonate grains:	1.000
Original intrabasinal non-carbonate grains:	1.000
Dolomite/Calcite ratio:	0.020

Photomicrographs

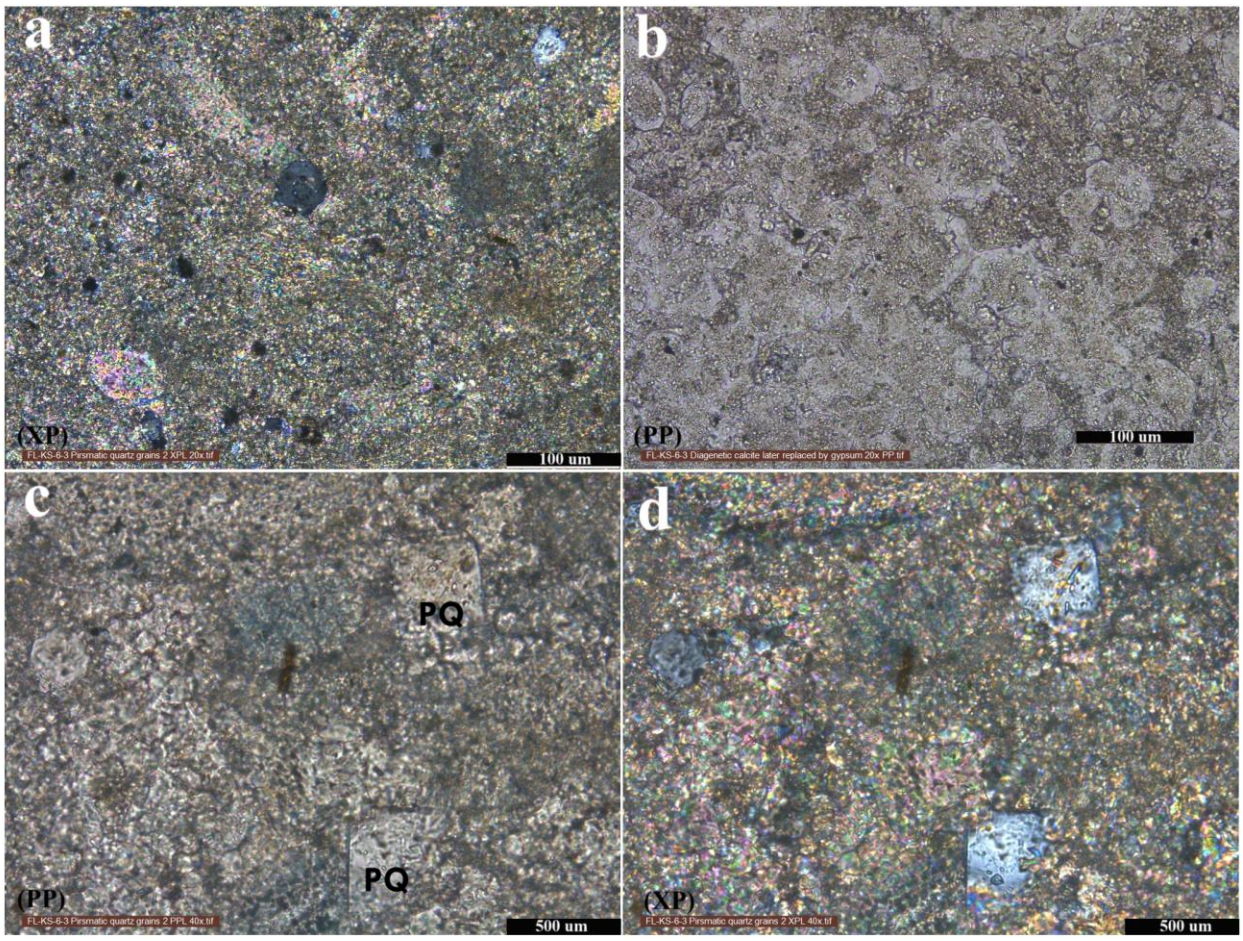

Figure A.16- (a and b) Prismatic quartz replaced by calcite within the cherty matrix. (c and d) Partially replaced euhedral prismatic quartz (PQ) with granules of anhydrite inside the grains.

Thin section ID: **FL-KS-7-1**

Summary

Wackestone (=micritic calcarenite) with abundant bioclasts (brachiopods, sponge spicules, undifferentiated bioclasts, and calcispheres) making about 35%. About 6% of the matrix was replaced by blocky calcite. Micrite and micrite-replacive silica are predominant, accounting for about 60%. Moldic and interparticle pores resulted from the dissolution of bioclasts and micrite. Stylolite and fractures.

Microscopic textural features

Structure(s): Lamination (0.002-0.006mm), Stylolite (0.0-0.0), Fractured (0.0-0.0)

Texture

Grain size range:	Clay (0.0 mm) to Coarse sand (0.8 mm)
Modal grain size:	Clay (0.0 mm)
Sand:	40.0%
Mud:	60.0%
Sorting:	Poorly sorted(2.0)
Sphericity:	Medium

Fabric

Orientation(s):	Chaotic
Support:	Matrix and matrix-replacive phase supported
Packing:	Loose (40)
Point contacts:	Common (85.0 %)
Long contacts:	Common (15.0 %)

Intrabasinal grains

1.7% Sponge spicule, As intrabasinal constituent;
1.0% Carbonate bioclast undifferentiated, As intrabasinal constituent;
0.7% Brachiopod bioclast, As intrabasinal constituent;
0.3% Calcisphere bioclast, As intrabasinal constituent;

Matrix

18.0% Micritic matrix syndepositional, As intrabasinal constituent;

Diagenetic Composition

31.3% Diagenetic silica, Microcrystalline, Interparticle replacive, Replacing <Primary-Constituent>, Micritic matrix syndepositional, As intrabasinal constituent;
13.3% Diagenetic silica, Coarsely-crystalline, Intraparticle replacive, Replacing <Primary-Constituent>, Carbonate bioclast undifferentiated, As intrabasinal constituent;
8.7% Diagenetic silica, Microcrystalline, Intraparticle replacive, Replacing <Primary-Constituent>, Carbonate bioclast undifferentiated, As intrabasinal constituent;
5.7% Diagenetic silica, Microcrystalline, Intraparticle replacive, Replacing <Primary-Constituent>, Calcisphere bioclast, As intrabasinal constituent;
2.3% Opal, Cryptocrystalline, Interparticle replacive, Replacing <Primary-Constituent>, Micritic matrix syndepositional, As intrabasinal constituent;
2.3% Diagenetic silica, Rosette, Interparticle replacive, Replacing <Primary-Constituent>, Micritic matrix syndepositional, As intrabasinal constituent;
2.3% Oil stain;
2.0% Diagenetic silica, Rosette, Interparticle continous pore-lining, Within <Primary-Constituent>, Micritic matrix syndepositional, As intrabasinal constituent;
2.0% Diagenetic iron oxide/hydroxide, Pelletoid, Interparticle replacive, Replacing <Primary-Constituent>, Micritic matrix syndepositional, As intrabasinal constituent;
1.0% Opal, Cryptocrystalline, Filling interparticle pore, Within <Primary-Constituent>, Micritic matrix syndepositional, As intrabasinal constituent;
1.0% Chalcedony, Spherulite, Intraparticle replacive, Replacing <Primary-Constituent>, Carbonate bioclast undifferentiated, Intraparticle replacive;
0.7% Diagenetic titanium mineral, Small rhomb, Interparticle replacive, Replacing <Primary-Constituent>, Micritic matrix syndepositional, As intrabasinal constituent;

Porosity

3.3% Interparticle pore, Interstitial, Dissolution of <Primary-Constituent>, Micritic matrix syndepositional, As intrabasinal constituent;
2.0% Moldic pore, Framework, Dissolution of <Primary-Constituent>, Carbonate bioclast undifferentiated, As intrabasinal constituent;
0.3% Fracture pore, Framework and interstitial;

Carbonate Classification:

Name of classification's method:	Grabau, Brankamp, Powers and Folk
Classification result:	Micritic/spathic calcarenite

Total Volumes

Framework:	37.000
Interstitial:	63.000
Cement:	3.000
Matrix:	18.000
Porosity:	5.666
Microporosity:	Not calculated
Total diagenetic constituents:	72.666
Rigid grains:	3.666
Intrabasinal constituents	
Intrabasinal constituents:	54.666
Present primary carbonate constituents:	20.000
Original primary carbonate constituents:	53.000
Intrabasinal grains:	33.333
Present carbonate allochems:	2.000
Original carbonate allochems:	31.666
Primary proportion of original carbonate allochems:	59.748
Present Carbonate bioclasts:	2.000
Original Carbonate bioclasts:	31.666
Present carbonate matrix:	18.000
Original carbonate matrix:	21.333
Primary proportion of original carbonate matrix:	40.251
Present intrabasinal non-carbonate grains:	1.666
Original intrabasinal non-carbonate grains:	1.666

Photomicrographs

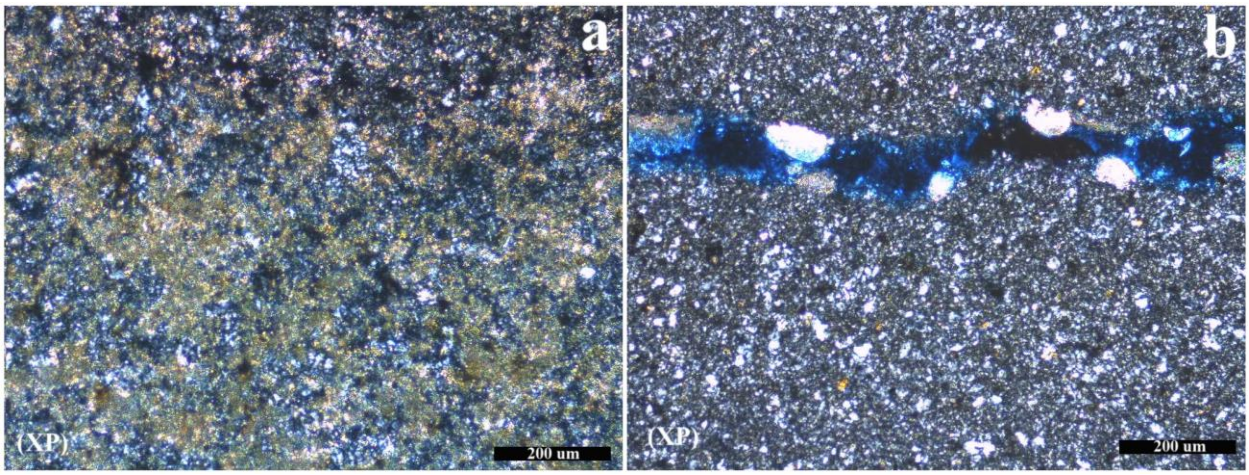

Figure A.17- (a) Mud micrite replaced by chert (b) A stylolite with opaline silica precipite. Later, opaline silica was replaced by blocky calcite crystals growing inwards.

Thin section ID: **FL-KS-7-2**

Summary

Wackestone (=micritic calcarenite) with abundant bioclasts (brachiopods, sponge spicules, bryozoans.

corals, gastropods, calcispheres, crinoids, and undifferentiated bioclasts) making about 20%. Micrite and micrite-replacive silica are predominant, accounting for about 60%. Micrite was mainly replaced by opaline silica along lines that formed wood-graining. Calcite replaces micrite and opaline silica/chert in the matrix and carbonate bioclasts. Rare moldic and interparticle pores resulted from the dissolution of bioclasts and micrite. Abundant opaline silica in wood-grained horizons.

Microscopic textural features

Structure(s):	Lamination (0.002-0.006mm)
Texture	
Grain size range:	Clay (0.0 mm) to Granule (2.8 mm)
Modal grain size:	Clay (0.0 mm)
Gravel:	3.0%
Sand:	37.0%
Mud:	60.0%
Sorting:	Poorly sorted(2.0)
Sphericity:	Medium
Fabric	
Orientation(s):	Chaotic
Support:	Matrix and matrix-replacive phase supported
Packing:	Loose (40)
Point contacts:	Common (85.0 %)
Long contacts:	Common (15.0 %)

Intrabasinal grains

3.7% Carbonate bioclast undifferentiated, As intrabasinal constituent;
3.0% Brachiopod bioclast, As intrabasinal constituent;
1.7% Calcisphere bioclast, As intrabasinal constituent;
1.7% Bryozoan bioclast, As intrabasinal constituent;
1.3% Sponge spicule, As intrabasinal constituent;
1.3% Coral bioclast, As intrabasinal constituent;
1.0% Gastropod bioclast, As intrabasinal constituent;
1.0% Crinoid bioclast, As intrabasinal constituent;
1.0% Bivalve bioclast, As intrabasinal constituent;

Matrix

32.7% Micritic matrix syndepositional, As intrabasinal constituent;

Diagenetic Composition

16.7% Opal, Cryptocrystalline, Interparticle replacive, Replacing <Primary-Constituent>, Micritic matrix syndepositional, As intrabasinal constituent;

11.7% Diagenetic silica, Microcrystalline, Interparticle replacive, Replacing <Primary-Constituent>, Micritic matrix syndepositional, As intrabasinal constituent;

6.7% Calcite, Blocky, Intraparticle replacive, Replacing <Primary-Constituent>, Carbonate bioclast undifferentiated, Framework;

3.0% Diagenetic silica, Coarsely-crystalline, Intraparticle replacive, Replacing <Primary-Constituent>, Carbonate bioclast undifferentiated, As intrabasinal constituent;

2.0% Diagenetic silica, Microcrystalline, Intraparticle replacive, Replacing <Primary-Constituent>, Carbonate bioclast undifferentiated, As intrabasinal constituent;

1.7% Diagenetic silica, Microcrystalline, Intraparticle replacive, Replacing <Primary-Constituent>, Calcisphere bioclast, As intrabasinal constituent;

1.0% Opal, Cryptocrystalline, Intraparticle replacive, Replacing <Primary-Constituent>, Carbonate bioclast undifferentiated, As intrabasinal constituent;

1.0% Diagenetic silica, Rosette, Interparticle continous pore-lining, Within <Primary-Constituent>, Micritic matrix syndepositional, As intrabasinal constituent;
1.0% Calcite, Blocky, Intraparticle replacive, Replacing <Diagenetic-Constituent>, Diagenetic silica, Intraparticle replacive;
1.0% Calcite, Blocky, Intraparticle replacive, Replacing <Primary-Constituent>, Calcisphere bioclast, As intrabasinal constituent;
1.0% Diagenetic titanium mineral, Small rhomb, Interparticle replacive, Replacing <Primary-Constituent>, Micritic matrix syndepositional, As intrabasinal constituent;
0.7% Diagenetic silica, Microcrystalline, Intraparticle replacive, Replacing <Primary-Constituent>, Brachiopod bioclast, As intrabasinal constituent;
0.7% Diagenetic silica, Rim, Intraparticle replacive, Replacing <Primary-Constituent>, Carbonate bioclast undifferentiated, As intrabasinal constituent;
0.7% Diagenetic silica, Rim, Intraparticle replacive, Replacing <Primary-Constituent>, Brachiopod bioclast, As intrabasinal constituent;
0.7% Chalcedony, Spherulite, Intraparticle replacive, Replacing <Diagenetic-Constituent>, Diagenetic silica, Intraparticle replacive;
0.7% Diagenetic iron oxide/hydroxide, Peloidal, Interparticle replacive, Replacing <Primary-Constituent>, Micritic matrix syndepositional, As intrabasinal constituent;

Porosity

1.0% Moldic pore, Framework, Dissolution of <Primary-Constituent>, Carbonate bioclast undifferentiated, As intrabasinal constituent;
0.7% Interparticle pore, Interstitial, Dissolution of <Primary-Constituent>, Micritic matrix syndepositional, As intrabasinal constituent;

Carbonate Classification:

Name of classification's method:	Grabau, Brankamp, Powers and Folk
Classification result:	Micritic/spathic calcarenite

Total Volumes

Framework:	35.666
Interstitial:	64.333
Cement:	1.000
Matrix:	32.666
Porosity:	1.666
Microporosity:	Not calculated
Total diagenetic constituents:	50.000
Rigid grains:	15.666

Intrabasinal constituents

Intrabasinal constituents:	60.666
Present primary carbonate constituents:	46.999
Original primary carbonate constituents:	59.333
Intrabasinal grains:	27.333
Present carbonate allochems:	14.333
Original carbonate allochems:	25.999
Primary proportion of original carbonate allochems:	43.820
Present Carbonate bioclasts:	14.333
Original Carbonate bioclasts:	25.999
Present carbonate matrix:	32.666
Original carbonate matrix:	33.333
Primary proportion of original carbonate matrix:	56.179

Present intrabasinal non-carbonate grains:	1.333
Original intrabasinal non-carbonate grains:	1.333

Photomicrographs

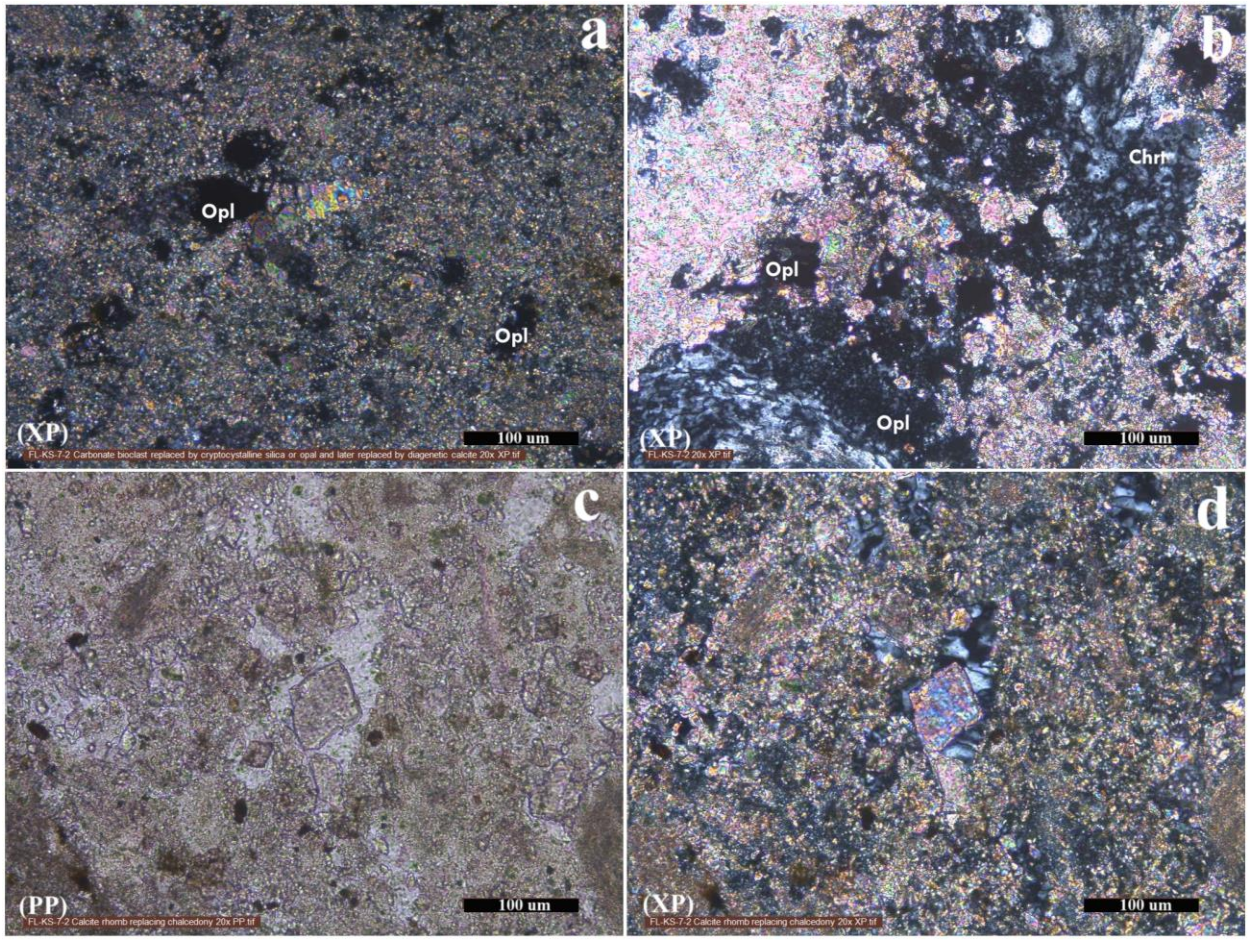

Figure A.18- (a and b) Opaline silica (Opl) replacing micrite and carbonate bioclasts. Opaline silica replaced by chert (Chrt) and blocky calcite. (c and d) Euhedral calcite rhomb replacing siliceous bioclast.

Thin section ID: **FL-KS-7-3**

Summary

Wackestone (=micritic calcarenite) with abundant bioclasts (brachiopods, sponge spicules, bryozoans, calcispheres, crinoids, and undifferentiated bioclasts) making about 35%. Calcite replaced both micrite and opaline silica/chert in the matrix and replaced carbonate bioclasts. Micrite and micrite-replacive silica are predominant, accounting for about 60%. Micrite was replaced by opaline silica, making about ~10%. Moldic and interparticle pores resulting from the dissolution of bioclasts and micrite are rare, and pores

are lined by silica rosettes.

Microscopic textural features

Structure(s):	Nodular (0.002-0.006mm)
Texture	
Grain size range:	Clay (0.0 mm) to Pebble (10.4 mm)
Modal grain size:	Clay (0.0 mm)
Gravel:	3.0%
Sand:	37.0%
Mud:	60.0%
Sorting:	Poorly sorted(2.0)
Sphericity:	Medium
Fabric	
Orientation(s):	Chaotic
Support:	Matrix and matrix-replacive phase supported
Packing:	Loose (40)
Point contacts:	Common (85.0 %)
Long contacts:	Common (15.0 %)

Intrabasinal grains

7.0% Carbonate bioclast undifferentiated, As intrabasinal constituent;
1.3% Sponge spicule, As intrabasinal constituent;
1.3% Brachiopod bioclast, As intrabasinal constituent;
1.0% Coral bioclast, As intrabasinal constituent;
0.7% Calcisphere bioclast, As intrabasinal constituent;
0.7% Bryozoan bioclast, As intrabasinal constituent;
0.7% Crinoid bioclast, As intrabasinal constituent;

Matrix

19.3% Micritic matrix syndepositional, As intrabasinal constituent;

Diagenetic Composition

25.3% Diagenetic silica, Microcrystalline, Interparticle replacive, Replacing <Primary-Constituent>, Micritic matrix syndepositional, As intrabasinal constituent;

12.3% Diagenetic silica, Coarsely-crystalline, Intraparticle replacive, Replacing <Primary-Constituent>, Carbonate bioclast undifferentiated, As intrabasinal constituent;

6.3% Opal, Cryptocrystalline, Interparticle replacive, Replacing <Primary-Constituent>, Micritic matrix syndepositional, As intrabasinal constituent;

3.7% Diagenetic silica, Microcrystalline, Intraparticle replacive, Replacing <Primary-Constituent>, Calcisphere bioclast, As intrabasinal constituent;

3.0% Diagenetic silica, Microcrystalline, Intraparticle replacive, Replacing <Primary-Constituent>, Carbonate bioclast undifferentiated, As intrabasinal constituent;

3.0% Chalcedony, Spherulite, Intraparticle replacive, Replacing <Diagenetic-Constituent>, Diagenetic silica, Intraparticle replacive;

1.7% Calcite, Blocky, Intraparticle replacive, Within <Primary-Constituent>, Carbonate bioclast undifferentiated, Framework;

1.3% Opal, Cryptocrystalline, Intraparticle replacive, Replacing <Primary-Constituent>, Carbonate bioclast undifferentiated, As intrabasinal constituent;

1.3% Diagenetic silica, Microcrystalline, Intraparticle replacive, Replacing <Primary-Constituent>, Brachiopod bioclast, As intrabasinal constituent;

1.3% Diagenetic silica, Rim, Intraparticle replacive, Replacing <Primary-Constituent>, Carbonate bioclast undifferentiated, As intrabasinal constituent;

1.0% Diagenetic silica, Rim, Intraparticle replacive, Replacing <Primary-Constituent>, Brachiopod bioclast, As intrabasinal constituent;
1.0% Diagenetic silica, Rosette, Interparticle continous pore-lining, Within <Primary-Constituent>, Micritic matrix syndepositional, As intrabasinal constituent;
1.0% Diagenetic silica, Rosette, Interparticle replacive, Replacing <Primary-Constituent>, Micritic matrix syndepositional, As intrabasinal constituent;
1.0% Calcite, Blocky, Intraparticle replacive, Within <Primary-Constituent>, Sponge spicule, Framework;
1.0% Oil stain;
0.7% Opal, Cryptocrystalline, Filling intraparticle pore, Within <Primary-Constituent>, Gastropod bioclast, As intrabasinal constituent;
0.7% Diagenetic iron oxide/hydroxide, Pelletoid, Interparticle replacive, Replacing <Primary-Constituent>, Micritic matrix syndepositional, As intrabasinal constituent;
0.7% Diagenetic titanium mineral, Small rhomb, Interparticle replacive, Replacing <Primary-Constituent>, Micritic matrix syndepositional, As intrabasinal constituent;

Porosity

1.0% Interparticle pore, Interstitial, Dissolution of <Primary-Constituent>, Micritic matrix syndepositional, As intrabasinal constituent;
0.7% Moldic pore, Framework, Dissolution of <Primary-Constituent>, Carbonate bioclast undifferentiated, As intrabasinal constituent;

Carbonate Classification:

Name of classification's method:	Grabau, Brankamp, Powers and Folk
Classification result:	Micritic/spathic calcarenite

Total Volumes

Framework:	44.666
Interstitial:	55.333
Cement:	1.000
Matrix:	19.333
Porosity:	1.666
Microporosity:	Not calculated
Total diagenetic constituents:	66.333
Rigid grains:	12.666
Intrabasinal constituents	
Intrabasinal constituents:	59.333
Present primary carbonate constituents:	30.666
Original primary carbonate constituents:	57.000
Intrabasinal grains:	39.000
Present carbonate allochems:	11.333
Original carbonate allochems:	36.666
Primary proportion of original carbonate allochems:	64.327
Present Carbonate bioclasts:	11.333
Original Carbonate bioclasts:	36.666
Present carbonate matrix:	19.333
Original carbonate matrix:	20.333
Primary proportion of original carbonate matrix:	35.672
Present intrabasinal non-carbonate grains:	1.333
Original intrabasinal non-carbonate grains:	2.333

Photomicrographs

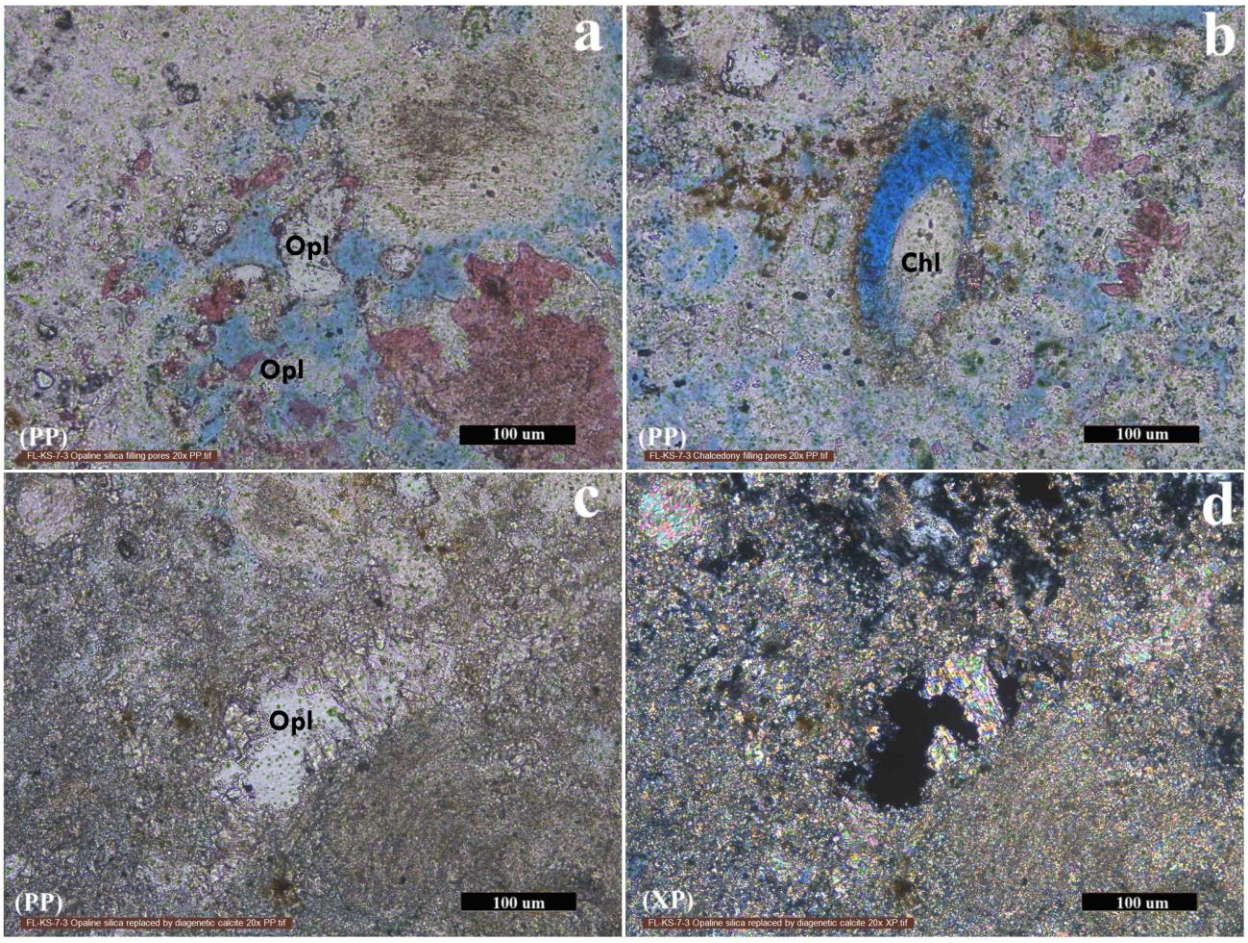

Figure A.19- (a) Dissolution pores filled by opaline silica (Opl) (b) A moldic pore partially filled by chalcedony (Chl) (c and d) Opaline silica (Opl) replaced by blocky calcite.

Thin section ID: **FL-KS-8**

Summary

Wackestone (=micritic calcarenite) with abundant bioclasts (brachiopods, sponge spicules, foraminiferas, calcispheres, crinoids, and undifferentiated bioclasts) making about 35%. Almost completely silicified, with about 60% of the thin section composed of silica replacing micrite (with hardly any micrite left). Calcite replacing silica. Silica rosette lining dissolution pores rarely replace micrite (?) and/or replacive chert. Abundant moldic, interparticle, and intraparticle pores due to dissolution of micrite and bioclasts.

Microscopic textural features

Structure(s): Nodular (0.002-0.006mm)

Texture

Grain size range: Clay (0.0 mm) to Pebble (5.6 mm)

Modal grain size: Clay (0.0 mm)

Gravel:	4.0%
Sand:	36.0%
Mud:	60.0%
Sorting:	Poorly sorted(2.0)
Sphericity:	Medium

Fabric

Orientation(s):	Chaotic
Support:	Matrix and matrix-replacive phase supported
Packing:	Loose (40)
Point contacts:	Common (85.0 %)
Long contacts:	Common (15.0 %)

Intrabasinal grains

3.7% Sponge spicule, As intrabasinal constituent;
2.0% Brachiopod bioclast, As intrabasinal constituent;
0.3% Gastropod bioclast, As intrabasinal constituent;

Matrix

9.3% Micritic matrix syndepositional, As intrabasinal constituent;

Diagenetic Composition

28.3% Diagenetic silica, Microcrystalline, Interparticle replacive, Replacing <Primary-Constituent>, Micritic matrix syndepositional, As intrabasinal constituent;
11.7% Diagenetic silica, Coarsely-crystalline, Intraparticle replacive, Replacing <Primary-Constituent>, Carbonate bioclast undifferentiated, As intrabasinal constituent;
9.0% Diagenetic silica, Microcrystalline, Intraparticle replacive, Replacing <Primary-Constituent>, Calcisphere bioclast, As intrabasinal constituent;
4.0% Chalcedony, Spherulite, Intraparticle replacive, Replacing <Diagenetic-Constituent>, Diagenetic silica, Intraparticle replacive;
3.7% Diagenetic silica, Microcrystalline, Intraparticle replacive, Replacing <Primary-Constituent>, Carbonate bioclast undifferentiated, As intrabasinal constituent;
3.3% Diagenetic silica, Microcrystalline, Intraparticle replacive, Replacing <Primary-Constituent>, Brachiopod bioclast, As intrabasinal constituent;
3.3% Diagenetic silica, Rosette, Interparticle replacive, Replacing <Primary-Constituent>, Micritic matrix syndepositional, As intrabasinal constituent;
3.0% Diagenetic silica, Microcrystalline, Intraparticle replacive, Replacing <Primary-Constituent>, Gastropod bioclast, As intrabasinal constituent;
2.3% Diagenetic silica, Rosette, Interparticle continous pore-lining, Within <Primary-Constituent>, Micritic matrix syndepositional, As intrabasinal constituent;
1.7% Diagenetic iron oxide/hydroxide, Pelletoid, Interparticle replacive, Replacing <Primary-Constituent>, Micritic matrix syndepositional, As intrabasinal constituent;
1.3% Opal, Cryptocrystalline, Interparticle replacive, Replacing <Primary-Constituent>, Micritic matrix syndepositional, As intrabasinal constituent;
1.0% Diagenetic silica, Microcrystalline, Intraparticle replacive, Replacing <Primary-Constituent>, Crinoid bioclast, As intrabasinal constituent;
1.0% Diagenetic silica, Microcrystalline, Intraparticle replacive, Replacing <Primary-Constituent>, Foraminifer bioclast undifferentiated, As intrabasinal constituent;
1.0% Diagenetic silica, Rim, Intraparticle replacive, Replacing <Primary-Constituent>, Carbonate bioclast undifferentiated, As intrabasinal constituent;
0.7% Opal, Cryptocrystalline, Filling intraparticle pore, Within <Primary-Constituent>, Gastropod bioclast, As intrabasinal constituent;

Porosity

6.0% Interparticle pore, Interstitial, Dissolution of <Primary-Constituent>, Micritic matrix syndepositional, As intrabasinal constituent;
2.0% Moldic pore, Framework, Dissolution of <Primary-Constituent>, Carbonate bioclast undifferentiated, As intrabasinal constituent;
1.3% Intraparticle pore, Framework, Within <Primary-Constituent>, Carbonate bioclast undifferentiated, As intrabasinal constituent;

Carbonate Classification:

Name of classification's method:	Grabau, Brankamp, Powers and Folk
Classification result:	Micritic/spathic calcarenite

Total Volumes

Framework:	47.666
Interstitial:	52.333
Cement:	2.333
Matrix:	9.333
Porosity:	9.333
Microporosity:	Not calculated
Total diagenetic constituents:	75.333
Rigid grains:	6.000
Intrabasinal constituents	
Intrabasinal constituents:	59.000
Present primary carbonate constituents:	11.666
Original primary carbonate constituents:	55.333
Intrabasinal grains:	43.666
Present carbonate allochems:	2.333
Original carbonate allochems:	40.000
Primary proportion of original carbonate allochems:	72.289
Present Carbonate bioclasts:	2.333
Original Carbonate bioclasts:	40.000
Present carbonate matrix:	9.333
Original carbonate matrix:	15.333
Primary proportion of original carbonate matrix:	27.710
Present intrabasinal non-carbonate grains:	3.666
Original intrabasinal non-carbonate grains:	3.666

Photomicrographs

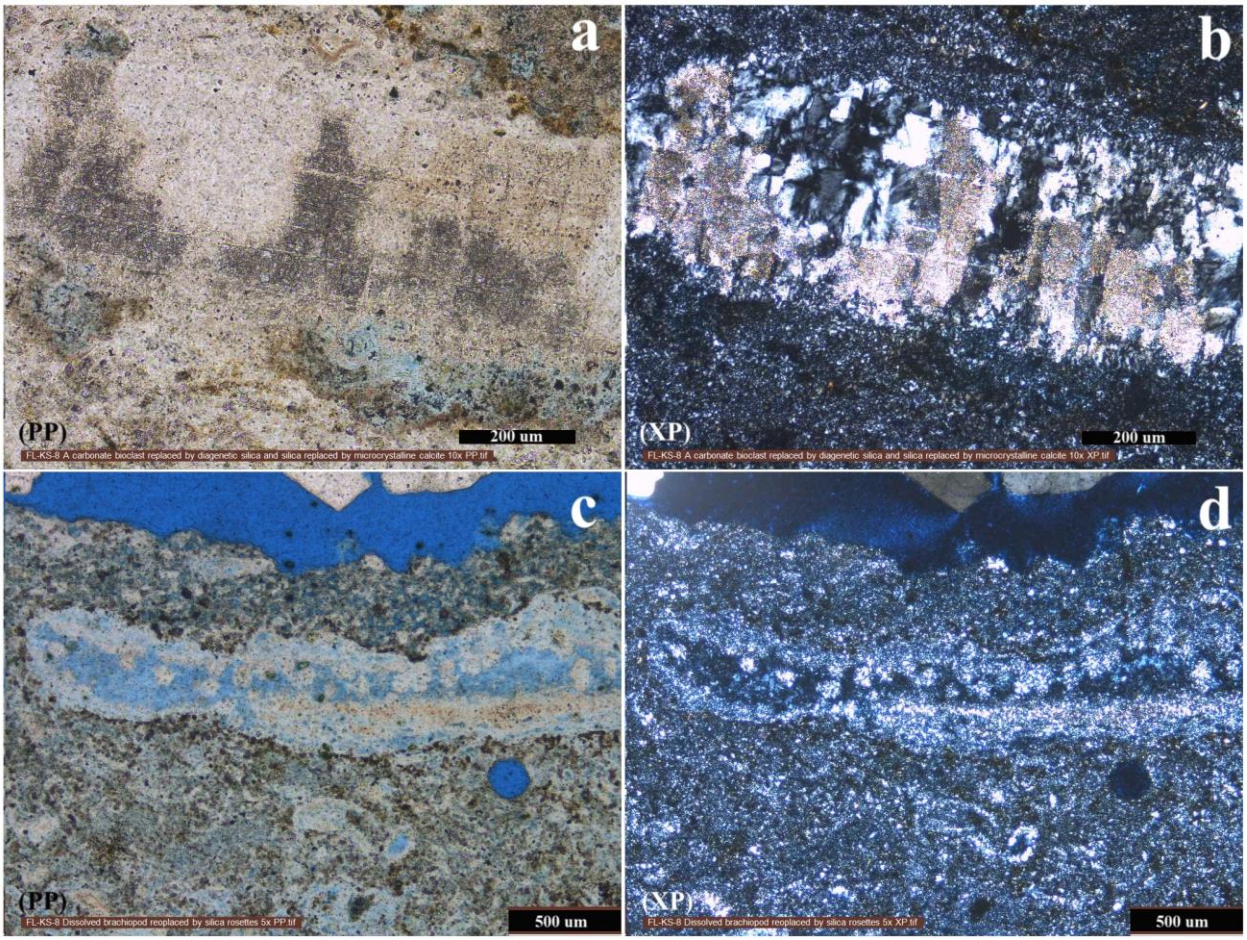

Figure A.20- (a and b) A carbonate bioclast replaced by chalcedony, the latter replaced by calcite. (c and d) Intraparticle dissolution of a brachiopod shell, with pore-filling silica rosettes.

Appendix B - Thin Section Quantification

Table B.1- Quantification of thin sections.

`Thin Section	FL-KS-1-1	FL-KS-1-2	FL-KS-2-1	FL-KS-2-2	FL-KS-3-1	FL-KS-3-2	FL-KS-4	FL-KS-5-1-1	FL-KS-5-1-2	FL-KS-5-2-1	FL-KS-5-2-2	FL-KS-5-2-3	FL-KS-5-3	FL-KS-6-1	FL-KS-6-2	FL-KS-6-3	FL-KS-7-1	FL-KS-7-2	FL-KS-7-3	FL-KS-8	Avg.	Max.
Constituents (Below in percentages)																						
Bivalve bioclast - As intrabasinal constituent -	0	0	0	0	0	0	0	0	0	0	0	0	0	0	0	0	0	1	0	0	0.1	1
Brachiopod bioclast - As intrabasinal constituent -	2	1	4	3.67	2.67	1	3	1.33	1	1.33	1	1	3.67	1.33	2.33	5.67	0.67	3	1.33	2	2.2	5.7
Bryozoan bioclast - As intrabasinal constituent -	1	1	1	1	1.67	1	0.33	0	0	0	0	0.33	0.67	0	0.67	1	0	1.67	0.67	0	0.6	1.7
Calcisphere bioclast - As intrabasinal constituent -	0	2	3.33	0	0	0.67	2.67	0	0.33	0	1	0	0.33	0.33	0	1.33	0.33	1.67	0.67	0	0.7	3.3
Carbonate bioclast undifferentiated - As intrabasinal constituent -	1.33	11.33	5.33	5.33	7.33	3.67	3.67	1.33	1.33	1.67	1	2	3.33	0	1	4.67	1	3.67	7	0	3.3	11.3
Carbonate peloid - As intrabasinal constituent -	0	0	3	3.67	1.67	0	0	0	0.67	0	0	0	0	0	0	0	0	0	0	0	0.5	3.7
Coral bioclast - As intrabasinal constituent -	0	0	0	1.33	0	2.33	1.33	0.33	0	0	0	0	0.33	0	0	0	0	1.33	1	0	0.4	2.3
Crinoid bioclast - As intrabasinal constituent -	1	0	0	0	0	0	0	0	0	0	0	0	0	0.33	0	0	0	1	0.67	0	0.2	1
Gastropod bioclast - As intrabasinal constituent -	1	0	0	1.67	1.33	0	0	0.33	0	0	0	0	0	0	0	1.67	0	1	0	0.33	0.4	1.7
Glauconite grain - As intrabasinal constituent -	0	0	0	0	0	1.33	0	0	0	0	0	0	0	0	0	0	0	0	0	0	0.1	1.3
Micritic matrix syndepositional - As intrabasinal constituent -	0	17	6	25	38	10	10.33	7	5.67	5.67	10.67	17.67	33	1.33	3.33	38	18	32.67	19.33	9.33	15.4	38
Phosphate bioclast undifferentiated - As intrabasinal constituent -	0	0	0	0	0	0	0	0	0	0	0.33	0	0	0	0	0	0	0	0	0	0	0.3
Radiolarian - As intrabasinal constituent -	0	1	1.67	1.33	1.33	1	0.67	0	0	0	0	0	0	0	0	0	0	0	0	0	0.4	1.7

Sponge spicule - As intrabasinal constituent -	2.67	2.67	3	1.67	4.33	5.67	2	9.67	10	1.33	0.33	0.33	3	1	1.33	1	1.67	1.33	1.33	3.67	2.9	10
Anhydrite - Prismatic - Interparticle displacive - - Displacing <Primary-Constituent> - Micritic matrix syndepositional - As intrabasinal constituent	0	0	0	0	0	0	0	0	0	0	0	0	0	1.67	0	0	0	0	0	0	0.1	1.7
Baryte - Coarsely-crystalline - Interparticle replacive - - Replacing <Diagenetic-Constituent> - Anhydrite - Concretions/nodules	0	0	0	0	0	0	0	0	0	0	0	0	0	20.33	0	0	0	0	0	0	1	20.3
Baryte - Prismatic - Interparticle replacive - - Replacing <Diagenetic-Constituent> - Anhydrite - Concretions/nodules	0	0	0	0	0	0	0	0	0	0	0	0	0	9.67	0	0	0	0	0	0	0.5	9.7
Calcite - Blocky - Filling intraparticle pore - - Within <Diagenetic-Constituent> - Diagenetic silica - Intraparticle replacive	0	0	0	0	0	0	0	0.67	0	0	0	0	0	0	0	0	0	0	0	0	0	0.7
Calcite - Blocky - Filling intraparticle pore - - Within <Primary-Constituent> - Brachiopod bioclast - As intrabasinal constituent	0	0	0	0	0	0	0.67	0.33	0	0	0	0	0	0	0	0	0	0	0	0	0.1	0.7
Calcite - Blocky - Filling intraparticle pore - - Within <Primary-Constituent> - Calcisphere bioclast - Framework	0	0	0	0	0	0	0	0	0	0	0.33	0	0	0	0	0	0	0	0	0	0	0.3
Calcite - Blocky - Interparticle replacive - - Replacing <Diagenetic-Constituent> - Diagenetic silica - Interparticle replacive	0	2.33	0	0	0	0	5	10.67	3.33	0.33	0	0	0	0	0	0	0	0	0	0	1.1	10.7
Calcite - Blocky - Interparticle replacive - - Replacing <Primary-Constituent> - Micritic matrix syndepositional - As intrabasinal constituent	0	0	0	0	0	0	0	3.67	0.67	1	0	4	12.33	0	0	9	0	0	0	0	1.5	12.3
Calcite - Blocky - Intraparticle replacive - - Replacing <Diagenetic-Constituent> - Chalcedony - Intraparticle replacive	1.67	0	0	0	0	0	0	0	0	0	0	0	0	0	0	0	0	0	0	0	0.1	1.7
Calcite - Blocky - Intraparticle replacive - - Replacing <Diagenetic-Constituent> - Diagenetic silica - Intraparticle replacive	0	0	1	1.33	0	3.33	4.67	2	0.33	2.33	0.67	8.67	20	0	1.67	4	0	1	0	0	2.5	20
Calcite - Blocky - Intraparticle replacive - - Replacing <Diagenetic-Constituent> - Quartz - Interparticle replacive	0	0	0	0	0	0	0	0	0	0	0	0	0	0	0	2	0	0	0	0	0.1	2
Calcite - Blocky - Intraparticle replacive - - Replacing <Primary-Constituent> - Brachiopod bioclast - As intrabasinal constituent	0	0	0	0	0	0	0	0	0	0	0	0.33	0	0	0	0	0	0	0	0	0	0.3
Calcite - Blocky - Intraparticle replacive - - Replacing <Primary-Constituent> - Calcisphere bioclast - As intrabasinal constituent	0	0	0	0	0	0	0	0	0	0	0	0	0.33	0	0	0	0	1	0	0	0.1	1

Calcite - Blocky - Intraparticle replacive - - Replacing <Primary-Constituent> - Carbonate bioclast undifferentiated - As intrabasinal constituent	0	0	0	0	0	1	0.67	0.67	0.33	0.33	0	3	1	0	1.67	3.67	0	6.67	1.67	0	1	6.7
Calcite - Blocky - Intraparticle replacive - - Replacing <Primary-Constituent> - Sponge spicule - As intrabasinal constituent	0	0	0	0	1.33	1	0	0	0	0	0	0	0	0	0	0	0	0	1	0	0.2	1.3
Calcite - Rim - Intraparticle replacive - - Replacing <Primary-Constituent> - Carbonate bioclast undifferentiated - As intrabasinal constituent	0	0	0	0	0	0	0	0	0	0.33	0	0	0	0	0	0	0	0	0	0	0	0.3
Calcite - Rim - Intraparticle replacive - - Replacing <Primary-Constituent> - Sponge spicule - As intrabasinal constituent	0	0	0	0	0	0	0	0	0	0	0	0.33	0.33	0	0	0	0	0	0	0	0	0.3
Calcite - Small rhomb - Filling interparticle pore - - Within <Primary-Constituent> - Micritic matrix syndepositional - As intrabasinal constituent	0	1	0	0	0	0	0	0	0	0	0	0	0	0	0	0	0	0	0	0	0.1	1
Calcite - Small rhomb - Intraparticle replacive - - Replacing <Diagenetic-Constituent> - Chalcedony - Intraparticle replacive	0	1	0	0	0	0	0	0	0	0	0	0	0	0	0	0	0	0	0	0	0.1	1
Calcite - Small rhomb - Intraparticle replacive - - Replacing <Diagenetic-Constituent> - Diagenetic silica - Intraparticle replacive	0	3.67	0	0	0	0	0	0	0	0	0	0	0	0	0	0	0	0	0	0	0.2	3.7
Calcite - Small rhomb - Intraparticle replacive - - Replacing <Primary-Constituent> - Carbonate bioclast undifferentiated - As intrabasinal constituent	0	1.33	0	0	0	0	0	0	0	0	0	0	0	0	0	0	0	0	0	0	0.1	1.3
Total calcite	1.7	9.3	1	1.3	1.3	5.3	11	18	4.7	4.3	1	16.3	34	0	3.3	18.7	0	8.7	2.7	0	7.1	34
Chalcedony - Rim - Interparticle replacive - - Replacing <Diagenetic-Constituent> - Baryte - Interparticle replacive	0	0	0	0	0	0	0	0	0	0	0	0	0	1.33	0	0	0	0	0	0	0.1	1.3
Chalcedony - Rim - Intraparticle replacive - - Replacing <Primary-Constituent> - Brachiopod bioclast - As intrabasinal constituent	0	0	0	0	0	0	0	0	0	0	0	0	0	0.67	0	0	0	0	0	0	0	0.7
Chalcedony - Spherulite - Interparticle replacive - - Replacing <Diagenetic-Constituent> - Baryte - Interparticle replacive	0	0	0	0	0	0	0	0	0	0	0	0	0	20	0	0	0	0	0	0	1	20
Chalcedony - Spherulite - Intraparticle replacive - - Replacing <Diagenetic-Constituent> - Diagenetic silica - Intraparticle replacive	0	0	0	0	0	0	0	0	0	1.67	1.33	0.67	1	0	1.67	0	0	0.67	3	4	0.7	4

Chalcedony - Spherulite - Intraparticle replacive - - Replacing <Primary-Constituent> - Brachiopod bioclast - As intrabasinal constituent	0	0	0	0	0	0	0	0	0	0	0	0	0.67	0	0	0	0	0	0	0	0	0.7
Chalcedony - Spherulite - Intraparticle replacive - - Replacing <Primary-Constituent> - Carbonate bioclast undifferentiated - As intrabasinal constituent	3.33	2.33	2.33	1.33	3	0	0.67	0.67	0	0	0	0	0	0	0	1	1	0	0	0	0.8	3.3
Total chalcedony	3.3	2.3	2.3	1.3	3	0	0.7	0.7	0	1.7	1.3	0.7	1.7	22	1.7	1	1	0.7	3	4	2.6	22
Diagenetic iron oxide/hydroxide - Pelletoid - - - Replacing <Primary-Constituent> - Micritic matrix syndepositional - As intrabasinal constituent	0	0	0	0	0	0	0	0	0	0	0	0	1	0	0	0	0	0	0	0	0.1	1
Diagenetic iron oxide/hydroxide - Pelletoid - Filling intraparticle pore - - Within <Primary-Constituent> - Micritic matrix syndepositional - As intrabasinal constituent	0	0	0	0	0	0	0	0	0	0.33	0	0	0	0	0	0	0	0	0	0	0	0.3
Diagenetic iron oxide/hydroxide - Pelletoid - Filling intraparticle pore - - Within <pore> - Moldic pore - Framework	0	0.67	3	0	1	0	0.33	0	0	0	0	0	0	0	0	0	0	0	0	0	0.3	3
Diagenetic iron oxide/hydroxide - Pelletoid - Filling vugular pore - - Within pore from dissolution of <Primary-Constituent> - Micritic matrix syndepositional - As intrabasinal constituent	0	0	1	0	0	0	0	0	0	0	0	0	0	0	0	0	0	0	0	0	0.1	1
Diagenetic iron oxide/hydroxide - Pelletoid - Interparticle replacive - - Replacing <Diagenetic-Constituent> - Baryte - Interparticle replacive	0	0	0	0	0	0	0	0	0	0	0	0	0	2.33	0	0	0	0	0	0	0.1	2.3
Diagenetic iron oxide/hydroxide - Pelletoid - Interparticle replacive - - Replacing <Primary-Constituent> - Micritic matrix syndepositional - As intrabasinal constituent	1.67	0.67	1	1.67	1	1	1.67	1.67	3.33	1.67	0.33	0	0	0	2	0.33	2	0.67	0.67	1.67	1.2	3.3
Total iron oxide	1.7	1.3	5	1.7	2	1	2	1.7	3.3	2	0.3	0	1	2.3	2	0.3	2	0.7	0.7	1.7	1.6	5
Diagenetic silica - Coarsely-crystalline - Filling intraparticle pore - - Replacing <Primary-Constituent> - Carbonate bioclast undifferentiated - As intrabasinal constituent	0	0	0	0	1	0	0	0	0	0	0	0	0	0	0	0	0	0	0	0	0.1	1
Diagenetic silica - Coarsely-crystalline - Intraparticle replacive - - Replacing <Primary-Constituent> - Carbonate bioclast undifferentiated - As intrabasinal constituent	1.33	0	1.67	0	0	1	1.33	1	14	21	0	8	3.33	0	5.33	2.67	13.33	3	12.33	11.67	5	21

Diagenetic silica - Fibrous - Intraparticle replacive - - Replacing <Primary-Constituent> - Carbonate bioclast undifferentiated - As intrabasinal constituent	0	0	0	0	0	0	0	0.67	0.33	0	0	0	0	0	0	0	0	0	0	0	0.1	0.7
Diagenetic silica - Microcrystalline - Filling interparticle pore - - Within <Primary-Constituent> - Micritic matrix syndepositional - As intrabasinal constituent	0	0	0	0	0	0	0.67	0	0	0	0	0	0	0	1.67	0	0	0	0	0	0.1	1.7
Diagenetic silica - Microcrystalline - Filling interparticle pore - - Within pore from dissolution of <Primary-Constituent> - Micritic matrix syndepositional - As intrabasinal constituent	1.33	0	0	0	0	0	0	0	0	0	0	0	0	0	0	0	0	0	0	0	0.1	1.3
Diagenetic silica - Microcrystalline - Filling intraparticle pore - - Within <Primary-Constituent> - Bryozoan bioclast - As intrabasinal constituent	2	0.33	1	1	0	0	0.67	0	0	0	0	0	0	0	0	0	0	0	0	0	0.3	2
Diagenetic silica - Microcrystalline - Filling intraparticle pore - - Within <Primary-Constituent> - Coral bioclast - As intrabasinal constituent	0	0	0	0	0	0.33	0	0	0	0	0	0	0	0	0	0	0	0	0	0	0	0.3
Diagenetic silica - Microcrystalline - Filling intraparticle pore - - Within <pore> - Moldic pore - Framework	1	0.33	1	0	0	0	0	0	0	0	0	0	0	0	0	0	0	0	0	0	0.1	1
Diagenetic silica - Microcrystalline - Interparticle replacive - - Replacing <Diagenetic-Constituent> - Baryte - Interparticle replacive	0	0	0	0	0	0	0	0	0	0	0	0	0	0.33	0	0	0	0	0	0	0	0.3
Diagenetic silica - Microcrystalline - Interparticle replacive - - Replacing <Primary-Constituent> - Micritic matrix syndepositional - As intrabasinal constituent	44.67	15.33	29	32.33	17.67	26.67	21.67	30.33	27.33	30.33	24.67	13.67	0.67	14.67	34.67	4.33	31.33	11.67	25.33	28.33	23.2	44.7
Diagenetic silica - Microcrystalline - Intraparticle pore-lining - - Replacing <Primary-Constituent> - Bryozoan bioclast - As intrabasinal constituent	0	0	0	0	0	0	0	0	0	0.33	0	0	0	0	0	0	0	0	0	0	0	0.3
Diagenetic silica - Microcrystalline - Intraparticle pore-lining - - Within <Primary-Constituent> - Carbonate bioclast undifferentiated - As intrabasinal constituent	0	0	0	0	0	0	0	0.33	0	0	0	0	0	0	0.33	0	0	0	0	0	0	0.3
Diagenetic silica - Microcrystalline - Intraparticle pore-lining - - Within <Primary-Constituent> - Micritic matrix syndepositional - As intrabasinal constituent	0	0	0	0	0	0	0	0	0	0	0	0.33	0	0	0	0	0	0	0	0	0	0.3

Diagenetic silica - Microcrystalline - Intraparticle replacive - - Replacing <Primary-Constituent> - Brachiopod bioclast - As intrabasinal constituent	3.33	0	0	0	0	0	1.67	0.33	0.67	1.67	0	0	0	2.67	0.33	0	0	0.67	1.33	3.33	0.8	3.3
Diagenetic silica - Microcrystalline - Intraparticle replacive - - Replacing <Primary-Constituent> - Calcisphere bioclast - As intrabasinal constituent	0	2	4.33	1	0	0	8.33	0	1.33	7	7.67	0.33	0	0.33	0	0	5.67	1.67	3.67	9	2.6	9
Diagenetic silica - Microcrystalline - Intraparticle replacive - - Replacing <Primary-Constituent> - Carbonate bioclast undifferentiated - As intrabasinal constituent	17	13	16	4.67	2.67	8.33	5.33	10.67	11	2.67	20.33	2.33	1.33	5.33	1.67	1.33	8.67	2	3	3.67	7.1	20.3
Diagenetic silica - Microcrystalline - Intraparticle replacive - - Replacing <Primary-Constituent> - Coral bioclast - As intrabasinal constituent	0	0	0	0	0	0.67	0	0	0	0	0	0	0	0	0	0	0	0	0	0	0	0.7
Diagenetic silica - Microcrystalline - Intraparticle replacive - - Replacing <Primary-Constituent> - Crinoid bioclast - As intrabasinal constituent	0	0	0	0	0	0	0	0	0	0	0	0	0	0	0	0	0	0	0	1	0.1	1
Diagenetic silica - Microcrystalline - Intraparticle replacive - - Replacing <Primary-Constituent> - Foraminifer bioclast undifferentiated - As intrabasinal constituent	0	0	0	0	0	0	0	0	0	0	0	0	0	0	0	0	0	0	0	1	0.1	1
Diagenetic silica - Microcrystalline - Intraparticle replacive - - Replacing <Primary-Constituent> - Gastropod bioclast - As intrabasinal constituent	0	0	0	0	0	0	0	0	0	0	0	0	0	0	0	0	0	0	0	3	0.2	3
Diagenetic silica - Microcrystalline - Intraparticle replacive - - Replacing <Primary-Constituent> - Sponge spicule - As intrabasinal constituent	0	0	3	0	0	0	0	0	0	0	0	0	0	0	0	0	0	0	0	0	0.2	3
Diagenetic silica - Microcrystalline - Intraparticle replacive - - Within <Primary-Constituent> - Brachiopod bioclast - As intrabasinal constituent	0	1	0	0	0	0	0	0	0	0	0	0	0	0	0	0	0	0	0	0	0.1	1
Diagenetic silica - Rim - Interparticle continous pore-lining - - Covering <Primary-Constituent> - Bivalve bioclast - As intrabasinal constituent	0	0.33	0	0	0	0	0	0	0	0	0	0	0	0	0	0	0	0	0	0	0	0.3
Diagenetic silica - Rim - Interparticle continous pore-lining - - Covering <Primary-Constituent> - Brachiopod bioclast - As intrabasinal constituent	0	0	0	0	0	0	1.33	0	0	0	0	0	0	0	0	0	0	0	0	0	0.1	1.3
Diagenetic silica - Rim - Interparticle continous pore-lining - - Covering <Primary-Constituent> - Carbonate bioclast undifferentiated -	0	0	0	0	0	0.33	0	0	0	0	0	0	0	0	0	0	0	0	0	0	0	0.3

Diagenetic silica - Rim - Interparticle continous pore-lining - - Covering <Primary-Constituent> - Coral bioclast - As intrabasinal constituent	0	0	0	0	0	1	0.67	0	0	0	0	0	0	0	0	0	0	0	0	0	0.1	1
Diagenetic silica - Rim - Interparticle replacive - - Covering <Primary-Constituent> - Brachiopod bioclast - As intrabasinal constituent	0	0	0	0	0	0	0	0.33	0	0	0	0	0	0	0	0	0	0	0	0	0	0.3
Diagenetic silica - Rim - Interparticle replacive - - Covering <Primary-Constituent> - Sponge spicule - As intrabasinal constituent	0	0	0	0	0	0.67	0	0	0	0	0	0	0	0	0	0	0	0	0	0	0	0.7
Diagenetic silica - Rim - Intraparticle replacive - - Replacing <Primary-Constituent> - Coral bioclast - As intrabasinal constituent	0	0	0	0	0	1	0	0	0	0	0	0	0	0	0	0	0	0	0	0	0.1	1
Diagenetic silica - Rim - Intraparticle replacive - - Replacing <Primary-Constituent> - Bryozoan bioclast - As intrabasinal constituent	0	0	0	0	0	1	0	0	0	0	0	0	0	0	0	0	0	0	0	0	0.1	1
Diagenetic silica - Rim - Intraparticle replacive - - Replacing <Primary-Constituent> - Brachiopod bioclast - As intrabasinal constituent	0	0	0	0	0	0.33	0.33	0	0.33	1.33	1	2.67	0.33	0	0.67	0	0	0.67	1	0	0.4	2.7
Diagenetic silica - Rim - Intraparticle replacive - - Replacing <Primary-Constituent> - Carbonate bioclast undifferentiated - As intrabasinal constituent	1	0	0	0	0	1.33	0	0	0	0.33	0	0	0	0	1.33	0	0	0.67	1.33	1	0.3	1.3
Diagenetic silica - Rim - Rock fracture-lining - - Within <pore> - Fracture pore - Framework and interstitial	0	0	0	0	0	0	0	0	0	0	0	0	0	0	0.33	0	0	0	0	0	0	0.3
Total chert	71.7	32.3	56	39	21.3	42.7	42	43.7	55	64.7	53.7	27.3	5.7	23.3	46.3	8.3	59	20.4	48	62	41.1	71.7
Diagenetic silica - Rosette - Filling interparticle pore - - Within <Primary-Constituent> - Micritic matrix syndepositional - As intrabasinal constituent	0	1.67	0	0	0	6.33	4.33	0.33	3.33	2.67	0	0	0	0	9.67	0	0	0	0	0	1.4	9.7
Diagenetic silica - Rosette - Filling intraparticle pore - - Within <Primary-Constituent> - Brachiopod bioclast - As intrabasinal constituent	0	0	0	0	0	0	0	0	0	0	0.33	0	0	0	0	0	0	0	0	0	0	0.3
Diagenetic silica - Rosette - Filling intraparticle pore - - Within <Primary-Constituent> - Coral bioclast - As intrabasinal constituent	0	0	0	0	0	1	0	0	0	0	0	0	0	0	0	0	0	0	0	0	0.1	1

Diagenetic silica - Rosette - Interparticle continous pore-lining - - Within <Primary-Constituent> - Micritic matrix syndepositional - As intrabasinal constituent	0	0	0	0	0	0	0	0	0	0	0	5.67	0	0	0	0	2	1	1	2.33	0.6	5.7
Diagenetic silica - Rosette - Interparticle replacive - - Replacing <Primary-Constituent> - Micritic matrix syndepositional - As intrabasinal constituent	0	0	0	3.33	0	6.67	5.33	0.33	6	5.33	12.67	10	0	0	5.67	0	2.33	0	1	3.33	3.1	12.7
Diagenetic silica - Rosette - Interparticle replacive - - Within <Primary-Constituent> - Micritic matrix syndepositional - As intrabasinal constituent	0	2	0	0	0	0	0	0	0	0	0	0	0	0	0	0	0	0	0	0	0.1	2
Diagenetic silica - Rosette - Intraparticle pore-lining - - Within <pore> - Moldic pore - Framework	2	0	0	0	0	0	0	0	0	0	0	0	0	0	0	0	0	0	0	0	0.1	2
Diagenetic silica - Rosette - Intraparticle replacive - - Replacing <Primary-Constituent> - Brachiopod bioclast - As intrabasinal constituent	0	0	0	0	0	1	0	0	0	0	0	0	0	0	0	0	0	0	0	0	0.1	1
Diagenetic silica - Rosette - Lining interparticle pore - - Within <Primary-Constituent> - Micritic matrix syndepositional - As intrabasinal constituent	0	0	0	0	0	0	0	0	0	0	3.33	0	0	0	0	0	0	0	0	0	0.2	3.3
Diagenetic silica - Rosette - Moldic pore-filling - - Within <Primary-Constituent> - Carbonate bioclast undifferentiated - As intrabasinal constituent	0	0	0	0	0	0	0	0	0	0	1.67	0	0	0	0	0	0	0	0	0	0.1	1.7
Diagenetic silica - Rosette - Moldic pore-lining - - Within <pore> - Moldic pore - Framework	0	1	2.33	2.67	0	2	0.67	0.33	0.67	0.67	0.67	1.33	0	0	1.33	0	0	0	0	0	0.7	2.7
Diagenetic silica - Rosette - Rock fracture-lining - - Within <pore> - Fracture pore - Framework and interstitial	0	0	0	0	0	0	0	0	0	0.33	0	0	0	0	0	0	0	0	0	0	0	0.3
Total silica rosettes	2	4.7	2.3	6	0	17	10.3	1	10	9	18.7	17	0	0	16.7	0	4.3	1	2	5.7	6.4	18.7
Diagenetic titanium mineral - Small rhomb - Interparticle replacive - - Replacing <Primary-Constituent> - Micritic matrix syndepositional - As intrabasinal constituent	0	0.33	0.33	0.67	0	0	0.33	0.33	0.67	0.67	0.67	0.67	0	0	0	0.33	0.67	1	0.67	0	0.4	1
Dolomite - Blocky - Intraparticle replacive - - Replacing <Diagenetic-Constituent> - Calcite - Intraparticle replacive	0	0	0	0	0	0	0	0	0	0	0	0	1	0	0	0	0	0	0	0	0.1	1
Dolomite - Blocky - Intraparticle replacive - - Replacing <Diagenetic-Constituent> - Diagenetic silica - Intraparticle replacive	0	0	0	0	0	0	0	0	0	0	0	0	0	0	0	0.33	0	0	0	0	0	0.3

Dolomite - Microcrystalline - Filling interparticle pore - - Within pore from dissolution of <Primary-Constituent> - Micritic matrix syndepositional - As intrabasinal constituent	0	0	0	0	0	0	0.67	0	0	0	0	0	0	0	0	0	0	0	0	0	0	0	0.7
Dolomite - Microcrystalline - Intraparticle replacive - - Replacing <Diagenetic-Constituent> - Diagenetic silica - Intraparticle replacive	0	0	0	0	0	0	2.33	0	0	0	0	0	0	0	0	0	0	0	0	0	0	0.1	2.3
Dolomite - Microcrystalline - Intraparticle replacive - - Replacing <Primary-Constituent> - Calcisphere bioclast - As intrabasinal constituent	0	0	0	0	0	0	0.33	0	0	0	0	0	0	0	0	0	0	0	0	0	0	0	0.3
Dolomite - Small rhomb - Interparticle replacive - - Replacing <Diagenetic-Constituent> - Calcite - Interparticle replacive	0	0	0	0	0	0	0	0	0	0	0	1.33	1	0	0	0	0	0	0	0	0	0.1	1.3
Dolomite - Small rhomb - Interparticle replacive - - Replacing <Primary-Constituent> - Micritic matrix syndepositional - As intrabasinal constituent	0	0	0	0	0	0	0	1	0.33	0.67	0	0	0	0	0	0	0	0	0	0	0	0.1	1
Dolomite - Small rhomb - Intraparticle replacive - - Replacing <Diagenetic-Constituent> - Calcite - Intraparticle replacive	0	0	0	0	0	0	0.33	1	0.33	0.67	0	0	0	0	0	0	0	0	0	0	0	0.1	1
Dolomite - Small rhomb - Intraparticle replacive - - Replacing <Diagenetic-Constituent> - Diagenetic silica - Intraparticle replacive	0	0	0	0	0	0	0	0	0	0	0	0.33	6	0	0	0	0	0	0	0	0	0.3	6
Total dolomite	0	0	0	0	0	0	3.7	2	0.7	1.3	0	1.7	8	0	0	0.3	0	0	0	0	0	0.9	8
Oil stain - - - - - -	0	0	0	0	0	0	0	0	0	0	0	0	0	0	0	0	2.33	0	1	0	0.2	2.3	
Opal - Cryptocrystalline - Filling interparticle pore - - Within <Primary-Constituent> - Micritic matrix syndepositional - As intrabasinal constituent	0	0	0	0	0	0	0	0	0	0	0	0	0	0	0	0	1	0	0	0	0.1	1	
Opal - Cryptocrystalline - Filling intraparticle pore - - Within <Primary-Constituent> - Brachiopod bioclast - As intrabasinal constituent	0	0	0	0	0	0	0	0.33	0	0	0	0	0	0	0	0	0	0	0	0	0	0.3	
Opal - Cryptocrystalline - Filling intraparticle pore - - Within <Primary-Constituent> - Gastropod bioclast - As intrabasinal constituent	0	0	0	0	0	0	0	0	0	0	0	0	0	0	0	0	0	0	0.67	0.67	0.1	0.7	

Opal - Cryptocrystalline - Interparticle replacive - - Replacing <Diagenetic-Constituent> - Dolomite - Interparticle replacive	0	0	0	0	0	0	0	0.33	0	0	0	0	0	0	0	0	0	0	0	0	0	0	0.3
Opal - Cryptocrystalline - Interparticle replacive - - Replacing <Primary-Constituent> - Micritic matrix syndepositional - As intrabasinal constituent	0	1.33	0	0	11.67	0	0	9.67	1	1.67	6.67	7	5.33	0	8	4.67	2.33	16.67	6.33	1.33	4.2	16.7
Opal - Cryptocrystalline - Intraparticle replacive - - Replacing <Primary-Constituent> - Carbonate bioclast undifferentiated - As intrabasinal constituent	0	0	0	0	0	0	0	0	0	0	0	0	0	0	0	0	0	1	1.33	0	0.1	1.3
Opal - Microcrystalline - Interparticle replacive - - Replacing <Primary-Constituent> - Micritic matrix syndepositional - As intrabasinal constituent	0	0	0	0	0	0	0	0	0	0	0	0	0	5.33	0	0	0	0	0	0	0.3	5.3
Total opaline silica	0	1.3	0	0	11.7	0	0	10.3	1	1.7	6.7	7	5.3	5.3	8	4.7	3.3	17.7	8.3	2	4.7	17.7
Quartz - Prismatic - Interparticle replacive - - Replacing <Primary-Constituent> - Micritic matrix syndepositional - As intrabasinal constituent	0	0	0	0	0	0	0	0.67	0	0	0	0	0	0	0	6.67	0	0	0	0	0.4	6.7
Quartz - Prismatic - Intraparticle replacive - - Replacing <Primary-Constituent> - Carbonate bioclast undifferentiated - As intrabasinal constituent	0	0	0	0	0	0	0	0	0	0	0	0	0	0	0	3.67	0	0	0	0	0.2	3.7
Fracture pore - Framework and interstitial - - - -	1.67	0	0	0	0	0	0	0	0	1.67	0	0.67	0	0	0.67	0	0.33	0	0	0	0.3	1.7
Interparticle pore - Interstitial - - Dissolution of <Primary-Constituent> - Micritic matrix syndepositional - As intrabasinal constituent	4.33	4.33	1.67	3.67	2.33	4.33	5	1	3.67	2	2	5.33	0	0.67	10	2	3.33	0.67	1	6	3.2	10
Intraparticle pore - Framework - - Dissolution of <Primary-Constituent> - Carbonate bioclast undifferentiated - As intrabasinal constituent	1.67	2	0	0	0	0	0	0	0	0	0	0	0	0	0	0	0	0	0	1.33	0.3	2
Intraparticle pore - Framework - - Within <Primary-Constituent> - Coral bioclast - As intrabasinal constituent	0	0	0	0	0	3	0	0	0	0	0	0	0	0	0	0	0	0	0	0	0.2	3
Moldic pore - Framework - - Dissolution of <Diagenetic-Constituent> - Anhydrite - Interparticle displacive	0	0	0	0	0	0	0	0	0	0	0	0	0	9.67	0	0	0	0	0	0	0.5	9.7
Moldic pore - Framework - - Dissolution of <Primary-Constituent> - Bivalve bioclast - As intrabasinal constituent	0	0	0	0	0	0	0	0	0	0	0	0	0	0.33	0	0	0	0	0	0	0	0.3

Moldic pore - Framework - - Dissolution of <Primary-Constituent> - Carbonate bioclast undifferentiated - As intrabasinal constituent	3	6	4	1.67	0	0	1	0.67	2	1	1.33	2	0	0	2.33	0.67	2	1	0.67	2	1.6	6
Vug pore - Framework and interstitial - Enlarged by dissolution - - -	0	0	0	0	0	0	0	0	0	0	0	0	0	0.33	0.33	0	0	0	0	0	0	0.3

Table B.2- Summary of the Quantification.

Thin Section	**1-1**	**1-2**	**2-1**	**2-2**	**3-1**	**3-2**	**4**	**5-1-1**	**5-1-2**	**5-2-1**	**5-2-2**	**5-2-3**	**5-3**	**6-1**	**6-2**	**6-3**	**7-1**	**7-2**	**7-3**	**8**	**Av**	**Max.**
Totals (Below in percentages)																						
Framework	48.00	53.67	62.00	33.33	29.33	43.00	43.00	32.67	44.67	48.00	39.00	34.67	47.67	22.33	25.00	34.67	37.00	35.67	44.67	47.67	40.3	62.0
Interstitial	52.00	46.33	38.00	66.67	70.67	57.00	57.00	67.33	55.33	52.00	61.00	65.33	52.33	77.67	75.00	65.33	63.00	64.33	55.33	52.33	59.7	77.7
Cement	1.33	7.33	0.00	0.00	0.00	8.33	12.67	11.67	6.67	3.00	3.33	7.00	1.00	55.67	11.33	0.00	3.00	1.00	1.00	2.33	6.8	55.7
Matrix	0.00	17.00	6.00	25.00	38.00	10.00	10.33	7.00	5.67	5.67	10.67	17.67	33.00	1.33	3.33	38.00	18.00	32.67	19.33	9.33	15.4	38.0
Porosity	**10.67**	**12.33**	**5.67**	**5.33**	**2.33**	**7.33**	**6.00**	**1.67**	**5.67**	**4.67**	**3.33**	**8.00**	**0.00**	**11.00**	**13.33**	**2.67**	**5.67**	**1.67**	**1.67**	**9.33**	**5.9**	**13.3**
Total diagenetic constituents	80.33	51.67	67.00	50.00	39.33	66.00	70.00	78.33	75.33	85.33	82.33	70.67	55.67	84.67	78.00	44.00	72.67	50.00	66.33	75.33	67.1	85.3
Rigid grains	9.00	19.00	18.33	16.00	18.67	15.33	13.67	13.00	12.67	4.33	3.67	3.67	11.33	3.00	5.33	15.33	3.67	15.67	12.67	6.00	11.0	19.0
Ductile grains	0.00	0.00	3.00	3.67	1.67	1.33	0.00	0.00	0.67	0.00	0.00	0.00	0.00	0.00	0.00	0.00	0.00	0.00	0.00	0.00	0.5	3.7
Intrabasinal primary constituents	52.00	72.33	74.00	63.33	70.67	54.00	52.00	37.33	54.00	49.33	50.00	48.33	51.67	14.33	35.00	68.33	55.67	67.33	61.00	59.00	54.5	74.0
Present primary carbonate constituents	6.33	32.33	22.67	41.67	52.67	18.67	21.33	10.33	9.00	8.67	13.67	21.00	41.33	3.33	7.33	52.33	20.00	47.00	30.67	11.67	23.6	52.7
Original primary carbonate constituents	46.33	66.67	60.00	57.67	62.67	43.00	48.33	27.33	43.33	47.33	48.67	46.33	48.33	13.33	32.33	67.33	54.00	66.00	58.67	55.33	49.6	67.3
Intrabasinal grains	47.67	51.00	66.33	34.67	30.33	39.67	36.67	29.33	44.67	41.67	37.33	25.33	18.67	12.33	21.67	28.33	34.33	34.00	40.67	43.67	35.9	66.3
Present carbonate allochems	6.33	15.33	16.67	16.67	14.67	8.67	11.00	3.33	3.33	3.00	3.00	3.33	8.33	2.00	4.00	14.33	2.00	14.33	11.33	2.33	8.2	16.7
Original carbonate allochems	42.00	45.33	52.33	29.00	22.33	28.67	33.00	19.33	34.00	39.67	36.00	23.33	15.33	11.33	19.00	27.33	32.67	32.67	38.33	40.00	31.1	52.3
Primary proportion of original carbonate allochems	90.65	68.00	87.22	50.29	35.64	66.67	68.28	70.73	78.46	83.80	73.97	50.36	31.72	85.00	58.76	40.59	60.49	49.49	65.34	72.29	64.4	90.6
Present carbonate bioclasts	6.33	15.33	13.67	13.00	13.00	8.67	11.00	3.33	2.67	3.00	3.00	3.33	8.33	2.00	4.00	14.33	2.00	14.33	11.33	2.33	7.7	15.3
Original carbonate bioclasts	**39.00**	**43.33**	**43.00**	**22.67**	**19.67**	**26.67**	**32.00**	**19.00**	**32.67**	**39.00**	**35.33**	**22.00**	**15.33**	**11.33**	**17.67**	**27.33**	**32.67**	**32.67**	**38.33**	**40.00**	**29.5**	**43.3**
Carbonate peloids/pellets	0.00	0.00	3.00	3.67	1.67	0.00	0.00	0.00	0.67	0.00	0.00	0.00	0.00	0.00	0.00	0.00	0.00	0.00	0.00	0.00	0.4	3.7
Present carbonate matrix	0.00	17.00	6.00	25.00	38.00	10.00	10.33	7.00	5.67	5.67	10.67	17.67	33.00	1.33	3.33	38.00	18.00	32.67	19.33	9.33	15.4	38.0
Original carbonate matrix	4.33	21.33	7.67	28.67	40.33	14.33	15.33	8.00	9.33	7.67	12.67	23.00	33.00	2.00	13.33	40.00	21.33	33.33	20.33	15.33	18.6	40.3
Primary proportion of original carbonate matrix	**9.35**	**32.00**	**12.78**	**49.71**	**64.36**	**33.33**	**31.72**	**29.27**	**21.54**	**16.20**	**26.03**	**49.64**	**68.28**	**15.00**	**41.24**	**59.40**	**39.51**	**50.51**	**34.66**	**27.71**	**35.6**	**68.3**
Carbonate cement	0.00	3.33	0.00	0.00	0.00	0.00	5.67	10.67	3.33	0.33	0.00	1.33	1.00	0.00	0.00	0.00	0.00	0.00	0.00	0.00	1.3	10.7
Present intrabasinal non-carbonate grains	2.67	3.67	4.67	3.00	5.67	8.00	2.67	9.67	10.00	1.33	0.67	0.33	3.00	1.00	1.33	1.00	1.67	1.33	1.33	3.67	3.3	10.0
Original intrabasinal non-carbonate grains	5.67	5.67	14.00	5.67	8.00	11.00	3.67	10.00	10.67	2.00	1.33	2.00	3.33	1.00	2.67	1.00	1.67	1.33	2.33	3.67	4.8	14.0
Dolomite/Calcite ratio	0.00	0.00	0.00	0.00	0.00	0.00	0.33	0.11	0.14	0.31	0.00	0.10	0.23	0.00	0.00	0.02	0.00	0.00	0.00	0.00		0.3
Original siliceous bioclasts	**2.67**	**3.67**	**7.67**	**3.00**	**6.99**	**8.34**	**2.67**	**9.67**	**10.00**	**1.33**	**0.33**	**0.66**	**3.33**	**1.00**	**1.33**	**1.00**	**1.67**	**1.33**	**2.33**	**3.67**	**3.6**	**10.0**

Gravel	4.00	1.00	2.00	4.00	4.00	5.00	7.00	2.00	2.00	2.00	2.00	0.00	0.00	4.00	3.00	3.00	0.00	3.00	3.00	4.00	2.8	7.0
Sand	31.00	34.00	30.00	24.00	26.00	35.00	38.00	38.00	38.00	28.00	33.00	25.00	35.00	35.00	32.00	32.00	40.00	37.00	37.00	36.00	33.2	40.0
Mud	65.00	65.00	68.00	72.00	70.00	60.00	55.00	60.00	60.00	70.00	65.00	75.00	65.00	61.00	65.00	65.00	60.00	60.00	60.00	60.00	64.1	75.0

Thin Section	**1-1**	**1-2**	**2-1**	**2-2**	**3-1**	**3-2**	**4**	**5-1-1**	**5-1-2**	**5-2-1**	**5-2-2**	**5-2-3**	**5-3**	**6-1**	**6-2**	**6-3**	**7-1**	**7-2**	**7-3**	**8**
Rock Classification	Wackestone	Wackestone	Wackestone	Wackestone	Wackestone	Wackestone	Wackestone	Wackestone	Wackestone	Wackestone	Wackestone	Wackestone	Wackestone	Wackestone	Wackestone	Wackestone	Wackestone	Wackestone	Wackestone	Wackestone
Modal grain size	Clay	Silt	Silt	Clay	Clay	Clay	Clay	Clay	Clay	Clay	Clay	Clay	Clay	Clay	Clay	Clay	Clay	Clay	Clay	Clay
Sorting	Moderately sorted	Moderately sorted	Moderately sorted	Moderately sorted	Moderately sorted	Poorly sorted	Poorly sorted	Poorly sorted	Poorly sorted	Poorly sorted	Moderately sorted	Poorly sorted	Poorly sorted	Poorly sorted	Poorly sorted	Poorly sorted	Poorly sorted	Poorly sorted	Poorly sorted	Poorly sorted

Appendix C - Raman Spectroscopy Data

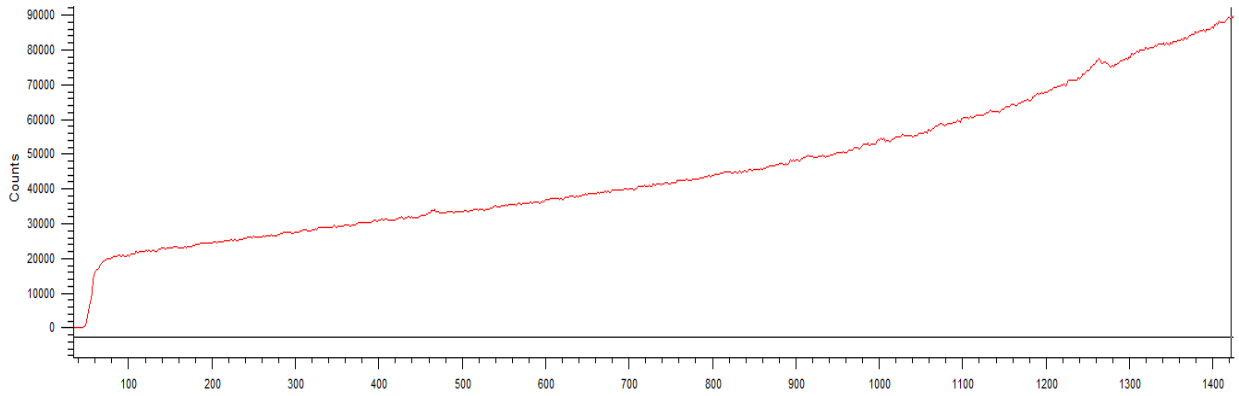

Figure C.21- FL-KS-1-2 Wood-grained chert full signal.

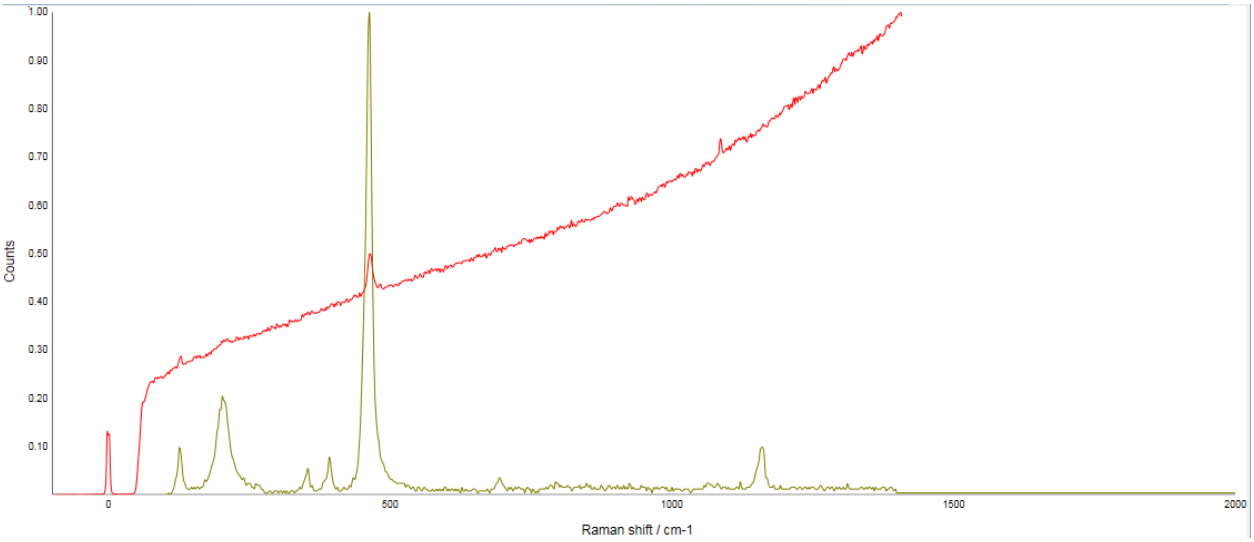

Figure C.22- Complete FL-KS-1-2 chert reference signal (top) overlapped with quartz reference signal (below).

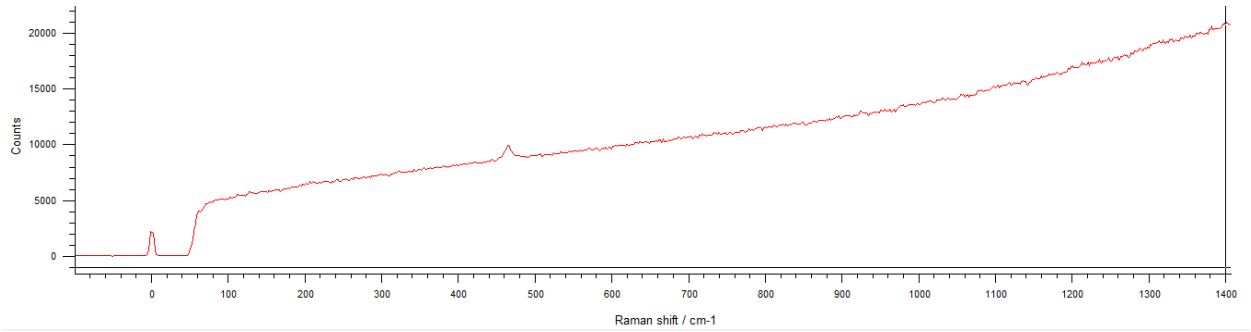

Figure C.23- Full signal for FL-KS-2-2 with a peak around 464 cm^{-1}.

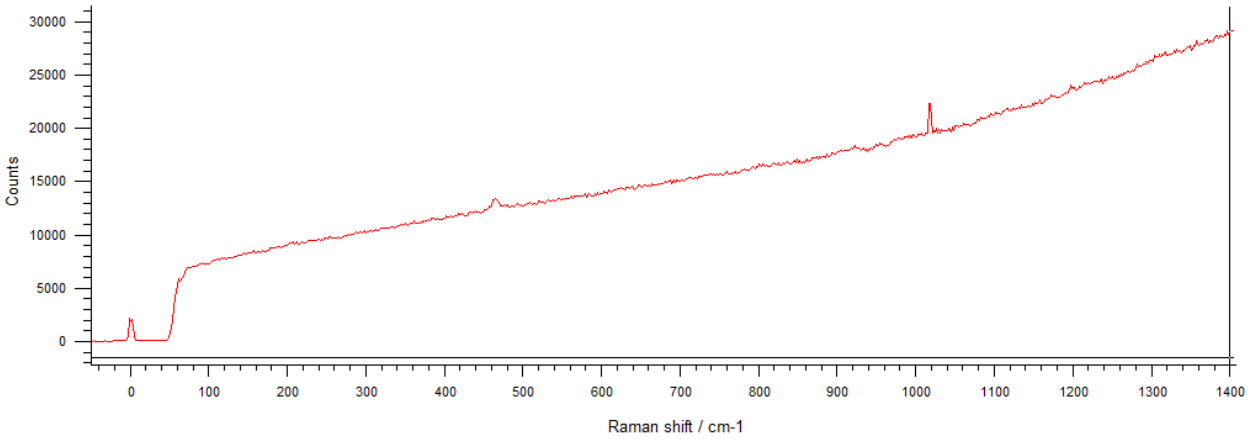

Figure C.24-Full signal for FL-KS-3-1 for wood-grained chert boundary. Peaks around 464 cm^{-1} (quartz) and 1019 cm^{-1} (calcite) were observed.

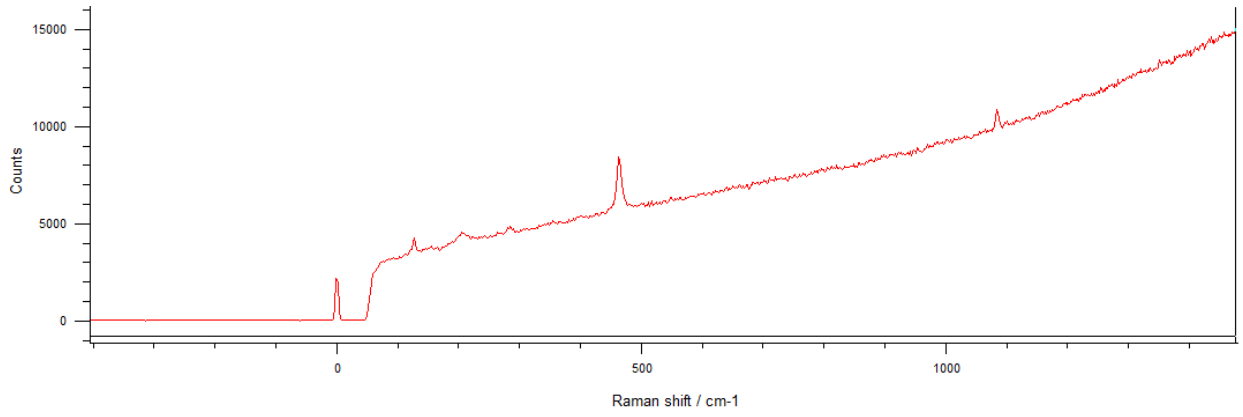

Figure C.25- Full signal observed for FL-KS-3-2 silicified bioclast with peak signal around 464 cm^{-1}.

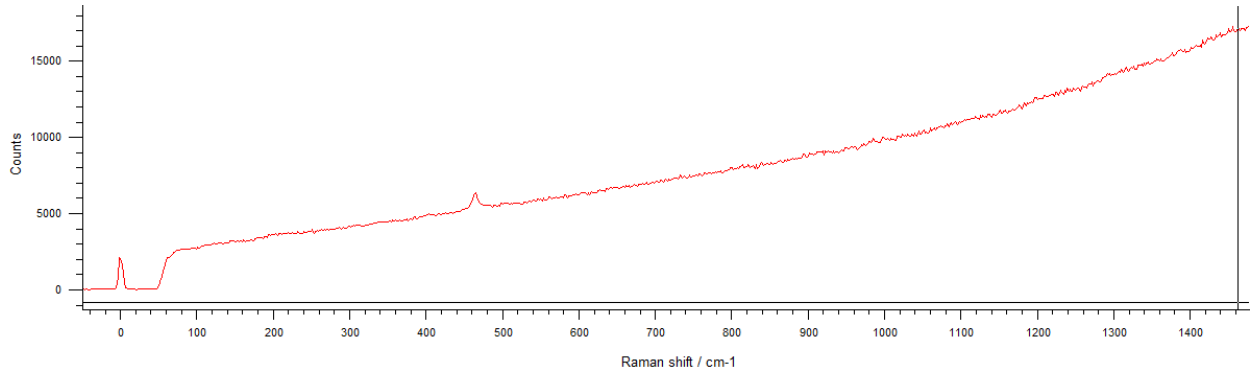

Figure C.26-FL-KS-4 Full signal with 464cm^{-1} peak for chert matrix.

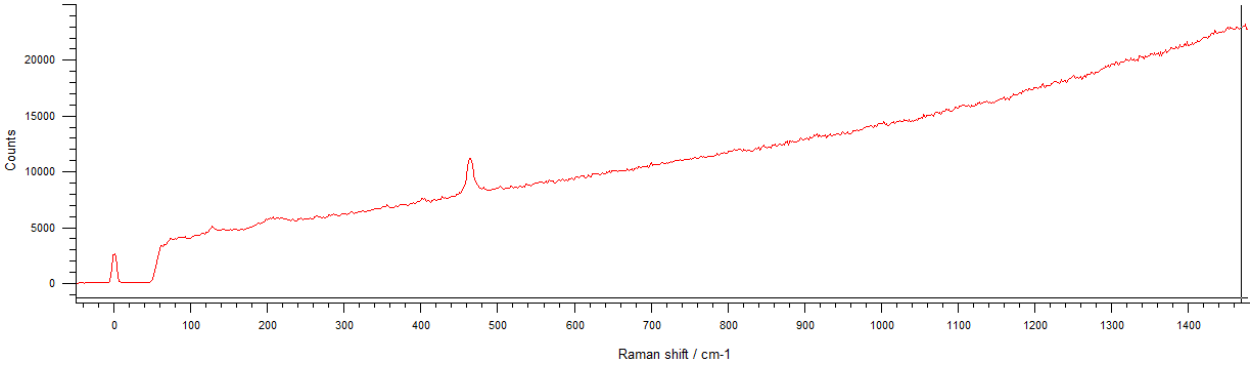

Figure C.27- Full signal for FL-KS-5-2-1.

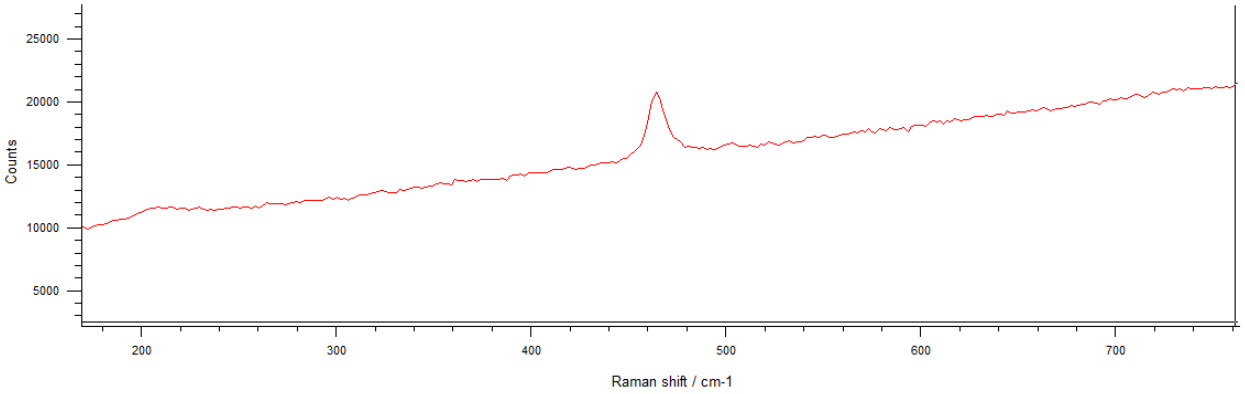

Figure C.28- Truncated signal wave with a peak around 464.23 cm^{-1} for micrite-replacing silica.

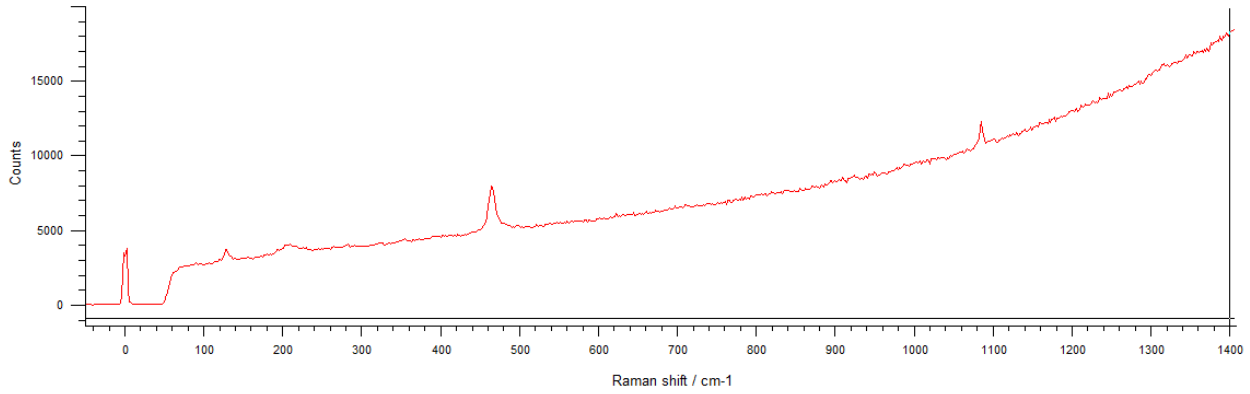

Figure C.29- Full signal for FL-KS-5-3, silicified bioclast boundary with peaks observed around 127.23cm^{-1} (quartz), 206.53 cm^{-1} (quartz), 464.06 cm^{-1}(quartz) and 1086.37 cm^{-1} (calcite).

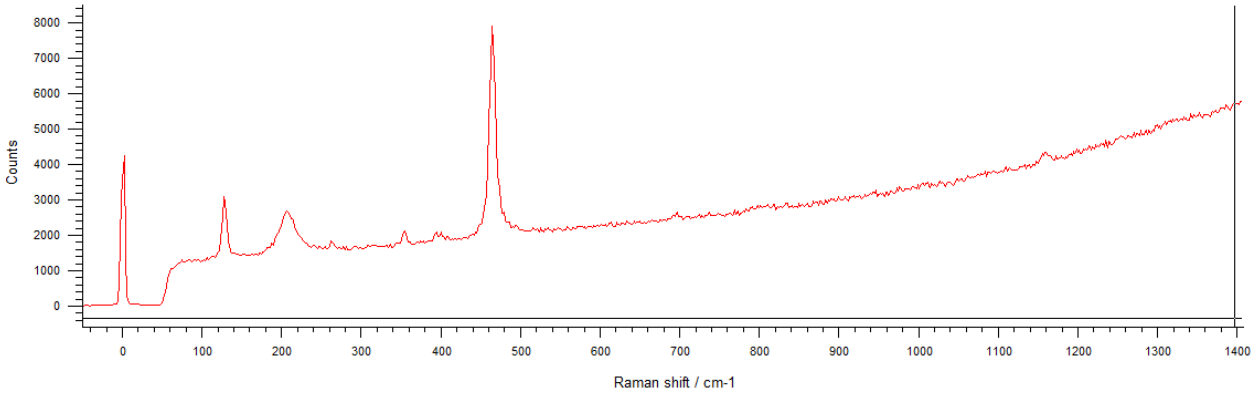

Figure C.30- Full signal for Chalcedony and megaquartz associations in FL-KS-6-1.

Appendix D - ICP-MS Analysis Data

Table D.1- ICP-MS concentration values for sample elements in ppm.

LB #	Sample	^{23}Na	^{25}Mg	^{27}Al	^{30}Si	^{43}Ca	^{51}V	^{55}Mn	^{59}Co	^{60}Ni	^{63}Cu	^{69}Ga	^{74}Ge	^{89}Y	^{91}Zr
13	2-2_1	209	143	220	465163	20628	1.19	7.36	0.20	3.83	13.51	33.88	0.58	1.54	1.88
14	2-2_2	595	882	5349	465163	14144	16.31	15.64	0.55	5.90	23.21	4.78	0.55	2.25	10.38
15	2-2_3	397	322	1750	465163	10474	5.81	7.85	0.23	2.95	33.31	2.27	0.59	0.76	5.33
16	2-2_4	992	1109	9388	465163	1377	25.90	20.65	1.09	8.24	3.97	7.03	0.61	1.22	9.28
17	2-2_5	901	1005	8493	465163	1833	25.52	20.03	0.78	6.79	2.06	6.83	0.60	2.13	9.72
18	5-2_1	379	3061	2477	465163	260387	7.43	118.84	0.83	4.46	1.89	1.96	0.34	5.62	5.80
19	5-2_2	711	12267	2865	465163	1200857	11.16	533.29	2.90	9.71	2.63	2.53	0.44	25.44	4.94
20	5-2_3	461	2277	3097	465163	167189	11.59	81.05	0.67	7.62	5.30	2.19	0.40	5.87	4.67
21	5-2_4	406	2592	2644	465163	207177	8.57	98.17	0.72	4.25	2.26	1.71	0.35	5.13	3.62
22	5-2_5	514	5445	2170	465163	491617	7.35	225.26	1.35	6.02	1.21	1.52	0.36	11.02	3.08
23	6-2_1	224	136	1222	465163	2724	10.46	2.47	0.10	2.57	26.89	1.22	0.20	1.05	2.84
24	6-2_2	201	116	1056	465163	3551	8.17	2.57	0.07	1.62	20.90	1.01	0.17	0.54	1.78
25	6-2_3	281	146	1235	465163	1032	13.18	3.88	0.15	3.38	19.90	2.34	0.33	0.52	2.51
26	6-2_4	319	95	1263	465163	990	9.20	1.33	0.07	1.61	13.16	1.63	0.27	0.72	1.40
27	6-2_5	161	67	772	465163	2052	7.39	1.36	0.05	1.83	22.06	0.71	0.20	0.69	1.43
34	6-3_1	635	12397	544	465163	1089420	6.04	508.48	1.70	4.46	18.27	0.95	0.10	25.37	1.39
35	6-3_2	234	6927	596	465163	629331	7.08	374.89	1.76	11.56	20.28	0.66	0.23	14.33	2.47
36	6-3_3	306	2857	1287	465163	180228	10.55	58.97	0.56	8.34	25.38	1.23	0.26	5.14	3.41
37	6-3_4	136	1539	941	465163	97691	7.35	50.05	0.38	5.24	2.50	1.44	0.27	3.08	1.94
38	6-3_5	1594	12108	97	465163	1260197	3.56	628.87	1.68	4.41	15.73	1.19	0.17	27.90	0.73
39	7-1_1	486	166	2003	465163	1826	4.07	3.23	0.11	1.88	2.27	2.21	0.30	0.84	2.17
40	7-1_2	596	209	2618	465163	2114	5.38	4.52	0.19	2.36	1.49	2.13	0.34	0.66	4.95
41	7-1_3	698	363	3702	465163	1666	7.74	5.77	0.35	3.50	3.08	3.81	0.49	1.17	3.78
42	7-1_4	599	247	2646	465163	879	5.22	5.23	0.20	1.83	4.63	1.86	0.39	0.49	3.20
43	7-1_5	724	266	3089	465163	1381	6.07	5.32	0.18	2.20	4.78	1.92	0.45	0.51	4.06
44	7-2_1	391	1813	244	46516	145987	8.25	64.08	0.4	5.85	1.09	2.26	0.4	5.78	2.69

				1	3				8				2		
45	7-2_2														
46	7-2_3	437	34	1066	465163	459	0.42	-0.01	0.00	0.95	3.24	1.75	0.36	0.01	0.70
47	7-2_4	332	714	1968	465163	41935	5.77	25.05	0.25	3.40	92.62	1.26	0.41	1.89	1.95
48	7-2_5	386	797	2089	465163	46621	6.54	20.87	0.28	3.45	4.28	1.54	0.43	2.26	2.25